Attachment A-7

Results of Resonant Column/Cyclic Torsional Shear Testing

ATTACHMENT A-7

Results of Resonant Column/Cyclic Torsional Shear Testing

This attachment contains the results of resonant column/cyclic torsional shear testing that was conducted at the University of Texas at Austin, under the supervision of Professor Kenneth H. Stokoe. The following information is presented to provide an overview of the work carried out by Professor Stokoe.

Sample Selection and Shipping

Seven undisturbed samples were sent to Professor Stokoe for testing in the Fall of 2002. The samples were selected by CH2M HILL's geotechnical staff based on the location of the samples within the soil profile and on the quality of sample. Samples that were judged as either *Excellent* or *Very Good* in quality were selected for testing by the University of Texas. An *Excellent* sample had no indentations at the tip of the sample, while a *Very Good* sample was one with only minor indentations of less than a quarter inch.[1] Samples of lesser quality have larger indentations or other tube disturbance, and have not been used in tests performed by the University of Texas.

Samples were shipped to the University of Texas in special shipping containers. Before shipping the samples were protected by wrapping the sample tube with multiple layers of bubble wrap, then placing the bubble-wrapped tube in a shipping container, and then finally packing the shipping container in "popcorn" within another shipping container. This method of sample shipping was selected after discussing shipping requirements with Professor Stokoe before shipping. It was Professor Stokoe's experience that this method of shipping resulted in samples that had little if any damage.

The shipping method described above was considered appropriate for these samples, given their very stiff consistency and general lack of potential for densification or remolding. The project area had been over-ridden by glaciers in the past – resulting in the samples being subjected to much higher loads than exist currently at the site (referred to as overconsolidation). Samples in a highly overconsolidated state are resistant to the effects of vibrations and other shock loading because of their denseness or hardness. In the case of the samples from the EGC ESP Site, the cohesive content of most samples provides "binder" to preserve this stiff condition.

[1] The indentations in the sampling tube occur when the sampling tube is pushed into very hard soils. If the soils are highly overconsolidated, as in the case of the samples from the EGCESP Site, the thin wall sampling tubes deform if they encounter a gravel particle – because it is difficult to push the gravel aside. The indentation results in some disturbance to the outer surface of the sample, proportionate to the amount of indentation of the sampling tube. A tube with no indentations is usually judged to be excellent quality as long as full sample recovery occurred. A sample with small indentations is judged better in quality than a sample with large indentations. Categories of Excellent, Very Good, Good, Fair, and Poor were assigned to the samples during the field work.

Resonant Column/Cyclic Torsional Shear Testing Method

Six of the seven samples sent to the University of Texas were selected by CH2M HILL for testing.

Samples were extruded from the sampling tube and then hand trimmed from their original diameter of 2.875 to a diameter of approximately 2 inches (in) and a height of approximately 4 in. Soil from the trimming was used for classification testing of the sample.

Each sample was tested separately in a combined resonant column/cyclic torsion test device. The test procedure involved setting the sample on a pedestal at the base of the test equipment, placing a top cap on the sample, and then enclosing the sample with a rubber membrane. A silicon-filled fluid bath was placed around the sample; a coil-magnet drive system was attached to the top cap; and then the entire assembly was placed in a confining pressure system.

The test method involved confining the sample to the desired test pressure, and then subjecting the top of the sample to either low-frequency torsional loading (torsional shear) or high frequency loading (resonant column). The frequency of loading during torsional shear tests was under 10 Hz. The resonant column test was typically performed at 50 Hz or more. The frequencies of loading for the resonant column test are much higher than the frequencies of primary interest for earthquake loading. However, by vibrating the soil sample at resonance in the resonant column test, it was possible to obtain higher shearing strain amplitudes. Past studies have shown that frequency effects are minimal for shear modulus measurements, but can be important for material damping measurements. For this reason, cyclic torsional tests were used to augment the resonant column data. The lower frequency testing resulted in more representative material damping values, but did not provide the range of shearing strain amplitudes.

The test pressure for each test was selected on the basis of the estimated mean effective confining pressure for the sample (i.e., $\sigma_o' = [(\sigma_v' + 2\sigma_h')/3]$). The first test was normally conducted at $0.25\sigma_o'$. Once the test sequence was conducted at this pressure, the pressure was increased to twice this amount, and the testing sequence repeated. Tests were conducted at $0.25\sigma_o'$, $0.5\sigma_o'$, $1.0\sigma_o'$, $2.0\sigma_o'$, and $4.0\sigma_o'$ in this manner. The intent of the pressure sequence was to obtain information showing the variation in shear modulus and damping with confining pressure. This information provides fundamental information about the soil behavior. It can also be used to estimate the change in shear modulus or material damping if the confining conditions occur at a site – for example under the weight of a very heavy power block structure.

The test sequence after increasing the confining pressure was not started until the low-strain shear modulus was into the secondary portion of the confining pressure modulus response. Typically, secondary response was achieved after a day of confinement. Once the secondary condition was observed, the testing sequence was started. The testing sequence for each confining pressure involved the application of high frequency (resonant column) or low frequency (cyclic torsion) cyclic loading to the top of the soil sample.

- For resonant column tests the frequency and amplitude of loading to the top of the sample were varied until resonance was achieved at a desired shearing strain amplitude. The resonance and calibration data for the accelerometer mounted on the top cap were

used to determine the amplitude of loading. This information was used to compute the shear modulus of the soil based on the resonant frequency, the size and weight of the sample, and the characteristic of the drive system using a one dimensional model of the vibrating sample. Both the frequency response and free decay methods were used to obtain the damping of the sample.

- For cyclic torsional tests, the load was applied at the top of the sample and displacements determined using proximity sensors. Torque and displacement measurements are used to determine the relationship between shearing stress and shearing strain. The resulting relationship was plotted as a hysteresis loop. The shear modulus of the soil was determined from the slope of the line between the end points of the hysteresis loop; material damping was determined on the basis of the area within the hysteresis loop relative to the maximum potential energy stored in each cycle of motion as represented by the triangular area beneath the modulus strain plot.

Resonant column and cyclic torsional shear tests for a given confining pressure were conducted by imposing low levels of loading to the top of the sample, corresponding to low shearing strain amplitudes, and then progressively working up to high levels of shearing strain. The range of shearing strains varied from less than 10^{-4} percent to 0.1 to 0.5 percent. The maximum shearing strain was determined by the maximum force that could be developed by the coil-magnet drive system, in combination with the stiffness of the soil. As confining pressures increased, the soil became stiffer – which then required more force to achieve the desired displacement or shearing strain.

Following each test series, the test system was disassembled and final weights and dimensions obtained for the test specimen.

Test Results

The results of the resonant column/cyclic torsional shear tests are presented in the exhibits to the University of Texas report. The plots in the exhibits present

- The shear modulus – duration of confinement plot. The change in slope from a relatively flat to a steeper constant slope is defined as the transition from the primary to secondary behavior. This transition typically occurs after several hundred minutes of confinement. The break in the curve is usually more apparent at higher confining pressures and with more cohesive soils.

- The material damping – duration of confinement curve. This curve is approximately the opposite of the modulus – confining pressure curve. As the modulus increases, the damping typically decreases.

- The low amplitude shear wave velocity (or shear modulus) – confining pressure curve. A break in the modulus –confining pressure curve is often noted at the approximate preconsolidation pressure of the soil sample.

- The low amplitude damping – confining pressure curve. Similar to previous discussions, the damping plots are essentially the opposite of the modulus – confining pressure plot in that damping decreases with increasing confining pressure (i.e., as the sample becomes stiffer).

- Shear modulus – shearing strain plots both in absolute terms (i.e., G) and normalized for the low strain shear modulus (i.e., G/G_{max}). The normalized curve is referred to as the modulus shape curve. It is used to adjust the modulus measured in situ to account for shearing strain amplitude effects; i.e., $G_{field} = [G_{max\ field} \times (G/G_{max})]$ where $G_{max\ field}$ is obtained from in situ values of shear wave velocity and G/G_{max} is selected from the results of laboratory tests at the shearing strain amplitude of interest.
- Material damping – shearing strain plots. One of the observations from these plots is that the material damping values from the resonant column test is typically several percentage points higher than the data from the cyclic torsion tests. The higher damping reflects the rate effects that occur from the higher frequency (i.e., > 50 Hz) of resonant column loading relative to cyclic torsional shear testing (<10 Hz). Generally, these frequency effects are observed for damping but not for modulus.
- Material damping – frequency of loading plots. These plots show the effects of frequency from the different test methods. The frequencies range from 0.1 Hz (loading over a 10 second period) to greater than 100 Hz (loading in 0.01 seconds). As noted previously, frequency effects seem to be most noticeable at frequencies greater than 10 Hz.

Observations

The results of the resonant column/cyclic torsional tests are consistent with published curves with one exception as discussed in the next paragraph of this summary. The consistency was verified by comparing the plots of shear modulus ratio (G/G_{max}) and material damping ratio (D) versus shearing strain amplitude (γ) from the ESP samples to plots developed from standard relationships recommended by EPRI (1993), Vucetic and Dobry (1991), and Sun et al. (1988). These plots are presented in Section 5 of the Geotechnical Report, and in the University of Texas report that follows.

One set of data (UTA-34-E) from a depth of 208 ft (Sample ESP B-3 (S-37)) gave unusually low shear modulus ratio and unusually high material damping ratio data relative to the other test results for samples from the EGC ESP Site and relative to published data. This unique behavior was discussed with Professor Stokoe. The conclusion from the discussions was that the conditions of the sample led to the unusual behavior. Apparently, when the sample was extruded from the sampling tube, a number of very small, horizontal fissures were observed. These fissures were attributed to stress relief occurring when the sample was removed from 208 ft below the ground surface and then extruded from the sampling tube. When the sample was subjected to the test pressures in the test device, the sample went out of alignment as the fissures closed. The misalignment became more prevalent as confining pressures increased, and resulted in a much lower modulus and higher material damping than would be expected.

In view of this unusual modulus ratio and damping ratio plots relative to both the data obtained for other samples from the EGC ESP Site and published data, it was decided to discard this set of data. Remaining portions of the sample in the sampling tube had similar fissures, and therefore, it was decided that additional testing of this sample would result in similar erratic data.

References

Electrical Power Research Institute "Guidelines for Determining Design Basis Ground Motions," Final Report, EPRI TR-102293, Palo Alto, CA, November 1993.

Sun, J.J., Golesorkhi, R., and H.B. Seed. *Dynamic Moduli and Damping Ratios for Cohesive Soils,* Report No. EERC-88/15, Earthquake Engineering Research Center, University of California, Berkeley, 1988.

Vucetic , M. and R. Dobry. *Effect of Soil Plasticity on Cyclic Response,* Journal of Geotechnical Engineering, ASCE, Vol. 117, No. 1, pp. 89-107, 1991.

Linear and Nonlinear Dynamic Soil Properties Determined by Combined Resonant Column and Torsional Shear Tests: Exelon Generating Company, ESP Site, Illinois

Volume I: Test Results

for
CH2M HILL
777 108th Avenue NE
Bellevue, WA 98004-5118

by

Kenneth H. Stokoe, II
CelestinoValle
Won Kyoung Choi
Farn-Yuh Menq

May 9, 2003

Geotechnical Engineering Report GR03-4
Geotechnical Engineering Center
Civil Engineering Department
The University of Texas at Austin

TABLE OF CONTENTS – VOLUME 1

LIST OF TABLES

LIST OF FIGURES

1. INTRODUCTION

The dynamic properties of six intact soil specimens that were recovered from two boreholes at the Exelon Generating Company (EGC) Early Site Permit (ESP) Site in Illinois were evaluated in the Soil Dynamics Laboratory at the University of Texas at Austin (UTA). This work was conducted for CH2M HILL, Inc. as part of their work on the EGC ESP Application. The purpose of the study was to evaluate the linear and nonlinear shear modulus and material damping characteristics of the intact specimens. The work at UTA was funded by CH2M HILL, Inc. Dr. Donald G. Anderson was the Project Manager for CH2M HILL, Inc.

The report documenting the project at UTA is presented in two volumes. This volume, Volume I, presents: (1) an overview of the test program, (2) a discussion of the dynamic test results, and (3) exhibits containing all test data. The second volume, Volume II, contains all documentation associated with: (1) the testing and calibration procedures, (2) the QA program, and (3) the overall system checks conducted before and after dynamic testing was performed. The QA program met the general intent of ASTM 3740 "Standard Practice for Minimum Requirements for Agencies Engaged in Testing and/or Inspection of Soil and Rock as Used in Engineering Design and Construction". Specific test procedures and evaluation methods were in accordance with the Quality Assurance Program used by the Soil Dynamics Laboratory at UTA. This quality Assurance Program was developed for, accepted by, and used on the Department of Energy Program for the part of the Yucca Mountain Project that involved dynamic soil and rock property measurements at UTA.

1.1 Intact Samples Dynamically Tested at the University of Texas

Seven intact samples were delivered by express mail to the Soil Dynamic Laboratory at the University of Texas at Austin on September 23, 2002. Each specimen was shipped in the thin-walled steel ("Shelby") tube used during the field sampling operation. Each tube was wrapped in protective bubble wrap, surrounded by small pieces of styrofoam packing, and

placed in a cardboard box. This box was in turn surrounded by small pieces of styrofoam and packed in a larger cardboard shipping box. Each Shelby tube had an outside diameter (OD) of 3 in. (7.6 cm), a wall thickness of 1/16 in. (0.16 cm), and a length of about 30 in. (76.2 cm). A listing of the samples, boreholes and associated information such as a description of the soil and the date of sampling are presented in Table 1.

The samples were shipped to UTA in four cardboard boxes which contained two samples per box, except for one box which only contained one sample. Each outer shipping box was approximately 14 in. (88.9 cm) by 15 in. (38.1 cm) in plan dimensions and about 35 in. (88.9 cm) tall. The sample tubes inside the boxes were well protected and arrived undamaged at UTA.

Six of the seven samples were dynamically tested at UTA. The six intact specimens that were extruded from the Shelby tube samples are listed in Table 2. Just before testing these specimens, each sample tube was cut to the desired length. The sample length was generally 5.0 in. (12.7 cm) to 7.0 in (17.8 cm). After the tubes were cut to the proper length, the samples were removed by extruding the soils from the Shelby tubes using a piston operated with a hydraulic pump.

After each sample was removed from the metal tube, it was trimmed to the desired specimen size and then set up in the combined resonant column and torsional shear (RCTS) equipment. The specimen was dynamically tested as described in Section 2. All specimens except Specimen No. 5 were trimmed to a smaller size to remove the outer (and possibly somewhat disturbed) material. Generally, the final size of the test specimen was about 4.0 in. (10.2 cm) in height and 2.0 in. (5.1 cm) in diameter. The outer material of Specimen No. 5 could not be trimmed due to the horizontal layering and tendency to separate at the layer boundaries. All six specimens were tested as intact specimens. A summary of the initial properties of these specimens is presented in Table 2.

Table 1 Boreholes and Associated Information Given to UTA on the Seven Samples from the EGC ESP Site that were Dynamically Tested at the University of Texas

No.	Borehole	Specimen Identification	Specimen Depth ft (m)	Soil Description	Sample in the field ft(m)	Date of Sampling	Time of Sampling
1	B-2	S-7	31.5-33.5 (9.6-10.2)	Low Plasticity or Clay	1.7 (0.52	8/2/02	8:50
2	B-3	S-13	40-42 (12.2-12.8)	Lean Clay	2.0 (0.61)	7/26/02	12:50
3	B-3	S-23	70.5-73.5 (21.5-22.4)	Sandy Lean or Silt	2.4 (0.73)	7/29/02	11:35
4	B-3	S-33	115.5-118.5 (35.2-36.1)	Low Plasticity Clay	2.7 (0.82)	7/30/02	9:35
5	B-3	S-42	170-173 (51.8-52.7)	Lean Clay	2.7 (0.82)	8/2/02	16:05
6	B-3	S-37	205.5-208.5 (9.6-10.2)	Low Plasticity or Clay	2.8 (0.85)	8/2/02	9:10
7	B-2	S-38	240-243 (9.6-10.2)	Sandy Low Plasticity or Low Plasticity Silt	1.9 (0.58)	8/6/02	15:45

Table 2 Initial Properties of Specimens from the ECG ESP Project: Combined Resonant Column and Torsional Shear Testing at the University of Texas at Austin

No.	Specimen ID	Borehole No.	Specimen Depth ft(m)	Soil Type (Unified Soil Classification)	Water Content %	Dry Density pcf (gr/cm^3)	% Passing Sieve #200	Liquid Limit %	Plasticity Index	Void Ratio[1] e	Assumed Sp. Grav. G_3	Degree of Saturation (Sr, (%)
1	UTA-34-A	B-2 (S-7)	33 (10.06)	Sandy Lean Clay (CL)	13.2	125.7 (2.01)	69	27	12	0.34	2.70	100.0
2	UTA-34-B	B-3 (S-13)	42 (12.56)	Sandy Lean Clay (CL)	18.5	109.8 (1.76)	64	25	11	0.54	2.70	93.3
3	UTA-34-D	B-3 S-33	115 (35.05)	Sandy Lean Clay (CL)	6.7	136 (2.19)	61	22	9	0.24	2.70	76.5
4	UTS-34-C	B-3 S-42	171 (52.12)	Sandy Lean Clay (CL)	11.9	119.8 (1.92)	61	25	11	0.41	2.70	79.0
5	UTA-34-E	B-3 (S-47)	208 (63.40)	Silty Clay (CL-ML)	19.0	107.1 (1.72)	99	21	7	0.57	2.70	89.4
6	UTA-34-F	B-2 (S-38)	242 (73.76)	Silt (ML)	17.4	111.6 (1.79)	97	24	NP[2]	0.51	2.70	92.0

Notes:

1. Void ratios were calculated based on the assumed value
2. NP = Nonplastic

2. DYNAMIC LABORATORY TESTS

Combined resonant column and torsional shear (RCTS) equipment was used to evaluate the dynamic characteristics of all six specimens. A brief description of the RCTS equipment is presented in Exhibit A. All documentation associated with: (1) testing and calibration procedures, (2) the QA program, and (3) the overall system check are contained in Volume II of this report. The bulk of this documentation was originally generated for a companion project dealing with evaluation of the dynamic material properties of soil and tuff specimens from Yucca Mountain, Nevada. It is worth noting that the RCTS equipment had been calibrated to an NQA level in July 2000, and this level was reconfirmed in January, 2001 and March, 2002. All testing on this project was completed during the March, 2002 – February, 2003 operational cycle for the NQA level calibration

The dynamic characteristics of the six intact specimens that were evaluated with the RCTS measurements are the shear modulus, G, and the material damping ratio in shear, D. The influence of the following variables on G and D were evaluated:

1. Magnitude of the isotropic state of stress, σ_o.

   Five isotropic pressures were typically used for each specimen which ranged from below to above the estimated in situ mean effective stress, σ'_m. When the samples were above the water table, the total effective stresses were assumed equal, because the samples were unsaturated and the values of (negative) pore water pressure were unknown.

2. Time of confinement at each isotropic state of stress, t.

   Confinement times at each pressure were at least 1000 minutes for all specimens. Thus, all small-strain measurements of G and D at times of 1000 minutes were after primary consolidation for each specimen.

3. Shearing strain amplitude, γ.

   Strains ranged from the small-strain range, less than about 0.0005% to rather large strain amplitudes, above about 0.1% for many specimens. Testing was performed over this strain range at σ_m and 4 σ_m for many of the specimens.

4. Number of cycles of loading, N.

   Ten cycles of loading were used in the torsional shear (TS) test followed by about 1000 cycles in the resonant column (RC) test.

5. Excitation frequency, f.

   Frequencies ranging from 0.1 Hz to around 5 Hz were used in TS testing of the specimens. The frequency associated with resonance in the RC test varied with material stiffness and strain amplitude and ranged from about 59 Hz to slightly more than 264 Hz. Also, the maximum frequency in the TS test was ≤ 0.1 times the resonant frequency in the RC test.

6. Stress History.

   Small-strain values of G and D (G_{max} and D_{min}, respectively) were evaluated at the estimated in situ mean total stress, σ_m, and generally at two stress levels under and at two stress levels over the in situ mean total stress.

2.1 Test Program

Dynamic testing of each soil specimen involved the evaluation of G and D over a range of isotropic confining pressures. As noted above, five isotropic confining pressures were generally used in a loading sequence, with the isotropic confining pressure, σ_o, doubled upon completion of the required tests at the lower pressure. Low-amplitude resonant column testing was performed at each level of σ_o to determine the effects of magnitude of confinement and time of confinement on the small-strain shear modulus, G_{max}, and small-

strain material damping ratio, D_{min}. Low-amplitude dynamic tests are defined as those tests in which the resonant amplitude did not exceed 0.001% and was usually well below that level.

For each laboratory specimen, the range in confining pressures was based on the estimated in situ mean effective stress, σ'_m. The estimated in situ mean effective stress, σ'_m, was calculated by considering the following: (1) the depth of the water table which was equal to 30 ft (9.15 m), (2) the total unit weights of all soils above the specimen, which were taken from the values in Table 2, and the total unit weight of the test specimen that was determined by measuring the volume and weight of the trimmed specimen just before testing, and (3) the initial estimate of the in situ coefficient of lateral earth pressure at rest, K_o (assumed to be 1.0; given to UTA by Dr. Donald Anderson and is shown in Table 3). Once this value of σ'_m was determined, the range in confining pressures over which G and D would be evaluated was established.

All specimens were tested at small strains at the different confining pressures in an increasing confining pressure sequence. Each confining pressure sequence is listed in Table. 3. High-amplitude resonant column and torsional shear tests were performed during this loading sequence at the estimated in situ mean effective stress, σ'_m, (assuming $K_o = 1.0$) and, in this case, for five specimens, at four times the estimated in situ mean total stress. On the other hand, testing of Specimen No.5 had to be stopped during the loading sequence due to sample tilting which caused the drive plate to touch the magnets; hence high-amplitude testing was only performed at σ'_m.

High-amplitude testing was composed of two series of tests. The first involved cyclic torsional shear (TS) testing as illustrated in Figure 1. A complete set of torsional shear tests required about two hours to perform at each confining pressure. Torsional shear tests were conducted with the drainage line opened and involved shearing strains, γ, from less than 0.001% to above 0.02%. The majority of the measurements were performed at 0.5 Hz and are labeled as TS1 in Figure 1. However, two sets of TS tests at $\gamma \approx 0.001\%$ and $\gamma \approx 0.01\%$ were also conducted to evaluate the effect of excitation frequency on G and D at these strains. In

Table 3 Summary of Tests Performed at The University of Texas at Austin from EGC ESP Project: Combined Torsional Shear And Resonant Column Testing

No.	Borehole No.	Specimen Depth ft(m)	Estimated K[1]	In-Situ Effective Mean Stress σ_m[1], ksf (kPa)	Initial Specimen Size		Isotropic Test Pressures		
					Height In (cm)	Diameter In (cm)	Low-Amplitude RC and TS Tests ksf (kPa)	High-Amplitude RC Tests ksf (kPa)	High-Amplitude TS Tests ksf (kPa)
1	B-2 (S-7)	33 (10.06)	1	3.88 (186)	3.85 (9.78)	2.03 (5.16)	0.86, 1.87, 3.88, 7.77, 15.55 (41, 90, 186, 373, 746)	3.88, 15.55 (186, 746)	3.88, 15.56 (186, 746)
2	B-3 (S-13)	42 (12.56)	1	4.46 (214)	3.60 (9.14)	2.00 (5.08)	1.01, 2.16, 4.46, 8.64, 17.28 (48, 104, 214, 414, 828)	4.46, 17.28 (214, 828)	3.88, 15.56 (214, 828)
3	B-3 S-33	115 (35.05)	1	8.64 (414)	4.07 (10.34)	2.06 (5.23)	2.16, 4.32, 8.64, 17.28, 34.56 (104, 207, 414, 828, 1657)	8.64, 34.56 (414, 1657)	8.64, 34.56 (414, 1657)
4	B-3 S-42	171 (52.12)	1	12.96 (621)	3.87 (9.83)	2.03 (5.16)	4.75, 6.48, 12.96, 25.92, 51.84 (228, 311, 621, 1243, 2485)	12.96, 51.84 (621, 2485)	12.96, 51.84 (621, 2485)
5	B-3 (S-47)	208 (63.40)	1	14.40 (690)	3.63 (9.22)	1.98 (5.03)	3.60, 7.20, 14.40, 28.80, 57.60 (173, 345, 690, 1381, 2761)	14.4 (690)	14.4 (690)
6	B-2 (S-38)	242 (73.76)	1	17.28 (828)	3.72 (9.45)	2.00 (5.08)	4.32, 8.64, 17.28, 34.56, 57.60 (207, 414, 828, 1657, 2761)	17.28, 57.60 (828, 2761)	17.28, 57.60 (828, 2761)

Notes:

1. In-situ coefficient of lateral earth pressure at rest was given by Dr. Donald Anderson of CH2M HILL, Inc.
2. Based on the water table at a depth of 30 ft (from Dr. Anderson)

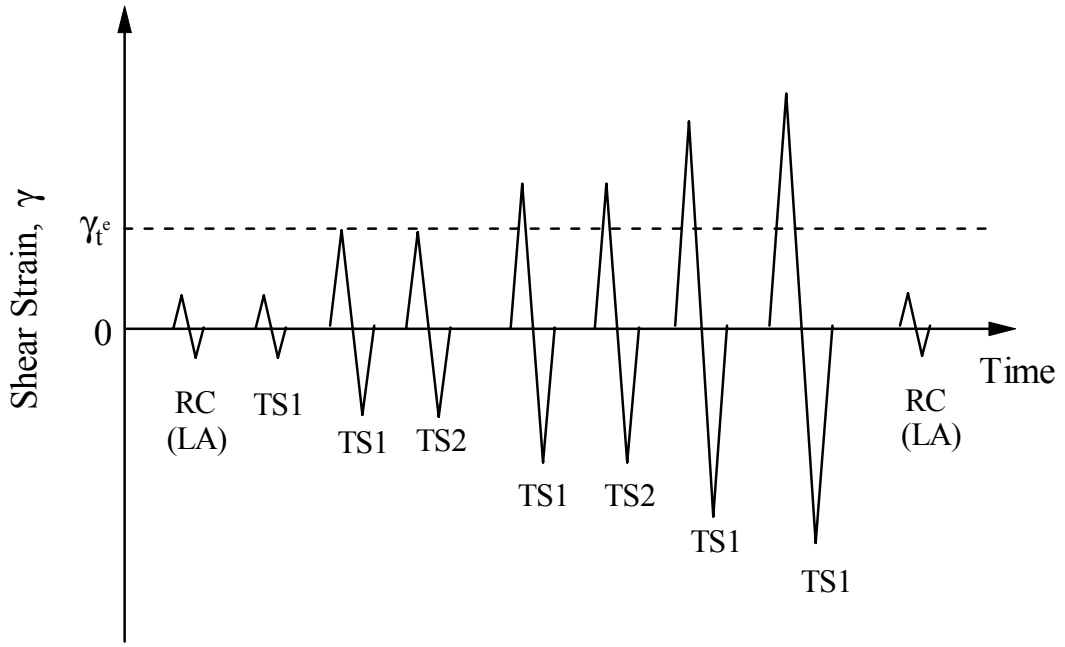

γt^e= elastic threshold strain; below γt^e, G is constant and equal to G_{max}

RC (LA) = resonant column test at low-amplitudes (strains < 0.001%)

TS1 = torsional shear test in which 10 cycles are applied at 0.5 Hz.

TS2 = torsional shear test in which 10 cycles are applied at each of four frequencies between 0.1 Hz to 5 Hz (0.1, 0.5, 1, and 5) for the soil specimens.

Figure 1 Testing Procedure Used in the Torsional Shear (TS) Test to Investigate the Effects of Strain Amplitude, Number of Loading Cycles, and Excitation Frequency on G and D of the Test Specimens.

these tests (denoted as TS2 in Figure 1), ten cycles of loading were applied at five different frequencies ranging from 0.1 Hz to 5 Hz.

After the TS tests were completed, confinement of the specimen was continued at the given confining pressure, and the specimens were allowed to re-gain any change in G_{max} for a period of one day. Then a series of high-amplitude resonant column (HARC) tests was performed. However, before high-amplitude RC testing commenced, small-strain RC tests were performed to determine any changes in the soil skeleton that might have occurred from the TS tests. No significant changes are defined herein as 5% in G_{max} and 10% in D_{min}.

High-amplitude resonant column testing was conducted to evaluate the influence of strain amplitude on G and D. This series of tests is illustrated in Figure 2. A complete set of resonant column tests took about two hours to perform, and these tests were performed with the drainage line opened just as in the case of the TS tests. The HARC tests typically involved shearing strains from less than 0.0005% to above 0.05%, depending on the soil stiffness and material damping. In these tests, about 1000 cycles of loading were applied at each strain amplitude.

Upon completion of the high-amplitude RC tests, low-amplitude RC tests were again performed to determine if any changes in the soil skeleton had occurred from the high-amplitude tests. (No significant changes were observed in G_{max} and D_{min} after the 1-day rest period.) Then, the next stage of testing (low-amplitude tests at a higher confining pressure) was undertaken.

2.2 Test Results

The results of the RC and TS tests are shown in Exhibits B through G for the six specimens. Each exhibit presents all test results from one specimen. As an example, consider the general presentation of dynamic test results for Specimen No. 1 that are presented in Exhibit B. The dynamic test results are presented as follows:

1. Figure B.1 shows the variation in low-amplitude shear modulus with magnitude and duration of isotropic confining pressure from resonant column tests.

2. Figure B.2 shows the variation in low-amplitude material damping ratio with magnitude and duration of isotropic confining pressure from resonant column tests.

3. Figure B.3 shows the variation in estimated void ratio with magnitude and duration of isotropic confining pressure from resonant column tests.

4. Figure B.4 shows the variation in low-amplitude shear wave velocity with isotropic confining pressure from resonant column tests.

5. Figure B.5 shows the variation in low-amplitude shear modulus with isotropic confining pressure from resonant column tests.

6. Figure B.6 shows the variation in low-amplitude material damping ratio with isotropic confining pressure from resonant column tests.

7. Figure B.7 shows the variation in estimated void ratio with isotropic confining pressure from resonant column tests.

8. Figure B.8 shows the variation in shear modulus with shearing strain and isotropic confining pressure.

9. Figure B.9 shows the variation in normalized shear modulus with shearing strain and isotropic confining pressure.

10. Figure B.10 shows the variation in material damping ratio with shearing strain and isotropic confining pressure.

11. Figure B.11 shows the variation in shear modulus with shearing strain at an isotropic confining pressure of 27 psi (= 3.89 ksf = 186 kPa) from both the RC and TS tests.

12. Figure B.12 shows the variation in normalized shear modulus with shearing strain at an isotropic confining pressure of 27 psi (= 3.89 ksf = 186 kPa) from both the RC and TS tests.

13. Figure B.13 shows the variation in material damping ratio with shearing strain at an isotropic confining pressure of 27 psi (= 3.89 ksf = 186 kPa) from both the RC and TS tests.

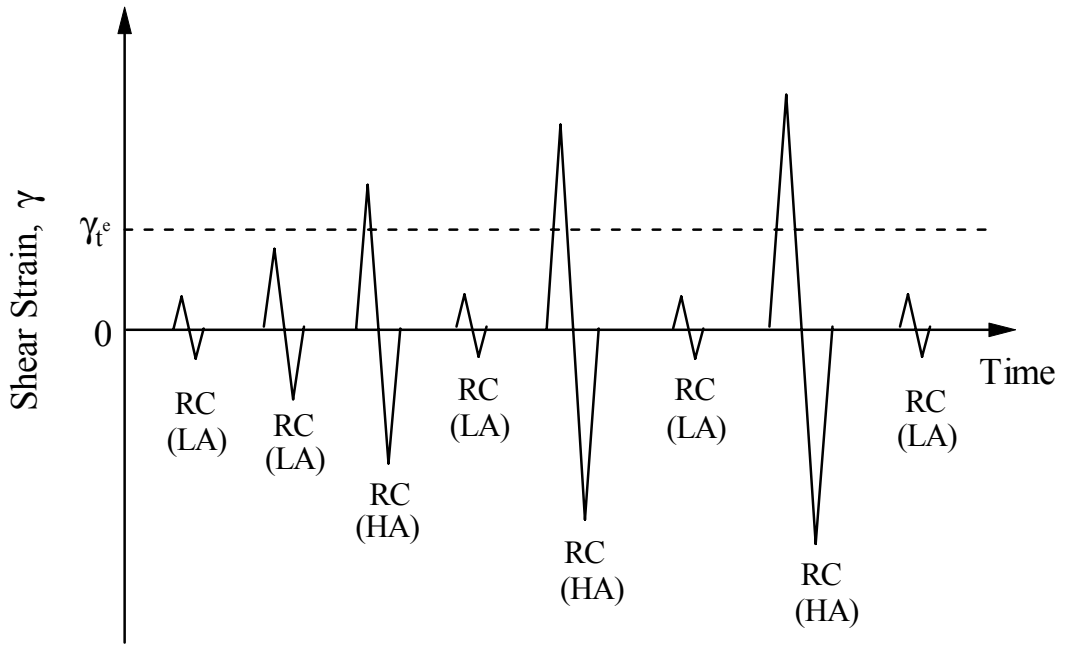

RC = resonant column test in which about 1000 cycles of loading are applied during each measurement

γt^e = elastic threshold strain; below γt^e, G is constant and equal to G_{max}

RC (LA) = resonant column test at low-amplitudes (strains < 0.001%)

RC (HA) = resonant column test at amplitudes above γt^e

Figure 2 Testing Procedure Used in the Resonant Column (RC) Test to Investigate the Effect of Strain Amplitude on G and D of the Test Specimens.

14. Figure B.14 shows the variation in shear modulus with loading frequency at an isotropic confining pressure of 27 psi (= 3.89 ksf = 186 kPa) from RCTS tests.

15. Figure B.15 shows the variation in material damping ratio with loading frequency at an isotropic confining pressure of 27 psi (= 3.89 ksf = 186 kPa) from RCTS tests.

16. Figure B.16 shows the variation in shear modulus with shearing strain at an isotropic confining pressure of 108 psi (=15.55 ksf = 746 kPa) from both the RC and TS tests.

17. Figure B.17 shows the variation in normalized shear modulus with shearing strain at an isotropic confining pressure of 108 psi (=15.55 ksf = 746 kPa) from both the RC and TS tests.

18. Figure B.18 shows the variation in material damping ratio with shearing strain at an isotropic confining pressure of 108 psi (=15.55 ksf = 746 kPa) from both the RC and TS tests.

19. Figure B.19 shows the variation in shear modulus with loading frequency at an isotropic confining pressure of 108 psi (=15.55 ksf = 746 kPa) from RCTS tests.

20. Figure B.20 shows the variation in material damping ratio with loading frequency at an isotropic confining pressure of 108 psi (=15.55 ksf = 746 kPa) from RCTS tests.

21. Table B.1 presents the tabulated results of the variation in low-amplitude shear wave velocity, low-amplitude shear modulus, low-amplitude material damping ratio and estimated void ratio with isotropic confining pressure from RC tests.

22. Table B.2 presents the tabulated results of the variation in shear modulus, normalized shear modulus and material damping ratio with shearing strains from RC tests at an isotropic confining pressure of 27 psi (= 3.89 ksf = 186 kPa).

23. Table B.3 presents the tabulated results of the variation in shear modulus, normalized shear modulus and material damping ratio with shearing strain from TS tests at an isotropic confining pressure of 27 psi (= 3.89 ksf = 186 kPa).

24. Table B.4 presents the tabulated results of the variation in shear modulus, normalized shear modulus and material damping ratio with shearing strains from RC tests at an isotropic confining pressure of 108 psi (=15.55 ksf = 746 kPa).

25. Table B.5 presents the tabulated results of the variation in shear modulus, normalized shear modulus and material damping ratio with shearing strain from TS tests at an isotropic confining pressure of 108 psi (=15.55 ksf = 746 kPa).

3. DISCUSSION OF DYNAMIC TEST RESULTS

The discussion of the dynamic test results from the combined RCTS tests is divided into two sections. The first one is this section, Section 3, which deals with the behavior of the specimens in the strain range where the dynamic properties are constant and independent of strain amplitude. This strain range is called the linear range, and measurements and dynamic properties in this range are often called small strain or low amplitude. The second section, Section 4, deals with the behavior of the specimens in the nonlinear range. In this strain range, the measurements and dynamic properties are often called large strain or high amplitude.

3.1 Small-Strain Shear Wave Velocity, Shear Modulus, and Material Damping Ratio

3.1.1 Small-Strain Shear Wave Velocity

The variations of small-strain shear wave velocity, V_S, with isotropic confining pressure, σ_o, for the six specimens are shown in Figure 3. Total confining pressure and not effective confining pressure is used because the samples were not saturated and the values of (negative) porewater pressure were unknown.

As seen in Figure 3, each specimen exhibited V_S increasing with increasing isotropic confining pressure, as expected. Relationships between small-strain shear wave velocity, confining pressure, and void ratio were fit to the data. The equation relating confining pressure, void ratio, and V_s (patterned after Hardin's 1978 equation for small-strain shear modulus) is:

$$V_s = (A_V / \sqrt{F(e)}) \cdot (\sigma_o / P_a)^{n_V} \quad (1)$$

where;

A_v = shear wave velocity at σ_o = 1 atm and e = 1.0,

$F(e) = 0.3 + 0.7e^2$,

e = void ratio,

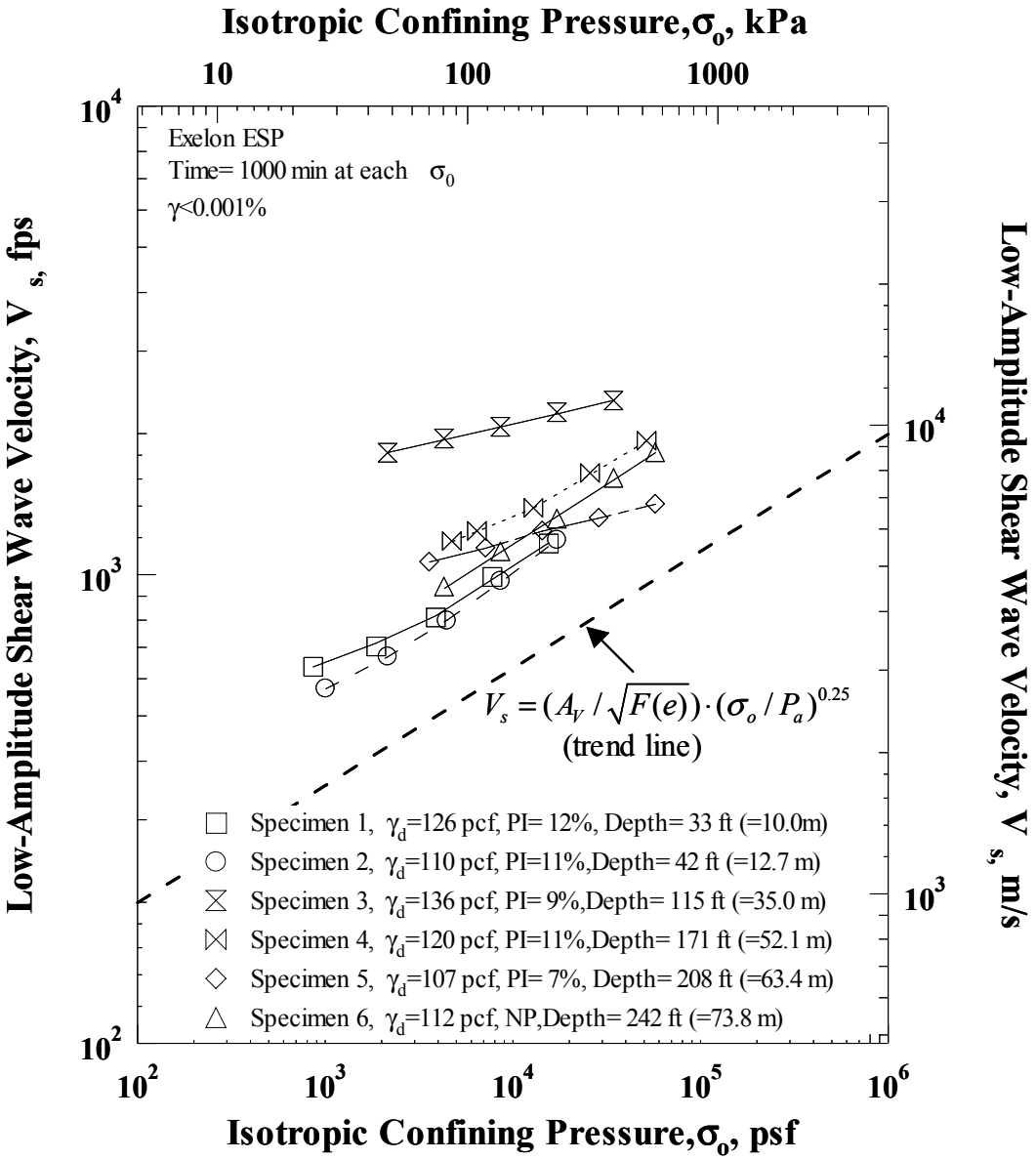

Figure 3 Variation in Low-Amplitude Shear Wave Velocity with Isotropic Confining Pressure of the Six Exelon ESP Specimens Determined from Resonant Column (RC) Tests

σ_o = total isotropic confining pressure in the same units as P_a,

P_a = one atmosphere (2117 psf or 100 kPa), and

n_v is a dimensionless exponent.

As noted above, total stress, σ_o, is used in place of effective stress, σ_o', in Equation 1. The best-fit lines from least-squares fitting of the loading results are presented in Figure 3 as dashed lines The constants determined for Equation 1 from the best-fit lines are summarized in Table 4**.** The log V_S – log σ_0 relationships and their relative similarities and differences are discussed below.

Three of the specimens, Specimen Nos. 1, 2 and 4, show a log V_S – log σ_0 relationship with two different slopes in the trend of increasing V_S with increasing σ_o. The initial region where V_S increases more slowly with a somewhat lower slope indicates the overconsolidated state of the specimen. The second region where V_S increases faster with a somewhat steeper slope represents the specimen in the normally consolidated state. Furthermore, the confining pressure at which there is a change in the slope for each specimen occurs at approximately the third pressure step (just slightly less for Specimen No. 2). The third confining pressure is the one estimated before testing commenced to be the in-situ mean effective stress if the specimen is overconsolidated with K_o of 1.0; hence, the initial estimation was good.

Two of the specimens, Specimen Nos. 3 and 5, did not show a trend of two slopes in the log V_S – log σ_0 relationship. Only one straight line can be drawn through each set of data points. The straight line shows a rather small increase in V_S with σ_0. This trend indicates that these specimens remained overconsolidated over the complete range in test pressures and/or they are cemented. This conclusion is supported by the lower values of n_v (0.09 and 0.10 in Table 4 for Specimens Nos. 3 and 5, respectively) relative to a value 0.25 as discussed below.

A normally consolidated material or a specimen that has not retained any history of past loading will exhibit a substantial increase in V_S with increasing σ_0. This increase translates to a value of n_v close to 0.25. This slope or exponent for σ_0 in Equation 1 is n_v = 0.25. The resulting trend is shown by the heavy dashed line in Figure 3. Specimen No. 6, a

Table 4 Constants and Exponents in Equations 1 through 3 from Least-Squares Fitting of the log V_s – log σ_0, log G_{max} – log σ_0 and log D_{min} – log σ_0 Relationships for the Six Specimens as Determined from Resonant Column (RC) Tests.

Specimen No.	UT Specimen ID	Specimen Depth ft (m)	Plasticity Index %	Isotropic Confining Pressure ksf (kPa)	Initial Void Ratio e_0	Shear Wave Velocity				Shear Modulus				Material Damping Ratio			
						O.C[3]		N.C[4]		O.C[3]		N.C[4]		O.C		N.C	
						A_v, fps (m/s)	n_v	A_v, fps (m/s)	n_v	A_G, ksf (MPa)	n_G	A_G, ksf (MPa)	n_G	A_D, %	n_D	A_D, %	n_D
1	UTA-34-A	33 (10.06)	12	3.88 (186)	0.34	440 (134.1)	0.13	431 (131.3)	0.25	855 (41.0)	0.25	827 (39.6)	0.50	4.91	-0.08	6.21	-0.15
2	UTA-34-B	42 (12.65)	11	4.46 (214)	0.54	468 (142.6)	0.20	457 (139.4)	0.27	887 (42.5)	0.40	898 (43.1)	0.51	2.96	-0.06	2.96	-0.06
3	UTA-34-D	115 (35.05)	9	8.64 (414)	0.24	1059 (322.7)	0.09	NA	NA	5049 (242.0)	0.19	NA	NA	3.30	-0.03	NA	NA
4	UTA-34-C	171 (52.12)	11	12.96 (621)	0.41	668 (203.5)	0.15	591 (180.0)	0.22	1849 (88.7)	0.31	1445 (69.3)	0.45	2.75	-0.05	2.75	-0.05
5	UTA-34-E	208 (63.40)	7	14.40 (690)	0.57	686 (209.1)	0.10	NA	NA	1995 (95.6)	0.20	NA	NA	1.41	-0.08	NA	NA
6	UTA-34-F	242 (73.76)	NP[2]	17.28 (828)	0.51	543 (165.4)	0.24	543 (165.4)	0.24	1185 (56.8)	0.50	1185 (56.8)	0.50	0.89	-0.17	0.89	-0.17

Notes:

1. Void ratios were calculated based on the assumed value for G_S
2. NP =Non Plastic
3. O.C =Overconsolidated state
4. N.C =Normally consolidated state
5. NA =Not Applicable

Note: *No change of slope in log G_{max} log σ'_o curve, thus OCR could not be estimated

nonplastic silt is an example of a specimen that did not retain any history of the past loading at the site and may be somewhat disturbed.

3.1.2 Small-Strain Shear Modulus

The variations of the small-strain shear modulus, G_{max}, with isotropic confining pressure, σ_o, for the six specimens are presented in Figure 4. Relationships have been fit to the small-strain shear moduli data using the generalized relationship presented by Hardin (1978). The Hardin (1978) equation relating shear modulus, void ratio, and confining pressure (slightly modified) is:

$$G_{\max} = (A_G / F(e)) \cdot (\sigma_o / P_a)^{n_G} \quad (2)$$

where;

A_G = shear modulus at σ_o = 1 atm and e = 1.0,

$F(e) = 0.3 + 0.7e^2$,

e = void ratio,

σ_o = isotropic confining pressure in the same units as P_a,

P_a = one atmosphere (2117 psf or 100 kPa), and

n_G is a dimensionless exponent.

As in Equation 1, total stress, σ_o, is used in place of effective stress, σ_o', in Equation 2. The best-fit lines determined by least-squares fitting of the loading results are shown in the Figure 4**.** The constants determined for Equation 2 from the best-fit lines are summarized in Table 4.

As cited in the discussion of trends in the log V_S – log σ_0 relationships, the change in G_{max} with σ_o predicted by Equation 2 (in terms of a trend line with $n_G = 0.50$) is shown by the heavy dashed line in Figure 4. If a specimen is normally consolidated, it will generally follow this trend line or exhibit an even slightly larger value of n_G. If a specimen has plasticity, is overconsolidated, and retains the stress history of the site, the log G_{max} – log σ_o relationship will be composed of two linear segments, with the initial segment in the overconsolidated

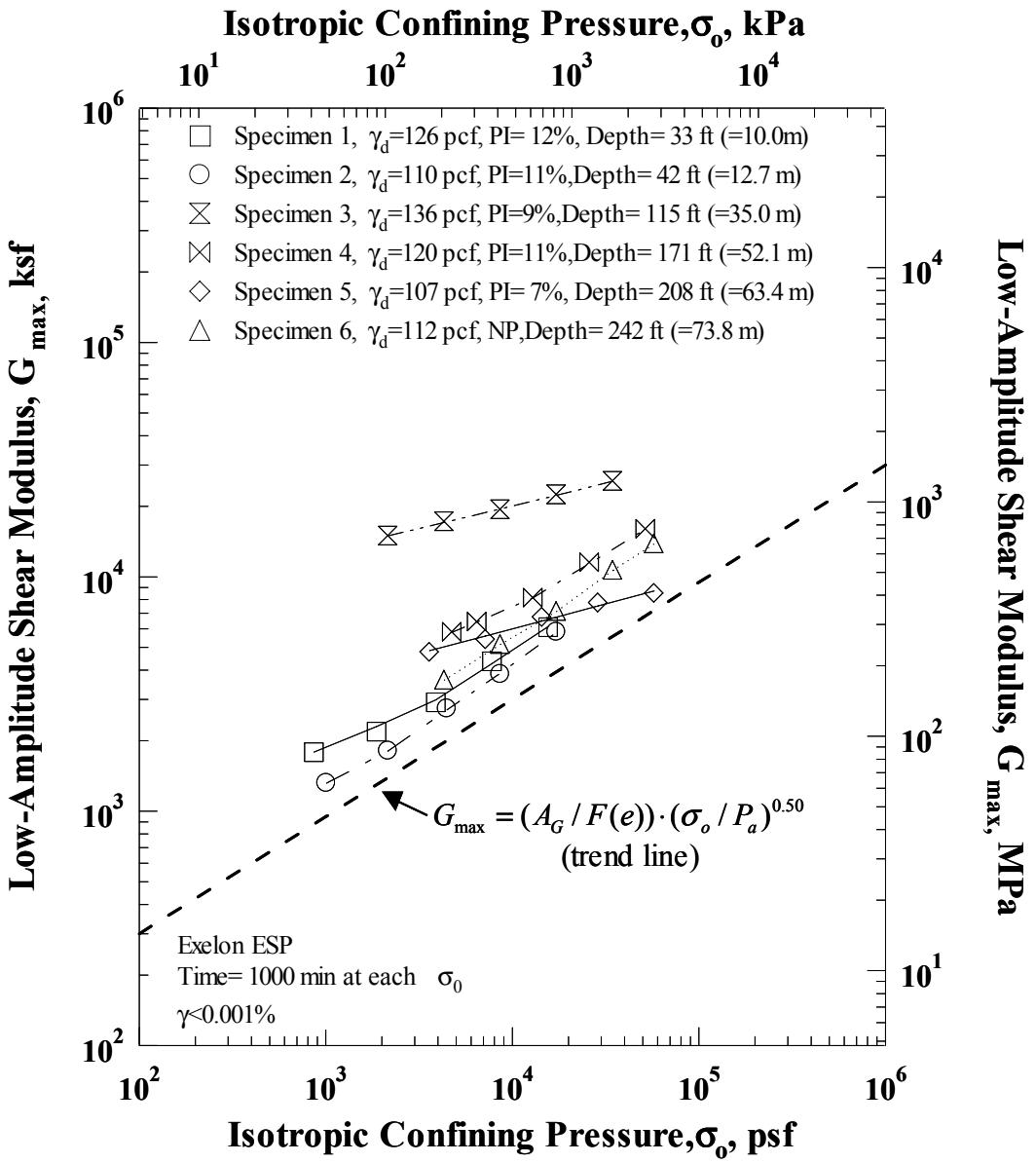

Figure 4 Variation in Low-Amplitude Shear Modulus with Isotropic Confining Pressure of the Six Exelon ESP Specimens Determined from Resonant Column (RC) Tests

range having a flatter slope and the segment in the normally consolidated range having a steeper slope (larger value of n_G). This relationship with two segments is shown by Specimens Nos. 1, 2 and 4 as discussed before. Moreover, the log G_{max} – log σ_o relationships differentiate the overconsolidated region a bit more readily than the log V_S – log σ_o relationships (because the vertical scale is expanded when G_{max} (= ρ V_S^2) is used). Specimen Nos. 3 and 5 are heavily overconsolidated and/or cemented. The test-pressure range did not exceed the maximum past pressure so the log G_{max} – log σ_o relationships show only one flat slope (n_G considerably less than 0.5). Unfortunately, Specimen No. 6 does not exhibit a trend indicating the stress history at the site, probably because the specimen is nonplastic and possibly because minor disturbance may have occurred.

3.1.3 Small-Strain Material Damping Ratio

The relationship between the small-strain material damping ratio, D_{min}, and isotropic confining pressure, σ_o, can be written as:

$$D_{\min} = A_D \cdot (\sigma_o / P_a)^{n_D} \tag{3}$$

where;

A_D =small-strain material damping ratio at σ_o = 1atm,

σ_o = isotropic confining pressure in the same units as P_a,

P_a = one atmosphere (2117 psf or 100 kPa), and

n_D is a dimensionless exponent.

As in Equations 1 and 2, total stress, σ_o, is used in place of effective stress, σ_o', in Equation 3. The best-fit lines calculated by least-squares fitting of the loading results are presented in Figure 5 and are summarized in Table 4.

All specimens except Specimen No. 2 exhibited the trend of material damping ratio decreasing as confining pressure increased (as expected). The values of n_D for Specimen Nos. 3 and 5, which are heavily overconsolidated and/or cemented, are generally smaller in absolute terms compared to the values of soils that are normally consolidated and/or possibly

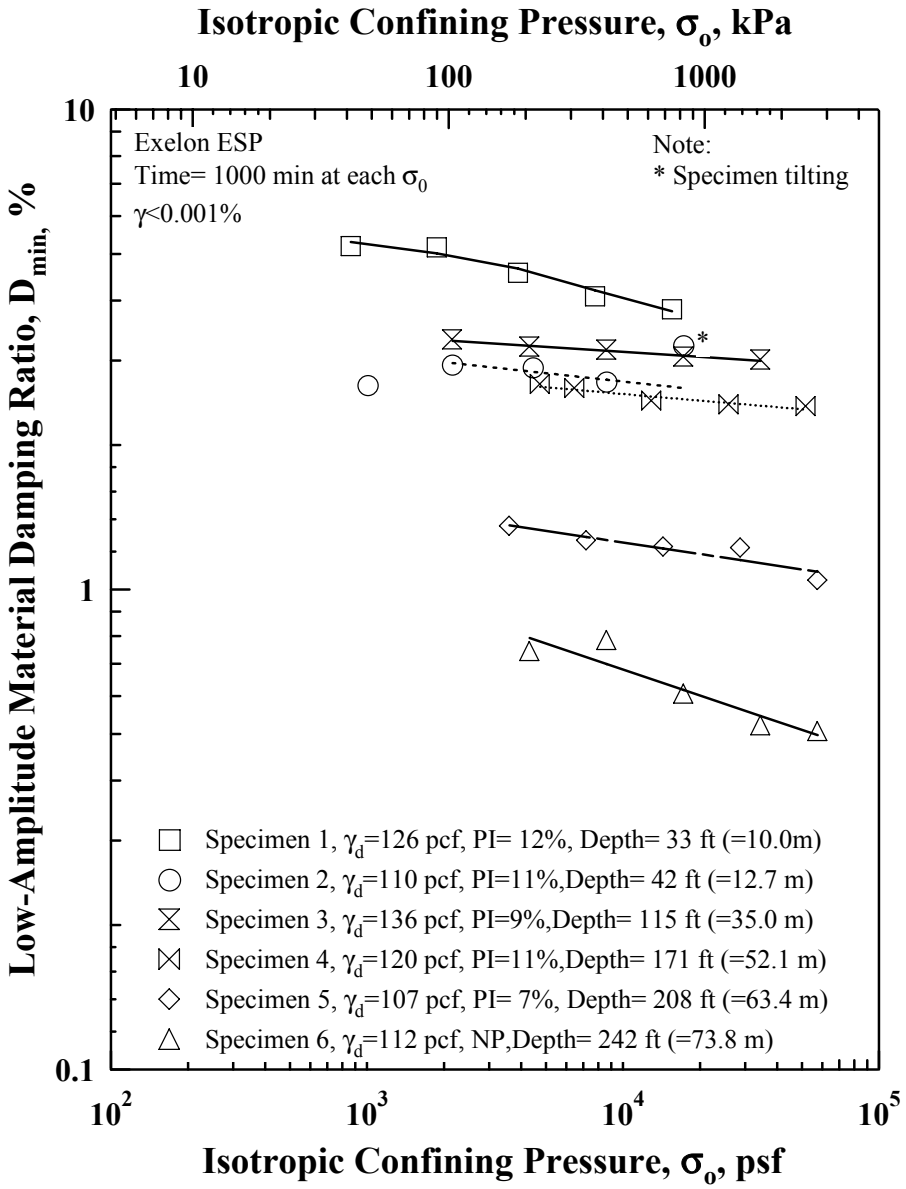

Figure 5 Variation in Low-Amplitude Material Damping Ratio, D_{min}, with Isotropic Confining Pressure of the Six Exelon ESP Specimens Determined from Resonant Column (RC) Tests

disturbed. Specimen No. 2 showed some variability in the log D_{min} – log σ_0 relationship and an increase in D_{min} at the last confining pressure. For this specimen, the confining chamber had to be opened after the fourth confining pressure due to sample tilting, and it is felt that this release and re-application of the pressure caused the damping value to increase at the final pressure. Additionally, it should be noted that, in the experience of the writers, the process of opening the confining chamber and then re-applying the confining pressure can lead to measurable changes in material damping, although it may only affect shear wave velocity and shear modulus marginally.

3.2 Variation of Void Ratio with Confining Pressure

The variations of void ratio, e, with isotropic confining pressure, σ_o, for the six specimens are presented in Figure 6. Normally consolidated or somewhat disturbed specimens exhibit relatively more compressibility under increasing confining pressure levels than overconsolidated specimens. The e – log σ_0 relationships shown in Figure 6 are consistent with the previous discussion.

3.3 Changes in G_{max} and D_{min} with Excitation Frequency

The effect of loading frequency on the small-strain shear modulus, G_{max} ($\gamma = 0.001$ %), of the six specimens is shown in Figure 7. The effect of loading frequency on the small-strain material damping ratio, D_{min} ($\gamma = 0.001$ %), for each specimen is shown in Figure 8. As noted in Section 2, ten cycles of loading were applied at four different frequencies (0.1, 0.5, 1, and 5 Hz) to each specimen. Both, the shear modulus, G_{max}, and the material damping ratio, D_{min}, have been normalized by the values measured in the torsional shear tests at 1 Hz. All measurements were performed at only one σ_o, the estimated in-situ σ_o, with the assumption of K_0 of 1.0.

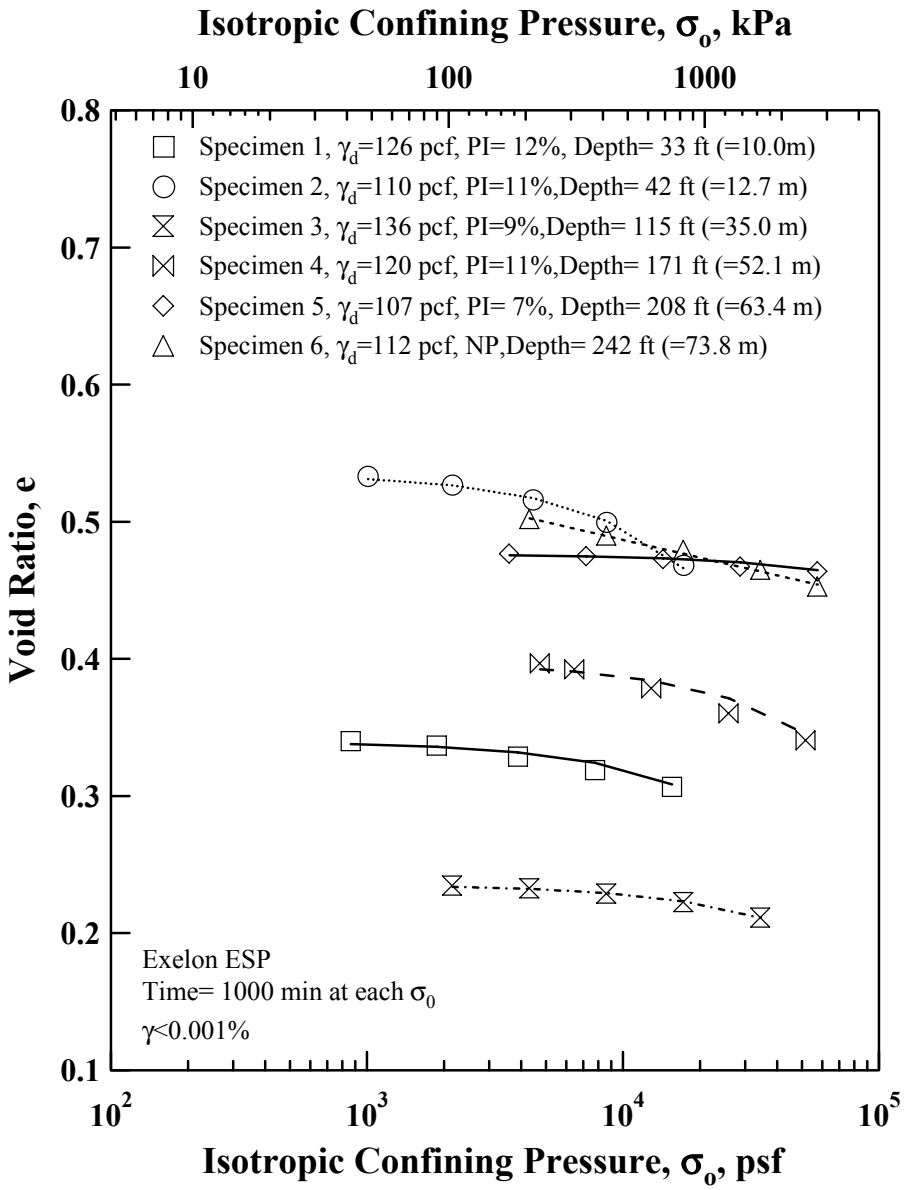

Figure 6 Variation in Void Ratio with Isotropic Confining Pressure of the Six Exelon ESP Specimens Determined during the Resonant Column (RC) Tests

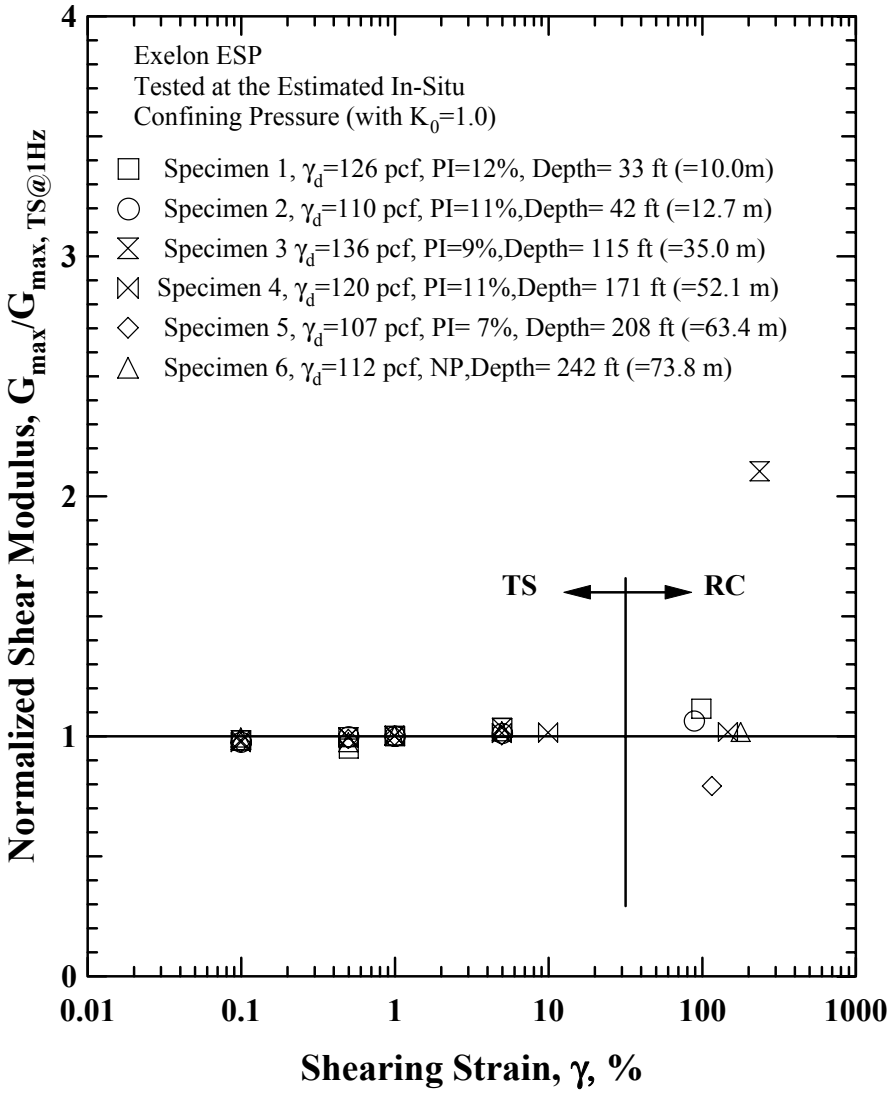

Figure 7 Variation in Normalized Low-Amplitude Shear Modulus with Loading Frequency of the Six Exelon ESP Specimens Determined from Resonant Column (RC) and Torsional Shear (TS) Tests at the Estimated In-Situ Confining Pressures

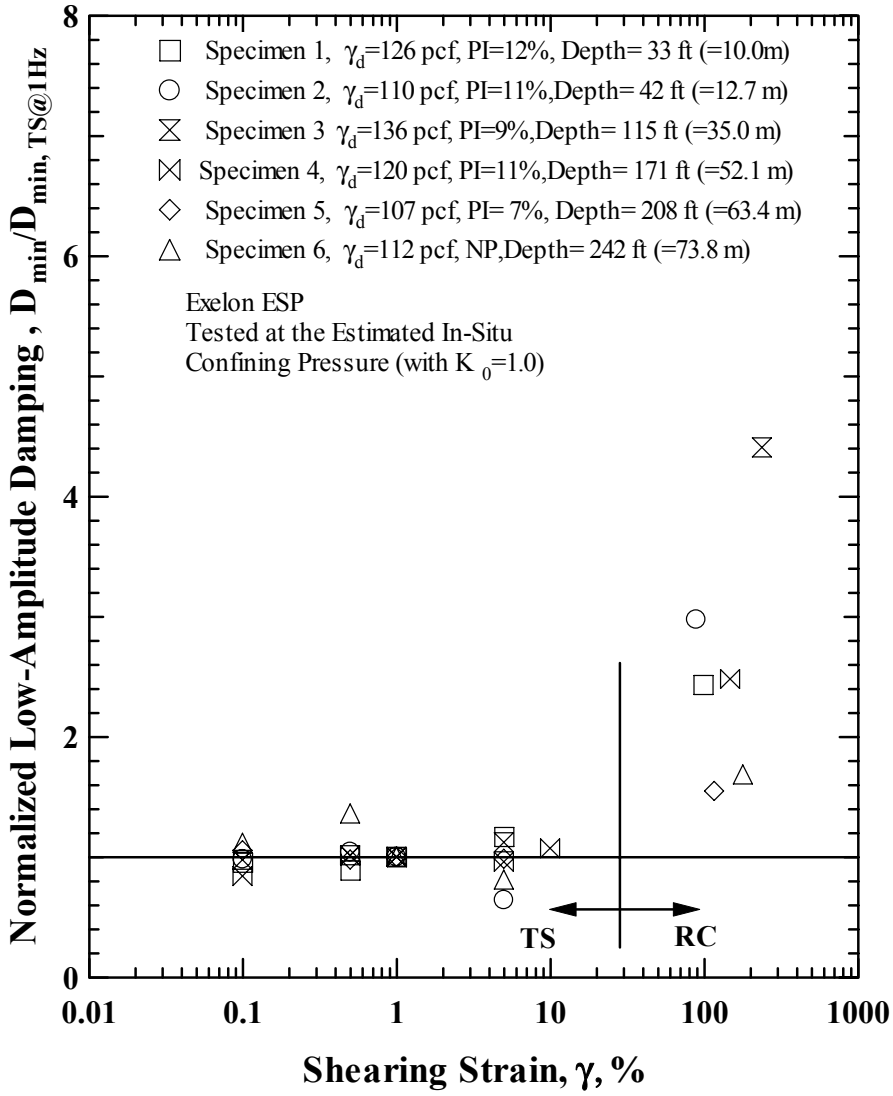

Figure 8 Variation in Normalized Low-Amplitude Material Damping Ratio with Loading Frequency of the Six Exelon ESP Specimens Determined from Resonant Column (RC) and Torsional Shear (TS) Tests at the Estimated In-Situ Confining Pressures

As shown in Figure 7, loading frequency generally had little effect on G_{max}. The shear moduli measured at frequencies around 100 Hz in the RC tests are, on average, only a few percent greater than the values measured at 1 Hz. The average change is about 4% for five of the specimens. The exception is Specimen No. 3. This specimen shows a significant difference between G_{max} obtained from the RC and TS tests. The reason for this difference is unknown.

A much larger effect of loading frequency occurs on D_{min} than on G_{max}. Since the RC test involves measurements at the resonant frequency of the specimen (59 to 264 Hz in these particular tests) and the TS test involves measurements at considerably lower frequencies (0.1 to 5 Hz), the frequency dependency of D_{min} is readily evaluated by combined RC and TS testing. Material damping ratios measured in the resonant column tests range from 1.5 to 4.4 times higher than those measured in the torsional shear tests at 1 Hz. The largest frequency effect was shown by Specimen No. 3.

4 NONLINEAR SHEAR MODULUS AND MATERIAL DAMPING RATIO

4.1 Nonlinear G - log γ Relationships

Results of the G - log γ measurements from the six specimens determined by the RC tests are presented in Figure 9 for measurements at the estimated in-situ confining pressure which ranges from of 3.88 ksf (186 kPa) through 17.28 ksf (828 kPa). As expected, shear moduli exhibit a linear range (where G is constant and equal to G_{max}) followed by a nonlinear range where G decreases with increasing shearing strain. Specimen No. 3 has the largest value of G_{max} even though it is from a depth of only 115 ft (35 m). This specimen is the densest and could be lightly cemented as indicated by the increased stiffness. Specimen No. 6 is from the same borehole as Specimen No. 3 (B-3) but is from a deeper depth. However, Specimen No. 6 has a G_{max} value much a lower than Specimen No. 3. Part of the difference between the specimens results from Specimen No. 6 not retaining the effect of overconsolidation and also possibly from some disturbance.

One point that must be addressed is the highly nonlinear behavior exhibited by Specimen No. 5 that is shown in Figure 9. This specimen exhibits nonlinearity even at shearing strains around $4x10^{-5}$ %. This behavior is atypical of soil and is attributed to disturbance in the specimen. The specimen had numerous, clearly-visible, horizontal partings (cracks). The presence of the horizontal cracks also precluded any trimming of the diameter of the specimen. It is recommended that the nonlinear behavior exhibited by Specimen No. 5 be thrown out as unrepresentative and empirical predictions presented subsequently be used.

A comparison of the G - log γ relationships measured in the RC and TS tests is shown in Figure 10 for Specimen No. 2 and No. 4. Comparisons for the other specimens are shown in the exhibits. Two points are clearly shown in Figure 10. First, similar G – log γ curves are measured in both tests, with the main difference related to the effect of excitation frequency. Second, the RC test can excite the specimens to larger strains because of dynamic amplification which enters the RC test but does not enter the “slow cyclic” TS test. This difference is especially important when testing stiffer specimens.

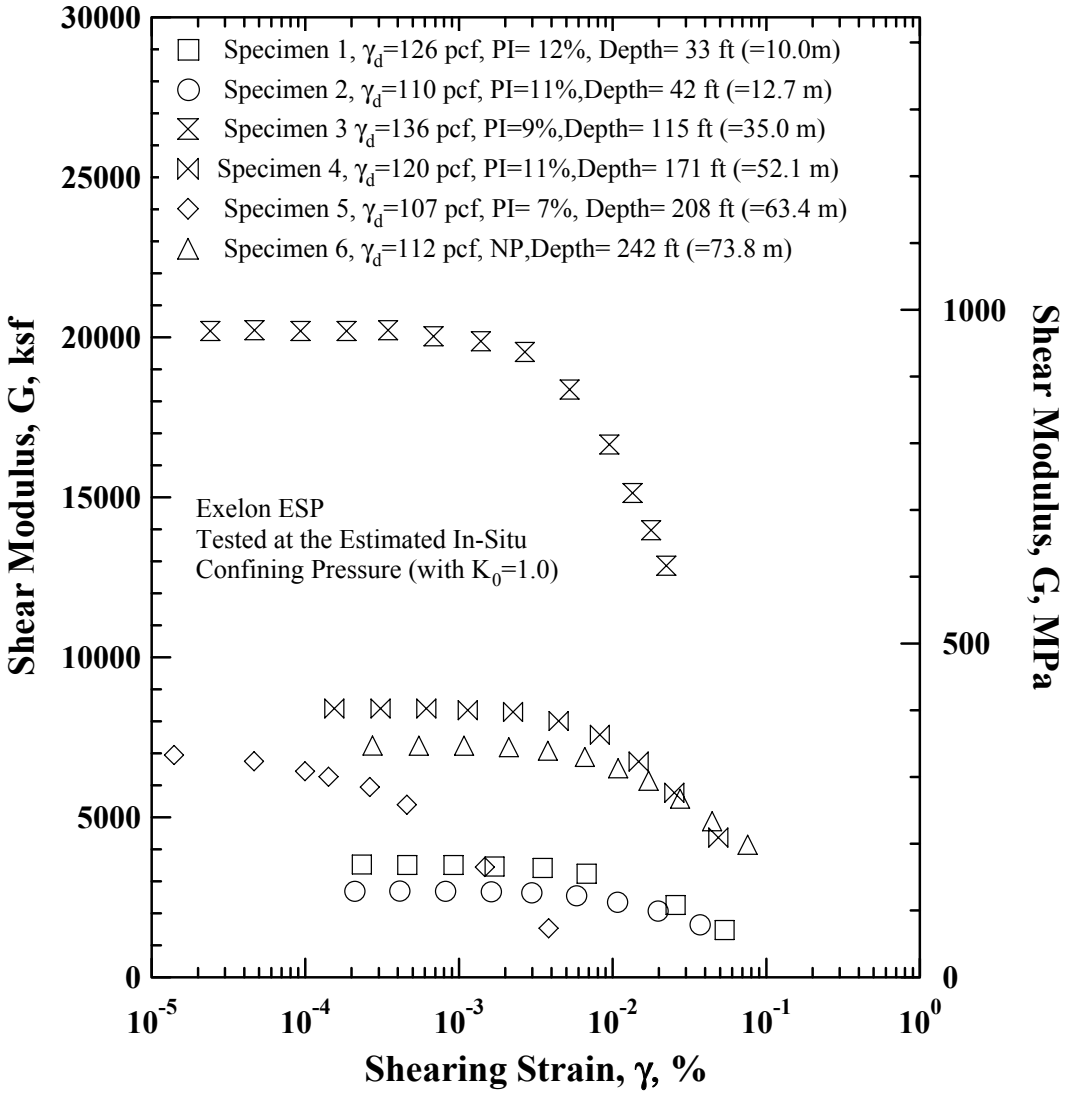

Figure 9 Variation in Shear Modulus with Shearing Strain from Resonant Column (RC) Tests of the Six Exelon ESP Specimens that were Tested at Their Estimated In-Situ Confining Pressures

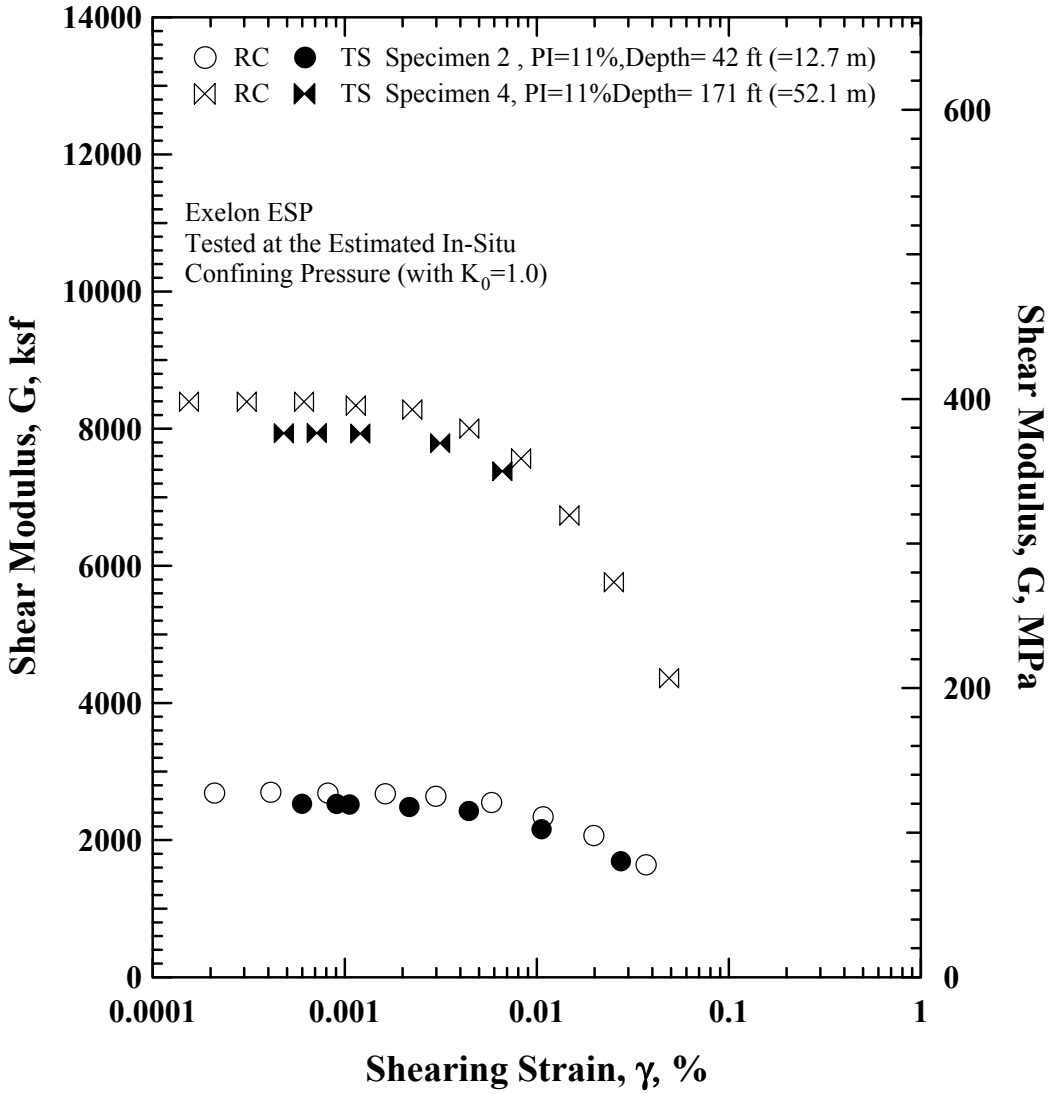

Figure 10 Variation in Shear Modulus with Shearing Strain from Resonant Column (RC) and Torsional Shear (TS) Tests of Specimen No. 2 and Specimen No. 4 that were Tested at Their Estimated In-Situ Confining Pressures

4.2 Nonlinear G/G_{max} - log γ Relationships

The normalized shear modulus reduction relationships (G/G_{max} - log γ) of the six specimens measured in the RC tests are shown in Figure 11. (The TS results are very similar and are not shown for clarity in the figure.) All specimens except Specimen No. 5 show very similar relationships. As noted above, the response of Specimen No. 5 is atypical and occurred because of disturbance (horizontal cracks in the specimen). The G/G_{max} - log γ curves for five of these specimens (Specimen No. 6 is deleted hereafter) are compared with well-known and new empirical relationships below. The new empirical relationship from Darendeli (2001) is also used to predict a G/G_{max} – log γ curve for Specimen No. 5 in Section 4.2.2.

4.2.1 Comparison of Measured G/G_{max} – log γ Relationships with Well-Known Empirical Relationships

Three well-known and widely used G/G_{max} - log γ relationships are:

1. Seed et al. (1986) for sands,
2. Electrical Power Research Institute (EPRI) (1993) for sands, which are also used as generic curves for soils in general, and
3. Vucetic and Dobry (1991) for soils with plasticity.

Comparisons of the measured G/G_{max}- log γ relationships with these empirical relationships are presented as follows.

1. First, the G/G_{max} – log γ curve of Specimen No. 6, the nonplastic silt (ML), is compared with the Seed et al. (1986) sand curves in Figure 12. In this case, Specimen No. 6 exhibits more linearity than the sand curves, partly due to the increased confining pressure at which the specimen was tested. (The normalized modulus reduction curves measured with the other specimens are not compared with the Seed et al curves because the other specimens have plasticity.)

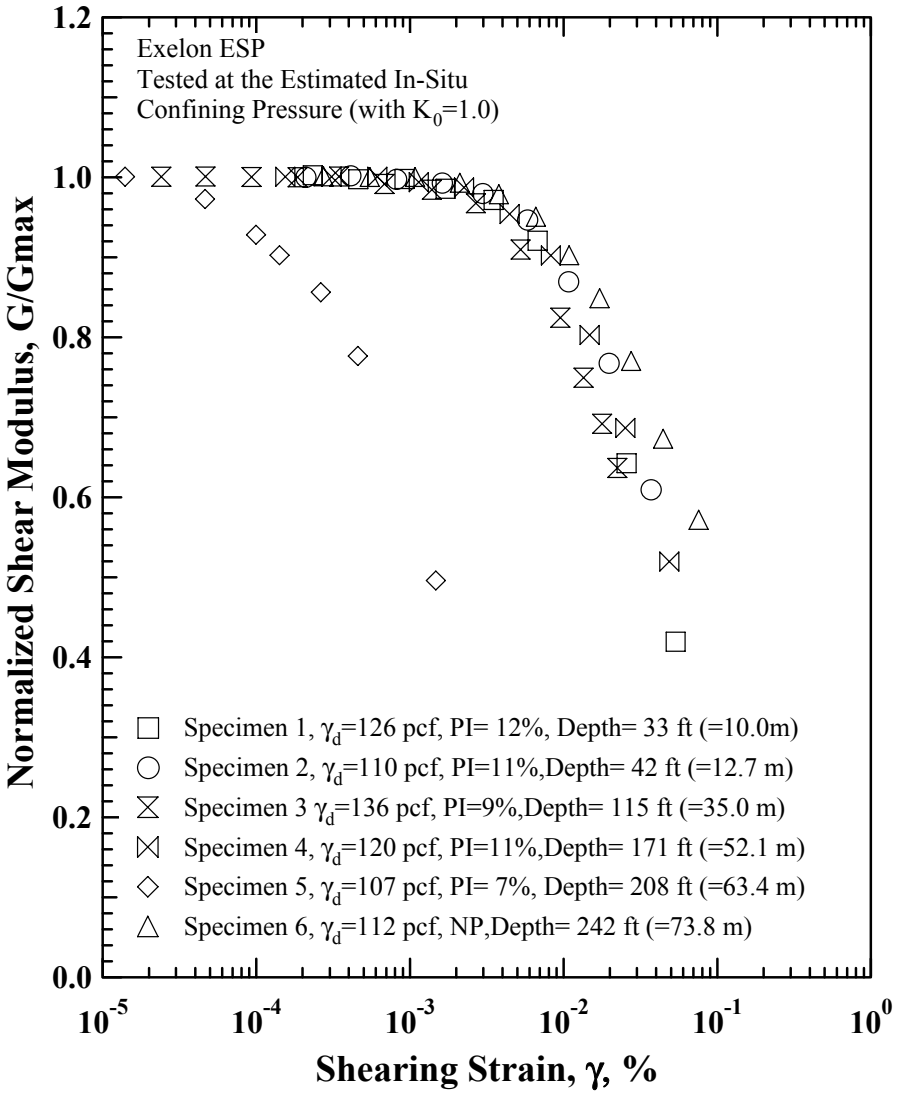

Figure 11 Variation in Normalized Shear Modulus with Shearing Strain from Resonant Column (RC) Tests of the Six Exelon ESP Specimens that were Tested at Their Estimated In-Situ Confining Pressures

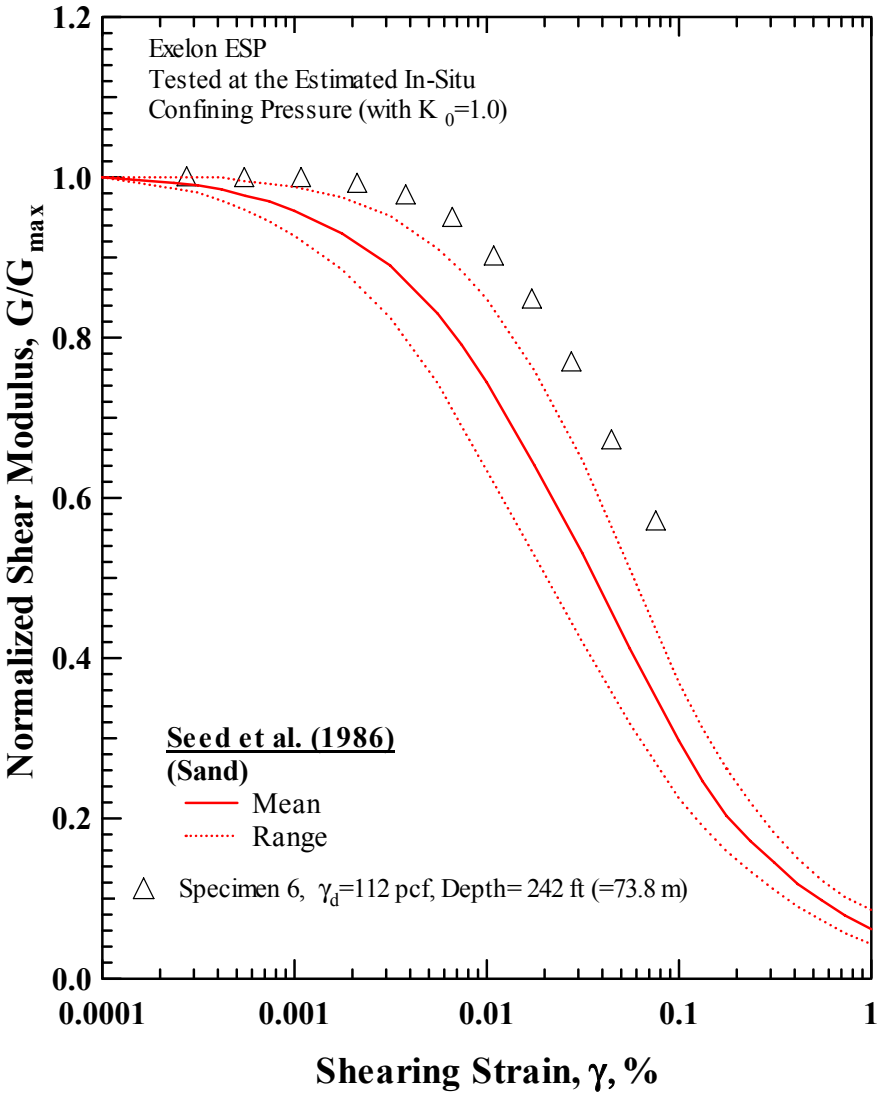

Figure 12 Comparison of the Seed et al. 1986 Sand Curves with the Variation in Normalized Shear Modulus with Shearing Strain from Resonant Column (RC) Tests of Specimen No. 6 that was Tested at Its Estimated In-Situ Confining Pressure

2. Next, the measured responses of the five specimens are compared with the EPRI (1993) curves. These comparisons are presented in Figures 13, 14 and 15 for Specimen Nos. 1 and 2, Specimen Nos. 3 and 4, and Specimen No. 6, respectively. The EPRI curves are used in this case as generic curves and not simply curves for sands. In general, these specimens exhibit nonlinear curves that are typically within one or two steps of the curves predicted for the specimen depth. This comparison is good and is helped by the fact that the highest PI value is 12 %. If, for example, a soil with a PI = 50 % was tested from a depth of 250 ft (76 m), the measured curve would be shifted significantly to higher strains (to the right in each figure).
3. Finally, the G/G_{max} – log γ relationships of the specimens are compared with the relationships suggested by Vucetic and Dobry (1991) in Figures 16, 17 and 18 for Specimen Nos. 1 and 2, Specimen Nos. 3 and 4, and Specimen No. 6, respectively. In this case, the specimens compare quite well with the curves predicted by the Vucetic and Dobry relationships for soils with a PI in the range of 0 to 30 %. The exception is Specimen No. 6 which exhibits more linearity than the Vucetic and Dobry curve for PI = 0 %, partly due to the increased confining pressure at which the specimen was tested.

4.2.2 Comparison with New G/G_{max} – log γ Relationships

In 2001, Mehmet Darendeli proposed a modified version of the hyperbolic equation originally recommended by Hardin and Drnevich (1972) to model the G/G_{max} – log γ relationship of soils. Darendeli's equation can be expressed as:

$$\frac{G}{G_{max}} = \frac{1}{1+\left(\frac{\gamma}{\gamma_r}\right)^a} \tag{4}$$

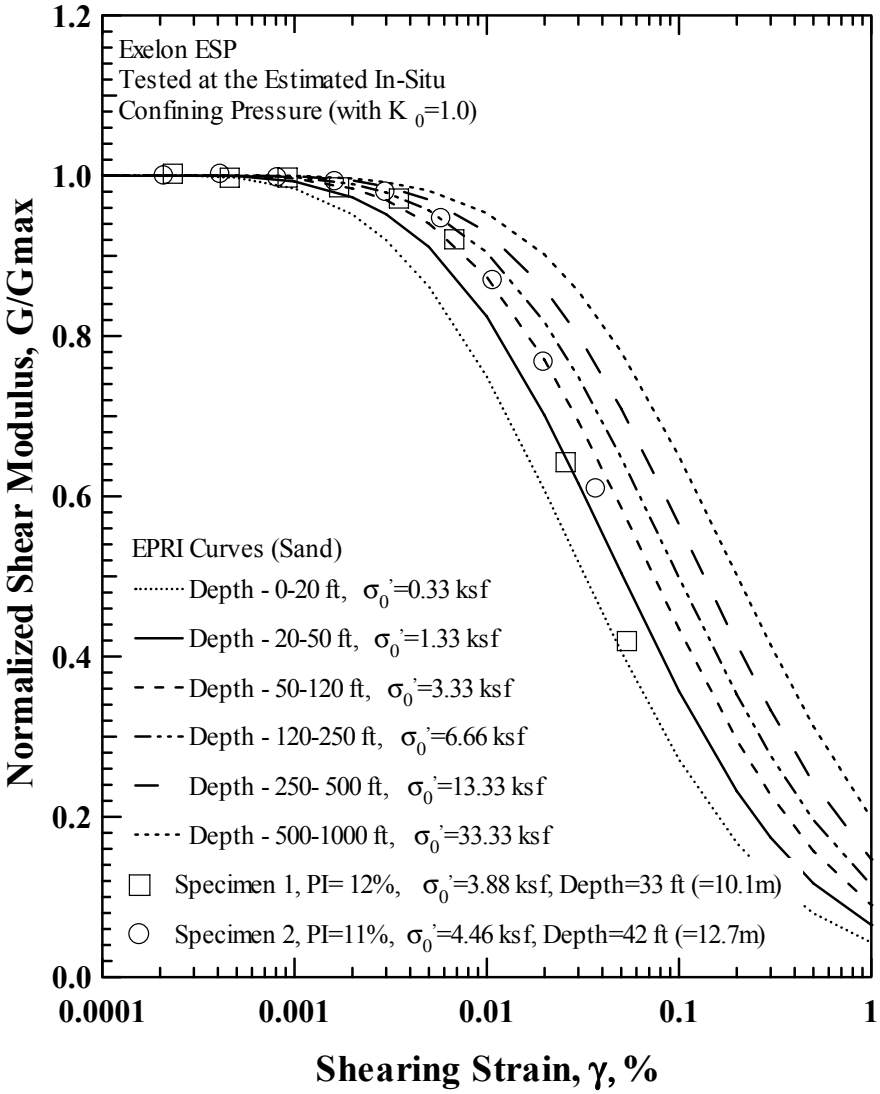

Figure 13 Comparison of the EPRI (1993) Curves with the Variation in Normalized Shear Modulus with Shearing Strain from Resonant Column (RC) Tests of Specimen No. 1 and Specimen No. 2 that were Tested at Their Estimated In-Situ Confining Pressures

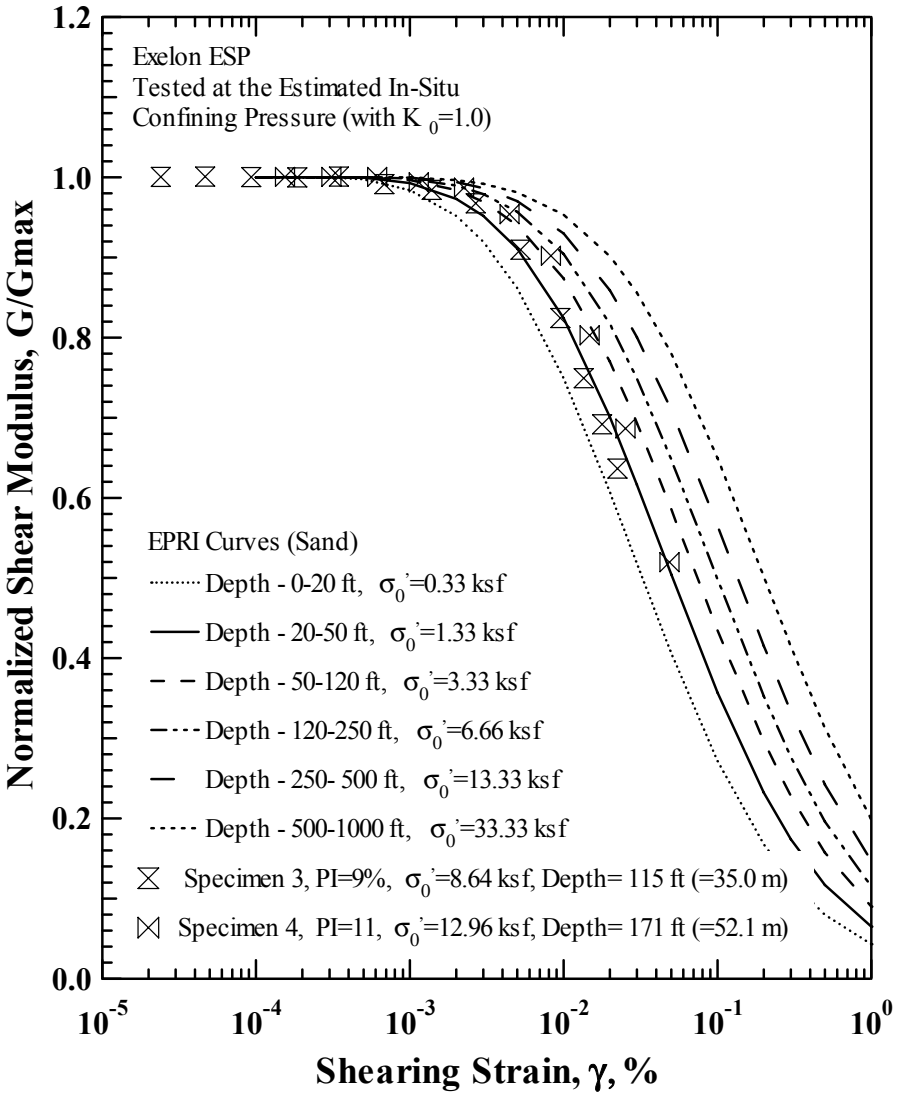

Figure 14 Comparison of the EPRI (1993) Curves with the Variation in Normalized Shear Modulus with Shearing Strain from Resonant Column (RC) Tests of the Specimen No. 3 and Specimen No. 4 that were Tested at Their Estimated In-Situ Confining Pressures

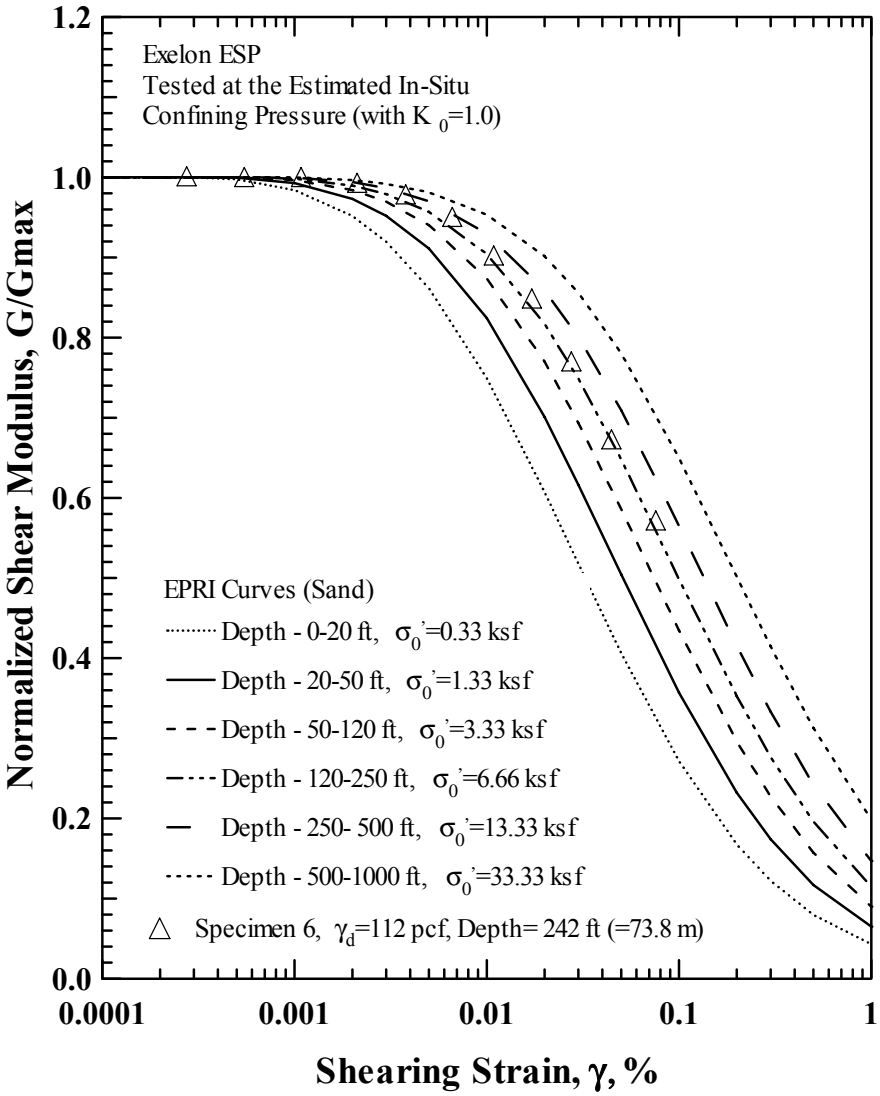

Figure 15 Comparison of the EPRI (1993) Curves with the Variation in Normalized Shear Modulus with Shearing Strain from Resonant Column (RC) Tests of Specimen No. 6 that was Tested at Its Estimated In-Situ Confining Pressure

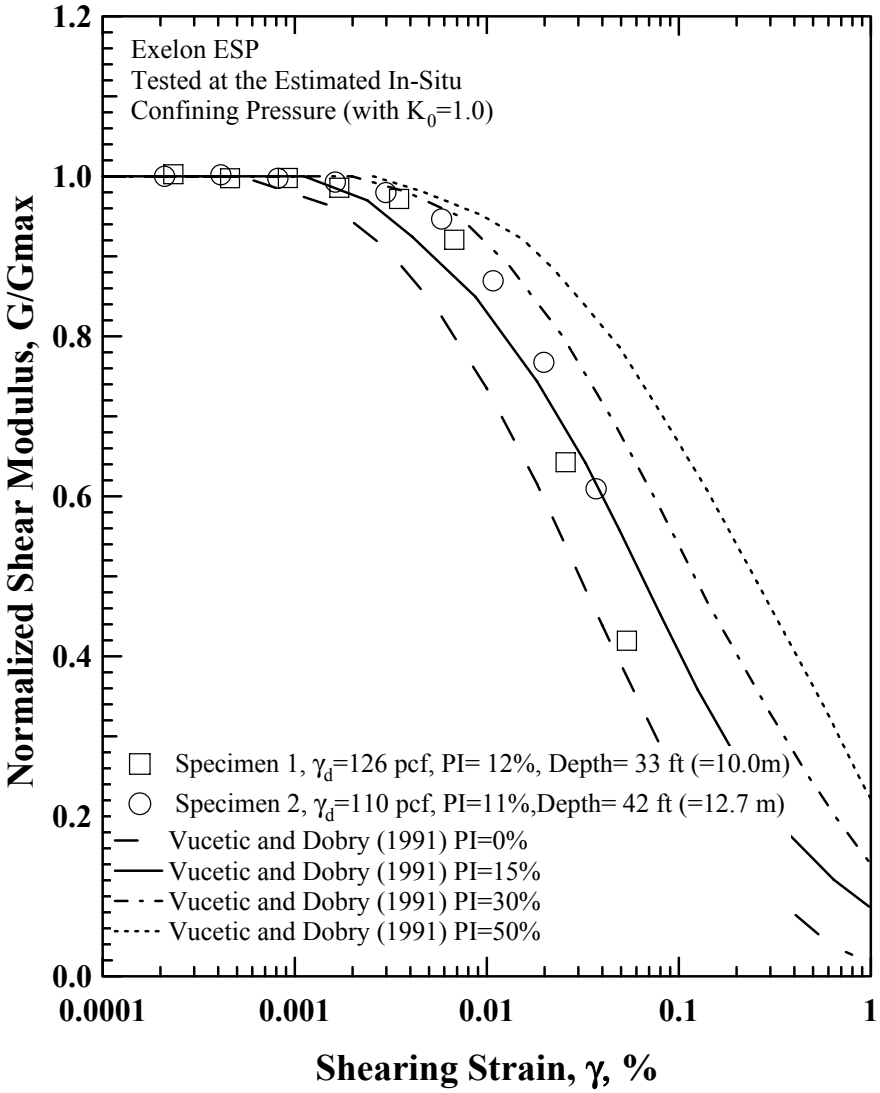

Figure 16 Comparison of the Vucetic and Dobry (1991) Curves with the Variation in Normalized Shear Modulus with Shearing Strain from Resonant Column (RC) Tests of Specimen No. 1 and Specimen No. 2 that were Tested at Their Estimated In-Situ Confining Pressures

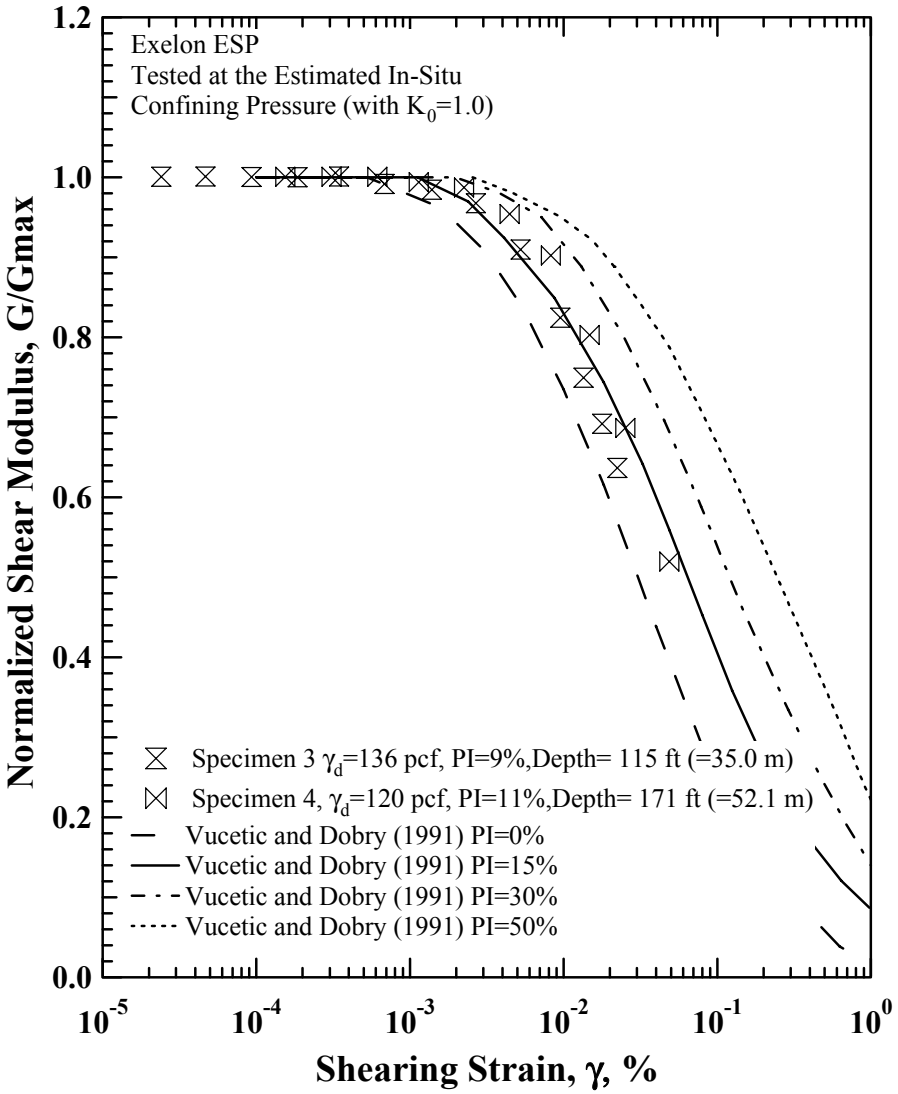

Figure 17 Comparison of the Vucetic and Dobry (1991) Curves with the Variation in Normalized Shear Modulus with Shearing Strain from Resonant Column (RC) Tests of Specimen No. 3 and Specimen No. 4 that were Tested at Their Estimated In-Situ Confining Pressures

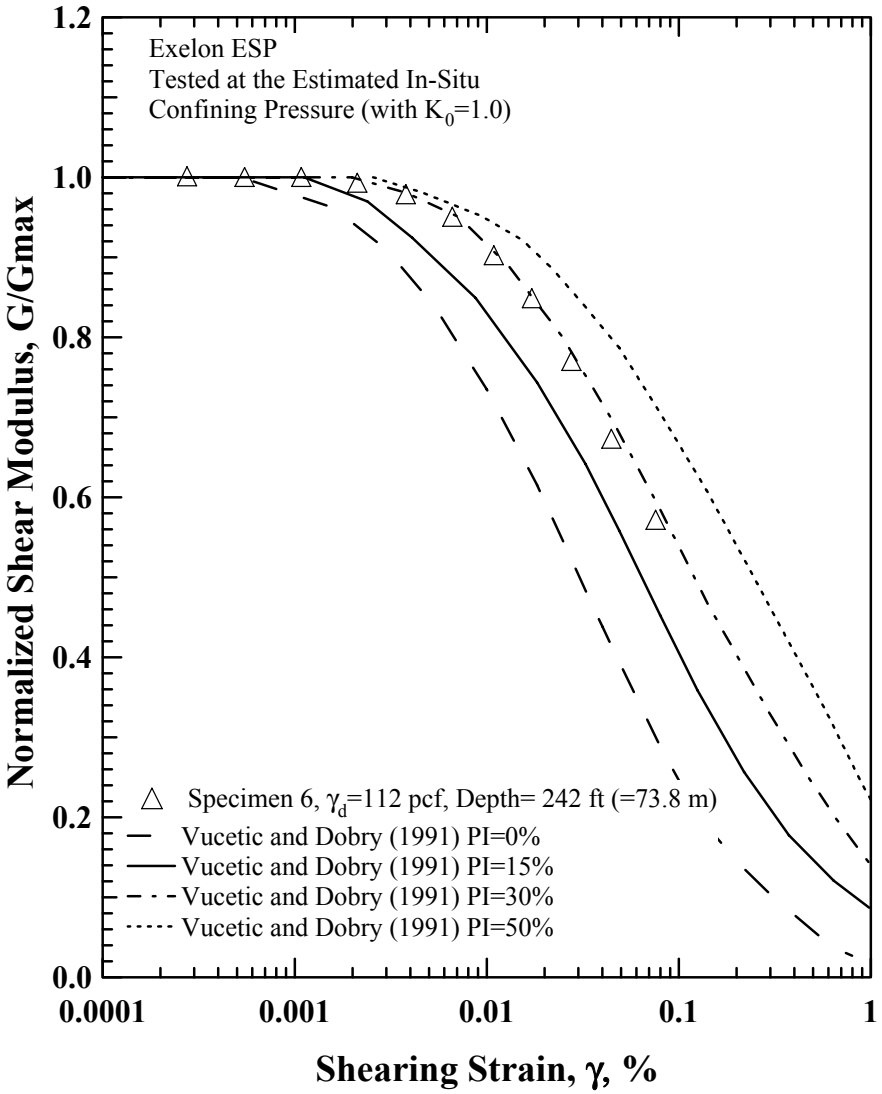

Figure 18 Comparison of the Vucetic and Dobry (1991) Curves with the Variation in Normalized Shear Modulus with Shearing Strain from Resonant Column (RC) Tests of Specimen No. 6 that was Tested at Its Estimated In-Situ Confining Pressure

in which γ = any given shearing strain,

γ_r = the reference shearing strain, and

a = dimensionless exponent.

The reference strain, γ_r, is used simply for curve fitting purposes in Darendeli's model and is defined as the value of γ equal to the shearing strain at which G/G_{max} equals 0.5. (This definition of γ_r is different from the one proposed by Hardin and Drnevich, 1972.) The reference strain is denoted as $\gamma_{r,G}$ hereafter. Values of $\gamma_{r,G}$ determined from the measured G/G_{max} – log γ curves for five of the six specimens (excluding Specimen No. 6) are listed in Table 5.

In this nonlinear model, Darendeli also developed empirical equations to estimate the values of $\gamma_{r,G}$ and a. These equations are:

$$\gamma_{r,G} = (\phi_1 + \phi_2 * PI * OCR^{\phi 3}) + \sigma_0'^{\,\phi 4} \quad (5)$$

$$a = \phi_5 \quad (6)$$

in which

σ_o' = mean effective confining pressure (atm),

PI = soil plasticity (%),

OCR = overconsolidation ratio,

ϕ_1 = 0.0352,

ϕ_2 = 0.0010,

ϕ_3 = 0.3246,

ϕ_4 = 0.3483, and

ϕ_5 = 0.9190.

As shown above, the input parameters required in Equations 5 and 6 are σ_0', PI and OCR. The values for these parameters for all six test specimens are listed in Table 6 (using σ_0 for σ_0').

Comparisons between "average" curves predicted by Darendeli's (2001) model and the measured G/G_{max} – log γ curves are presented in: (1) Figure 19 for Specimen Nos. 1 and 2, (2) Figure 20 for Specimen Nos. 3 and 4 and (3) Figure 21 for Specimen No. 6. ("Average" curves are determined using the average values (or single value for Specimen No. 6) of σ_0, PI, and OCR of the specimens in each set.) Darendeli's model also includes the

Table 5 Reference Strain ($\gamma_{r,G}$) Values Determined from the G/G_{max}-log γ Curves Measured at the In- Situ Confining Pressures

Specimen No.	UT Specimen ID	Specimen Depth ft (m)	Plasticity Index %	Confining Pressure ksf (kPa)	Reference Strain γ_r, %
1	UTA-34-A	33 (10.06)	12	3.88 (186)	0.045
2	UTA-34-B	42 (12.65)	11	4.46 (214)	0.06
3	UTA-34-D	115 (35.05)	9	8.64 (414)	0.04
4	UTA-34-C	171 (52.12)	11	12.96 (621)	0.05
6	UTA-34-F	242 (73.76)	NP	17.28 (828)	0.10

Table 6 Input Parameters Used in Equations (5) and (6) to Predict Nonlinear Behavior of the Six Specimens Using Darendeli's (2001) Model.

Spec. No.	Specimen ID	Borehole No.	Specimen Depth ft (m)	Soil Type (Unified Soil Classification)	Plasticity Index %	Estimated OCR	Estimated In-Situ Pressure ksf (atm)
1	UTA-34-A	B-2 (S-7)	33 (10.06)	Sandy Lean Clay (CL)	12	2	3.88(1.93)
2	UTA-34-B	B-3 (S-13)	42 (12.65)	Sandy Lean Clay (CL)	11	~1.5	4.46 (2.22)
3	UTA-34-D	B-3 (S-33)	115 (35.05)	Sandy Lean Clay (CL)	9	>8[2]	8.64 (4.30)
4	UTA-34-C	B-3 (S-42)	171 (52.12)	Sandy Lean Clay (CL)	11	2	12.96 (6.45)
5	UTA-34-E	B-3 (S-47)	208 (63.40)	Silty Clay (CL-ML)	7	>8[2]	14.40 (7.16)
6	UTA-34-F	B-2 (S-38)	242 (73.76)	Silt (ML)	NP[1]	–[3]	17.28 (8.60)

Notes: 1. NP = Nonplastic
2. No break in log G_{max} – log σ_0 curve because highly overconsolidated and/or cemented; assume OCR = 8
3. No break in log G_{max} – log σ_0 curve because sample did not retain stress history of site; assume OCR = 2

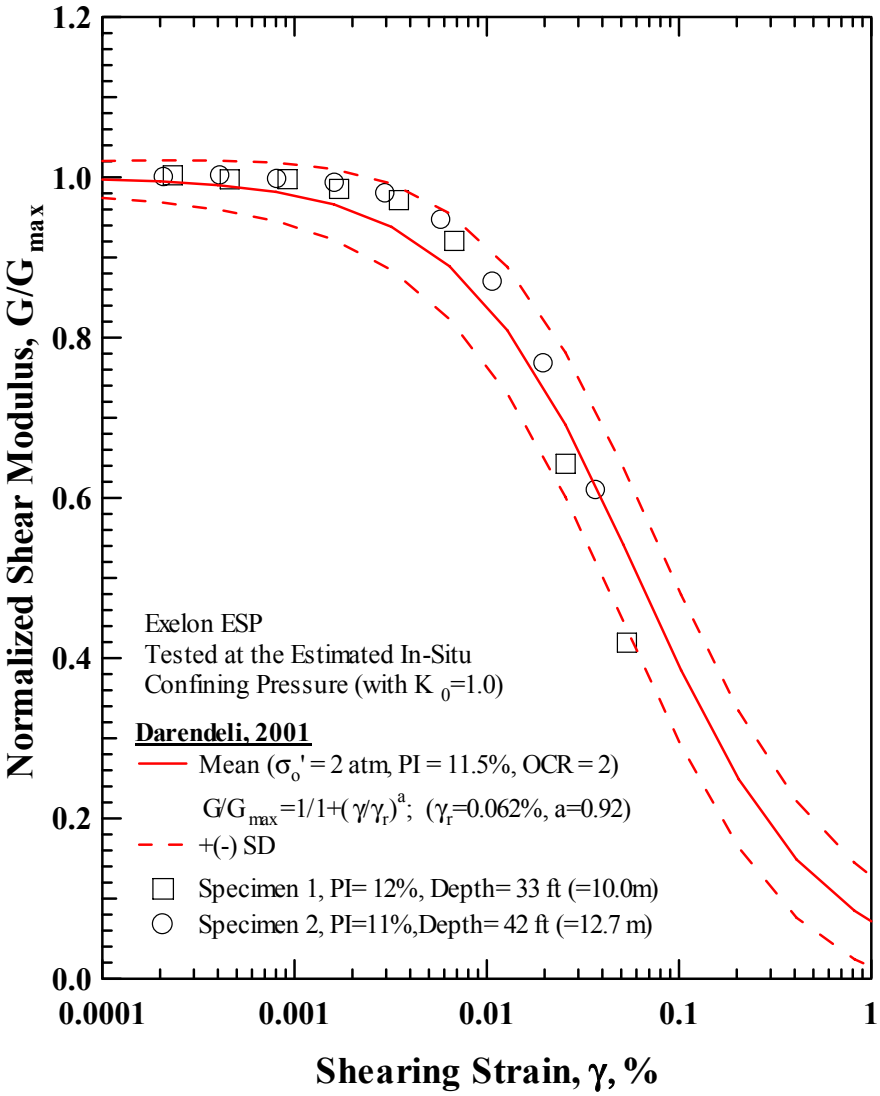

Figure 19 Comparison of the Average Nonlinear Curve Predicted by Darendeli (2001) with the Variations in Normalized Shear Modulus with Shearing Strain from Resonant Column (RC) Tests of Specimen No. 1 and Specimen No. 2 that were Tested at Their Estimated In-Situ Confining Pressures

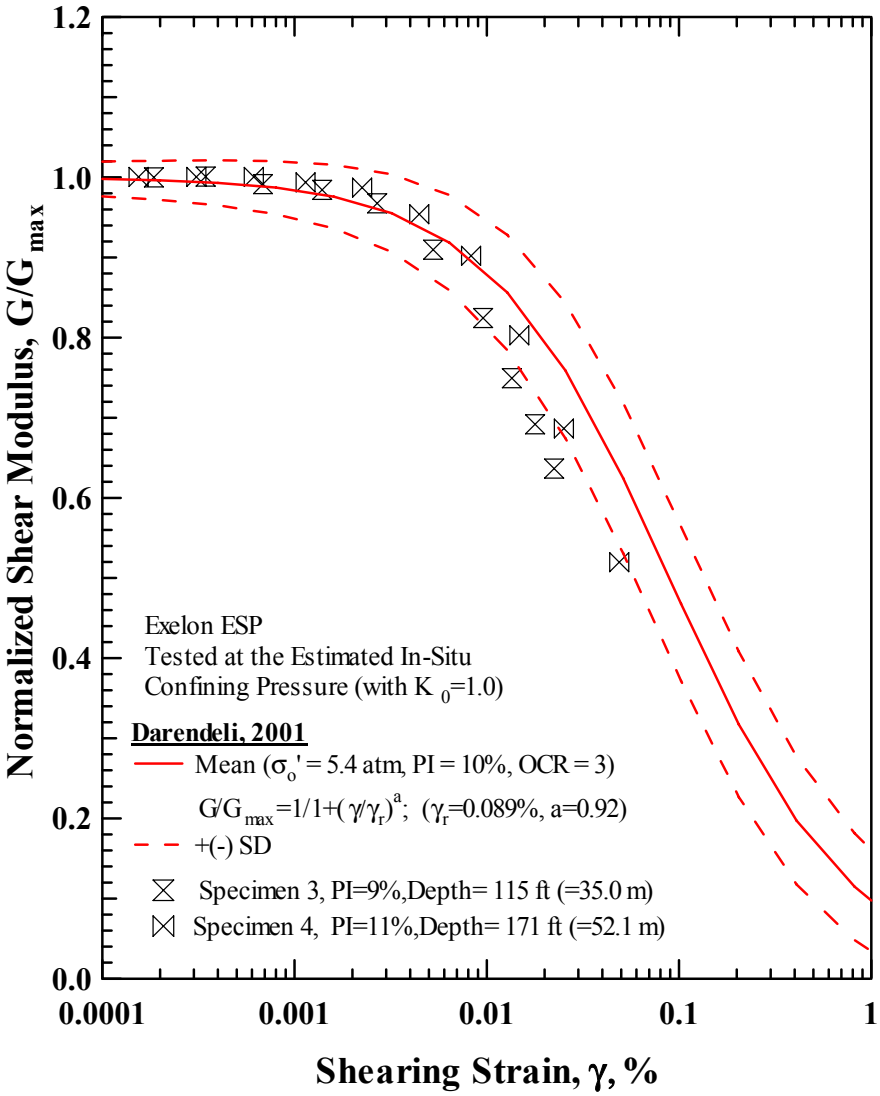

Figure 20 Comparison of the Average Nonlinear Curve Predicted by Darendeli (2001) with the Variations in Normalized Shear Modulus with Shearing Strain from Resonant Column (RC) Tests of Specimen No. 3 and Specimen No. 4 that were Tested at Their Estimated In-Situ Confining Pressures

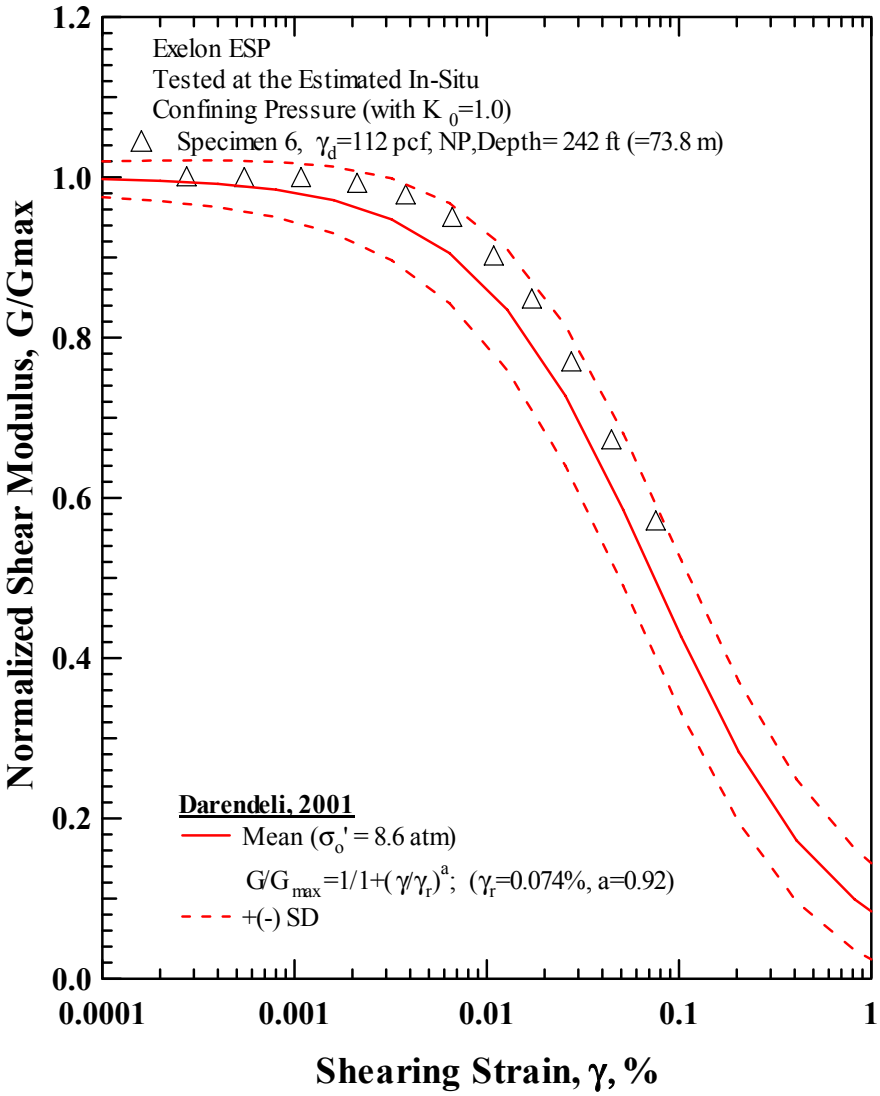

Figure 21 Comparison of the Nonlinear Curve Predicted by Darendeli (2001) with the Variation in Normalized Shear Modulus with Shearing Strain from Resonant Column (RC) Tests of Specimen No. 6 that was Tested at Its Estimated In-Situ Confining Pressure

variation to be expected in the normalized modulus degradation curves in terms of plus or minus one standard deviation, +/– σ. This range is also shown in each figure. As stated above, the term "average curve" or "average trend" is used in Figures 19 and 20 because the average values for the set of two specimens were used in the calculation of each empirical curve. The average values are noted in each figure.

It is also possible to generate a recommended G/G_{max} – log γ curve for Specimen No. 5 using Darendeli's model. The recommended curve (using the parameters in Table 6) is shown in Figure 22. As shown by the favorable comparisons between measured and predicted curves in Figures 19, 20 and 21, this curve is considered to be a good prediction. The nonlinear laboratory data for Specimen No. 5 that have been called atypical and have been deleted are shown in Figure 22 simply to illustrate how atypical they are.

4.3 D - log γ Relationships

Results of the D - log γ measurements from the six specimens that were determined by the RC tests are presented in Figure 23. As expected, material damping ratios exhibit a linear range (where D is constant and equal to D_{min}) followed by a nonlinear range where D increases with increasing shearing strain. There is a generalized trend for Specimen Nos. 1 through 4 of deeper specimens exhibiting lower values of low-amplitude material damping ratio, D_{min}. Specimen No. 5, the significantly disturbed specimen, exhibits an atypical response just as found for the G – log γ and G/G_{max} - log γ relationships. Specimen No. 5 is only considered hereafter in terms of an empirically predicted D – log γ curve. Also, Specimen No. 6 exhibits the lowest values of D (over the strain range tested) due to the high confining pressure and its nonplastic nature.

Comparison of the D - log γ relationships measured in the RC and TS tests for Specimen Nos. 2 and No. 4 are shown in Figure 24. Comparisons for the other specimens are shown in the exhibits. Two points are clearly shown in this figure. First, reasonably similar D – log γ curves are measured in both tests, with the main difference related to the effect of excitation frequency and possibly to the number of cycles of loading at strains above about 0.005 %. Also, the effect of excitation frequency is more important for D_{min} than it is

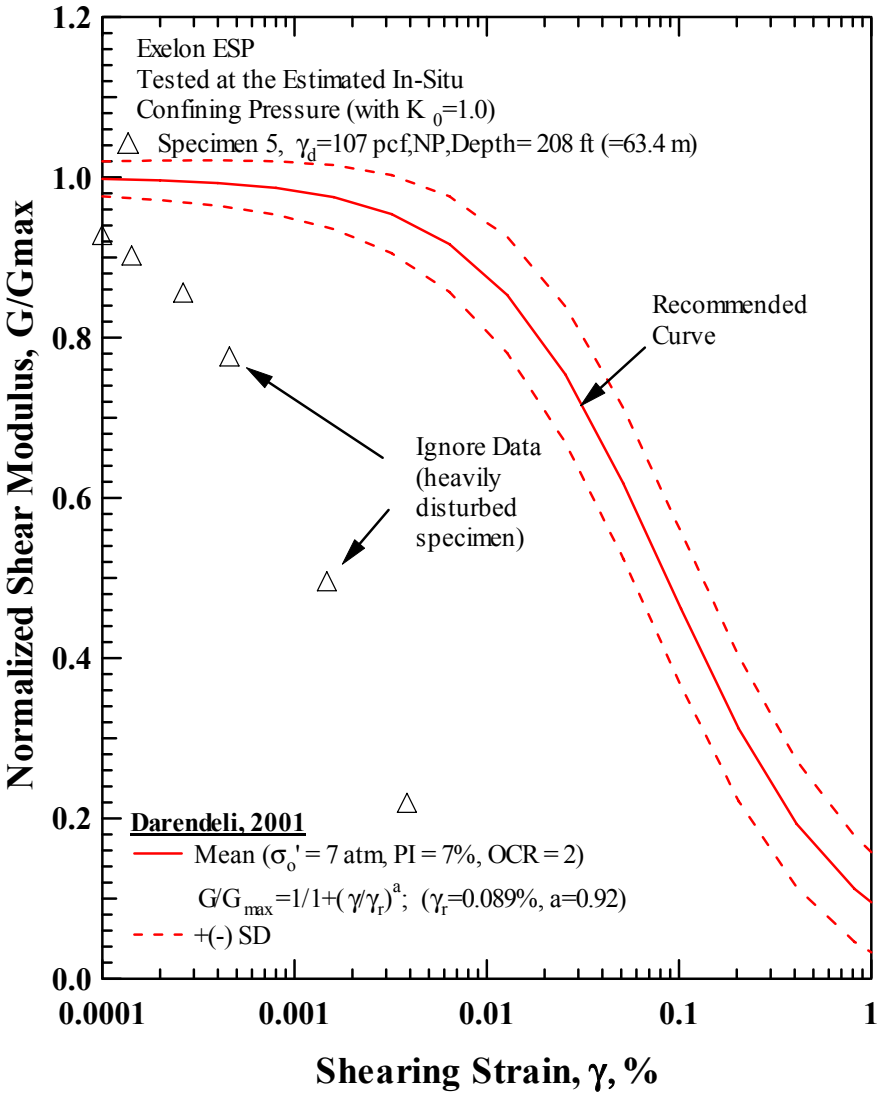

Figure 22 Recommended Variation in the Normalized Shear Modulus with Shearing Strain for Specimen No. 5 Based on Darendeli (2001)

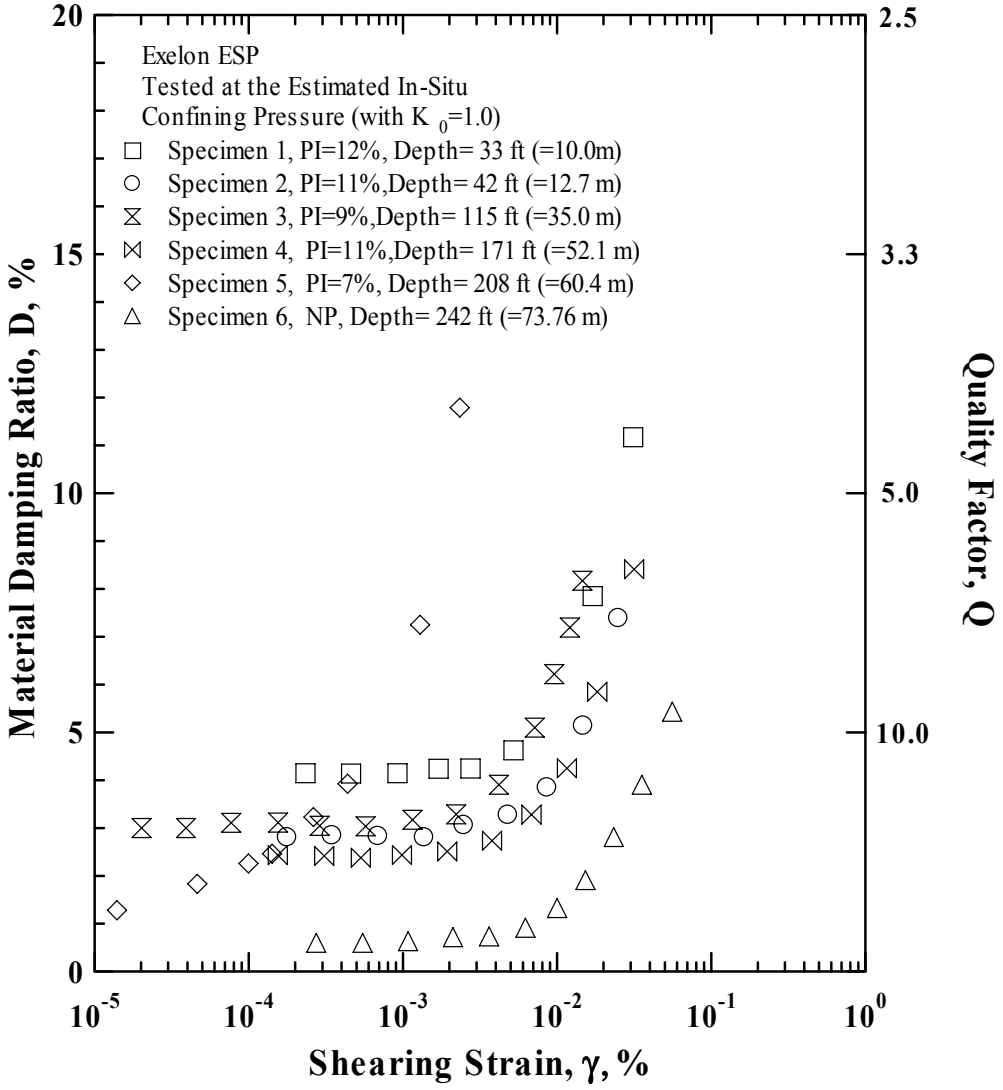

Figure 23 Variation in Material Damping Ratio with Shearing Strain from Resonant Column (RC) Tests of the Six Specimens of the Exelon ESP Project that were Tested at Their Estimated In-Situ Confining Pressures

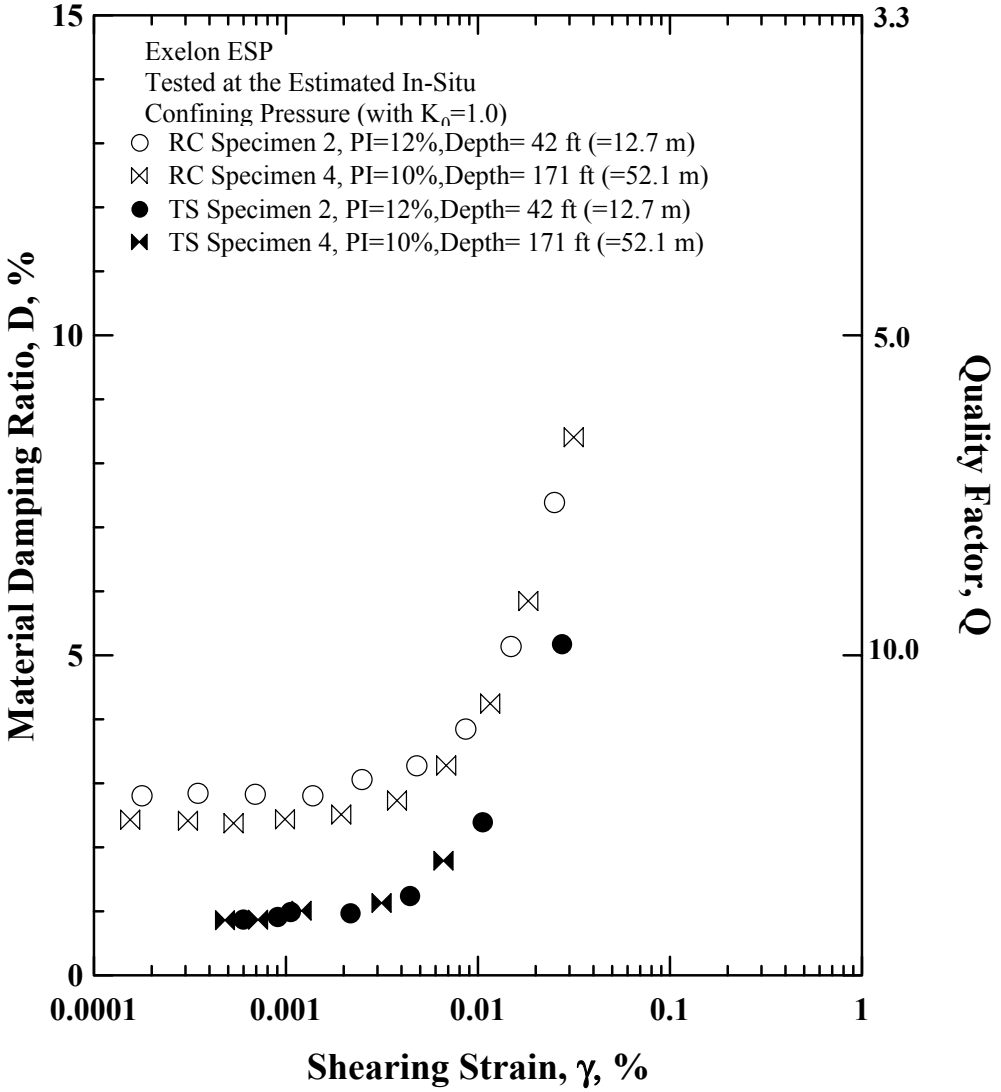

Figure 24 Comparison of the Variation in Material Damping Ratio with Shearing Strain from Resonant Column (RC) and Torsional Shear (TS) Tests of Specimen No. 2 and Specimen No. 4 that were Tested at Their Estimated In-Situ Confining Pressures

for G_{max} as discussed previously. Second, the RC test can excite the specimens to larger strains because of dynamic amplification which enters the RC test but does not enter the "slow cyclic" TS test as discussed previously.

4.3.1 Comparison of Measured D-log γ Relationships with Well-Known Empirical Relationships

Just as done with the G/G_{max} – log γ curves, the measured D – log γ curves are compared with the same three well-known and widely used D – log γ relationships. These relationships are:

1. Seed et al. (1986) for sands,
2. Electrical Power Research Institute (EPRI) (1993) for sands, which are also used as generic curves for soils in general, and
3. Vucetic and Dobry (1991) for soils with plasticity.

Also, it should be noted that the comparisons presented below only use the D – log γ relationships measured in the TS tests, except for Specimen No. 6 in which the RC results are also included. The TS test results are used so that excitation frequency and number of cycles of loading do not enter the comparisons in the four CL specimens.

1. First, the D – log γ curves of Specimen No. 6, the nonplastic silt (ML), are compared with the Seed et al. (1986) sand curves in Figure 26. In this case, the ML specimen exhibits considerably more linearity than the sand curves, partly due to the increased confining pressure at which this specimen was tested. Also, frequency and number of cycles has a small effect on the RC test results so they have been included.
2. Next, the measured responses of the five specimens are compared with the EPRI (1993) curves in Figures 27, 28 and 29 for Specimen Nos. 1 and 2, Specimen Nos. 3 and 4 , and Specimen No. 6, respectively. In this case, these specimens exhibit nonlinear curves that are within one or two steps of the curves predicted for the specimen depth (just as seen in the G/G_{max} – log γ comparisons).

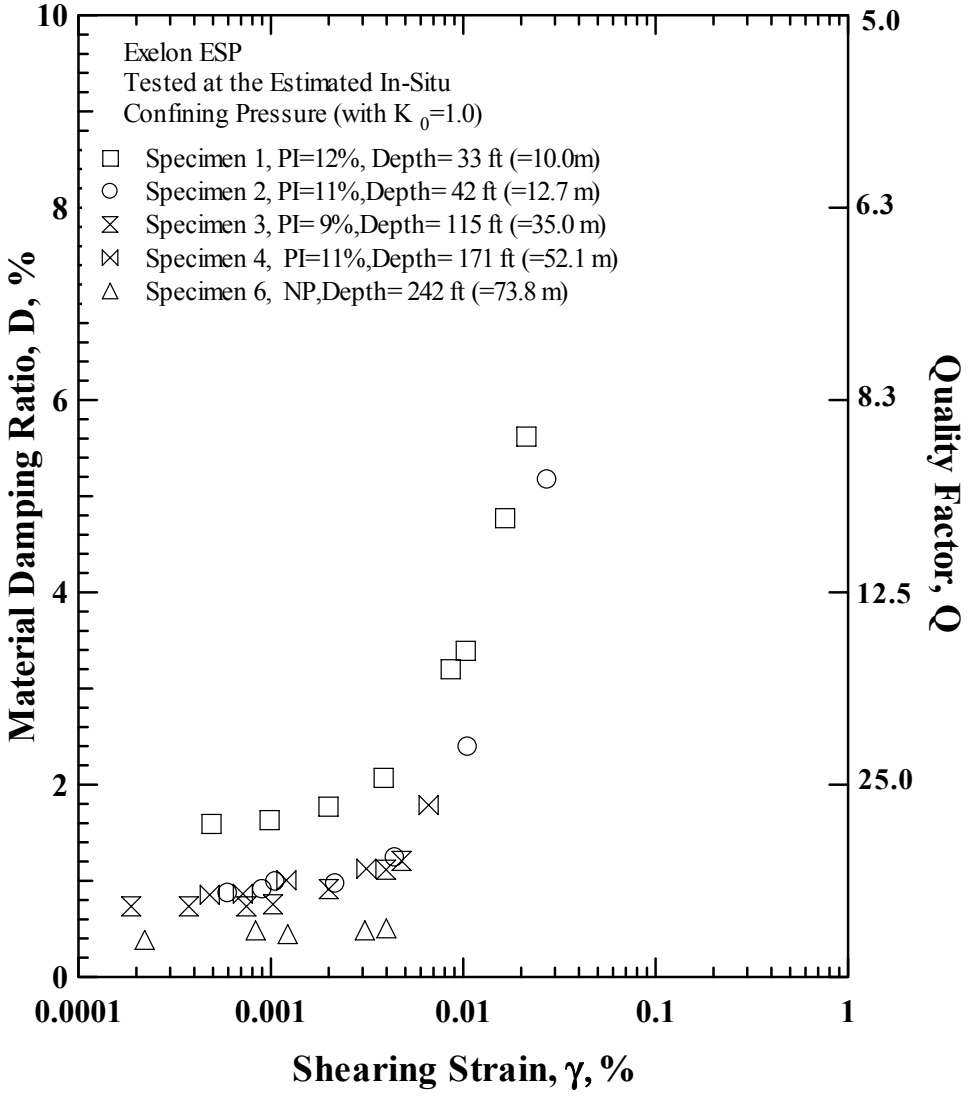

Figure 25 Variation in Material Damping Ratio with Shearing Strain from Torsional Shear (TS) Tests of Five Specimens from the Exelon ESP Project that were Tested at Their Estimated In-Situ Confining Pressures

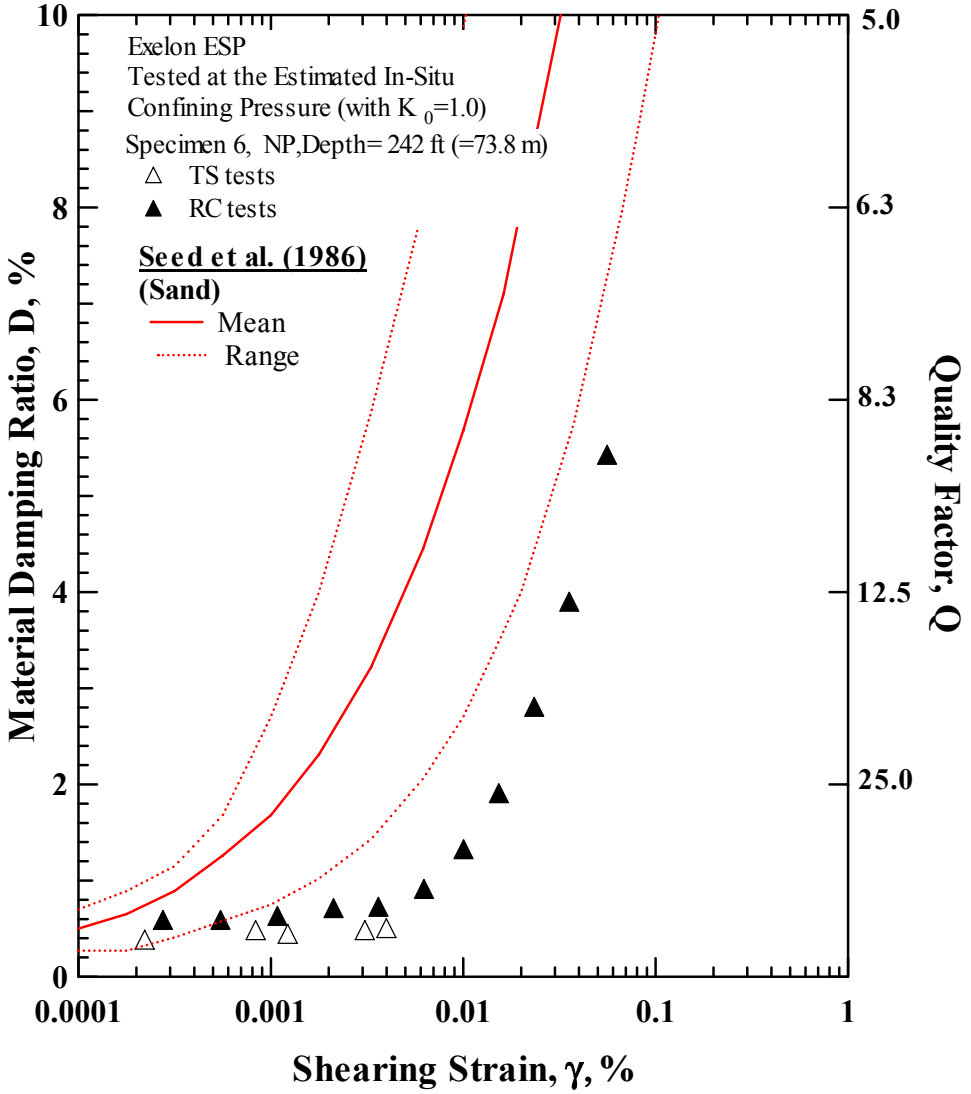

Figure 26 Comparison of the Seed et al. (1998) Sand Curves with the Variations in Material Damping Ratios with Shearing Strain from Resonant Column (RC) and Torsional Shear (TS) Tests of Specimens No. 6 that was Tested at Its Estimated In-Situ Confining Pressure

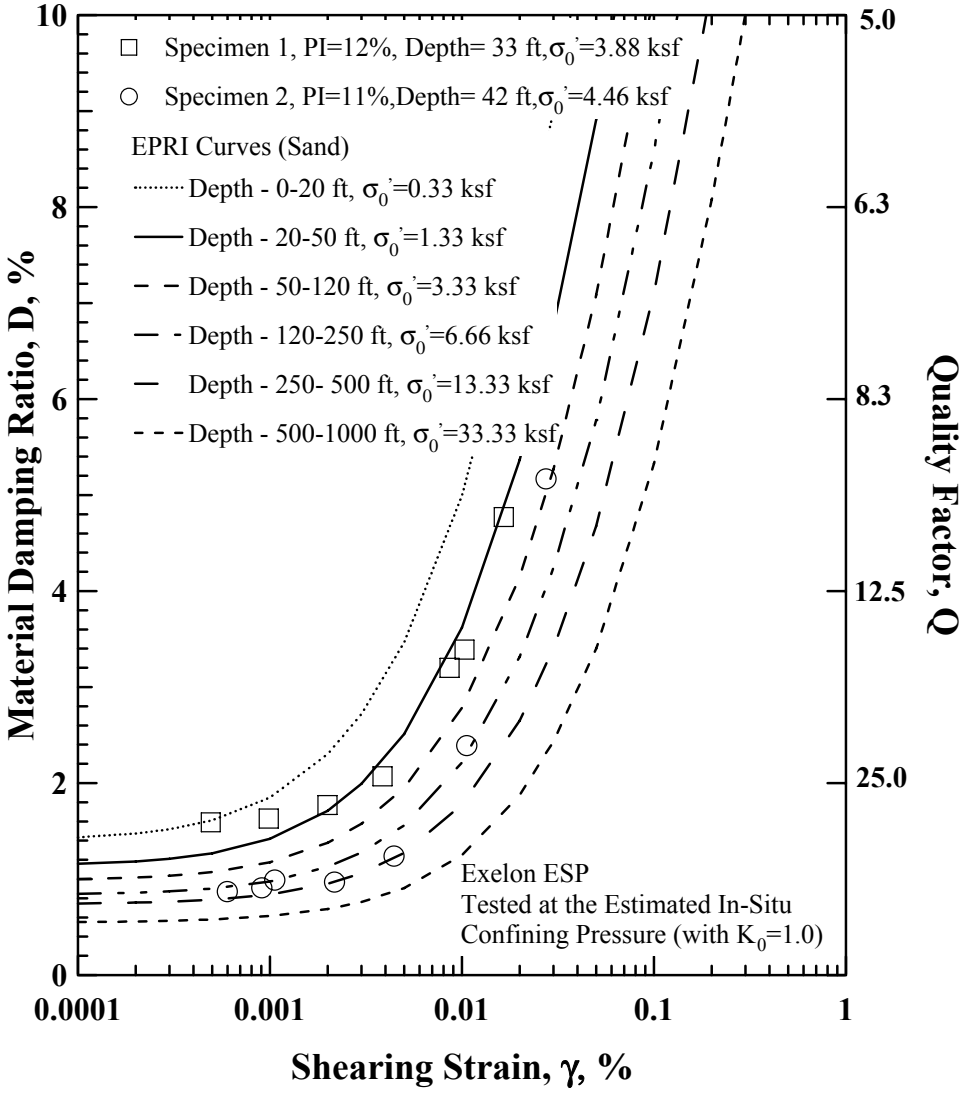

Figure 27 Comparison of the EPRI (1993) Sand Curves with the Variation in Material Damping Ratio with Shearing Strain from Torsional Shear (TS) Tests of Specimen No. 1 and Specimen No. 2 that were Tested at Their Estimated In-Situ Confining Pressures

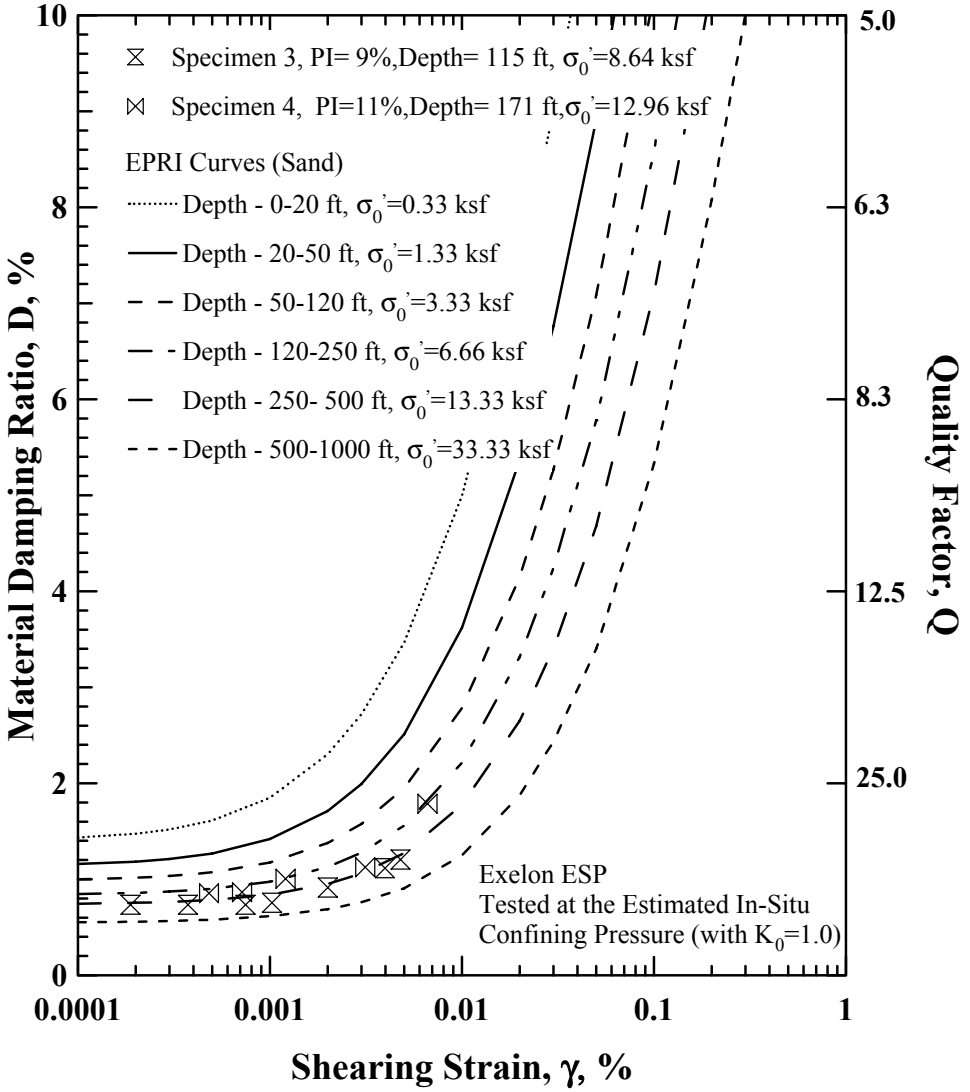

Figure 28 Comparison of the EPRI (1993) Sand Curves with the Variation in Material Damping Ratio with Shearing Strain from Torsional Shear (TS) Tests of Specimen No. 3 and Specimen No. 4 that were Tested at Their Estimated In-Situ Confining Pressures

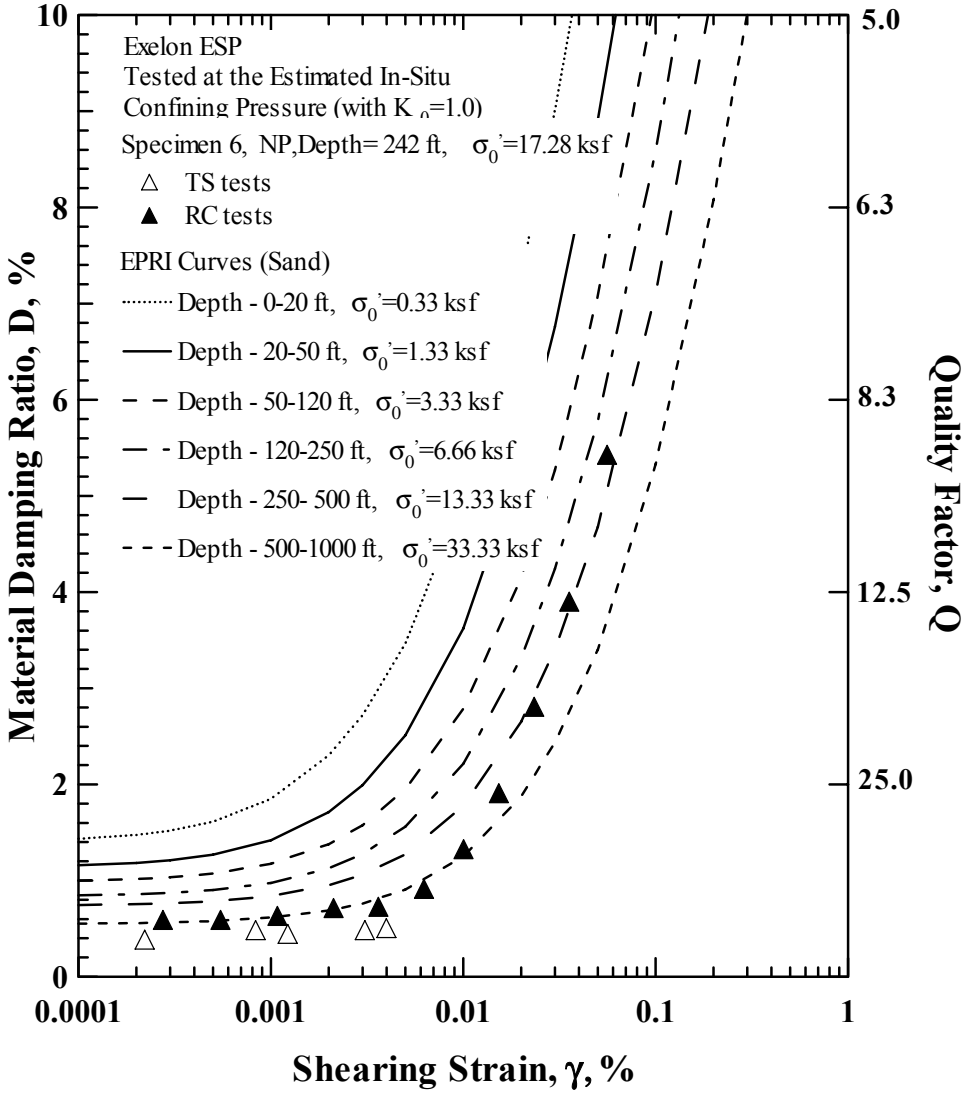

Figure 29 Comparison of the EPRI (1993) Sand Curves with the Variations in Material Damping Ratio with Shearing Strain from Resonant Column (RC) and Torsional Shear (TS) Tests of Specimen 6 that was Tested at Its Estimated In-Situ Confining Pressures

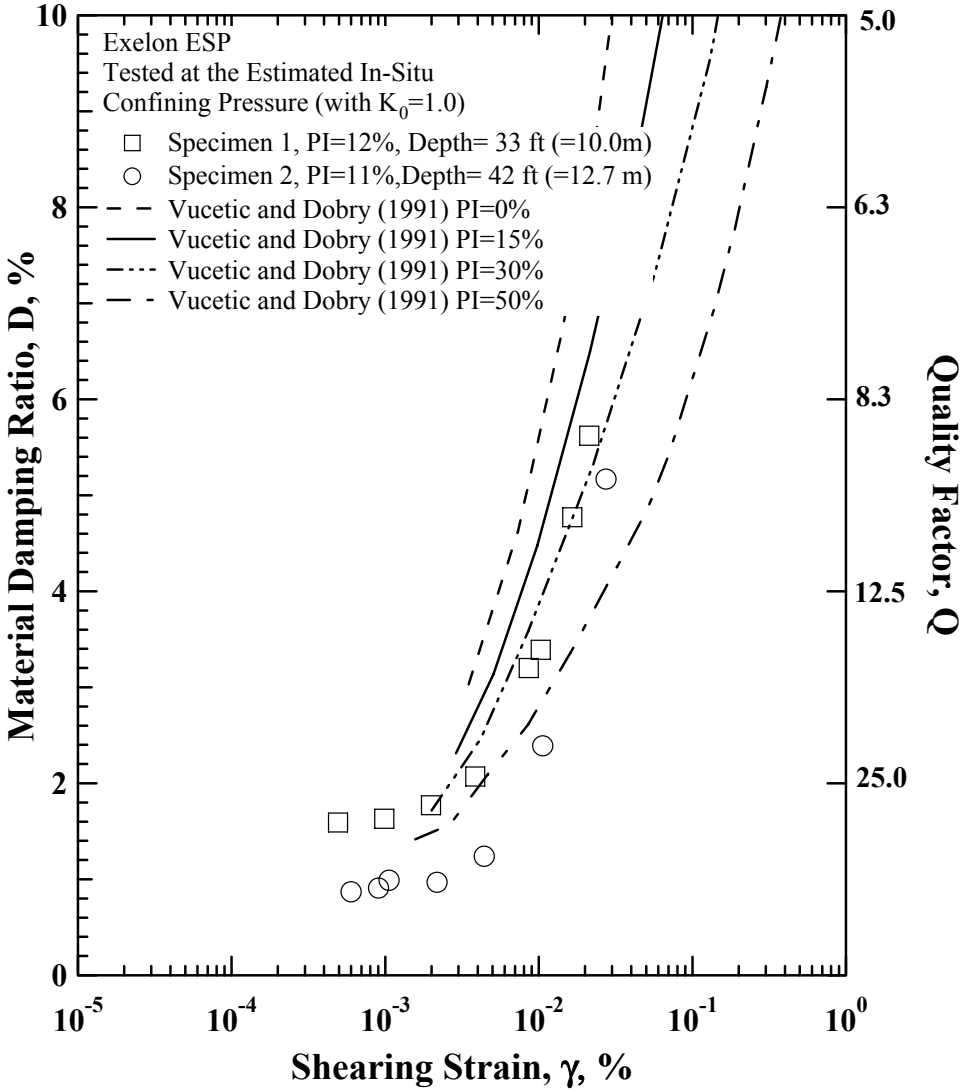

Figure 30 Comparison of the Vucetic and Dobry (1991) Curves with the Variation in Material Damping Ratio with Shearing Strain from Torsional Shear (TS) Tests of Specimen No. 1 and Specimen No.2 that were Tested at Their Estimated In-Situ Confining Pressures

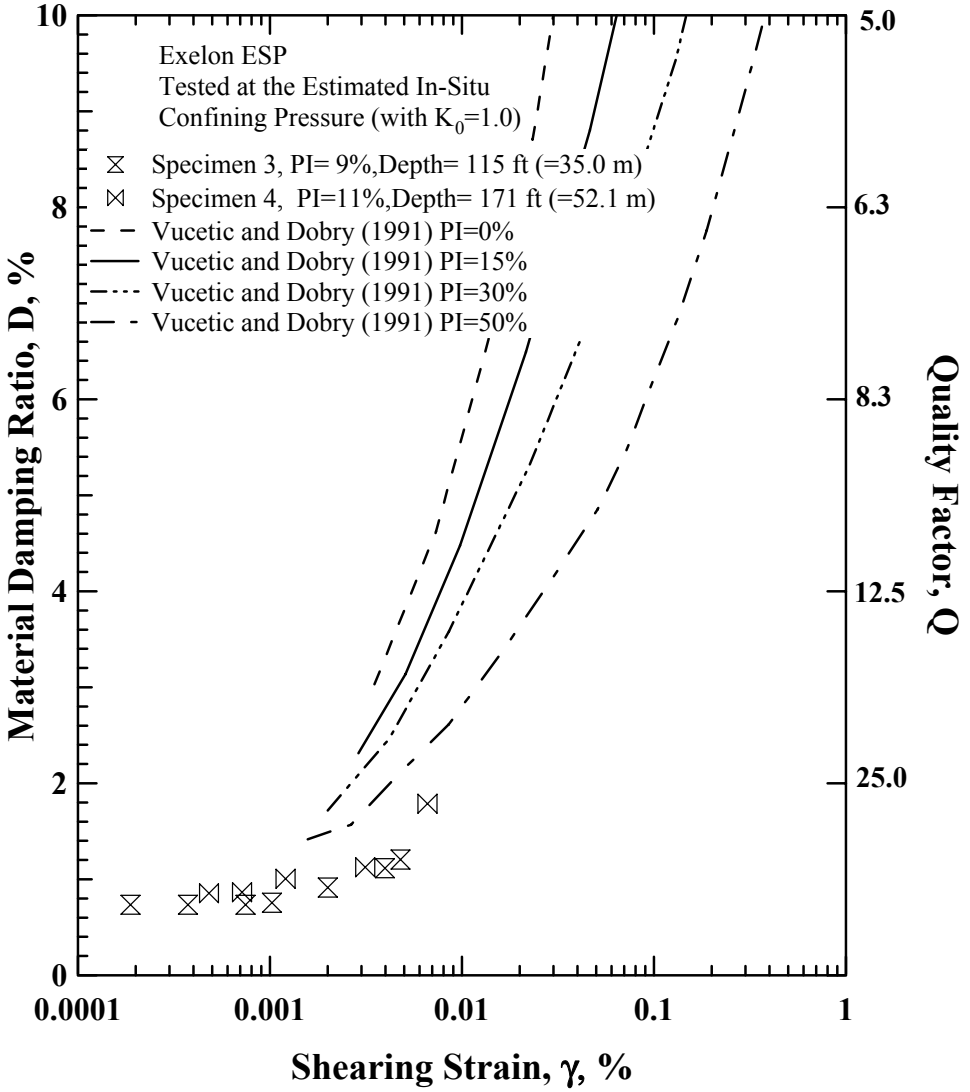

Figure 31 Comparison of the Vucetic and Dobry (1991) Curves with the Variations in Material Damping Ratio with Shearing Strain from Torsional Shear (TS) Tests of Specimen No. 3 and Specimen No. 4 that were Tested at Their Estimated In-Situ Confining Pressures

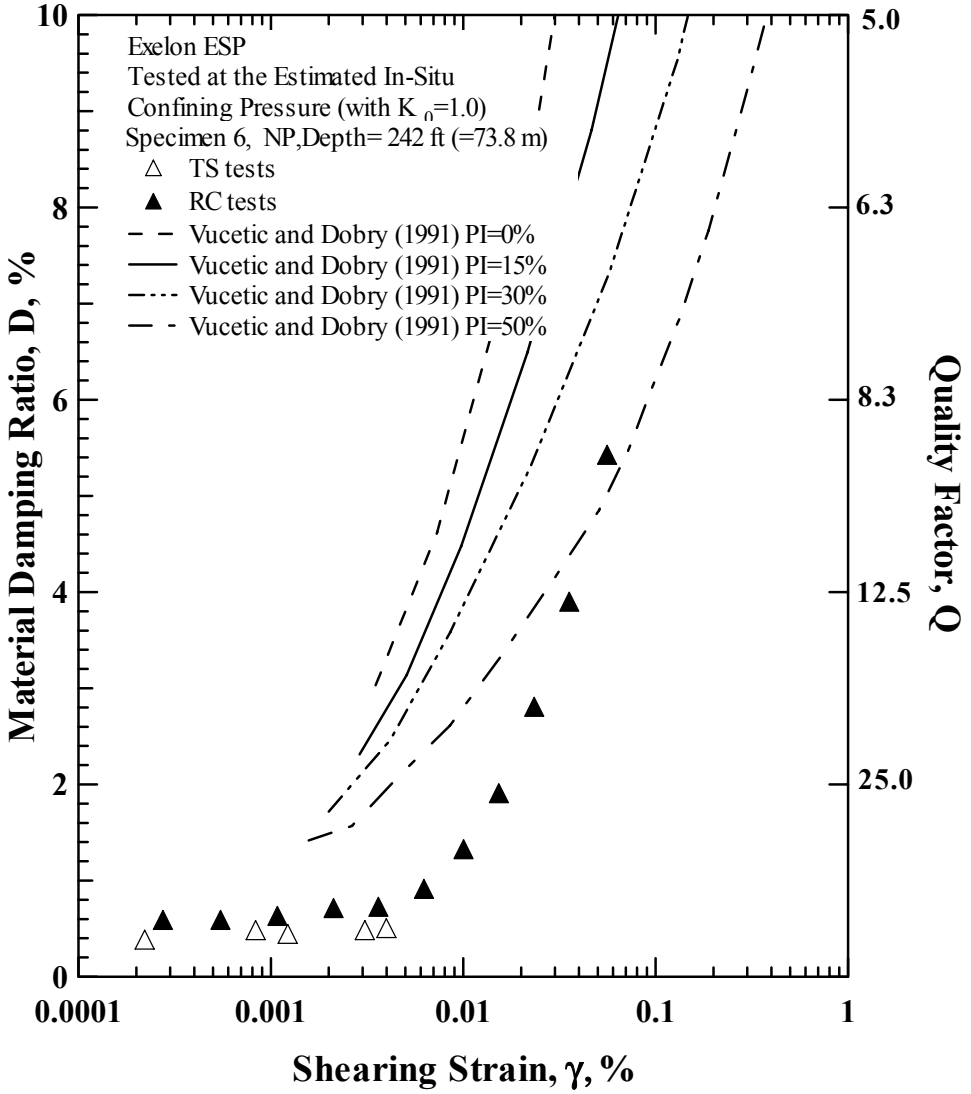

Figure 32 Comparison of the Vucetic and Dobry (1991) Curves with the Variations in Material Damping Ratio with Shearing Strain from Resonant Column (RC) and Torsional Shear (TS) Tests of Specimen No. 6 that was Tested at Its Estimated In-Situ Confining Pressure

3. The D – log γ relationships of the five specimens are compared with the relationships suggested by Vucetic and Dobry (1991) in Figures 30, 31 and 32 for Specimen Nos. 1 and 2, Specimen Nos. 3 and 4 and Specimen No. 6, respectively. In this case, the specimens show more linearity than predicted by the Vucetic and Dobry relationships for soils with a PI of about 15 %. Specimen No. 6 shows much more linearity than predicted by Vucetic and Dobry. Some of this difference is likely due to the higher confining pressure used in testing.

4.3.2 Comparison with New D – Log γRelationships

Mehmet Darendeli (2001) derived an equation for nonlinear damping curves based on the modified hyperbolic stress-strain curve and Masing behavior as:

$$D_{\text{Masing}} = c_1 D_{\text{Masing, a=1.0}} + c_2 D_{\text{Masing, a=1.0}}^{\ 2} + c_3 D_{\text{Masing, a=1.0}}^{\ 3} \tag{7}$$

$$D_{\text{Masing, a=1.0}} = \frac{100}{\Pi}\left[4\frac{\gamma - \gamma_r \ln\left(\frac{\gamma+\gamma_r}{\gamma_r}\right)}{\frac{\gamma^2}{\gamma+\gamma_r}} - 2\right](\%) \tag{8}$$

and

$\Pi = 3.1416$,

$\gamma_r = \gamma_{r,G}$,

$c_1 = -1.1143a^2 + 1.8618a + 0.2523$,

$c_2 = 0.0805a^2 - 0.0710a + 0.0095$, and

$c_3 = -0.0005a^2 + 0.0002a + 0.0003$.

This estimation of D, that is based solely on Masing behavior, yields higher damping ratios at higher strains than values reported in the literature (e.g., Seed et al, 1986 and Vucetic and Dobry, 1991). Also, Masing damping ratios lack the small-strain material damping ratio, D_{min}, because D_{Masing} goes to zero in the linear range. Therefore, Equations 7 and 8 were modified to take into account the experimental observations as follows:

$$D = F * D_{\text{Masing}} + D_{\text{min}} \tag{9}$$

$$F = b * \left(\frac{G}{G_{\max}} \right)^{0.1} \tag{10}$$

$$b = \phi_{11} + \phi_{12} * \ln(N) \tag{11}$$

and

$$D_{\min} = \left(\phi_6 + \phi_7 * PI * OCR^{\phi_8} \right) * \sigma_o'^{\phi_9} * \left[1 + \phi_{10} * \ln(freq) \right] \tag{12}$$

in which

σ_o' = mean effective confining pressure (atm),

PI = soil plasticity (%),

OCR = overconsolidation ratio,

freq = loading frequency,

N = number of cycles of loading,

$\phi_6 = 0.8005$,

$\phi_7 = 0.0129$,

$\phi_8 = -0.1069$,

$\phi_9 = -0.2889$,

$\phi_{10} = 0.2919$,

$\phi_{11} = 0.6329$, and

$\phi_{12} = -0.0057$.

As in the model equation for the G/G_{max} – log γ relationship (Equations 4 and 5), σ_o', PI and OCR are input parameters. In addition, loading frequency and number of loading cycles are now input parameters.

Comparisons between the measured D-log γ curves and the average trends predicted by Darendeli's model are presented in: (1) Figure 33 for Specimen Nos. 1 and 2, (2) Figure 34 for Specimen Nos. 3 and 4, and (3) Figure 35 for Specimen No. 6. The predicted curve for Specimen No. 5 is presented in Figure 36. Just as done with the G/G_{max} – log γ relationships, "average trends" are shown in each two-specimen set. Also the average values of the

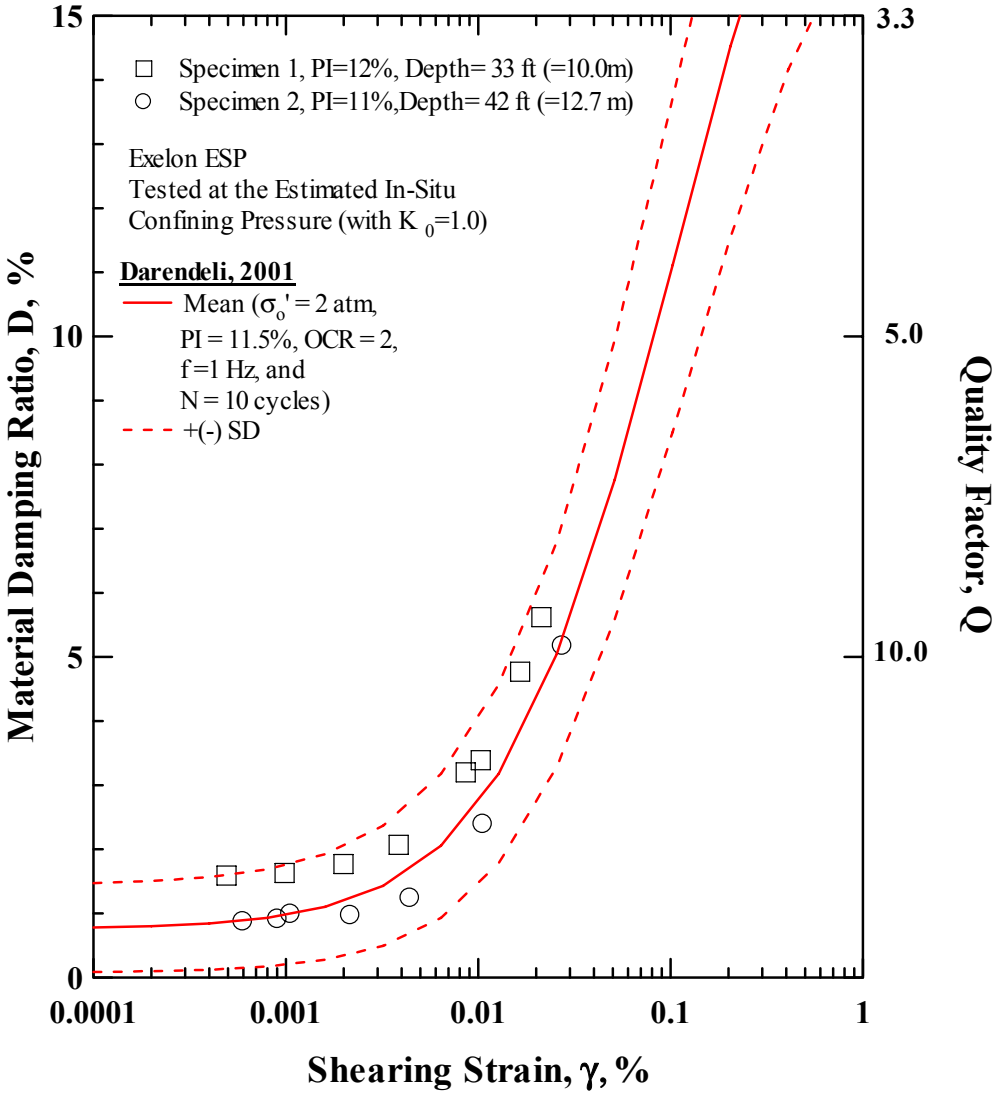

Figure 33 Comparison of the Average Nonlinear Curve Predicted by Darendeli (2001) with the Variations in Material Damping Ratio with Shearing Strain from Torsional Shear Tests of Specimen No. 1 and Specimen No. 2 that were Tested at Their Estimated In-Situ Confining Pressures

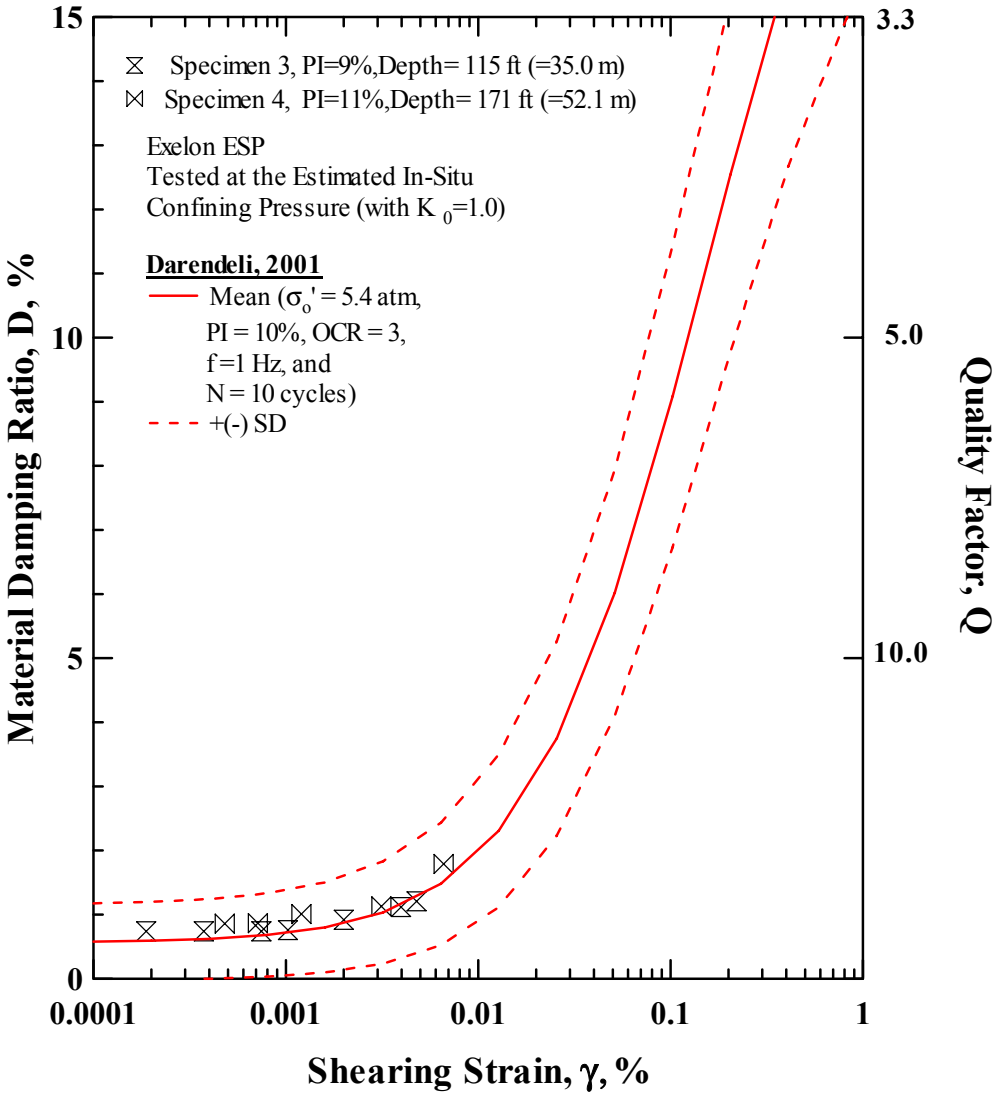

Figure 34 Comparison of the Average Nonlinear Curve Predicted by Darendeli (2001) with the Variations in Material Damping Ratio with Shearing Strain from Torsional Shear Tests of Specimen No. 3 and Specimen No. 4 that were Tested at Their Estimated In-Situ Confining Pressures

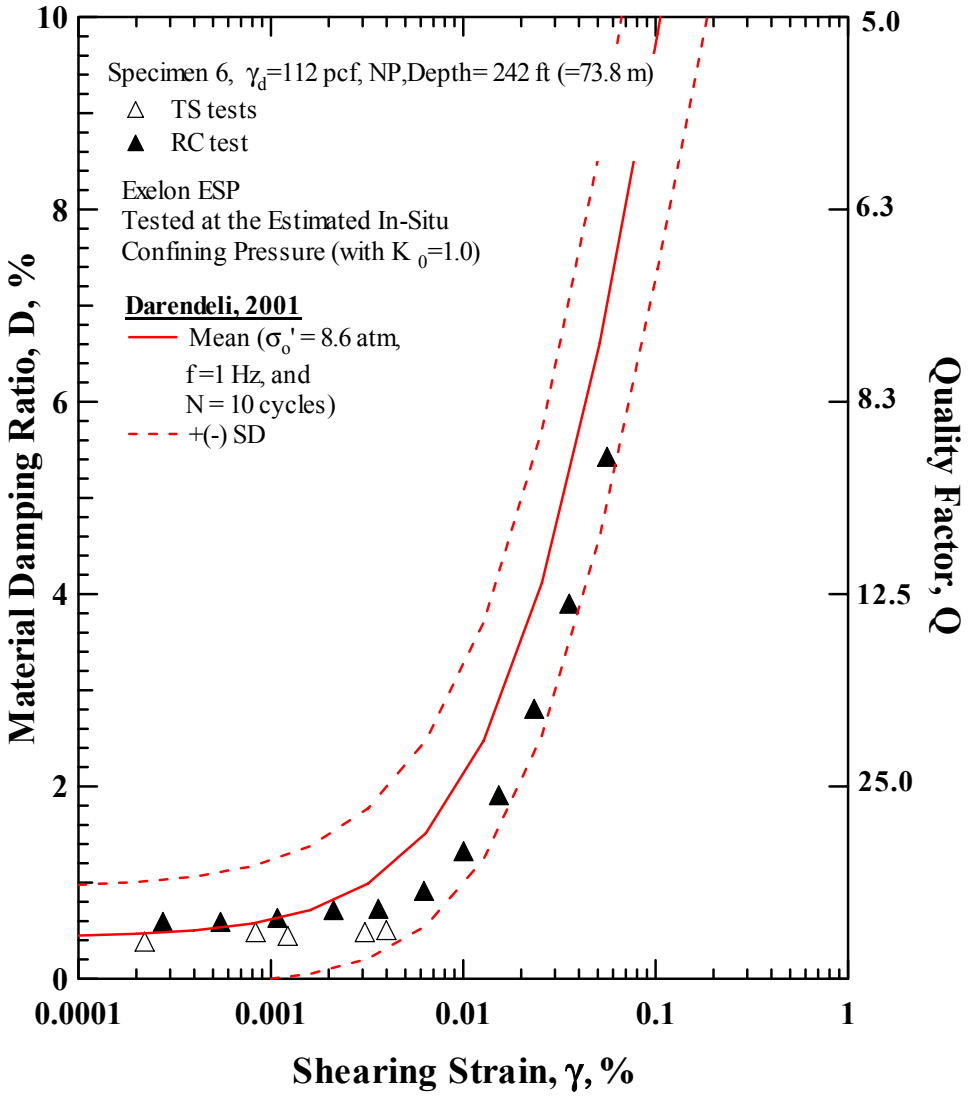

Figure 35 Comparison of the Nonlinear Curve Predicted by Darendeli (2001) with the Variations with the Material Damping Ratio with Shearing Strain from Resonant Column (RC) and Torsional Shear (TS) Tests of Specimen No. 6 that was Tested at Its In-Situ Confining Pressure

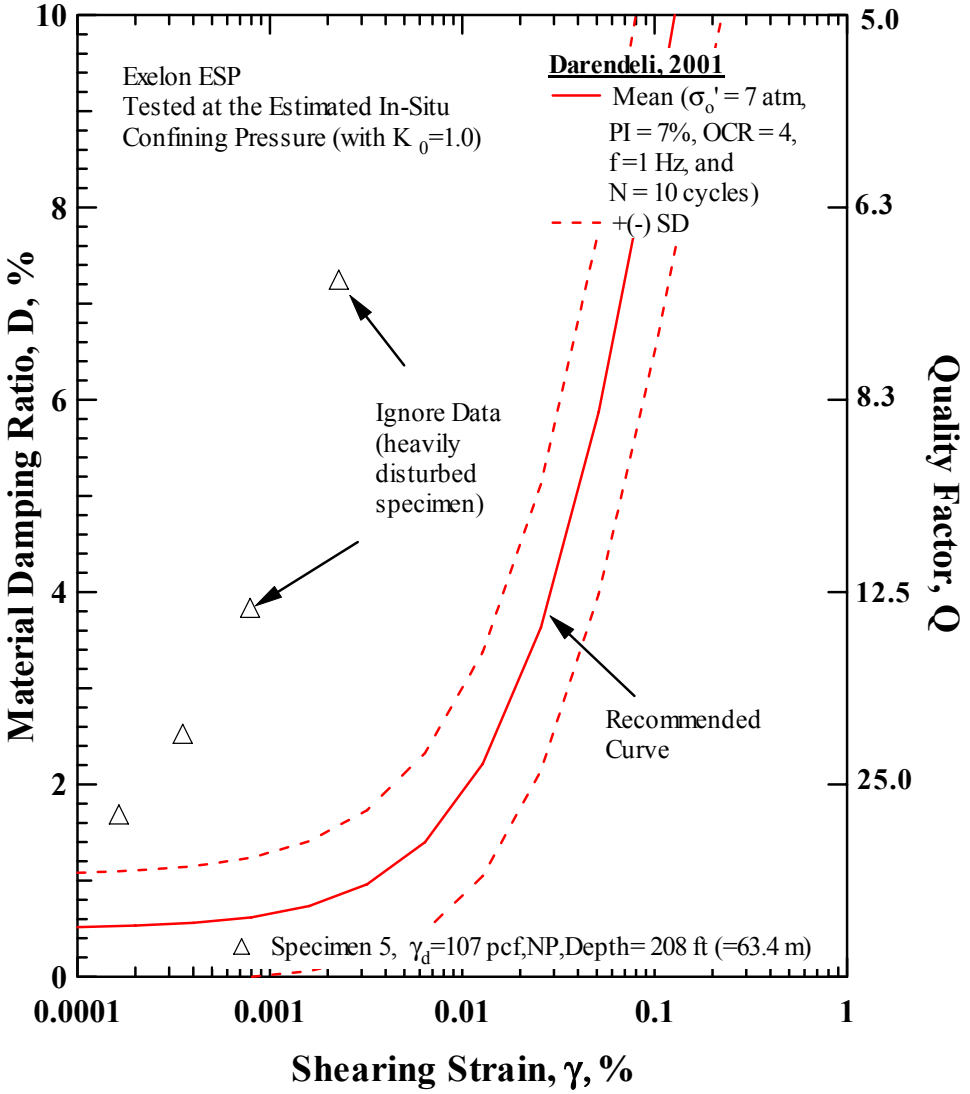

Figure 36 Recommended Variation in the Material Damping Ratio with Shearing Strain for Specimen No. 5 Based on Darendeli (2001)

parameters are shown in each figure. Darendeli's model also includes the variation to be expected in the D – log γ curves in terms of plus or minus one standard deviation, +/-σ. This range is shown in each figure. As seen in the figures, the average predicted curves approximated the TS measurements quite well. Also, the recommended curve for Specimen No. 5 in Figure 36 supports the conclusion that the laboratory results of the disturbed specimen were atypical for a soil.

5. SUMMARY

The linear and nonlinear dynamic properties of six intact soil specimens from the EGC ESP Project in Illinois were evaluated in the Soil Dynamics Laboratory at the University of Texas at Austin (UTA). Dynamic testing was performed with a fixed-free device that involved combined resonant column and torsional shear (RCTS) testing as described in Section 2. Initial properties of the six specimens are given in Table 2. All results from these tests are presented in graphical and tabular forms in Exhibits B through G for Specimens No. 1 through No. 6, respectively.

The variations in small-strain shear wave velocity, V_S, small-strain shear modulus, G_{max}, and small-strain material damping ratio, D_{min}, with isotropic confining pressure were determined for each specimen. The results of these measurements are summarized in Table 4 and in Figures 3 through 8. The nonlinear G – log γ, G/G_{max} – log γ and D – log γ relationships were also measured for each specimen at its estimated in-situ confining pressure. These results are presented in Section 4, along with comparisons with well-known and new empirical relationships.

In terms of overall summary comments, the dynamic laboratory testing went smoothly and was typical of other similar studies at UTA. The RCTS equipment worked well and passed the overall system checks before and after testing. The measured linear and nonlinear dynamic properties were within ranges expected for the soil types tested, with exception of the nonlinear properties of Specimen No. 5 which were atypical due to sample disturbance. The nonlinear properties of this specimen were predicted using Darendeli (2001).

6. REFERENCES

Darendeli, B. M. (2001) "Develop of a New Family of Normalize Modulus Reduction and Material Damping Curves" *Ph. D. Dissertation,* Univ. of Texas at Austin., 362 p.

Electrical Power Research Institute (1993), "Guidelines for Determining Design Basic Ground Motions," Final Report, EPRI TR-102293, Palo Alto, CA, November.

Hardin, B.O. and V.P. Drnevich (1972), "Shear Modulus and Damping in Soils: Design Equations and Curves," Journal of the Soil Mechanics and Foundations Division, ASCE, Vol. 98, No. SM6, Proc. Paper 9006, July.

Hardin, B.O. (1978), "The Nature of Stress-Strain Behavior of Soils," Proceedings, Geotech. Eng. Div. Specialty Conference on Earthquake Eng. And Soil Dynamics, Vol. 1 ASCE, Pasadena, June, pp. 3-90.

Hwang, S.K. (1997), "Investigation of the Dynamic Properties of Natural Soils," *Ph. D. Dissertation*, Univ. of Texas at Austin., 394 p.

Ni, S.H. (1997), "Dynamic Properties of Sand Under True Triaxial Stress States From Resonant Column/Torsional Shear Tests," *Ph. D. Dissertation,* Univ. of Texas at Austin., 421 p.

Seed, H.B., R.T. Wong, I.M. Idriss, and K. Tokimatsu (1986), "Moduli of Damping Factors For Dynamic Analyses of Cohesionless Soils," Journal of the Soil Mechanics and Foundations Division, Vol. 112, No. SM11, pp. 1016-1032.

Stokoe, K.H., II, Hwang, S.K., Lee, J. N.-K, and Andrus, R.D. (1994), "Effects of Various Parameters on the Stiffness and Damping of Soils at Small to Medium Strains," Proceedings, International Symposium on Prefailure Deformation Characteristics of Geomaterials, Vol. 2, Japanese Society of Soil Mechanics and Foundation Engineering, Sapporo, Japan, September, pp. 785-816.

Vucetic, Mladen and Dobry, Ricardo (1991), "Effect of Soil Plasticity on Cyclic Response," Journal of Geotechnical Engineering, Vol.117, No. 1, Jan. pp. 89-107

Exhibit A
to Attachment A-7

Brief Background on Combined RCTS Equipment

Background on Combined RCTS Equipment

The effects of various parameters on G and D are conveniently evaluated in the laboratory with combined RCTS equipment as discussed by Stokoe et al., 1994a. This equipment is of the fixed-free type, with the bottom of the specimen fixed and torsional excitation applied to the top as illustrated in Fig. A.1. The equipment has two important attributes. First, both resonant column (RC) and torsional shear (TS) tests can be performed with the same piece of equipment. Switching from one type of test to the other is simply done outside the confining chamber by changing: 1. the input excitation frequency used to drive the specimen and 2. the motion monitoring devices used to record the specimen response. As a result, variability due to testing different specimens is eliminated so that results from both tests can be compared effectively. Second, the loading frequency in the torsional shear test can be easily changed from 0.01 to about 10 Hz. Therefore, the effect of frequency and number of loading cycles on the deformational characteristics of intact specimens can be conveniently investigated.

The basic operational principle in the RC test is to vibrate the cylindrical specimen in first-mode torsional resonance. At the University of Texas (UT), this process is completely automated so that first-mode resonance can be quickly and accurately established as illustrated in Fig. A.2a (Ni, 1987). Determinations of resonant frequency and amplitude of vibration are made from the response curve. These values are then combined with equipment characteristics and specimen size to calculate shear wave velocity, V_S, shear modulus, G, and shearing strain amplitude, γ.

Material damping in the RC test is evaluated from the dynamic soil response using either the free-vibration decay curve or the half-power bandwidth method. The free-vibration decay curve is recorded by shutting off the driving force after the specimen is vibrating in steady-state motion at the resonant frequency. Figure A.3 shows an example of this process. The logarithmic decrement, δ, is defined from the decay curve as:

$$\delta = \ln(z_1/z_2) \qquad \text{(A.1)}$$

where z_1 and z_2 are the amplitudes of two successive cycles. Material damping ratio, D, can then be determined from δ by:

$$D = [\delta^2/(4\pi^2+\delta^2)]^{1/2} \qquad \text{(A.2)}$$

The half-power bandwidth method is based on measurement of the width of the dynamic response curve around the resonance peak. For small values of material damping, one can approximate damping as:

$$D \cong (f_2 - f_1)/2f_r \qquad \text{(A.3)}$$

where f_1 and f_2 are the two frequencies at which the amplitude is 0.707 times the amplitude at the resonant frequency , f_r, as illustrated in Fig. A.4.

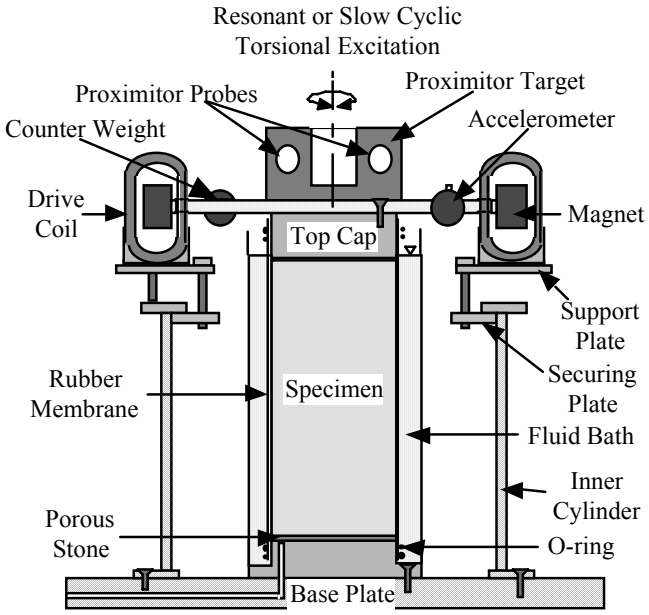

Figure A.1 Simplified Diagram of a Combined Resonant Column (RC) and Torsional Shear (TS) Device (Confining Chamber not Shown)

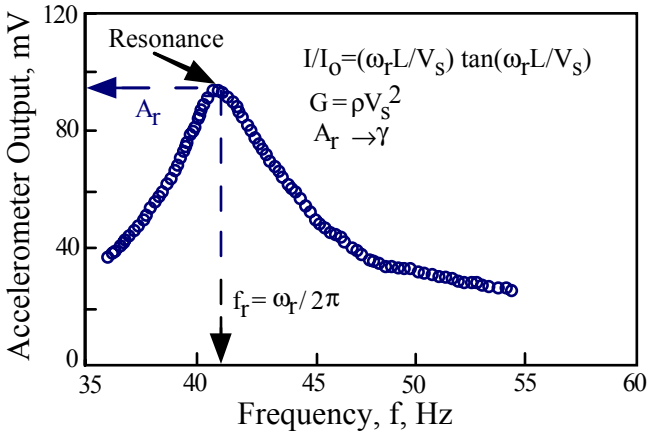

a) Dynamic Response Curve Measured in the RC Test

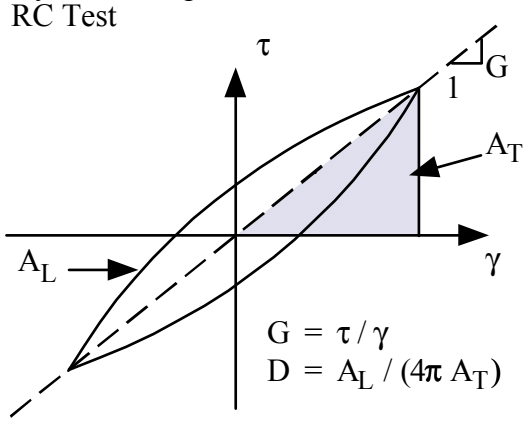

b) Hysteresis Loop Measured in the TS Test

Figure A.2 Examples of Measurements Performed in the RC and TS Tests

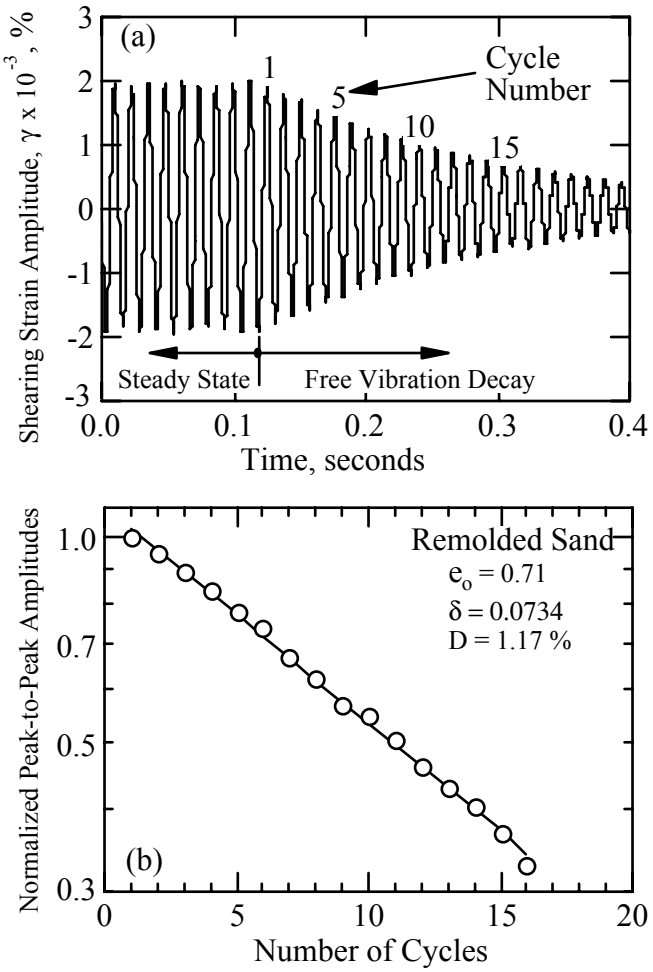

Figure A.3 Material Damping Measurement in the RC Test Using the Free-Vibration Decay Curve

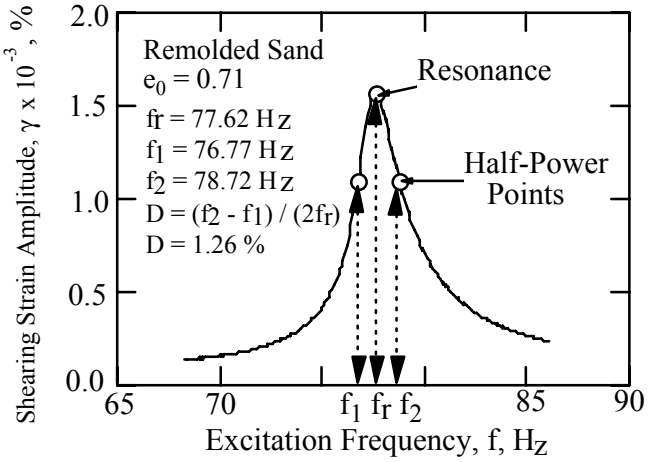

Figure A.4 Material Damping Measurement in the RC Test Using the Half-Power Bandwidth (Same Specimen as Shown in Fig. A.3)

For measurements at small strains ($\gamma<10^{-3}$ %), background noise can have a more adverse effect on the free-vibration decay curve than on the frequency response curve. On the other hand, at large strains, the assumptions implied in the derivation of Equation A.3 are no longer valid, and serious errors can be introduced into values of D determined by the half-power bandwidth method (Ni, 1987). In this study, both methods were used at shearing strains less than about 0.002 %, but only the free-vibration decay method was applied at larger strains. In addition, the strain at which the damping measurement was assumed to occur was taken as the average of the first three cycles of free vibration. This procedure is not conventionally employed at $\gamma > 0.002$ % but more correctly represents the strain associated with damping measurements from the free vibration decay curve.

In the TS test, shear modulus and material damping are measured using the same RCTS equipment, but the equipment is operated in slow cyclic torsional loading at a given frequency. Instead of determining the resonant frequency, the stress-strain hysteresis loop is determined from measuring the torque-twist response of the specimen as shown in Fig. A.2b. Proximitors are used to measure the angle of twist while the voltage applied to the coil is calibrated to yield torque. Shear modulus is calculated from the slope of a line through the end points of the hysteresis loop. Material damping is determined from the hysteresis loop as the ratio of the energy dissipated in one cycle of loading (A_L) to the peak strain energy stored during the cycle (A_T) times a factor of 4π as shown in Fig. A.2b.

As discussed by Stokoe et al., (1994a), the RCTS equipment at UT is calibrated so that equipment-generated damping can be subtracted from the measurements. Equipment-generated damping, D_{eq}, is measured along with material damping of the specimen when the damping measurements are performed following the procedures outlined in Figs. A.2 through A.4. Equipment-generated damping results from the back-electromagnetic force generated by the magnets moving through the drive coils. It is important to calibrate the drive system of each RCTS device over the entire range of frequencies used in testing so that equipment-generated damping can be determined before testing any specimens. Typical results for D_{eq} in

RC testing are shown in Fig. A.5 (Hwang, 1997). This damping is then subtracted from the combined measurement to yield material damping of the specimen. In all results where material damping ratios of soil specimens are presented, these values have been corrected by subtracting D_{eq} from the combined measurement of D.

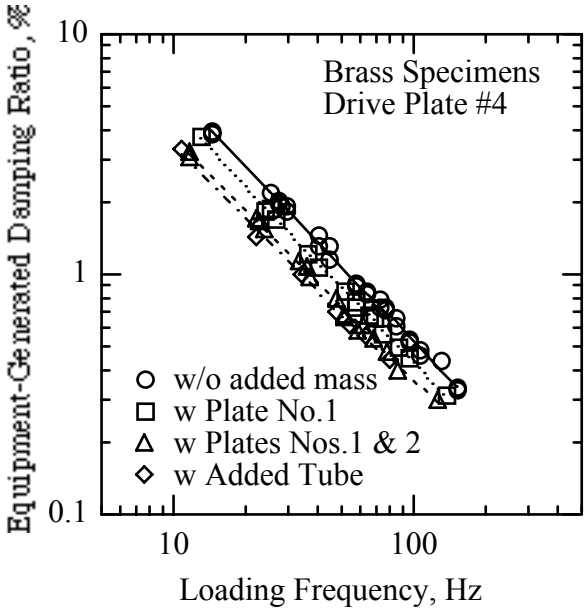

Figure A.5 Example of Equipment-Generated Damping Measured in the Resonant Column Device Using Metal Specimens (from Hwang, 1997)

Exhibit B

to Attachment A-7

Specimen No.1
UT Specimen: UTA-34-A
(Specimen No.1)

Exelon ESP B-2 (S-7)
Depth = 33ft (=10.1m)
Soil Type: Sandy Lean Clay (CL)

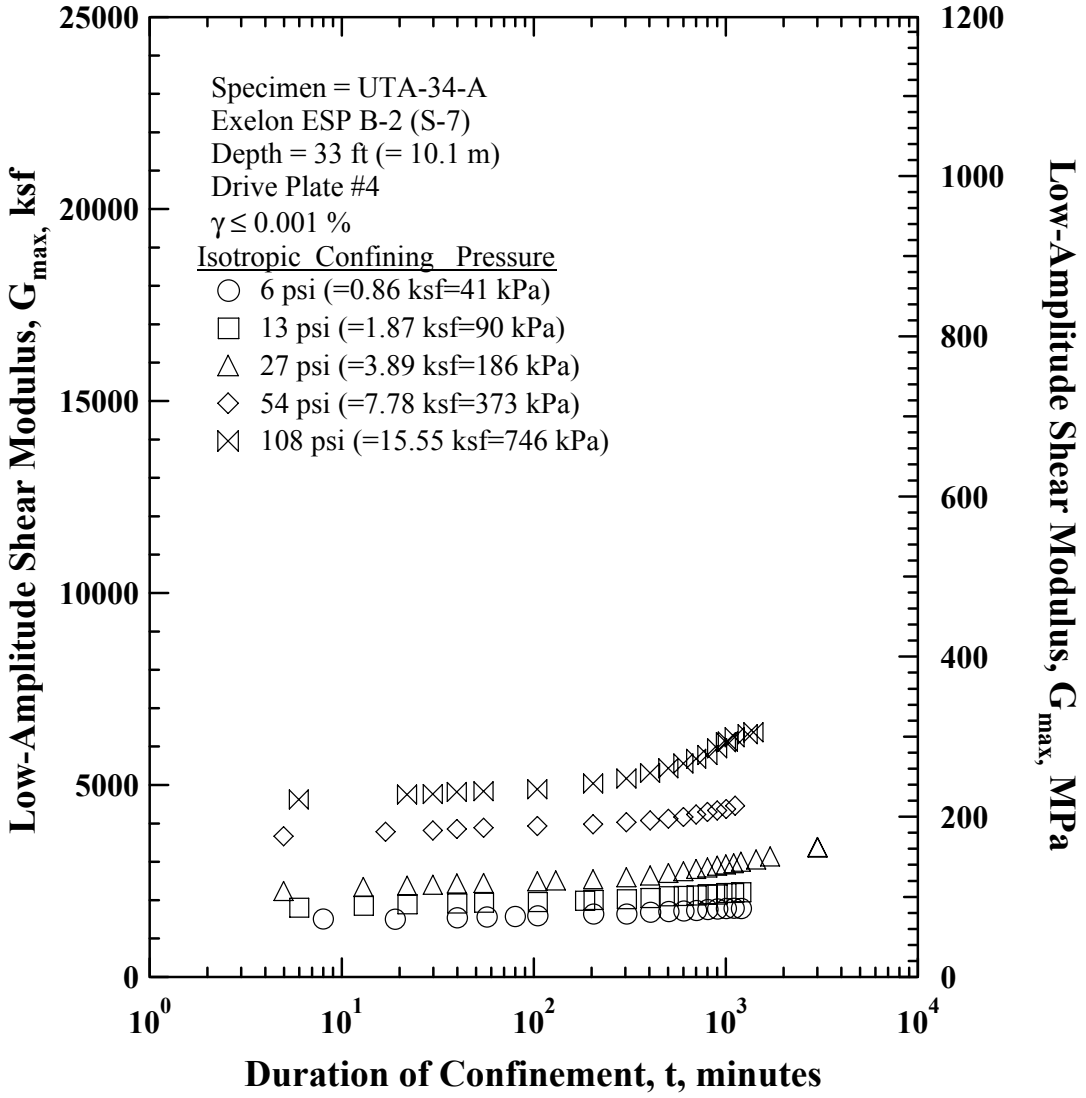

Figure B.1 Variation in Low-Amplitude Shear Modulus with Magnitude and Duration of Isotropic Confining Pressure from Resonant Column Tests of Specimen UTA-34-A (Specimen No.1).

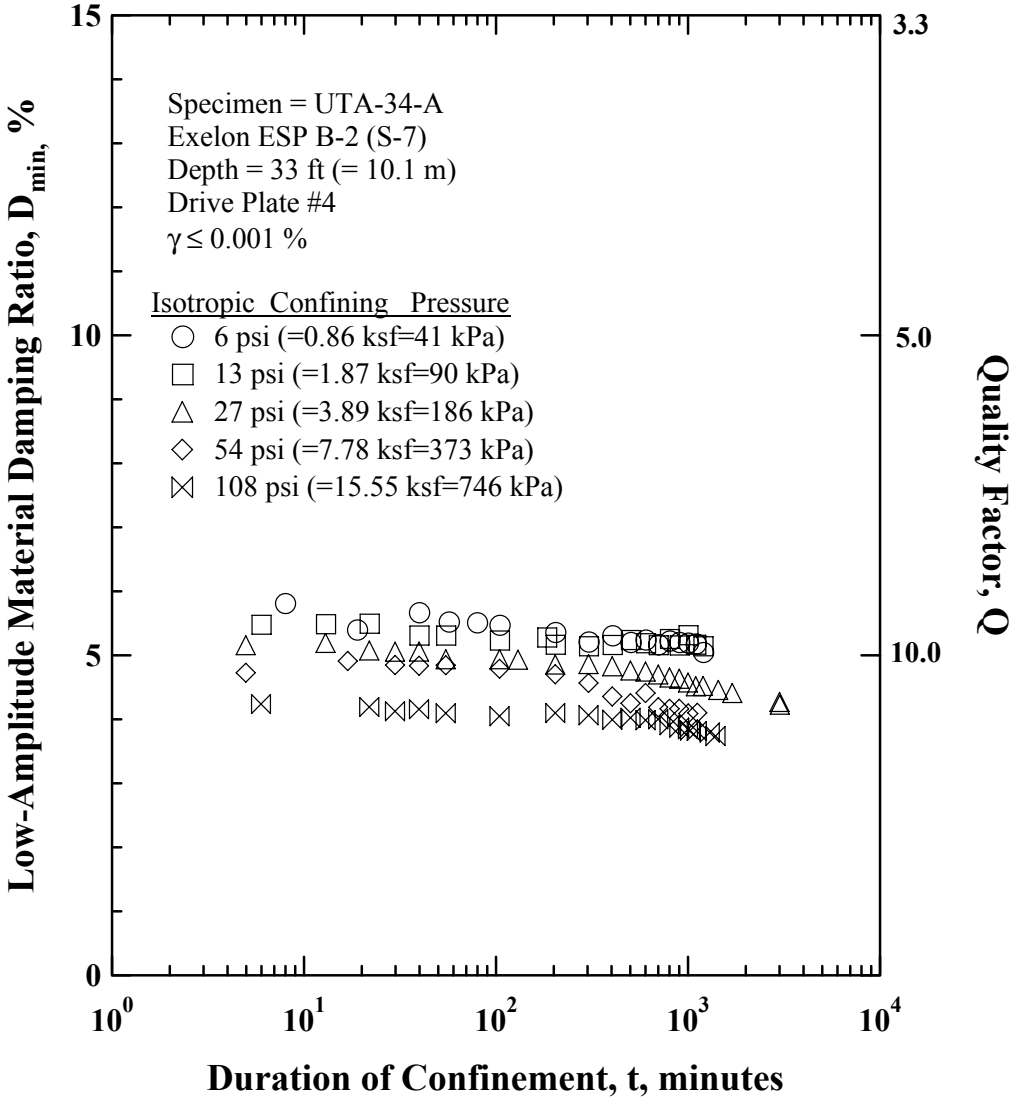

Figure B.2 Variation in Low-Amplitude Material Damping Ratio with Magnitude and Duration of Isotropic Confining Pressure from Resonant Column Tests of Specimen UTA-34-A (Specimen No.1).

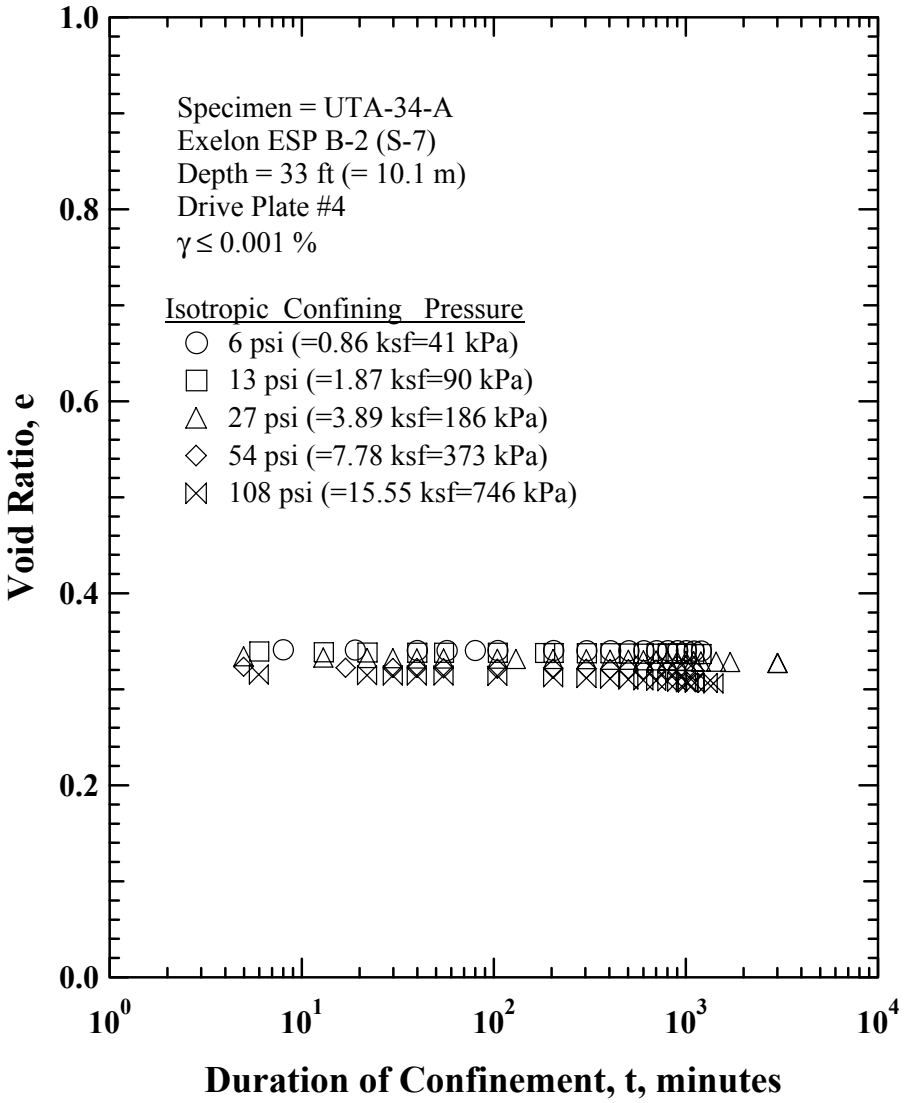

Figure B.3 Variation in Estimated Void Ratio with Magnitude and Duration of Isotropic Confining Pressure from Resonant Column Tests of Specimen UTA-34-A (Specimen No.1).

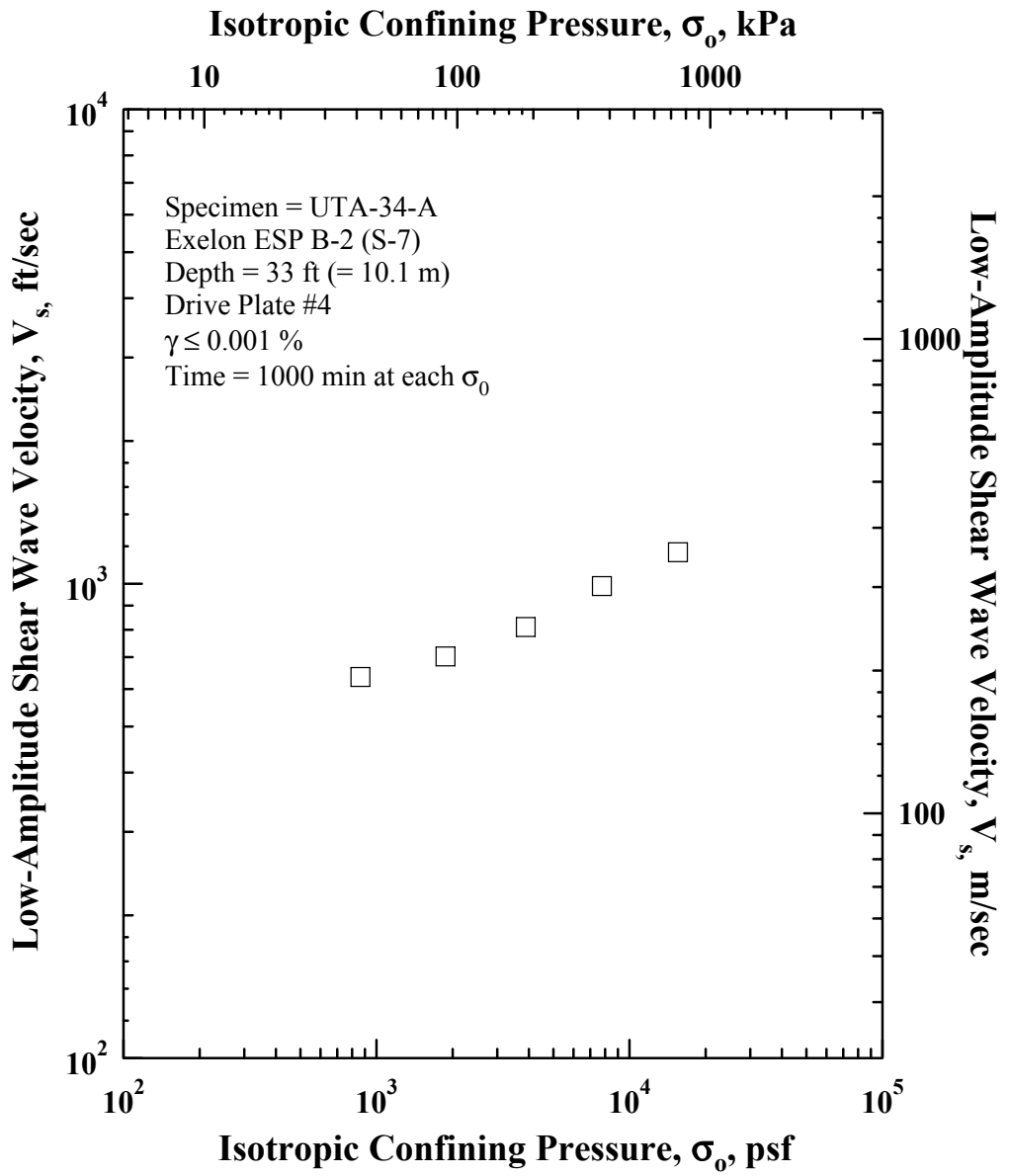

Figure B.4 Variation in Shear Wave Velocity with Isotropic Confining Pressure from Resonant Column Tests of Specimen UTA-34-A (Specimen No.1).

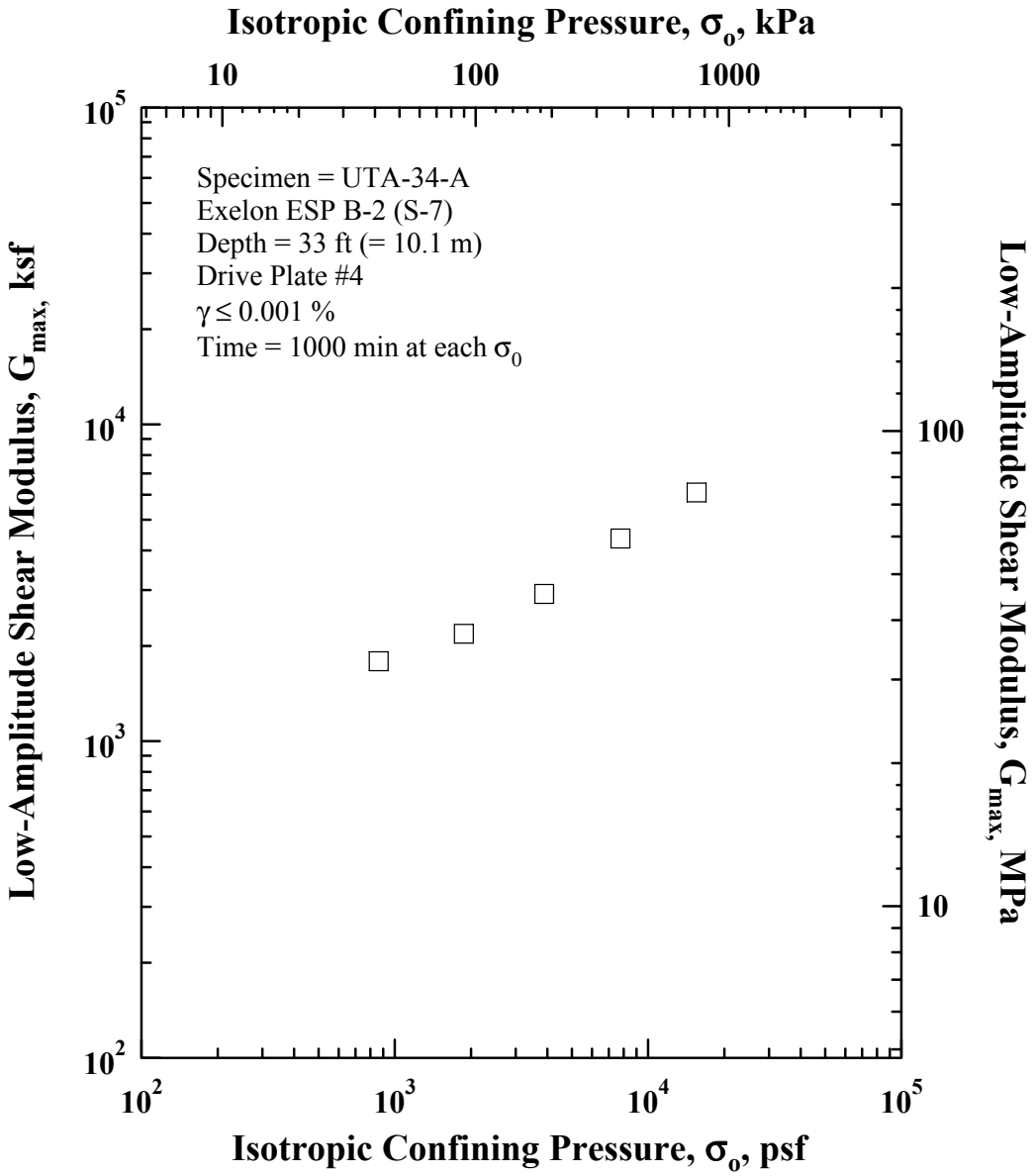

Figure B.5 Variation in Low-Amplitude Shear Modulus with Isotropic Confining Pressure from Resonant Column Tests of Specimen UTA-34-A (Specimen No.1).

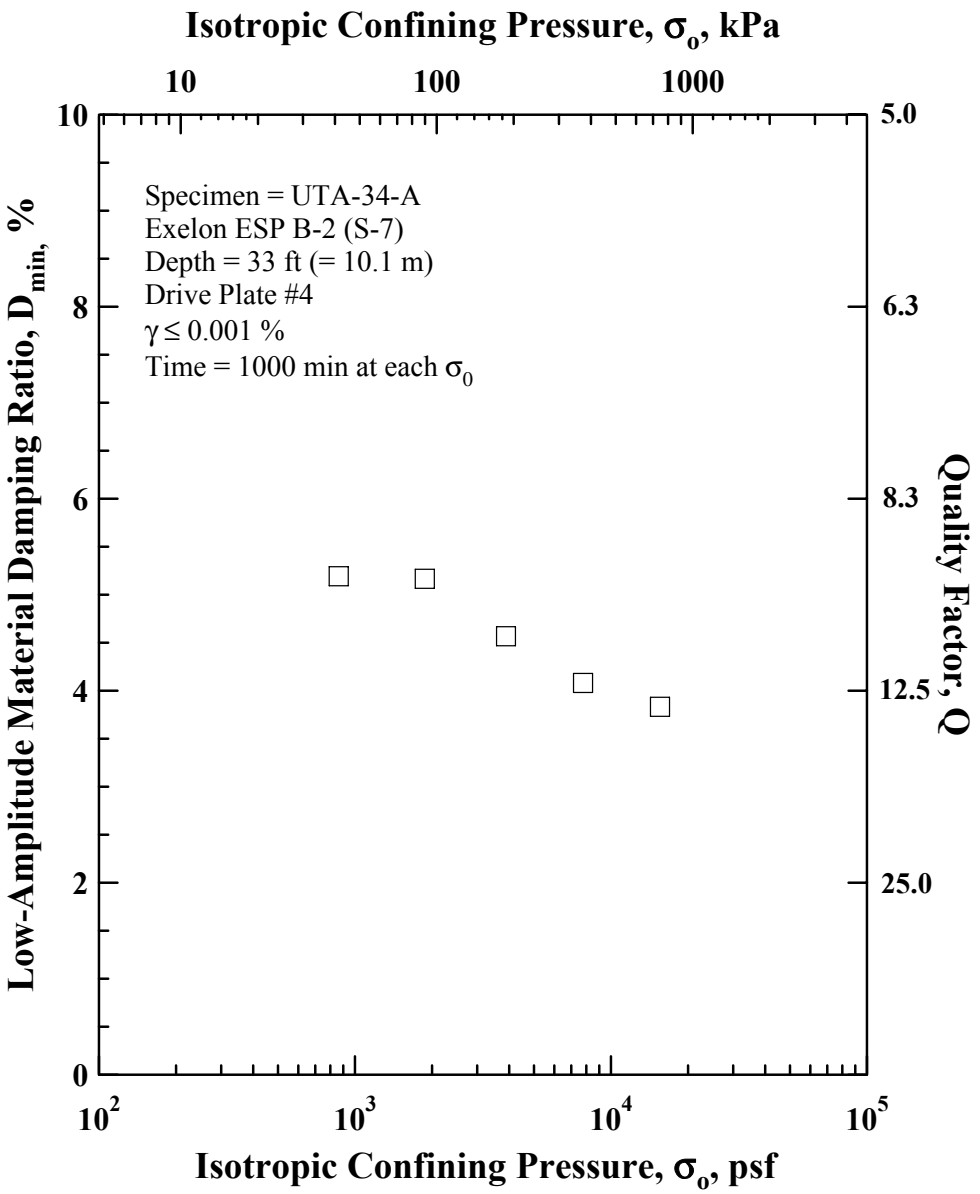

Figure B.6 Variation in Material Damping Ratio with Isotropic Confining Pressure from Resonant Column Tests of Specimen UTA-34-A (Specimen No.1).

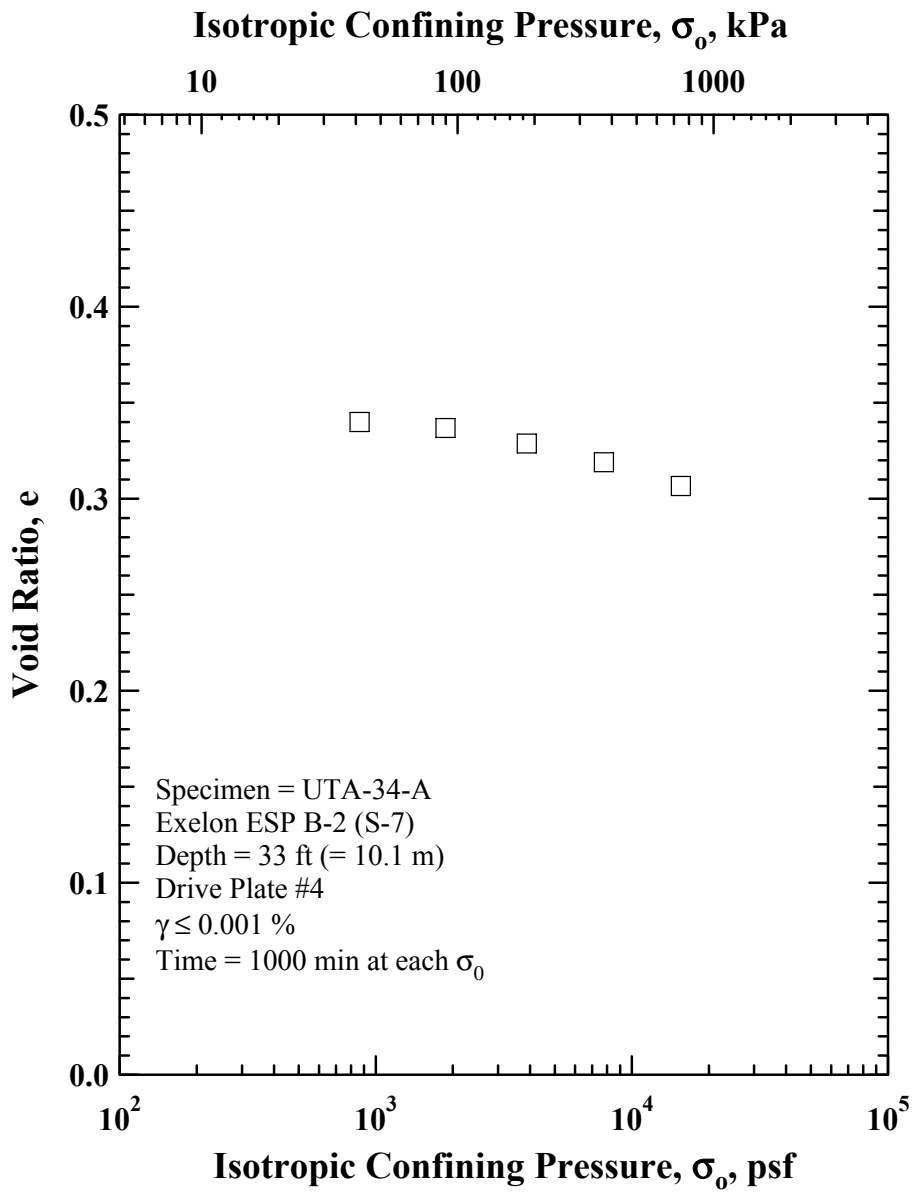

Figure B.7 Variation in Estimated Void Ratio with Isotropic Confining Pressure from Resonant Column Tests of Specimen UTA-34-A (Specimen No.1).

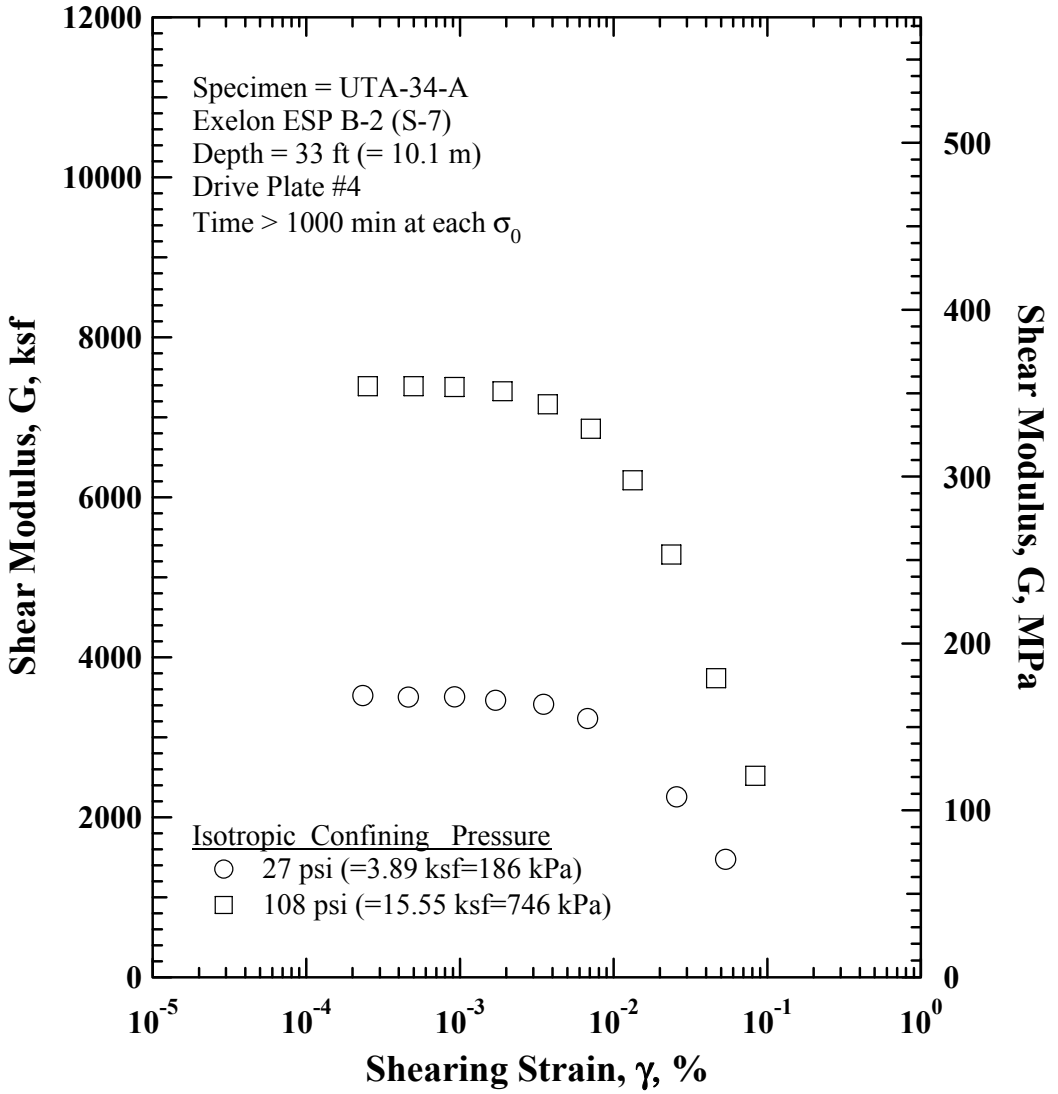

Figure B.8 Comparison of the Variation in Shear Modulus with Shearing Strain and Isotropic Confining Pressure from the Resonant Column Tests of Specimen UTA-34-A (Specimen No.1).

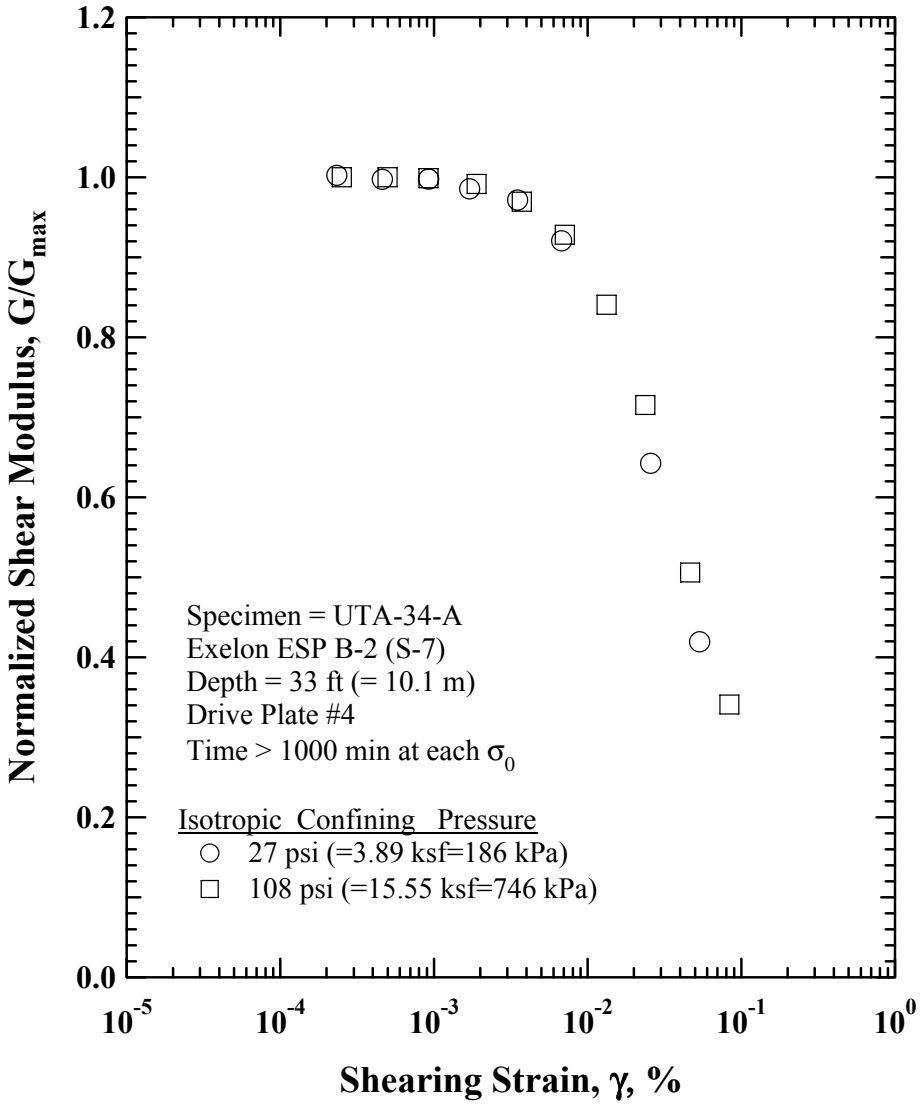

Figure B.9 Comparison of the Variation in Normalized Shear Modulus with Shearing Strain and Isotropic Confining Pressure from the Resonant Column Tests of Specimen UTA-34-A (Specimen No.1).

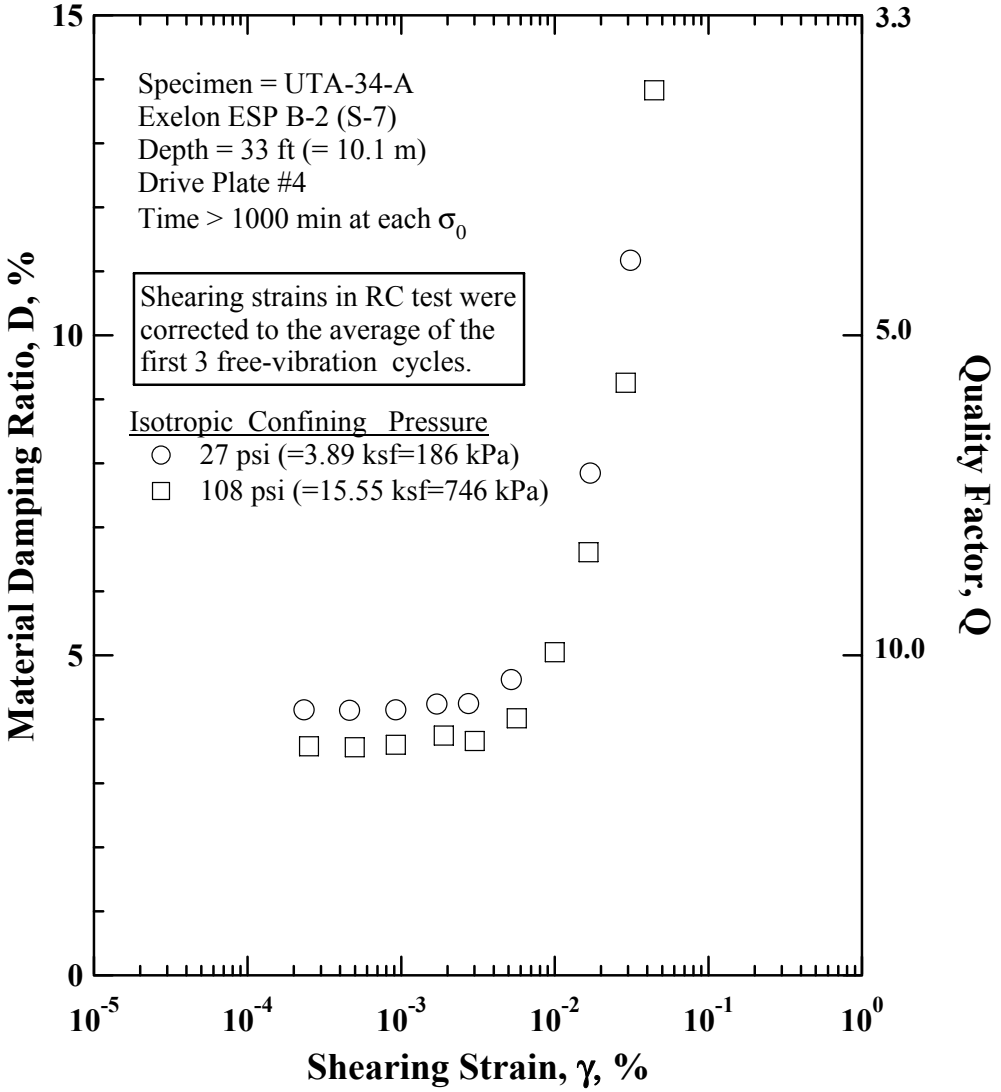

Figure B.10 Comparison of the Variation in Material Damping Ratio with Shearing Strain and Isotropic Confining Pressure from the Resonant Column Tests of Specimen UTA-34-A (Specimen No.1).

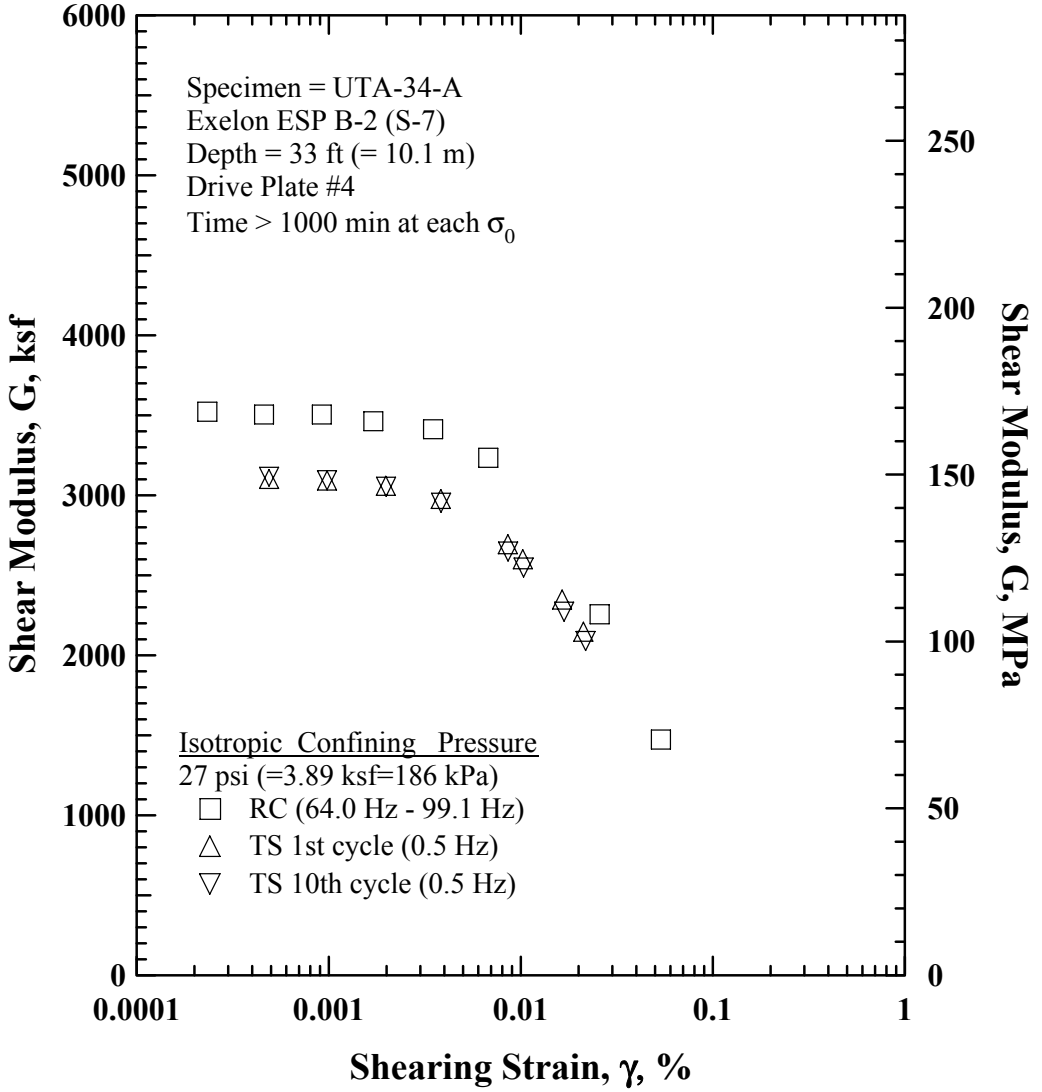

Figure B.11 Comparison of the Variation in Shear Modulus with Shearing Strain at an Isotropic Confining Pressure of 27 psi (=3.89 ksf=186 kPa) from the Combined RCTS Tests of Specimen UTA-34-A (Specimen No.1).

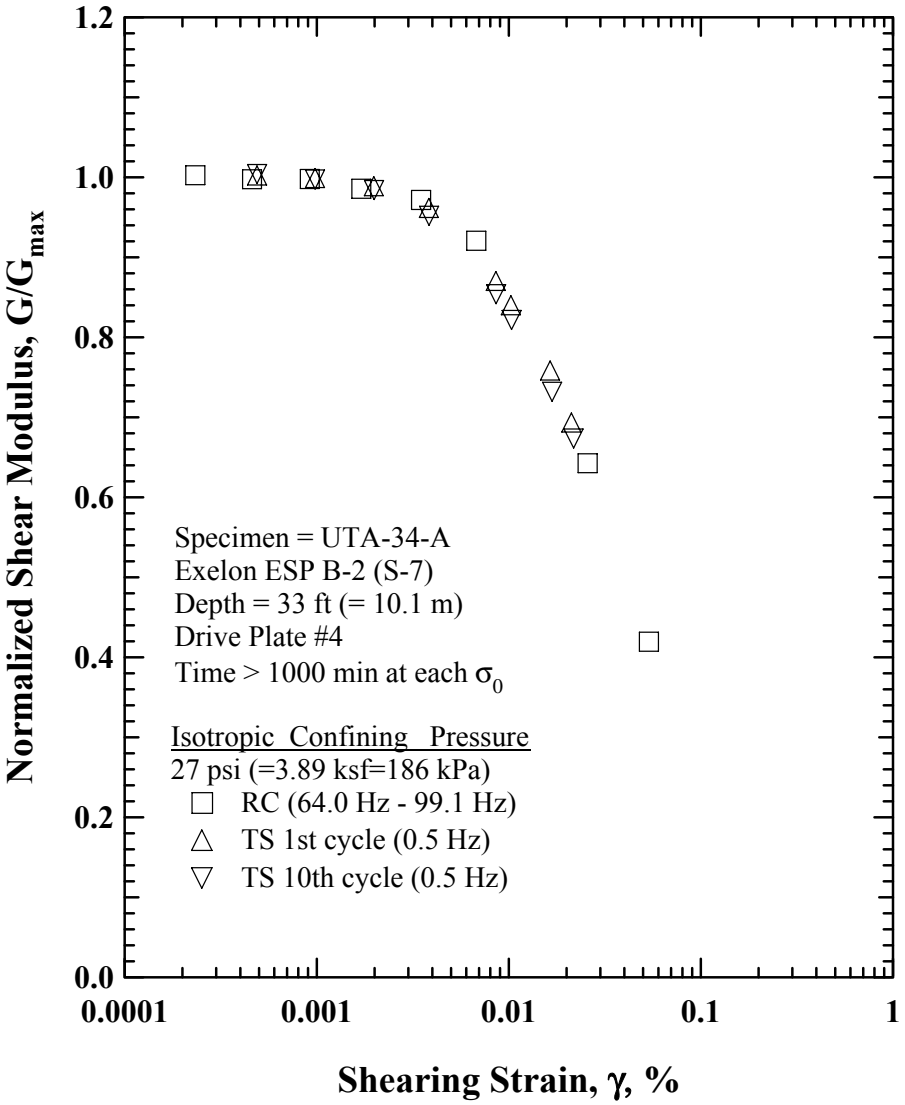

Figure B.12 Comparison of the Variation in Normalized Shear Modulus with Shearing Strain at an Isotropic Confining Pressure of 27 psi (=3.89 ksf=186 kPa) from the Combined RCTS Tests of Specimen UTA-34-A (Specimen No.1).

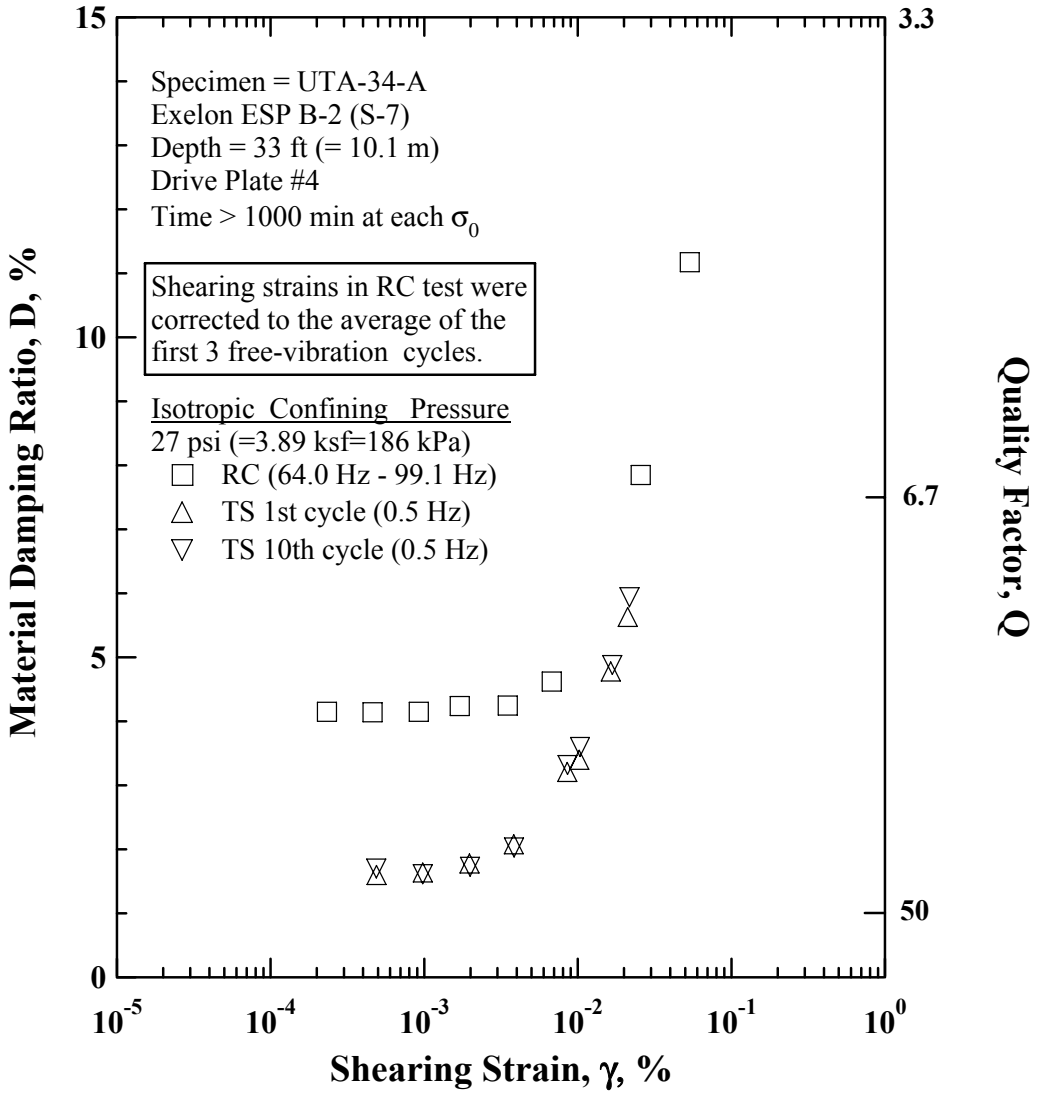

Figure B.13 Comparison of the Variation in Material Damping Ratio with Shearing Strain at an Isotropic Confining Pressure of 27 psi (=3.89 ksf=186 kPa) from the Combined RCTS Tests of Specimen UTA-34-A (Specimen No.1).

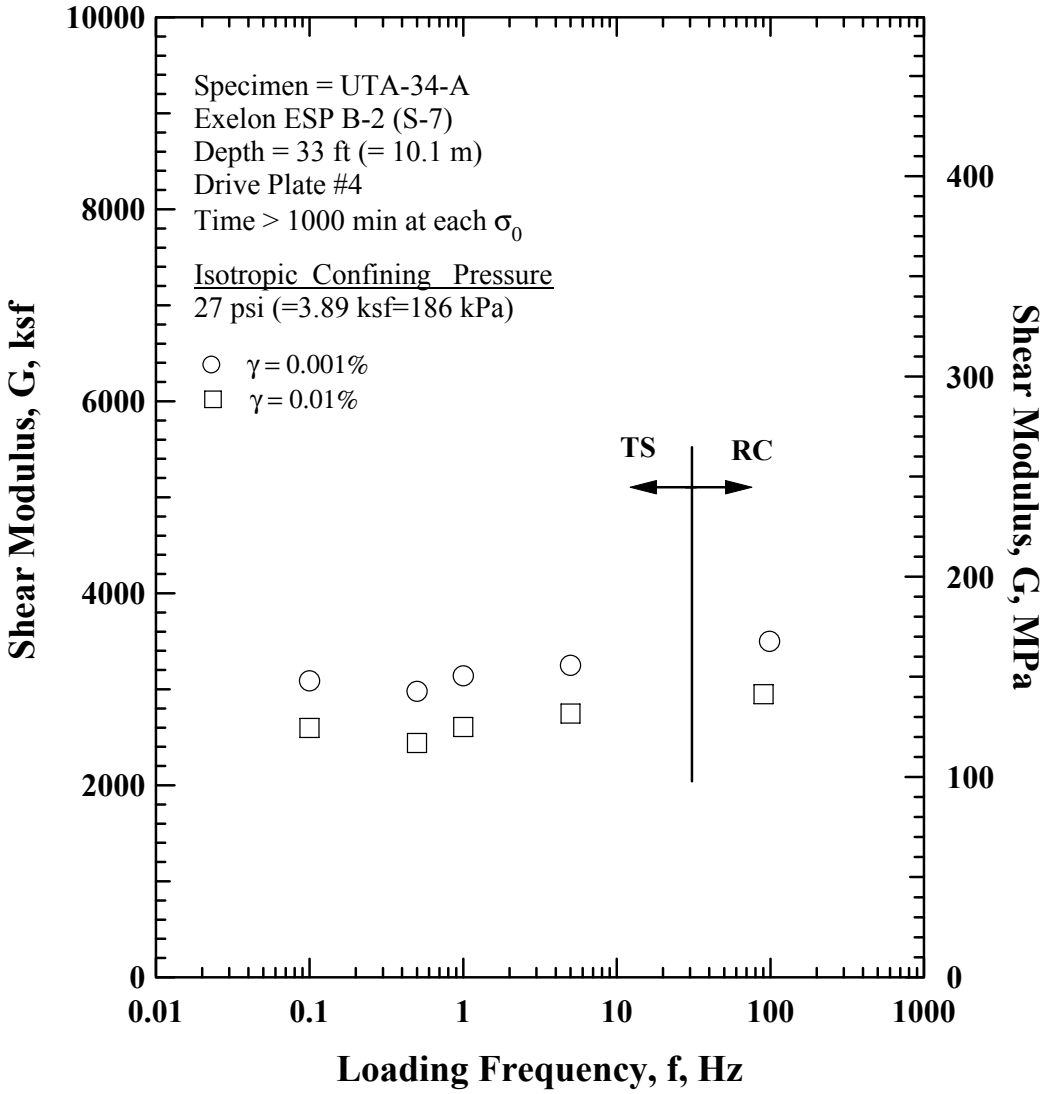

Figure B.14 Comparison of the Variation in Shear Modulus with Loading Frequency at an Isotropic Confining Pressure of 27 psi (=3.89 ksf=186 kPa) from the Combined RCTS Tests of Specimen UTA-34-A (Specimen No.1).

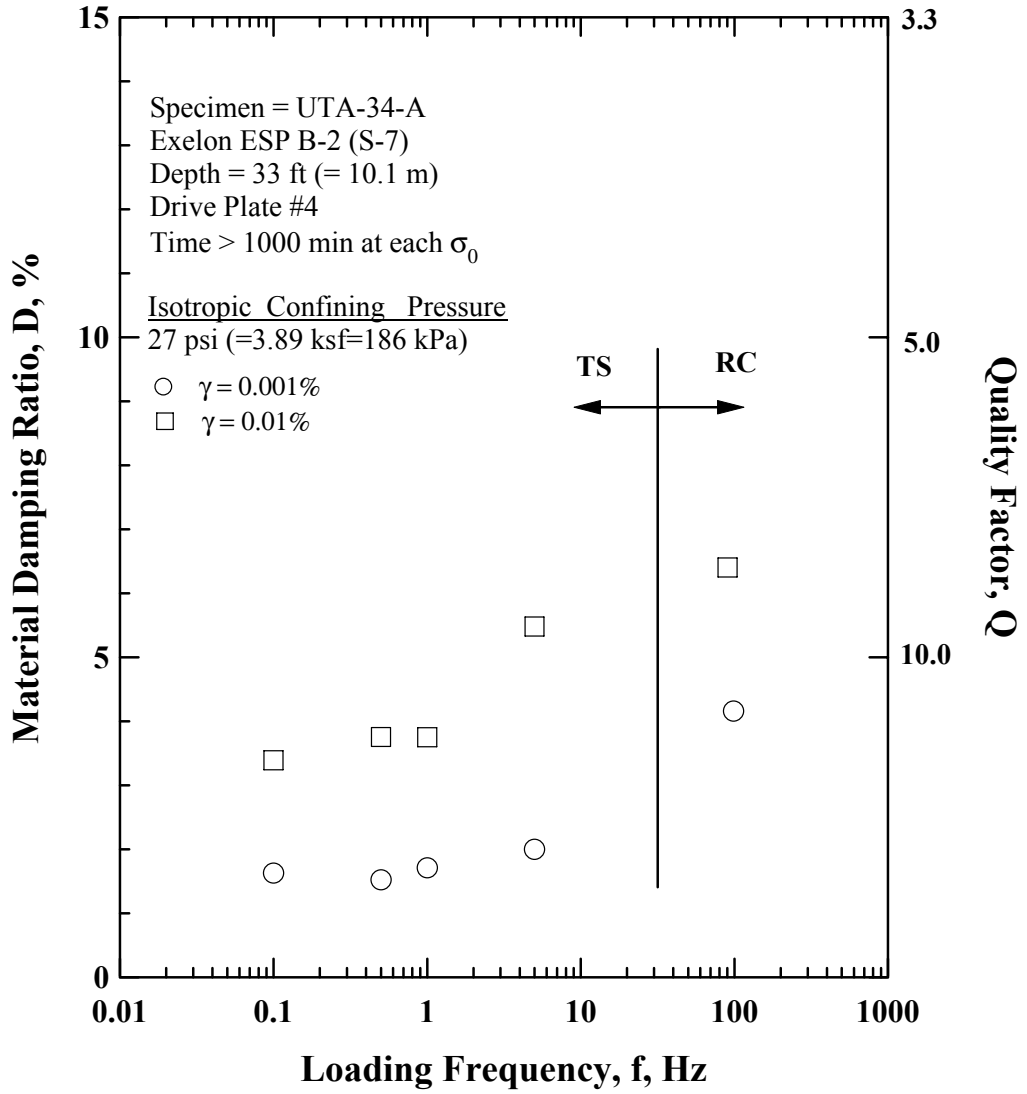

Figure B.15 Comparison of the Variation in Material Damping Ratio with Loading Frequency at an Isotropic Confining Pressure 27 psi (=3.89 ksf=186 kPa) from the Combined RCTS Tests of Specimen UTA-34-A (Specimen No.1).

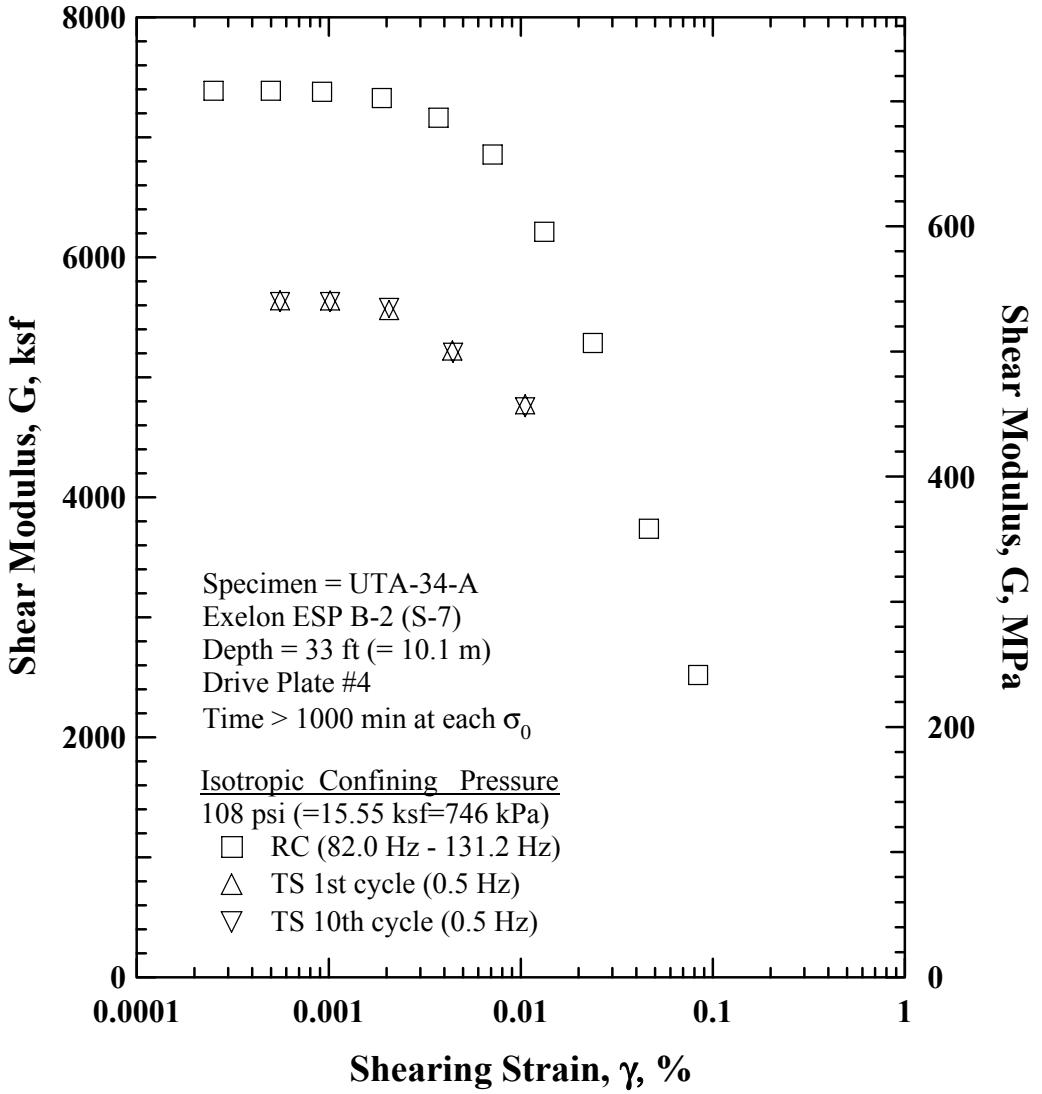

Figure B.16 Comparison of the Variation in Shear Modulus with Shearing Strain at an Isotropic Confining Pressure of 108 psi (=15.55 ksf=746 kPa) from the Combined RCTS Tests of Specimen UTA-34-A (Specimen No.1).

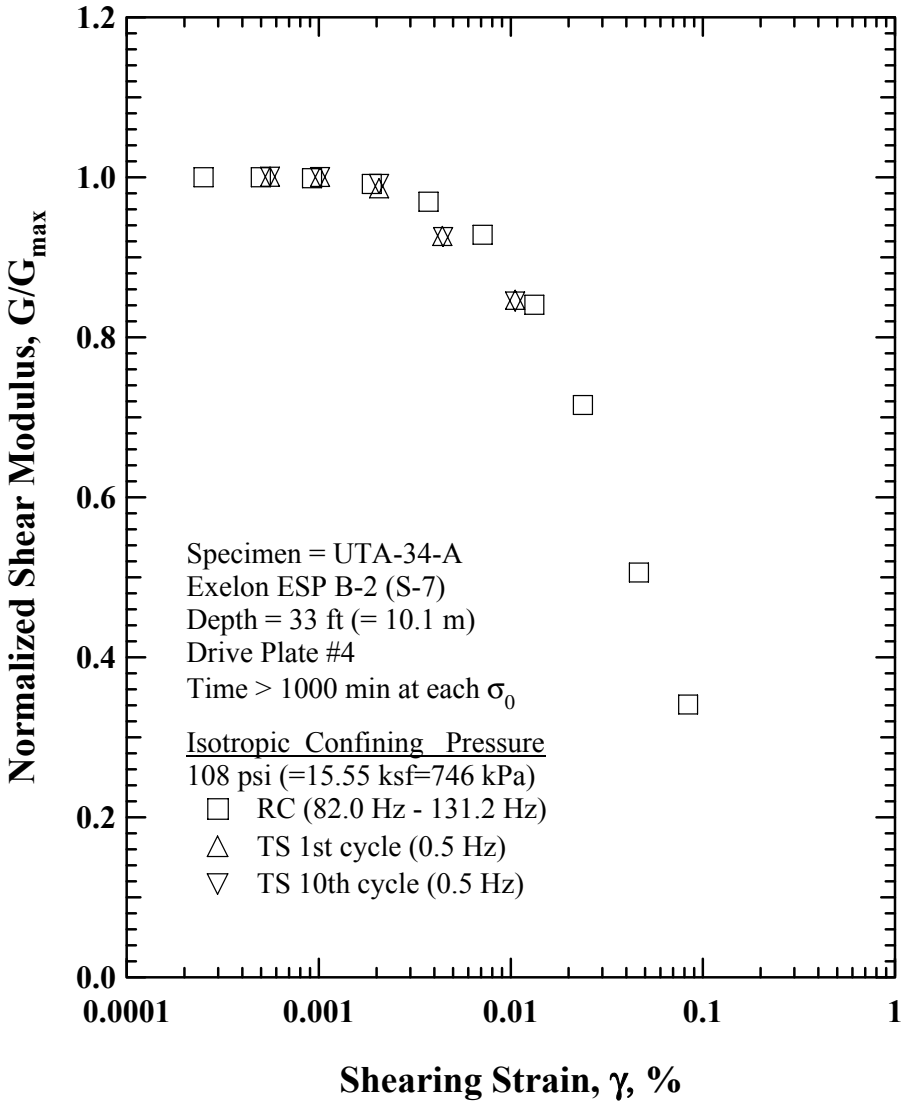

Figure B.17 Comparison of the Variation in Normalized Shear Modulus with Shearing Strain at an Isotropic Confining Pressure of 108 psi (=15.55 ksf=746 kPa) from the Combined RCTS Tests of Specimen UTA-34-A (Specimen No.1).

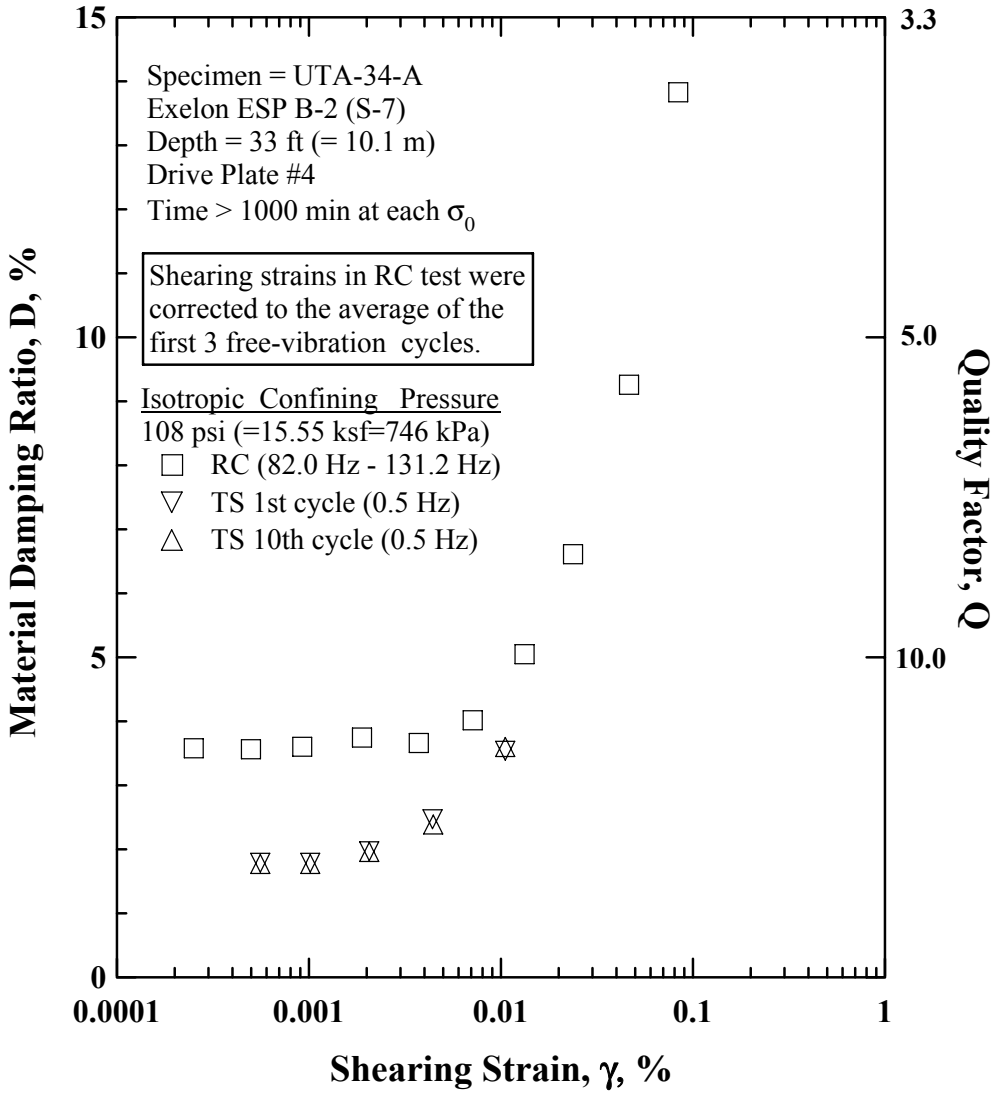

Figure B.18 Comparison of the Variation in Material Damping Ratio with Shearing Strain at an Isotropic Confining Pressure of 108 psi (=15.55 ksf=746 kPa) from the Combined RCTS Tests of Specimen UTA-34-A (Specimen No.1).

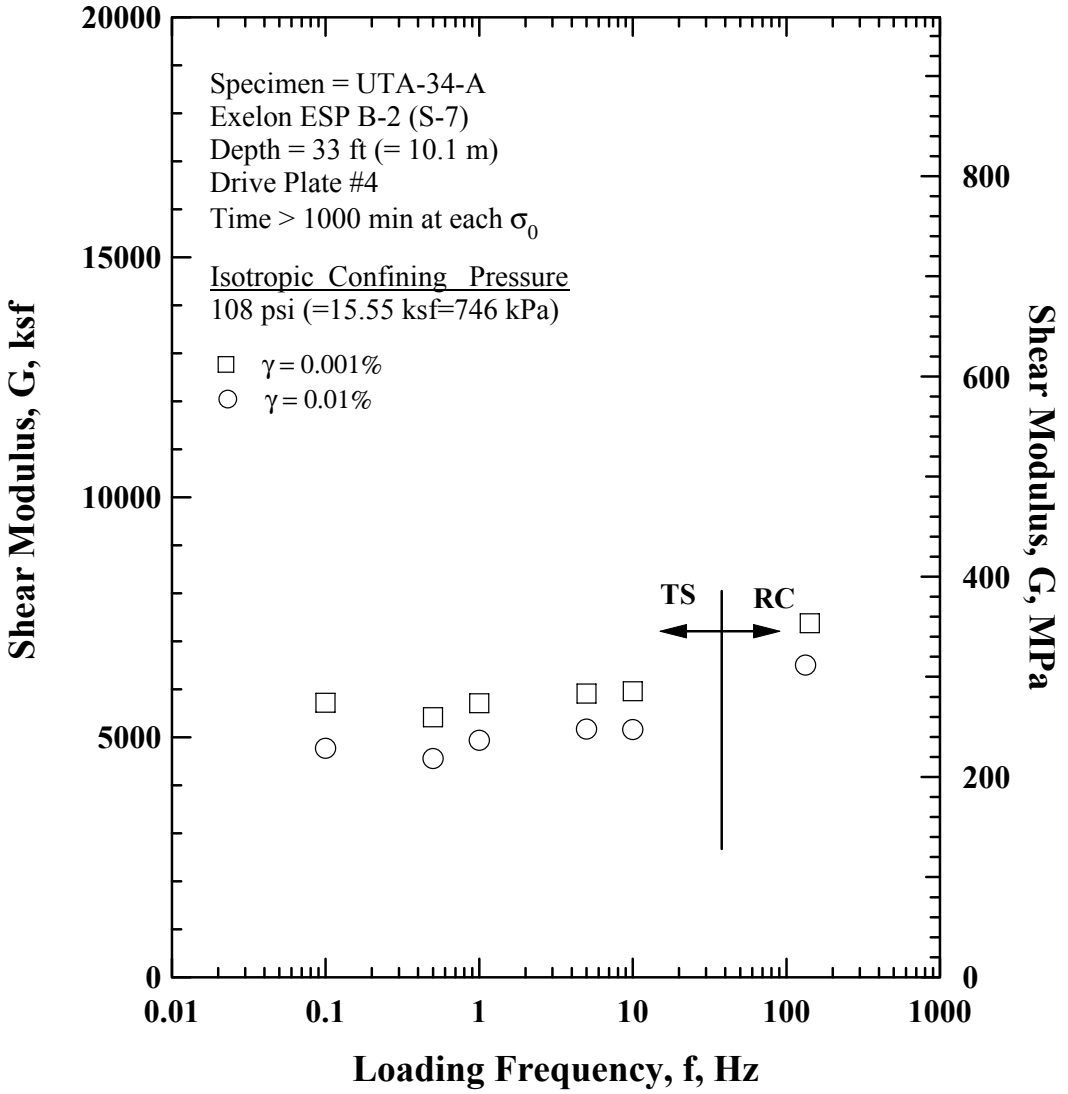

Figure B.19 Comparison of the Variation in Shear Modulus with Loading Frequency at an Isotropic Confining Pressure of 108 psi (=15.55 ksf=746 kPa) from the Combined RCTS Tests of Specimen UTA-34-A (Specimen No.1).

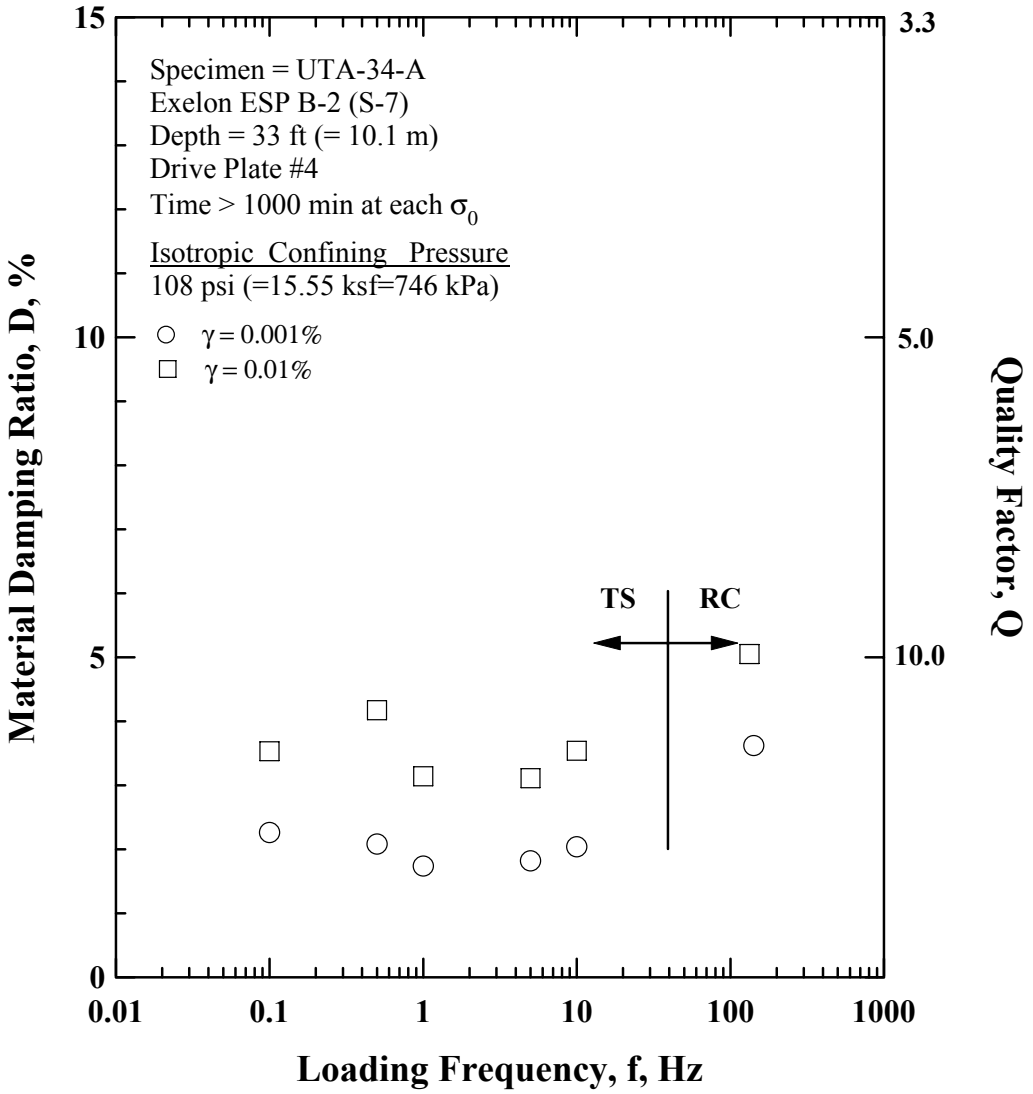

Figure B.20 Comparison of the Variation in Material Damping Ratio with Loading Frequency at an Isotropic Confining Pressure 108 psi (=15.55 ksf=746 kPa) from the Combined RCTS Tests of Specimen UTA-34-A (Specimen No.1).

Table B.1 Variation in Low-Amplitude Shear Wave Velocity, Low-Amplitude Shear Modulus, Low-Amplitude Material Damping Ratio and Estimated Void Ratio with Isotropic Confining Pressure from RC Tests of Specimen UTA-34-A.

Effective Isotropic Confining Pressure, σ_o'			Low-Amplitude Shear Modulus, G_{max}		Low-Amplitude Shear Wave Velocity, Vs	Low-Amplitude Material Damping Ratio, Dmin	Void Ratio, e
(psi)	(psf)	(kPa)	(ksf)	(MPa)	(fps)	(%)	
6	864	41	1786	85.6	636	5.19	0.34
13	1872	90	2184	104.7	703	5.17	0.34
27	3888	186	2917	139.9	811	4.57	0.33
54	7776	373	4365	209.2	989	4.08	0.32
108	15552	745.6	6098	292.4	1166	3.83	0.31

Table B.2 Variation in Shear Modulus, Normalized Shear Modulus and Material Damping Ratio with Shearing Strain from RC Tests of Specimen UTA-34-A; Isotropic Confining Pressure, σ_o =27 psi (=3.89 ksf =186 kPa).

Peak Shearing Strain, %	Shear Modulus, G, ksf	Normalized Shear Modulus, G/G_{max}	Average[+] Shearing Strain, %	Material Damping Ratio[x], D, %
0.00023278	3521.5	1.00245	0.00023278	4.14652
0.000460182	3504.3	0.997552	0.00046018	4.13927
0.000920377	3504.8	0.997694	0.00092038	4.14831
0.00170391	3462.4	0.985624	0.00170391	4.23918
0.00349335	3413.2	0.971619	0.0027391	4.24664
0.00677571	3233.6	0.920493	0.00521123	4.62261
0.0257104	2256.8	0.642432	0.0169982	7.8489
0.0535984	1473.7	0.419511	0.0310913	11.1722

[+] Average Shearing Strain from the First Three Cycles of the Free Vibration Decay Curve

[x] Average Damping Ratio from the First Three Cycles of the Free Vibration Decay Curve

Table B.3 Variation in Shear Modulus, Normalized Shear Modulus and Material Damping Ratio with Shearing Strain from TS Tests of Specimen UTA-34-A;Isotropic Confining Pressure, σ_o =27 psi (=3.89 ksf =186 kPa).

First Cycle				Tenth Cycle			
Peak Shearing Strain, %	Shear Modulus, G, ksf	Normalized Shear Modulus, G/G_{max}	Material Damping Ratio, D, %	Peak Shearing Strain, %	Shear Modulus, G, ksf	Normalized Shear Modulus, G/G_{max}	Material Damping Ratio, D, %
4.92E-04	3099	1.00	1.59	4.91E-04	3112	1.00	1.69
9.86E-04	3089	1.00	1.63	9.86E-04	3090	1.00	1.60
1.99E-03	3057	0.99	1.77	2.00E-03	3050	0.98	1.72
3.85E-03	2973	0.96	2.07	3.87E-03	2950	0.95	2.02
8.61E-03	2691	0.87	3.20	8.63E-03	2646	0.85	3.31
1.03E-02	2597	0.84	3.39	1.04E-02	2546	0.82	3.59
1.65E-02	2345	0.76	4.77	1.69E-02	2268	0.73	4.87
2.13E-02	2144	0.69	5.62	2.19E-02	2086	0.67	5.93

Table B.4 Variation in Shear Modulus, Normalized Shear Modulus and Material Damping Ratio with Shearing Strain from RC Tests of Specimen UTA-34-A; Isotropic Confining Pressure, σ_o =108 psi (=15.55 ksf =746 kPa).

Peak Shearing Strain, %	Shear Modulus, G, ksf	Normalized Shear Modulus, G/G_{max}	Average[+] Shearing Strain, %	Material Damping Ratio[x], D, %
2.51E-04	7388	1.00	2.51E-04	3.58
4.99E-04	7388	1.00	4.99E-04	3.56
9.22E-04	7379	1.00	9.22E-04	3.60
1.89E-03	7326	0.99	1.89E-03	3.74
3.72E-03	7163	0.97	3.01E-03	3.66
7.12E-03	6857	0.93	5.65E-03	4.02
1.33E-02	6212	0.84	9.99E-03	5.05
2.37E-02	5286	0.72	1.66E-02	6.61
4.65E-02	3738	0.51	2.90E-02	9.26
8.37E-02	2518	0.34	4.44E-02	13.83

[+] Average Shearing Strain from the First Three Cycles of the Free Vibration Decay Curve

[x] Average Damping Ratio from the First Three Cycles of the Free Vibration Decay Curve

Table B.5 Variation in Shear Modulus, Normalized Shear Modulus and Material Damping Ratio with Shearing Strain from TS Tests of Specimen UTA-34-A; Isotropic Confining Pressure, σ_o =108 psi (=15.55 ksf =746 kPa).

First Cycle				Tenth Cycle			
Peak Shearing Strain, %	Shear Modulus, G, ksf	Normalized Shear Modulus, G/G_{max}	Material Damping Ratio, D, %	Peak Shearing Strain, %	Shear Modulus, G, ksf	Normalized Shear Modulus, G/G_{max}	Material Damping Ratio, D, %
5.60E-04	5637	1.00	1.78	5.60E-04	5623	1.00	1.76
1.02E-03	5635	1.00	1.78	1.02E-03	5622	1.00	1.76
2.07E-03	5556	0.99	1.96	2.07E-03	5572	0.99	1.95
4.43E-03	5219	0.93	2.46	4.46E-03	5200	0.92	2.38
1.06E-02	4771	0.85	3.53	1.06E-02	4746	0.84	3.59

Exhibit C
to Attachment A-7

Specimen No.2
UTA-34-B

Exelon ESP B-3(S-13)
Depth = 41.5ft (=12.7m)
Soil Type: Sandy Lean Clay (CL)

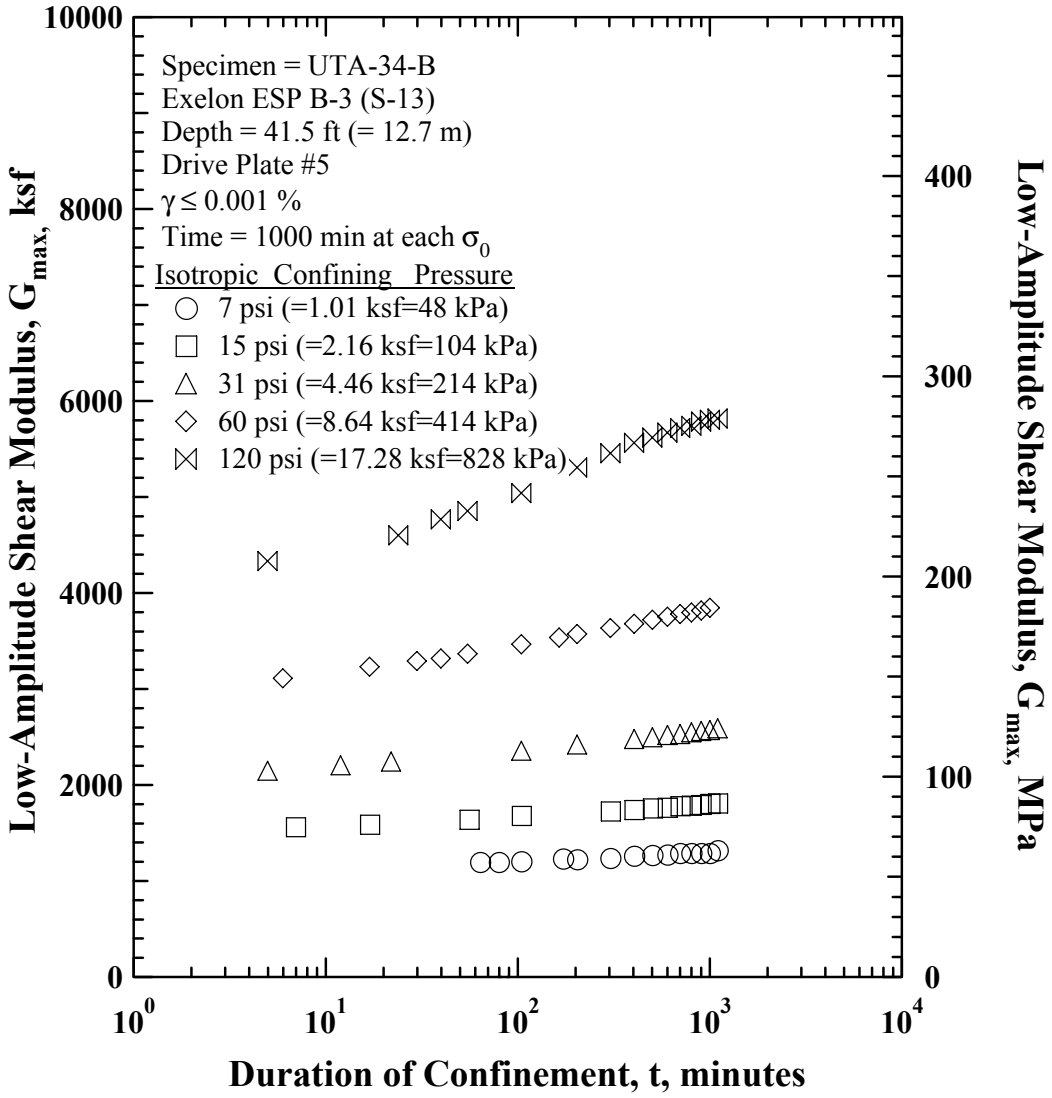

Figure C.1 Variation in Low-Amplitude Shear Modulus with Magnitude and Duration of Isotropic Confining Pressure from Resonant Column Tests of Specimen UTA-34-B (Specimen No.2).

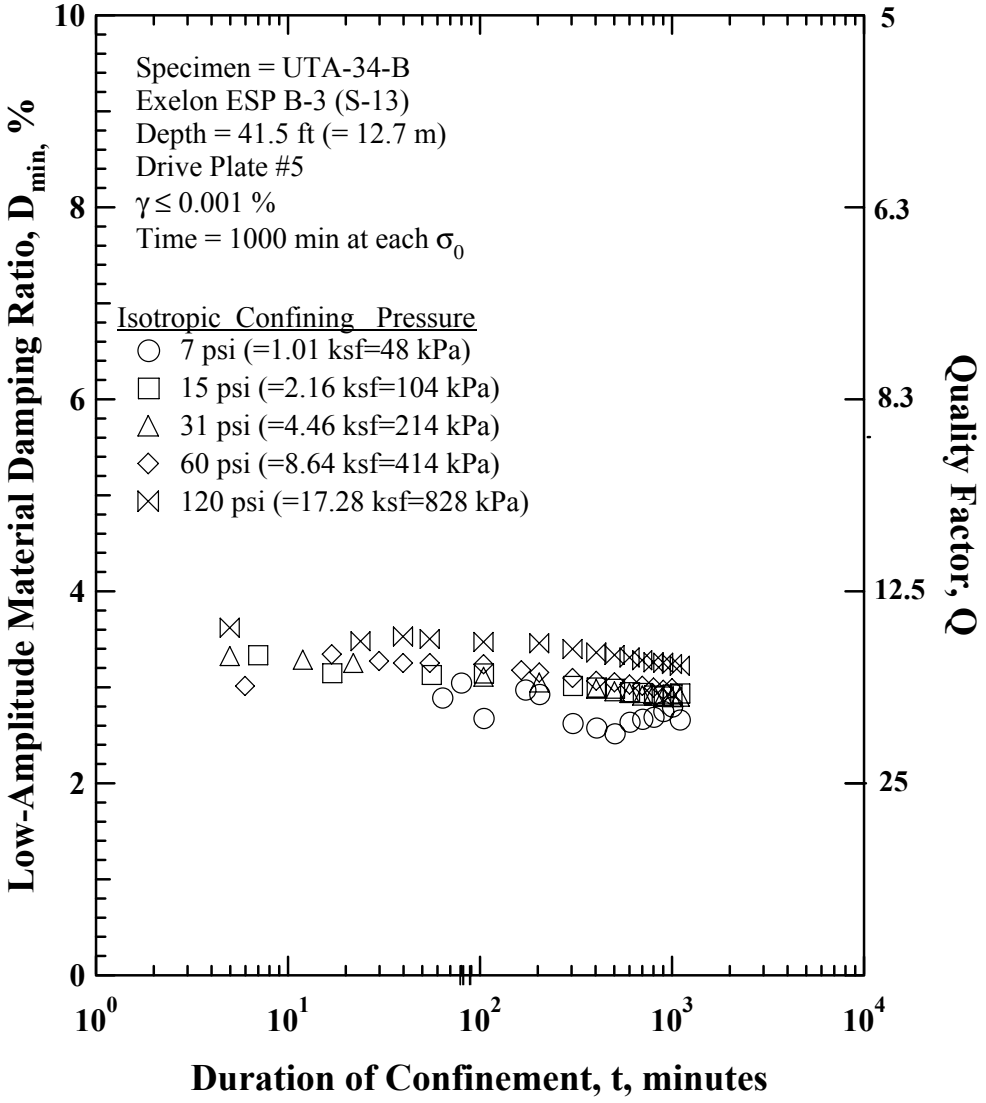

Figure C.2 Variation in Low-Amplitude Material Damping Ratio with Magnitude and Duration of Isotropic Confining Pressure from Resonant Column Tests of Specimen UTA-34-B (Specimen No.2).

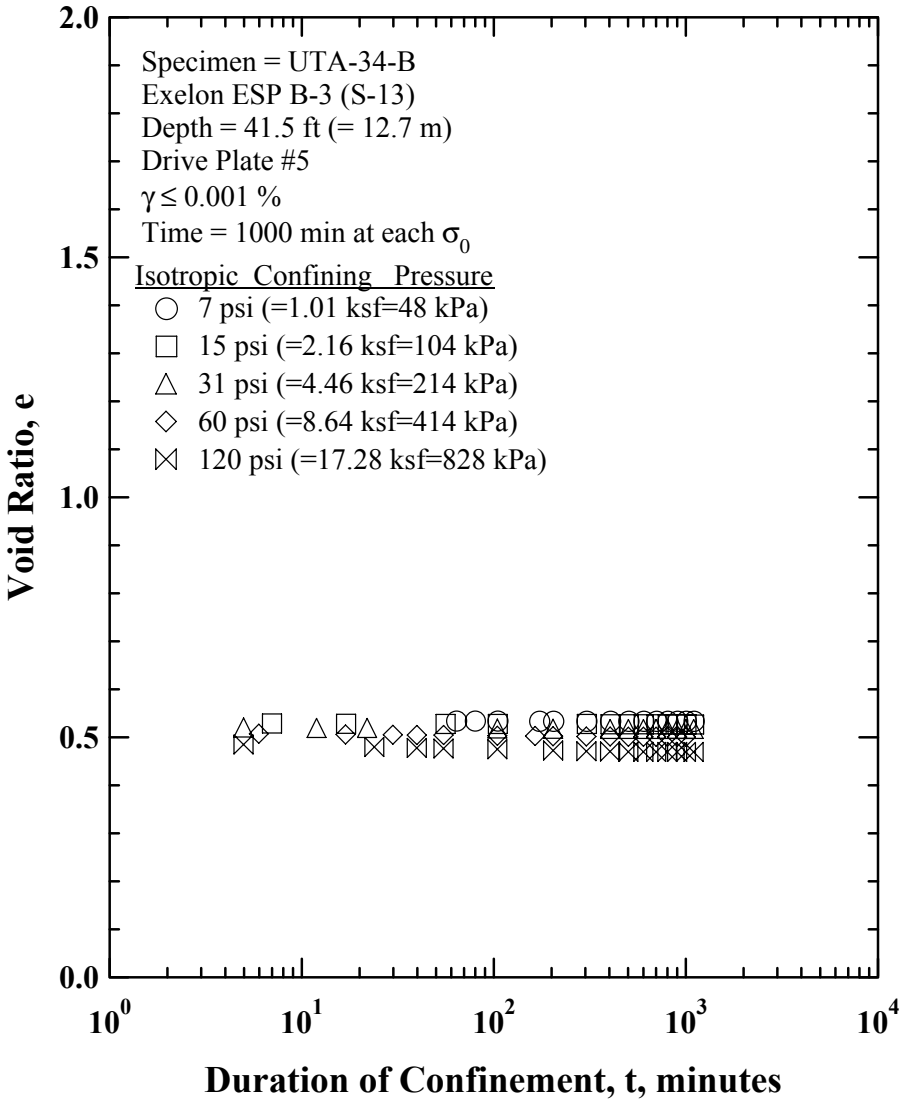

Figure C.3 Variation in Estimated Void Ratio with Magnitude and Duration of Isotropic Confining Pressure from Resonant Column Tests of Specimen UTA-34-B (Specimen No.2).

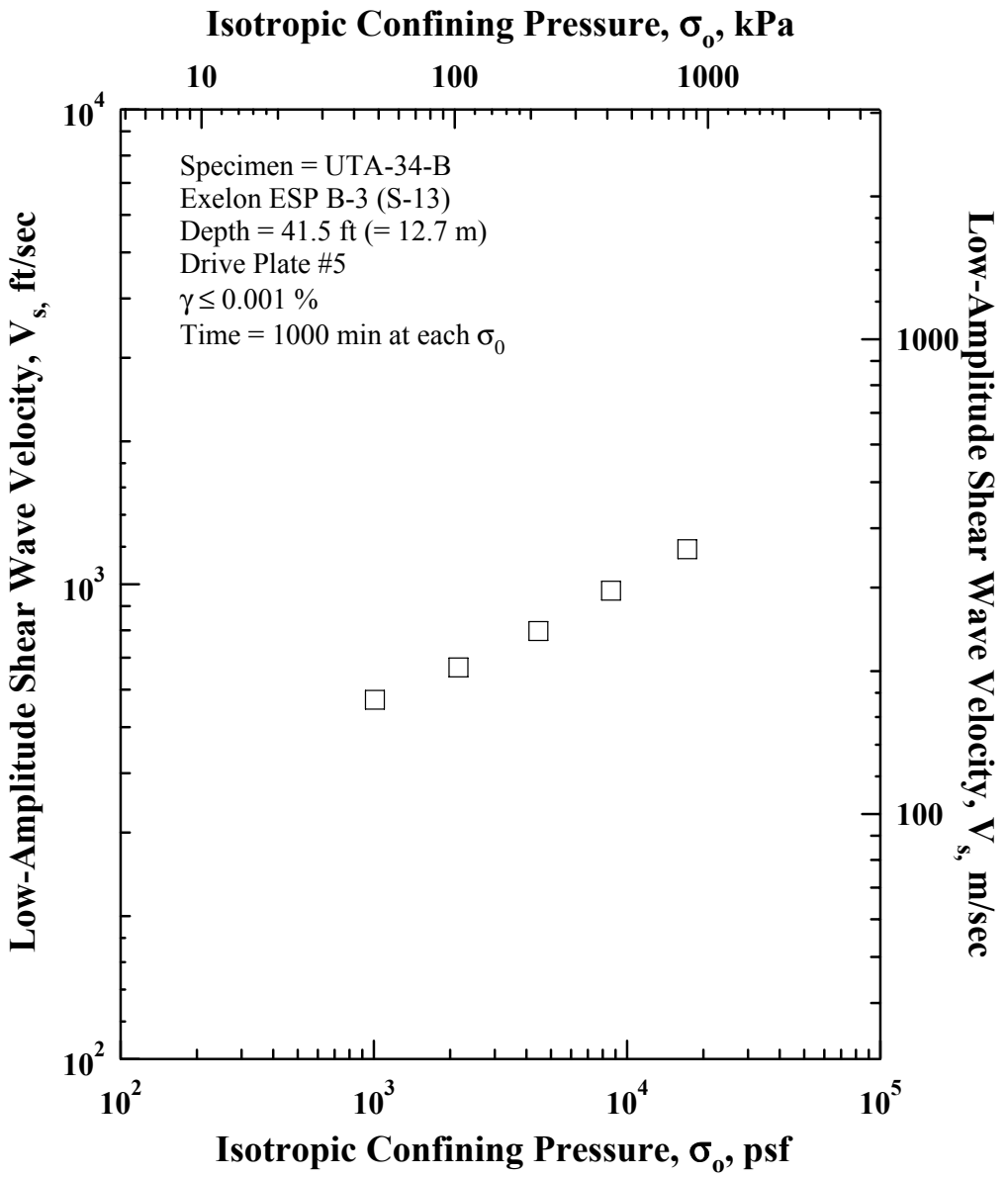

Figure C.4 Variation in Shear Wave Velocity with Isotropic Confining Pressure from Resonant Column Tests of Specimen UTA-34-B (Specimen No.2).

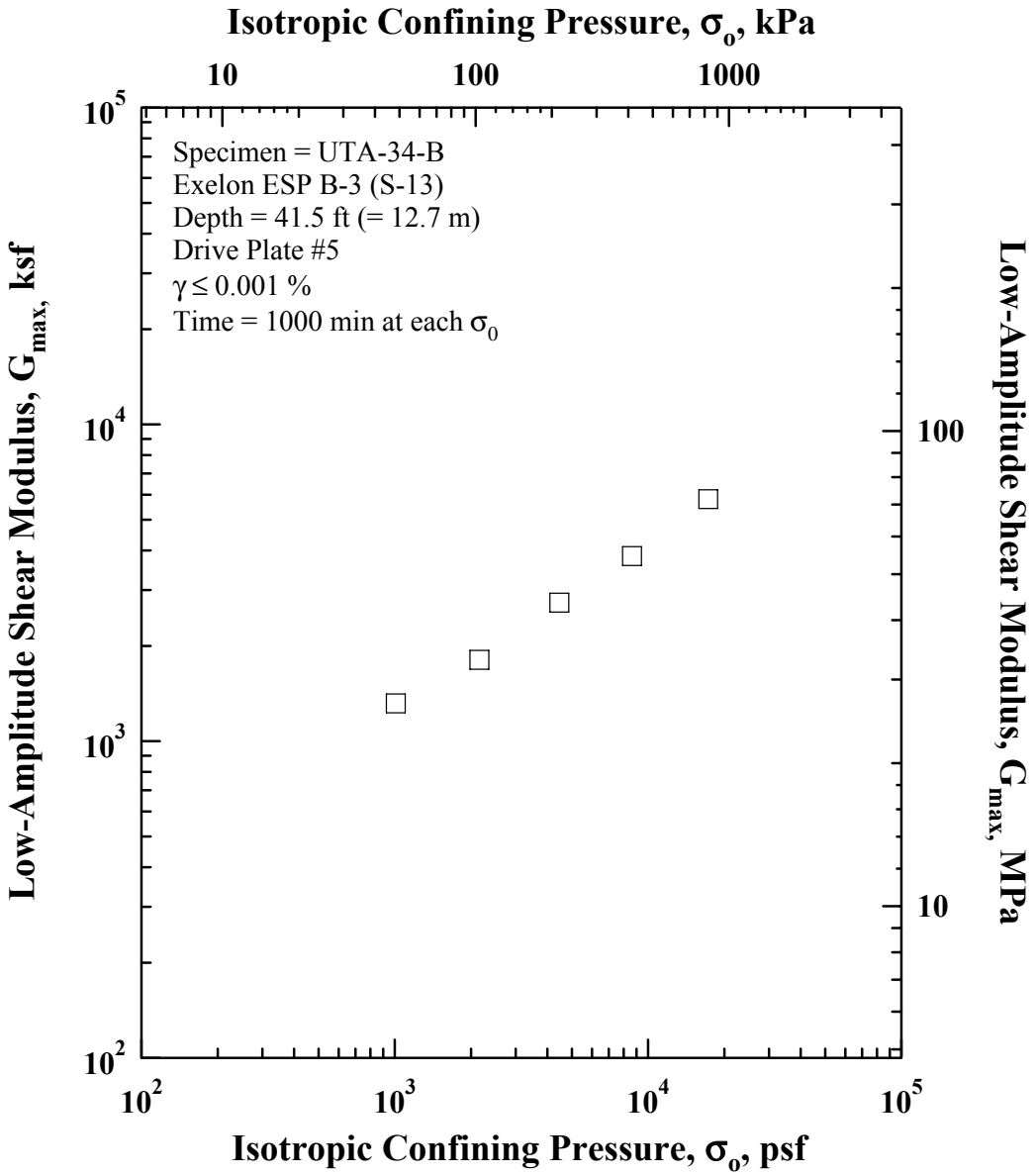

Figure C.5 Variation in Low-Amplitude Shear Modulus with Isotropic Confining Pressure from Resonant Column Tests of Specimen UTA-34-B (Specimen No.2).

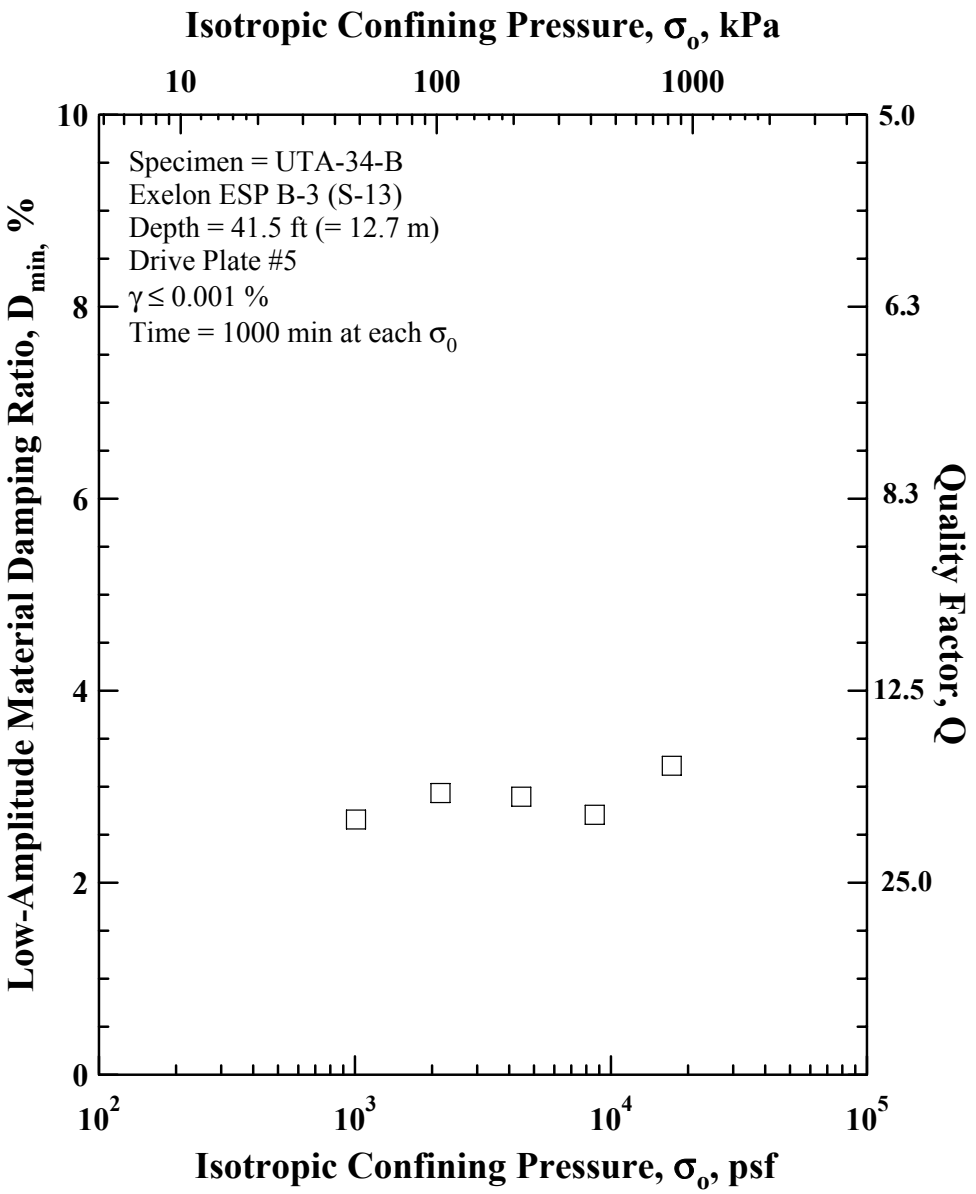

Figure C.6 Variation in Material Damping Ratio with Isotropic Confining Pressure from Resonant Column Tests of Specimen UTA-34-B (Specimen No.2).

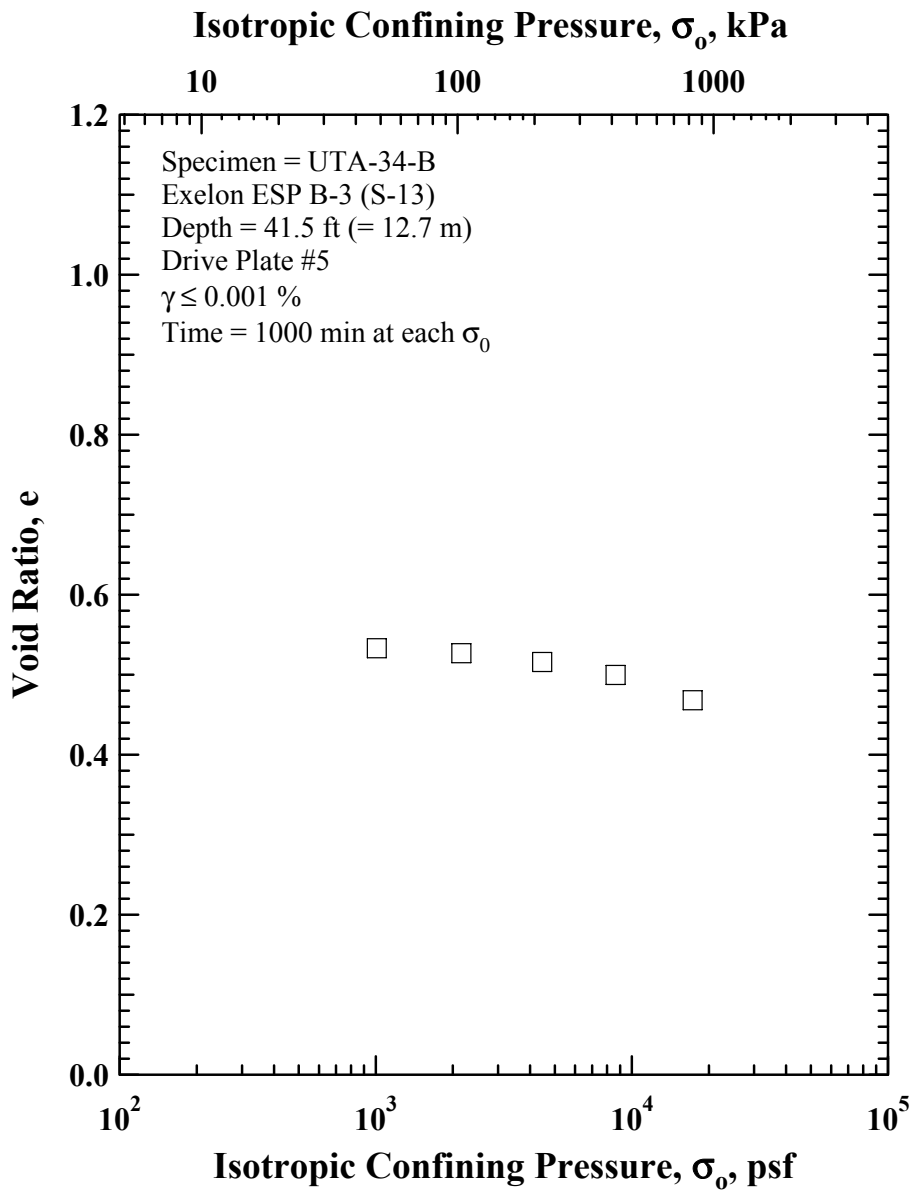

Figure C.7 Variation in Estimated Void Ratio with Isotropic Confining Pressure from Resonant Column Tests of Specimen UTA-34-B (Specimen No.2).

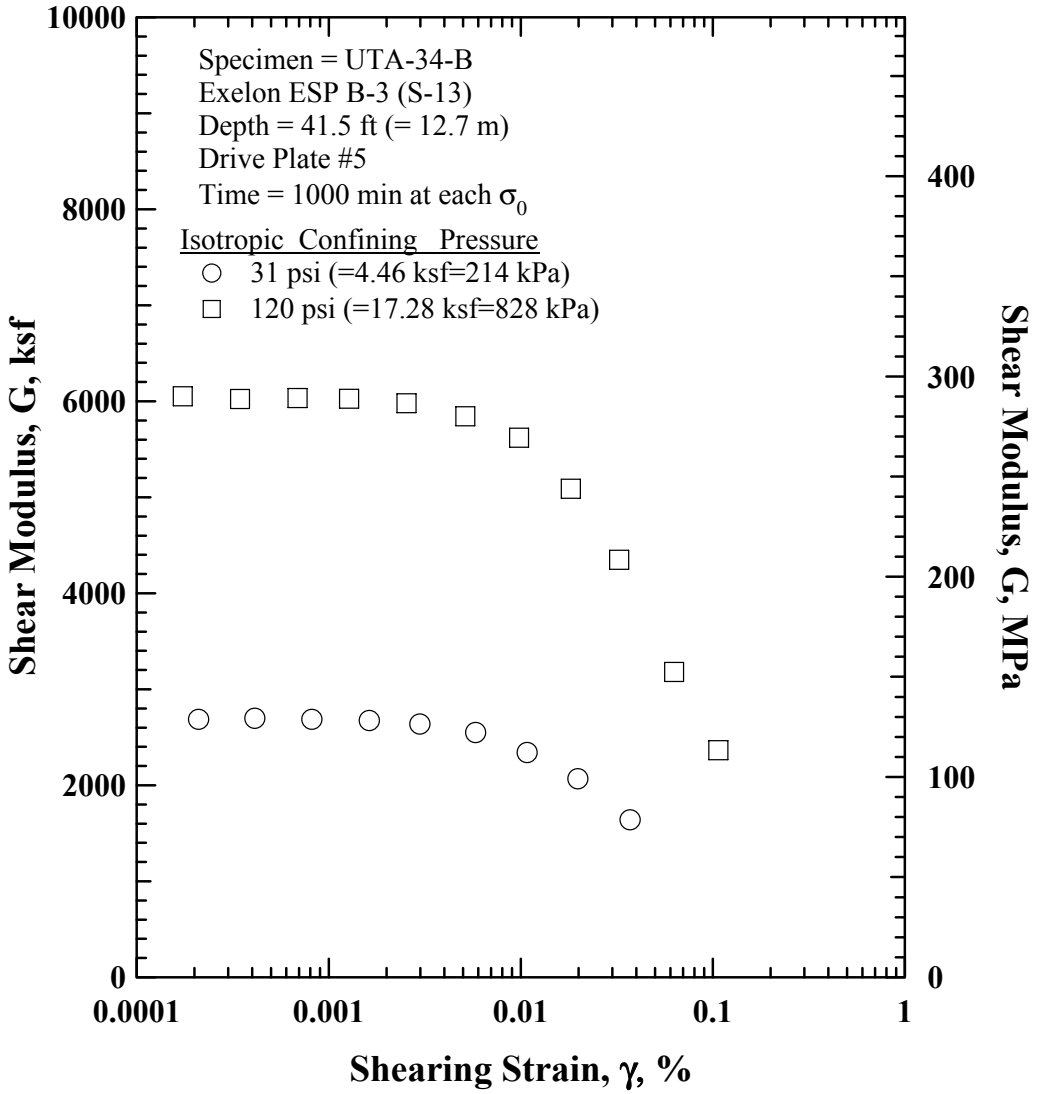

Figure C.8 Comparison of the Variation in Shear Modulus with Shearing Strain and Isotropic Confining Pressure from the Resonant Column Tests of Specimen UTA-34-B (Specimen No.2).

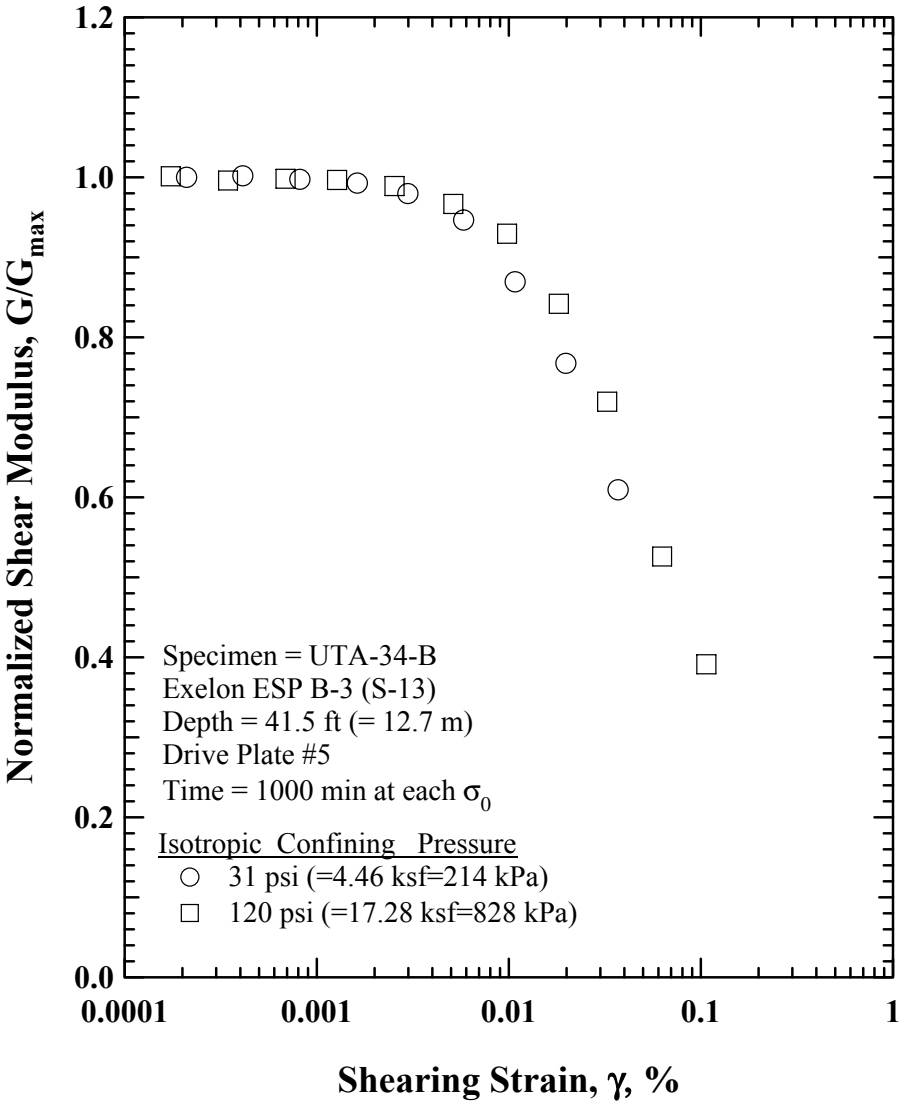

Figure C.9 Comparison of the Variation in Normalized Shear Modulus with Shearing Strain and Isotropic Confining Pressure from the Resonant Column Tests of Specimen UTA-34-B (Specimen No.2).

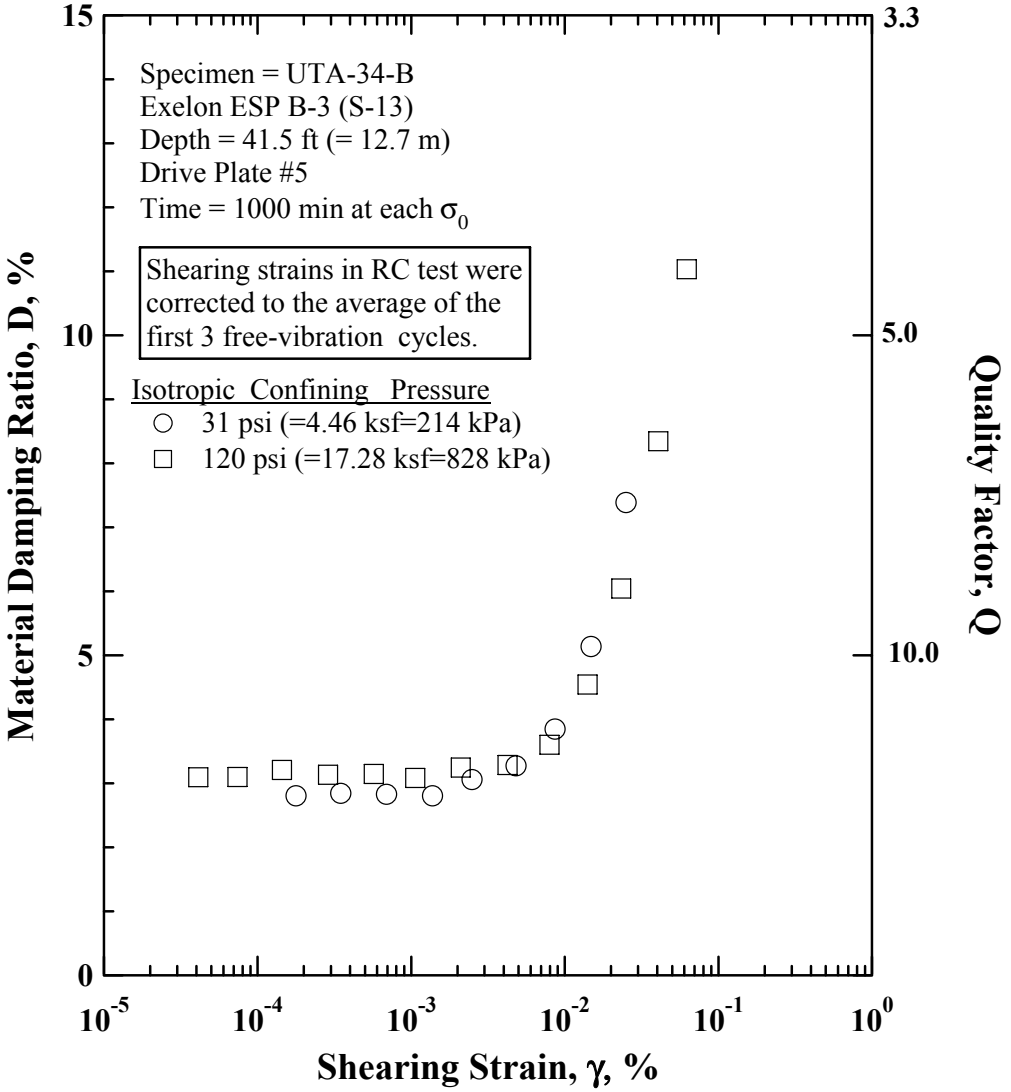

Figure C.10 Comparison of the Variation in Material Damping with Shearing Strain and Isotropic Confining Pressure from the Resonant Column Tests of Specimen UTA-34-B (Specimen No.2).

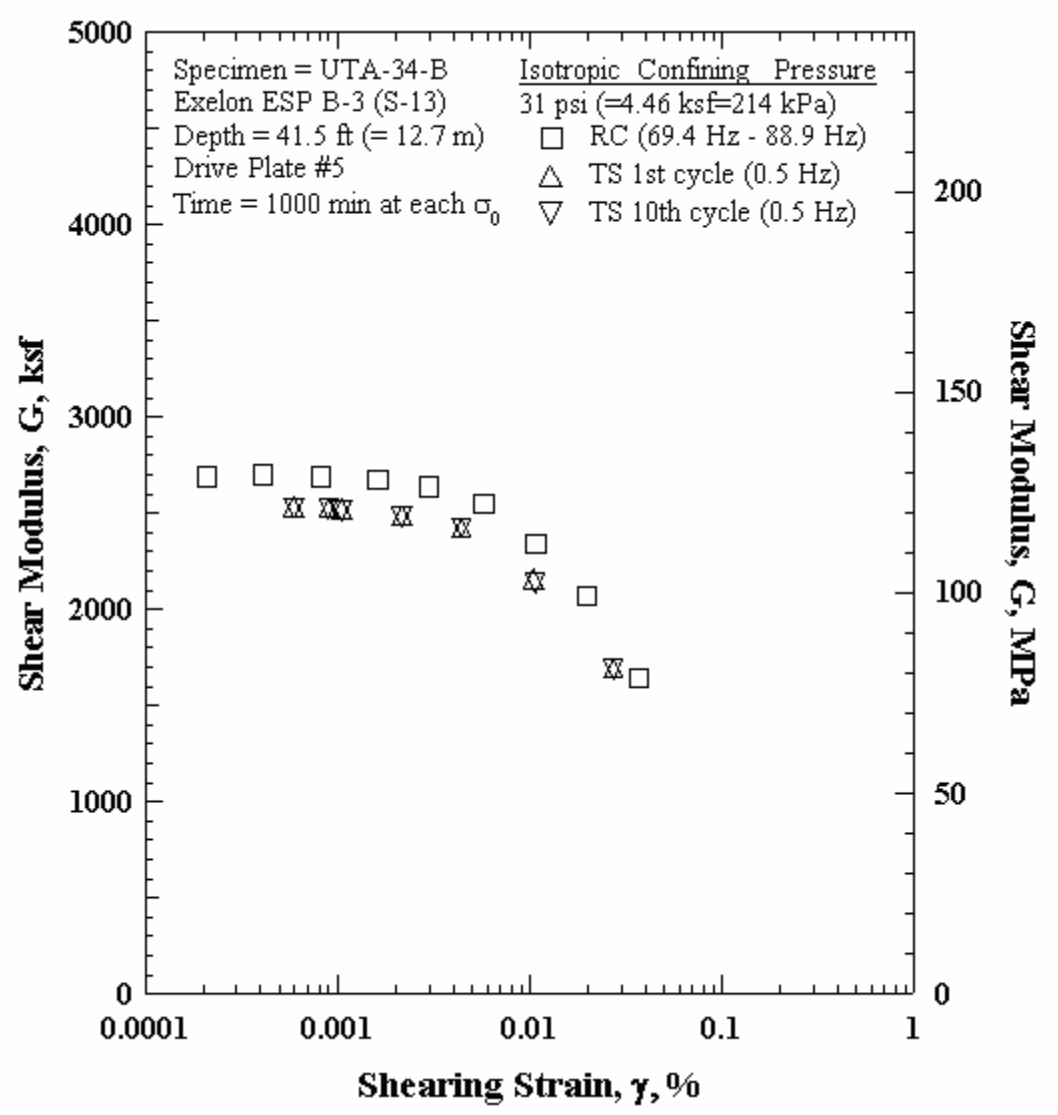

Figure C.11 Comparison of the Variation in Shear Modulus with Shearing Strain at an Isotropic Confining Pressure of 31 psi(=4.46 ksf=214 kPa)from the Combined RCTS Tests of UTA-34-B (Specimen No.2).

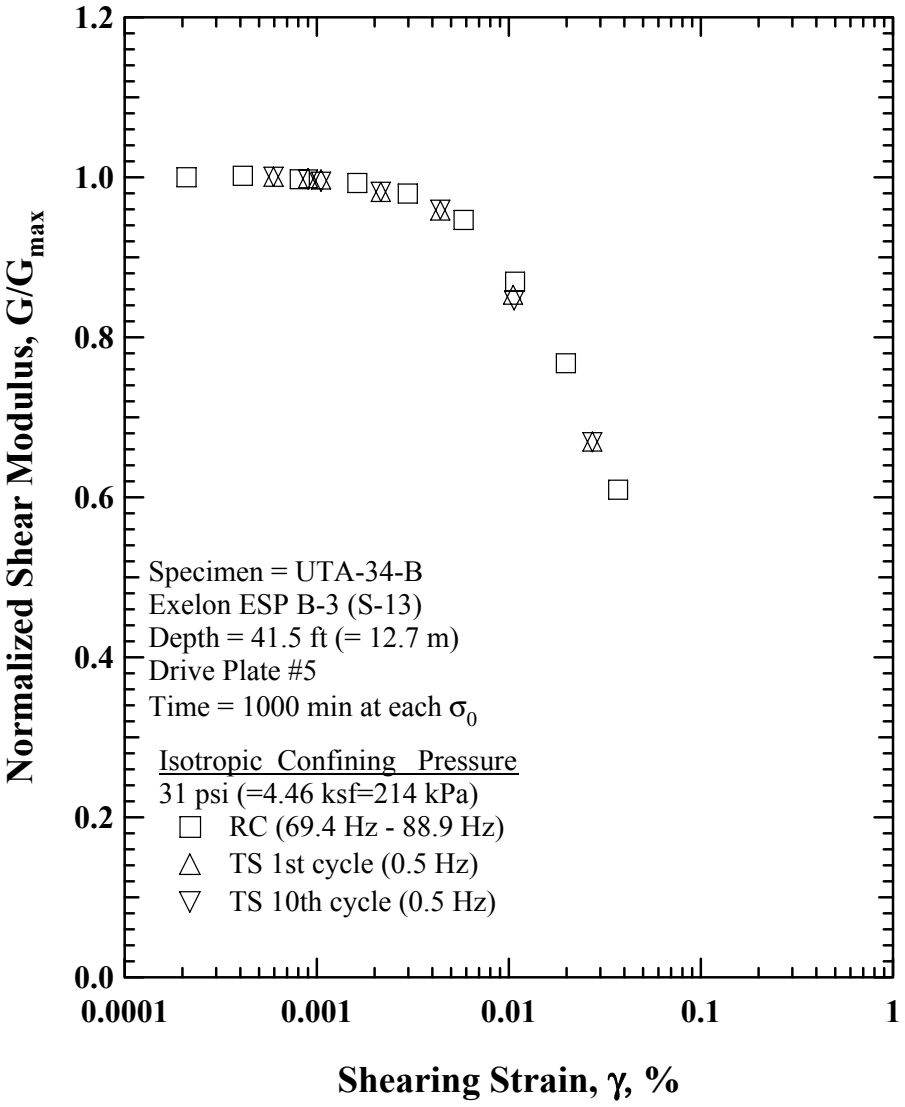

Figure C.12Comparison of the Variation in Normalized Shear Modulus with Shearing Strain at an Isotropic Confining Pressure of 31 psi(=4.46 ksf=214 kPa)from the Combined RCTS Tests of Specimen UTA-34-B (Specimen No.2).

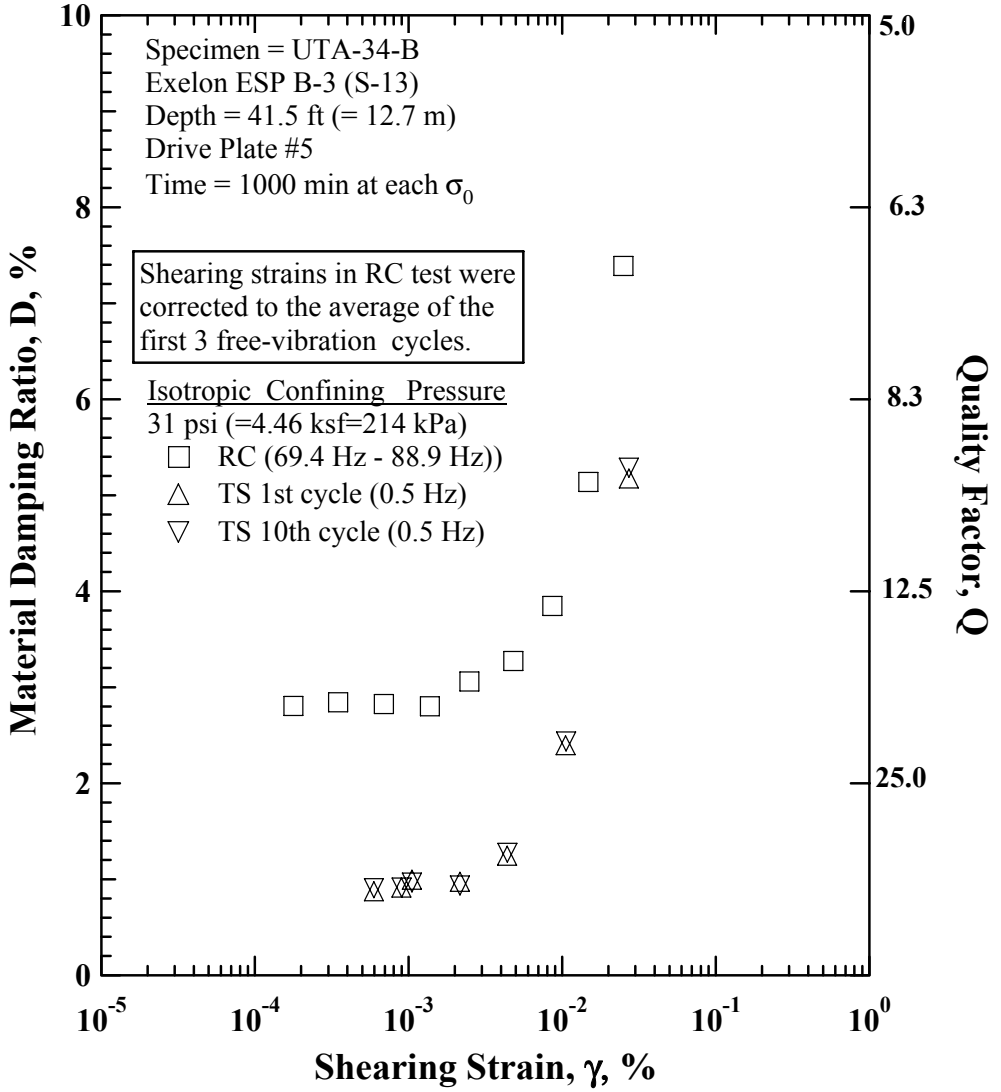

Figure C.13 Comparison of the Variation in Material Damping with Shearing Strain at an Isotropic Confining Pressure of 31 psi(=4.46 ksf=214 kPa)from the Combined RCTS Tests of Specimen UTA-34-B (Specimen No.2).

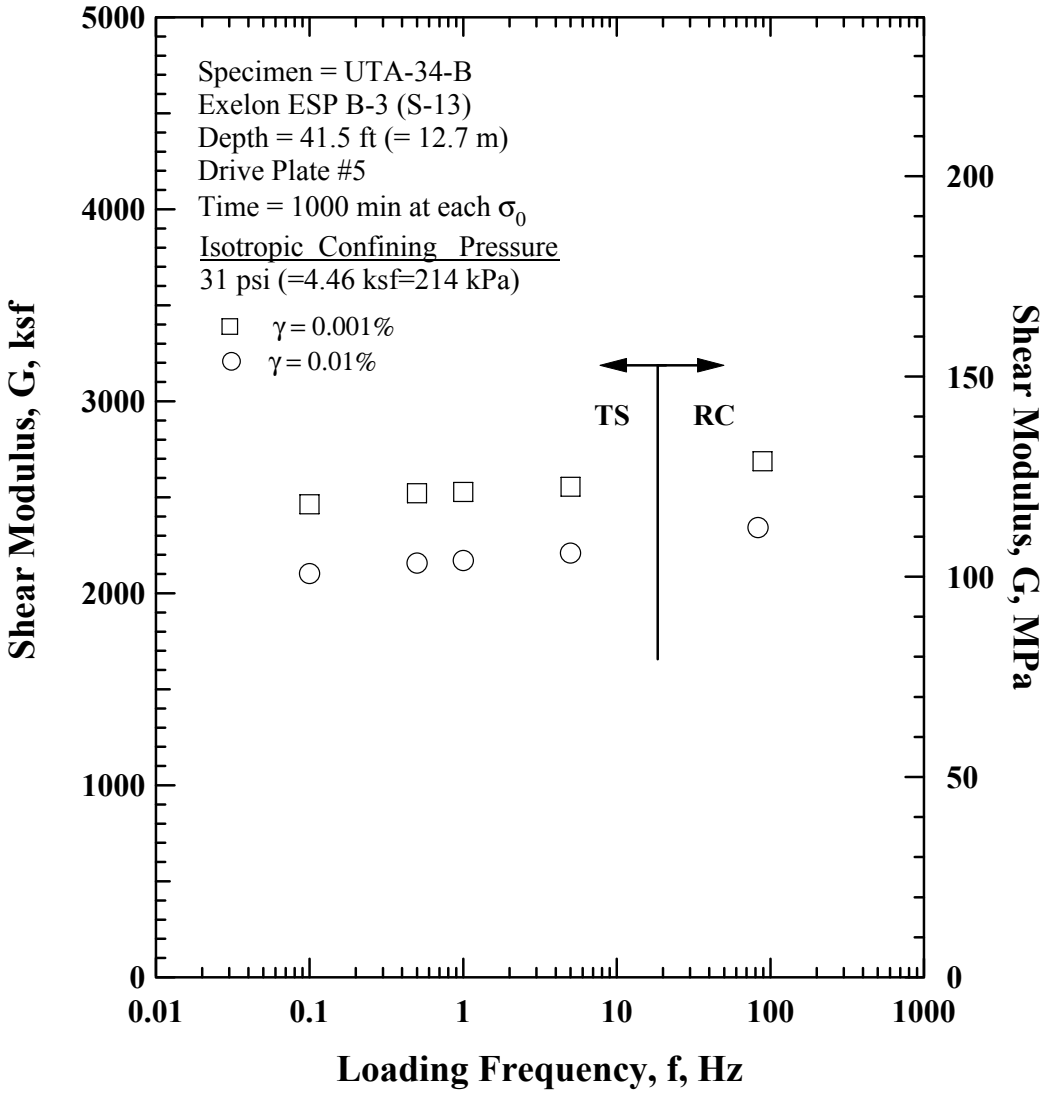

Figure C.14 Comparison of the Variation in Shear Modulus with Loading Frequency at an Isotropic Confining Pressure of 31 psi(=4.46 ksf=214 kPa)from the Combined RCTS Tests of Specimen UTA-34-B (Specimen No.2).

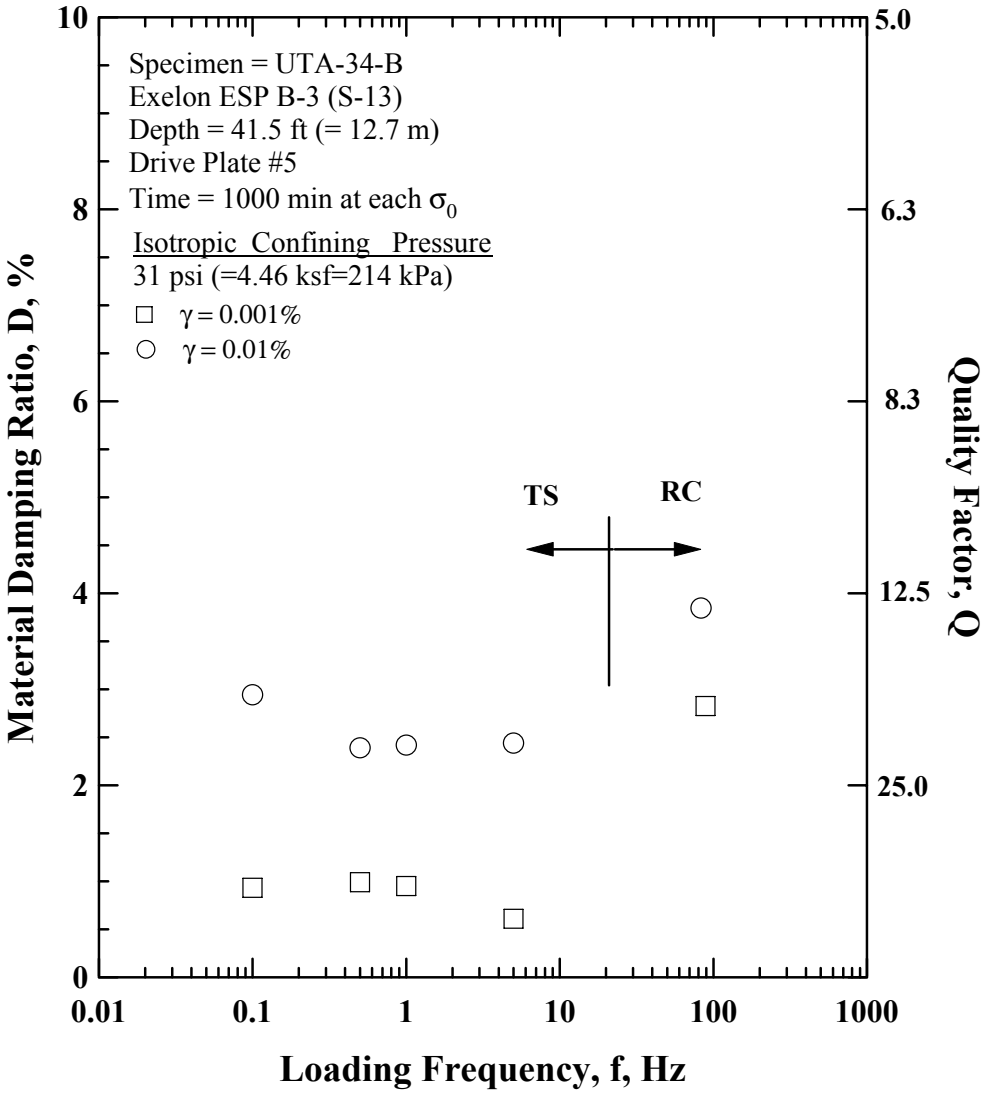

Figure C.15 Comparison of the Variation in Material Damping with Loading Frequency at an Isotropic Confining Pressure of 31 psi(=4.46 ksf=214 kPa)from the Combined RCTS Tests of Specimen UTA-34-B (Specimen No.2).

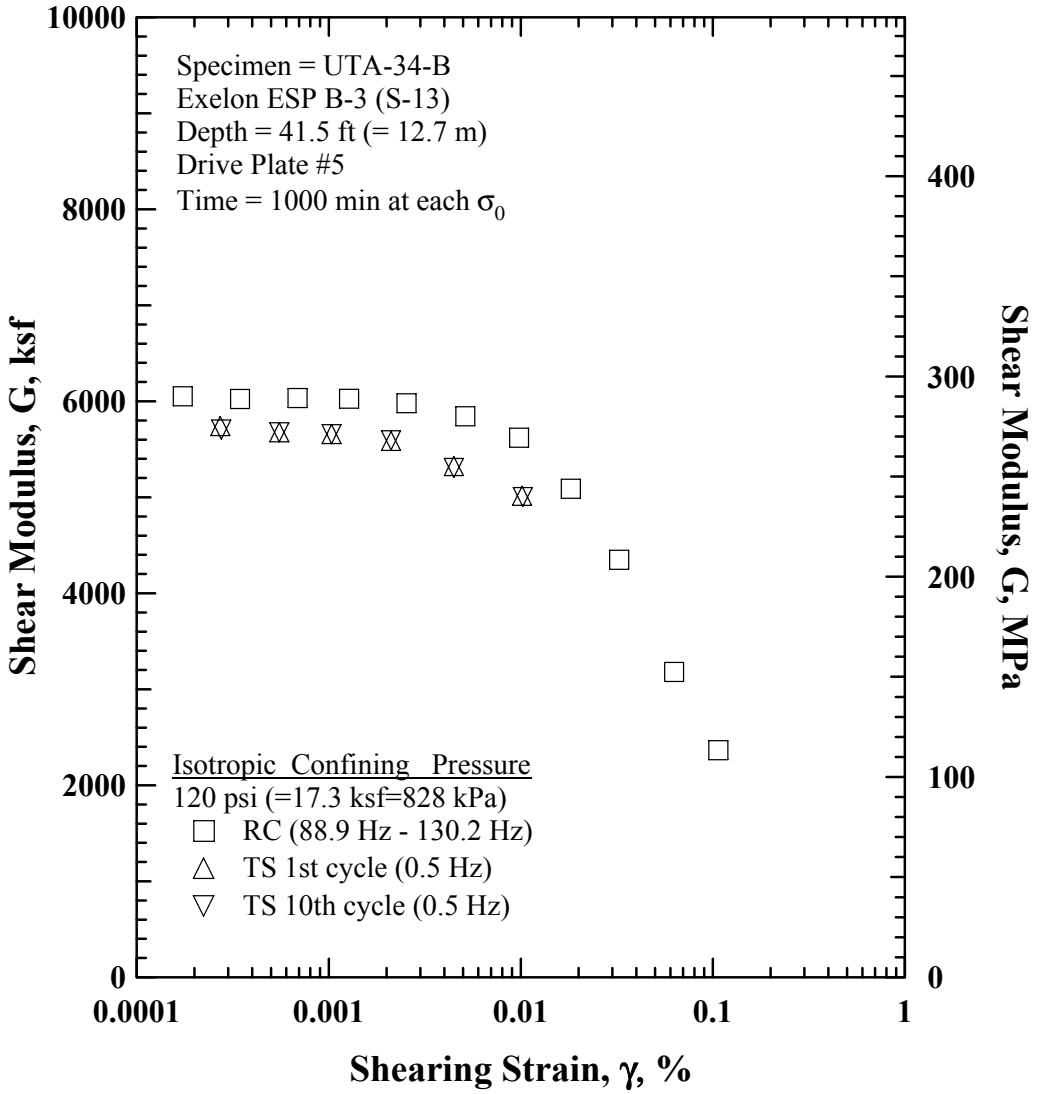

Figure C.16 Comparison of the Variation in Shear Modulus with Shearing Strain at an Isotropic Confining Pressure of 120 psi(=17.28 ksf=828 kPa)from the Combined RCTS Tests of Specimen UTA-34-B (Specimen No.2).

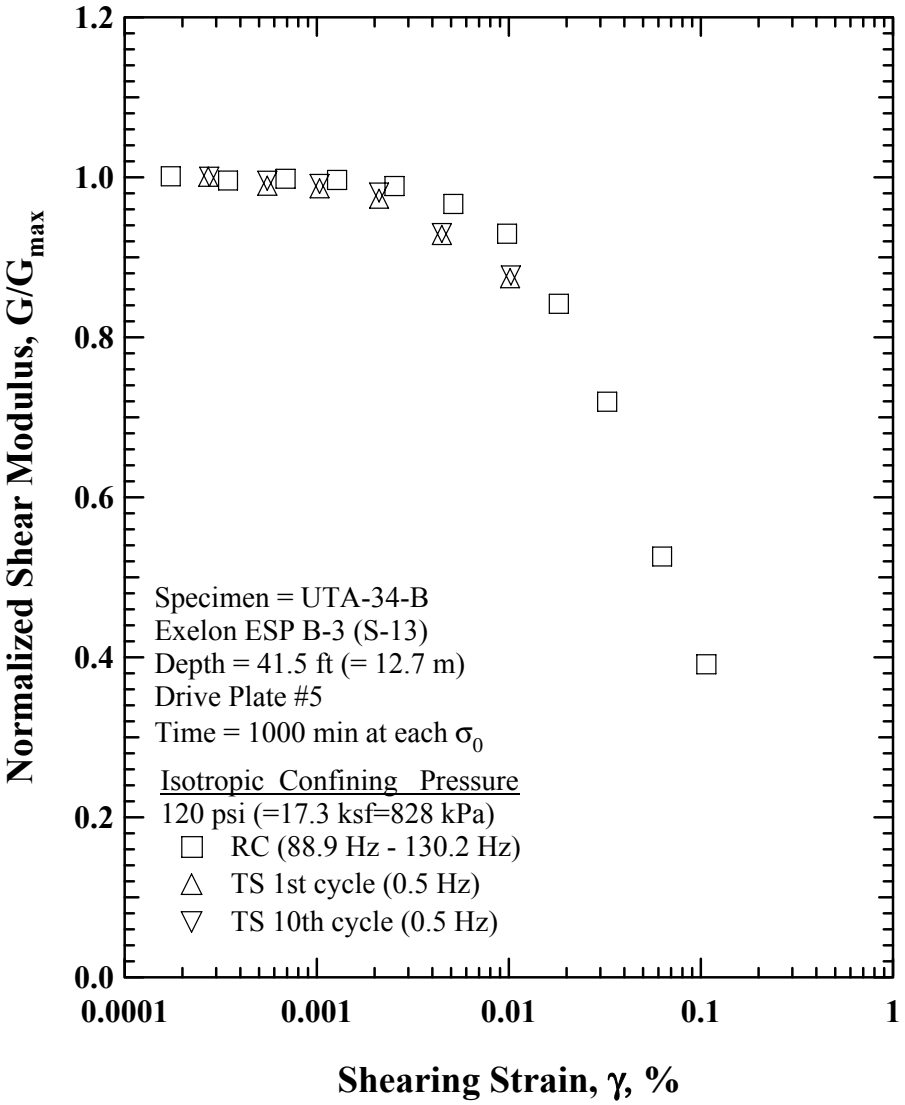

Figure C.17 Comparison of the Variation in Normalized Shear Modulus with Shearing Strain at an Isotropic Confining Pressure of 120 psi(=17.28 ksf=828 kPa) from the Combined RCTS Tests of Specimen UTA-34-B (Specimen No.2).

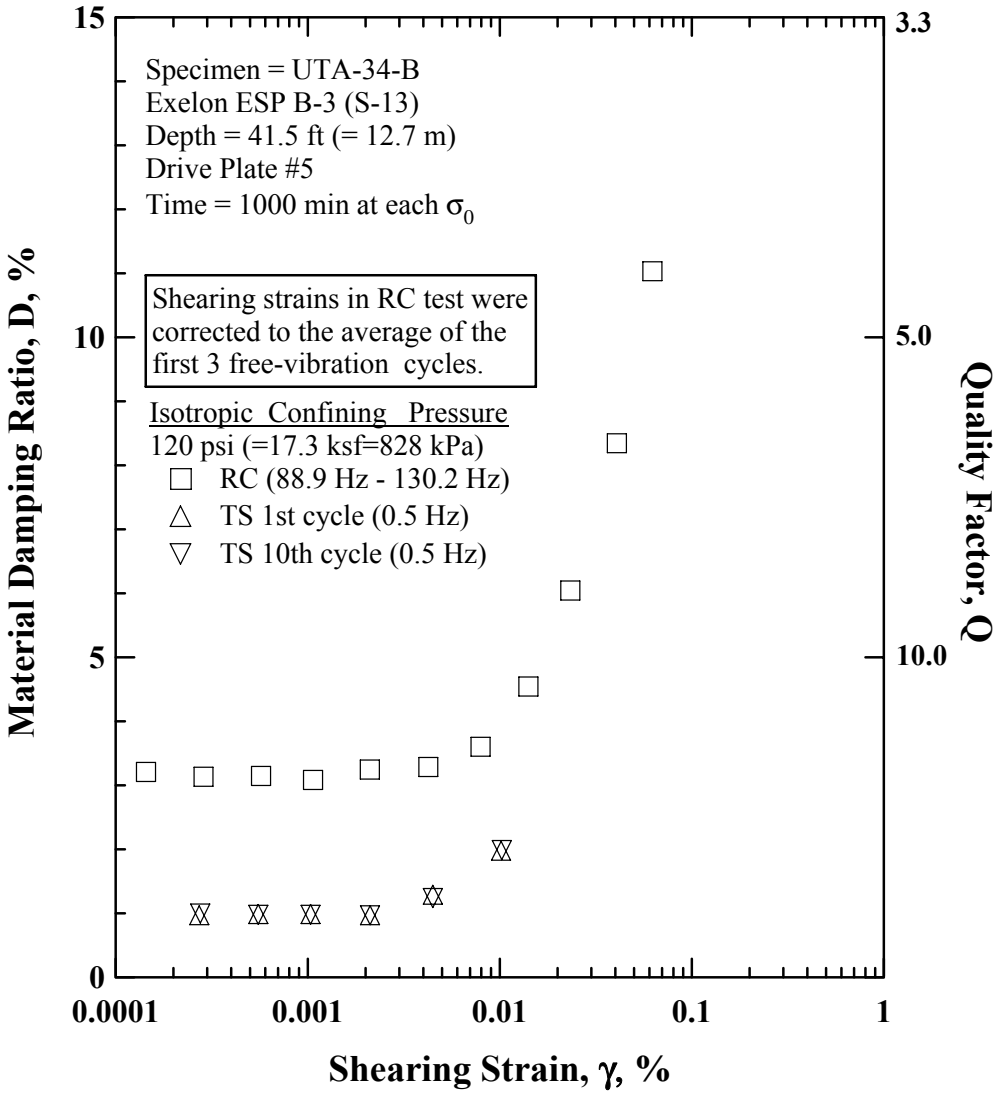

Figure C.18 Comparison of the Variation in Material Damping with Shearing Strain at an Isotropic Confining Pressure of 120 psi(=17.28 ksf=828 kPa)from the Combined RCTS Tests of Specimen UTA-34-B (Specimen No.2).

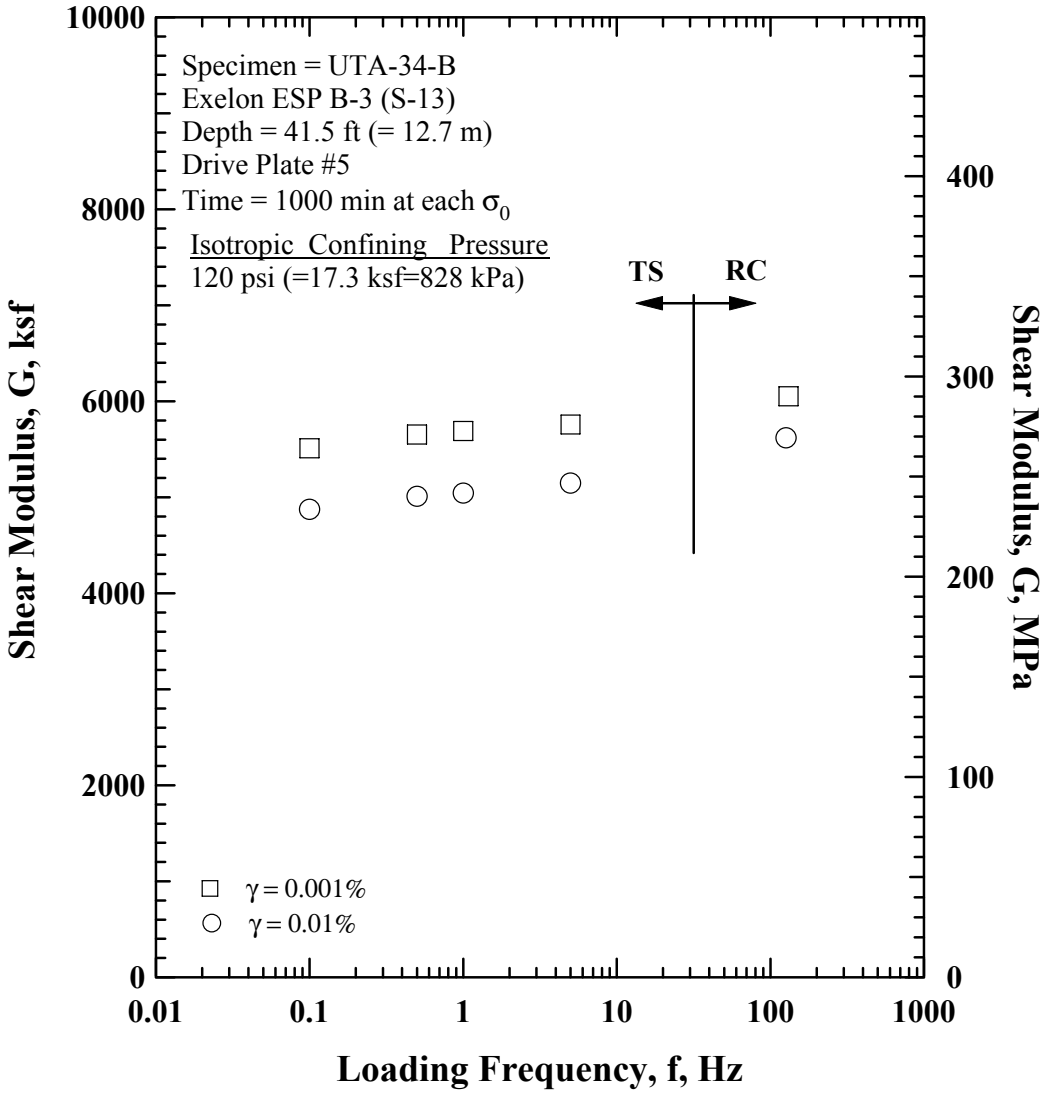

Figure C.19 Comparison of the Variation in Shear Modulus with Loading Frequency at an Isotropic Confining Pressure of 120 psi(=17.28 ksf=828 kPa)from the Combined RCTS Tests of Specimen UTA-34-B (Specimen No.2).

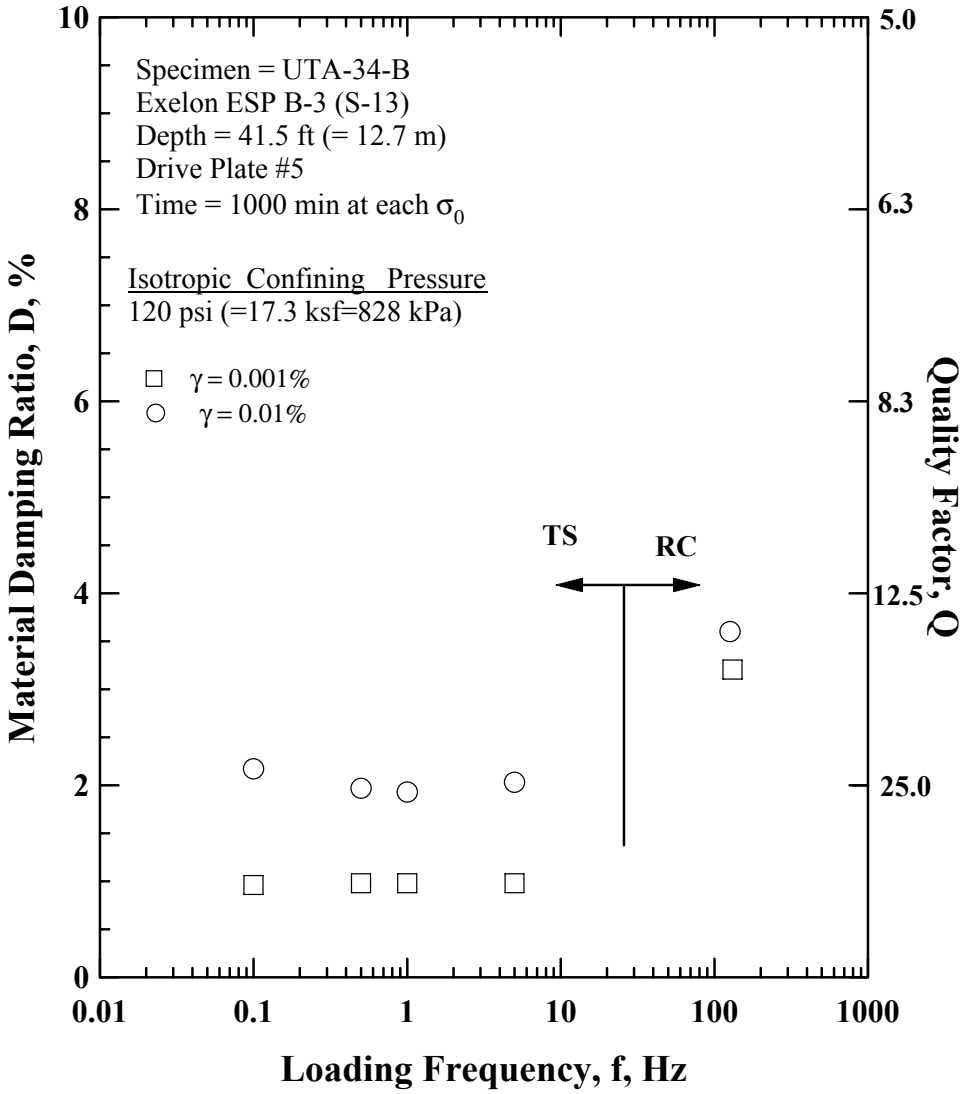

Figure C.20 Comparison of the Variation in Material Damping with Loading Frequency at an Isotropic Confining Pressure of 120 psi(=17.28 ksf=828 kPa)from the Combined RCTS Tests of Specimen UTA-34-B (Specimen No.2).

Table C.1 Variation in Low-Amplitude Shear Wave Velocity, Low-Amplitude Shear Modulus, Low-Amplitude Material Damping Ratio and Void Ratio with Isotropic Confining Pressure from RC Tests of Specimen UTA-34-B.

Effective Isotropic Confining Pressure, σ_o'			Low-Amplitude Shear Modulus, G_{max}		Low-Amplitude Shear Wave Velocity, Vs	Low-Amplitude Material Damping Ratio,	Void Ratio, e
(psi)	(psf)	(kPa)	(ksf)	(MPa)	(fps)	D_{min}, %	
7	1008	48.3	1316	63.1	571	2.66	0.533
15	2160	103.5	1808	86.7	668	2.93	0.527
31	4464	214.0	2737	131.2	797	2.90	0.516
60	8640	414.2	3842	184.2	969	2.71	0.500
120	17280	828.4	5813	278.7	1185	3.22	0.468

Table C.2 Variation in Shear Modulus, Normalized Shear Modulus and Material Damping Ratio with Shearing Strain from RC Tests of Specimen UTA-34-B; Isotropic Confining Pressure, σ_o = 31 psi(=4.46 ksf=214 kPa).

Peak Shearing Strain, %	Shear Modulus, G, ksf	Normalized Shear Modulus, G/G_{max}	Average^{+} Shearing Strain, %	Material Damping Ratio^{x}, D, %
2.10E-04	2689	1.00	1.78E-04	2.80
4.12E-04	2699	1.01	3.48E-04	2.84
8.17E-04	2687	1.00	6.91E-04	2.83
1.63E-03	2674	1.00	1.38E-03	2.80
2.98E-03	2639	1.00	2.49E-03	3.06
5.82E-03	2550	0.98	4.80E-03	3.27
1.08E-02	2342	0.95	8.63E-03	3.85
1.98E-02	2068	0.90	1.48E-02	5.14
3.71E-02	1641	0.81	2.50E-02	7.39

$^{+}$ Average Shearing Strain from the First Three Cycles of the Free Vibration Decay Curve

^{x} Average Damping Ratio from the First Three Cycles of the Free Vibration Decay Curve

Table C.3 Variation in Shear Modulus, Normalized Shear Modulus and Material Damping Ratio with Shearing Strain from TS Tests of Specimen UTA-34-B; Isotropic Confining Pressure, σ_o = 31 psi(=4.46 ksf=214 kPa).

First Cycle				Tenth Cycle			
Peak Shearing Strain, %	Shear Modulus, G, ksf	Normalized Shear Modulus, G/G_{max}	Material Damping Ratio, D, %	Peak Shearing Strain, %	Shear Modulus, G, ksf	Normalized Shear Modulus, G/G_{max}	Material Damping Ratio, D, %
5.99E-04	2530	1.00	0.87	5.98E-04	2527	1.00	0.90
9.05E-04	2525	1.00	0.91	9.07E-04	2518	1.00	0.91
1.06E-03	2521	1.00	0.99	1.06E-03	2511	0.99	0.96
2.17E-03	2482	0.98	0.97	2.17E-03	2480	0.98	0.93
4.42E-03	2423	0.96	1.24	4.43E-03	2423	0.96	1.27
1.06E-02	2157	0.85	2.39	1.07E-02	2136	0.85	2.43
2.74E-02	1693	0.67	5.17	2.74E-02	1688	0.67	5.28

Table C.4 Variation in Shear Modulus, Normalized Shear Modulus and Material Damping Ratio with Shearing Strain from RC Tests of Specimen UTA-34-B; Isotropic Confining Pressure, σ_o = 120 psi(=17.28 ksf=828 kPa).

Peak Shearing Strain, %	Shear Modulus, G, ksf	Normalized Shear Modulus, G/G_{max}	Average[+] Shearing Strain, %	Material Damping Ratio[x], D, %
4.92E-05	5965	1.00	4.10E-05	3.09
8.86E-05	6039	1.00	7.39E-05	3.10
1.74E-04	6053	1.00	1.44E-04	3.21
3.45E-04	6022	1.00	2.87E-04	3.13
6.87E-04	6034	1.00	5.71E-04	3.15
1.27E-03	6026	1.00	1.06E-03	3.08
2.54E-03	5980	0.99	2.10E-03	3.25
5.14E-03	5843	0.97	4.24E-03	3.29
9.79E-03	5619	0.93	7.94E-03	3.60
1.82E-02	5090	0.84	1.41E-02	4.54
3.25E-02	4349	0.72	2.33E-02	6.04
6.28E-02	3181	0.53	4.06E-02	8.34
1.07E-01	2366	0.39	6.22E-02	11.03

[+] Average Shearing Strain from the First Three Cycles of the Free Vibration Decay Curve

[x] Average Damping Ratio from the First Three Cycles of the Free Vibration Decay Curve

Table C.5 Variation in Shear Modulus, Normalized Shear Modulus and Material Damping Ratio with Shearing Strain from TS Tests of Specimen UTA-34-B; Isotropic Confining Pressure, σ_o= 120 psi(=17.28 ksf=828 kPa).

First Cycle				Tenth Cycle			
Peak Shearing Strain, %	Shear Modulus, G, ksf	Normalized Shear Modulus, G/G_{max}	Material Damping Ratio, D, %	Peak Shearing Strain, %	Shear Modulus, G, ksf	Normalized Shear Modulus, G/G_{max}	Material Damping Ratio, D, %
2.74E-04	5737	1.00	0.96	2.77E-04	5701	1.00	0.99
5.55E-04	5672	0.99	0.98	5.55E-04	5673	1.00	0.97
1.04E-03	5654	0.99	0.98	1.04E-03	5650	0.99	0.97
2.12E-03	5580	0.97	0.96	2.12E-03	5588	0.98	0.96
4.51E-03	5320	0.93	1.28	4.51E-03	5300	0.93	1.23
1.02E-02	5010	0.87	1.97	1.03E-02	4997	0.88	1.98

Exhibit D

to Attachment A-7

Specimen No. 3
UT Specimen: UTA-34-D

Exelon ESP B-3(S-33)
Depth = 115ft (=35m)
Soil Type: Sandy Lean Clay (CL)

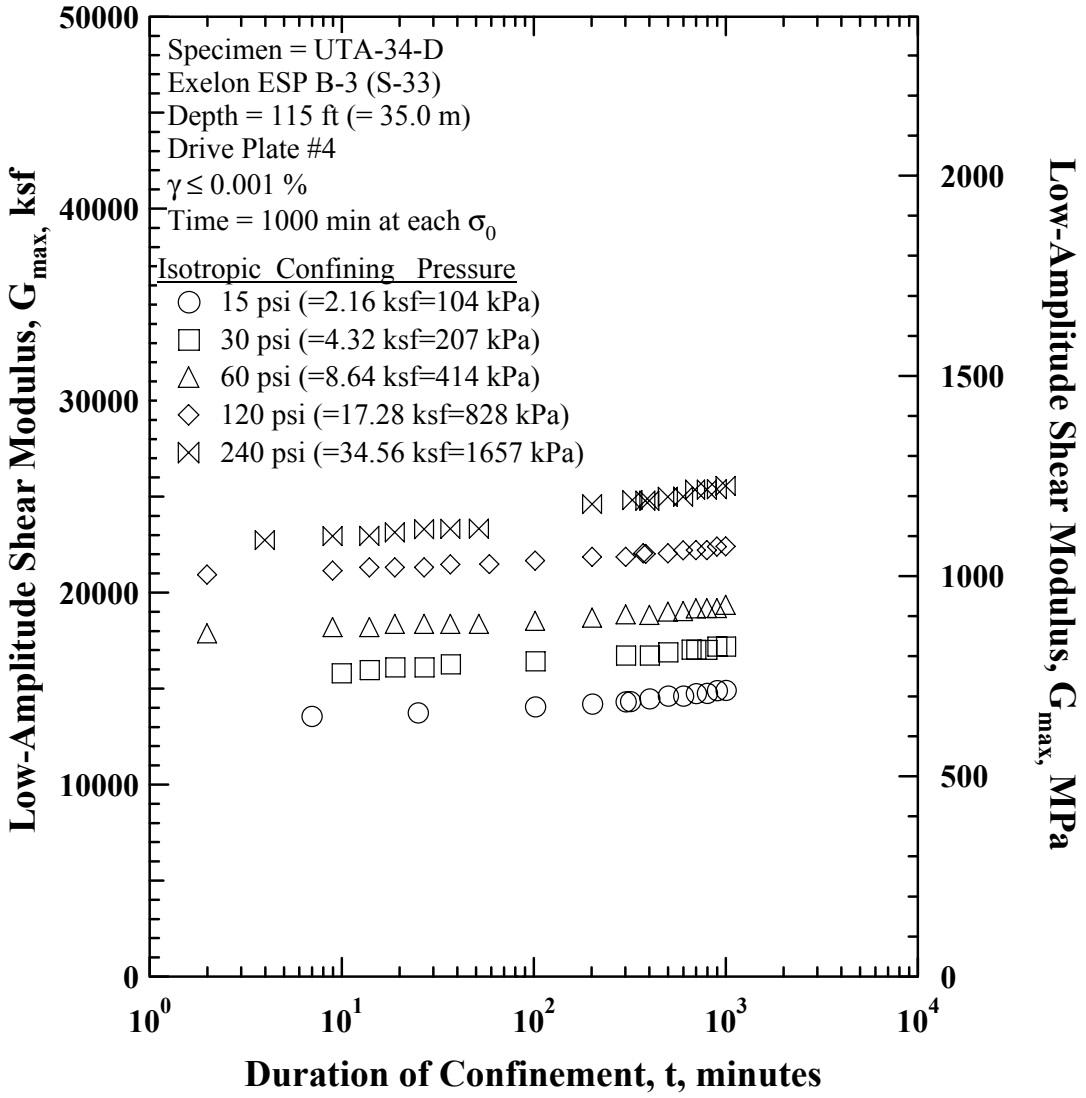

Figure D.1 Variation in Low-Amplitude Shear Modulus with Magnitude and Duration of Isotropic Confining Pressure from Resonant Column Tests of Specimen UTA-34-D (Specimen No. 3)

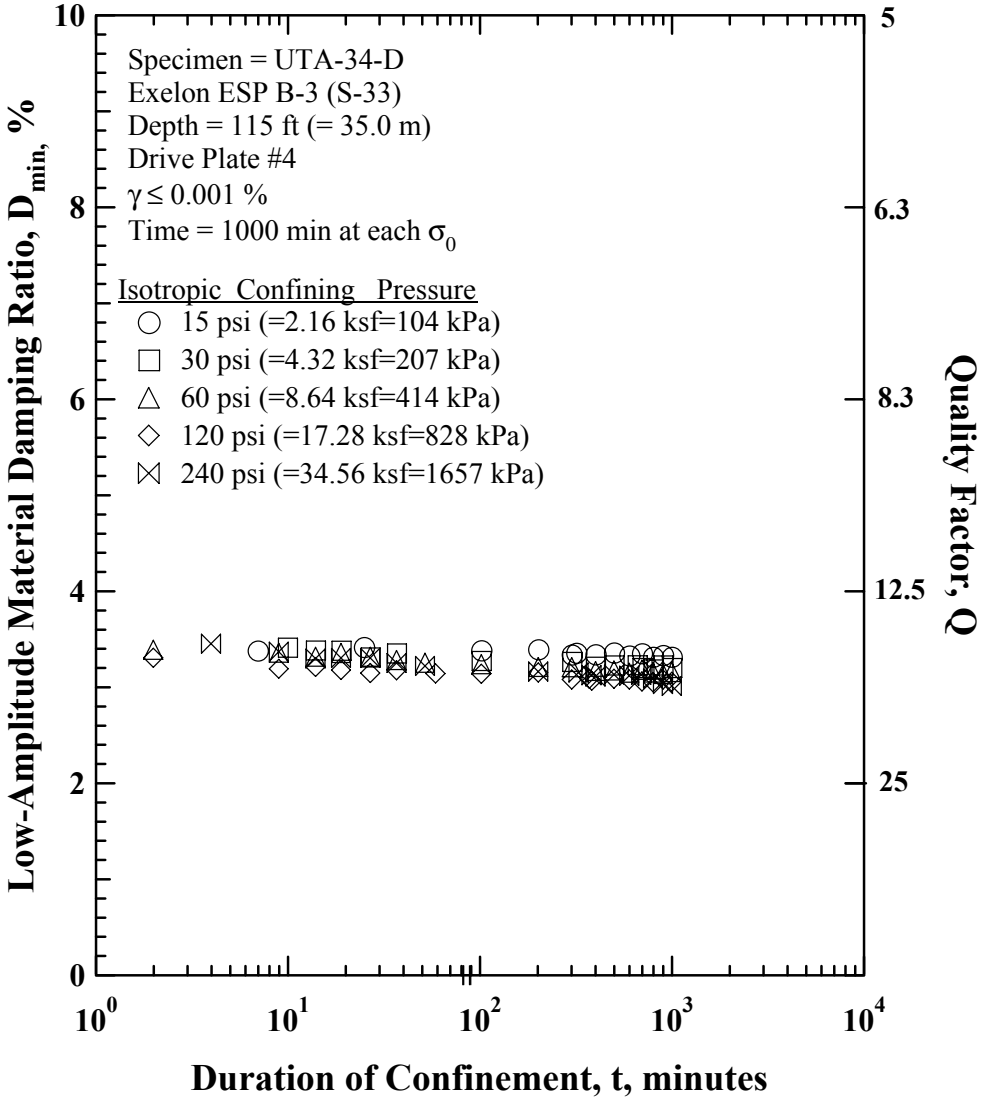

Figure D.2 Variation in Low Amplitude Material Damping Ratio with Magnitude and Duration of Isotropic Confining Pressure from Resonant Column Tests of Specimen UTA-34-D (Specimen No. 3)

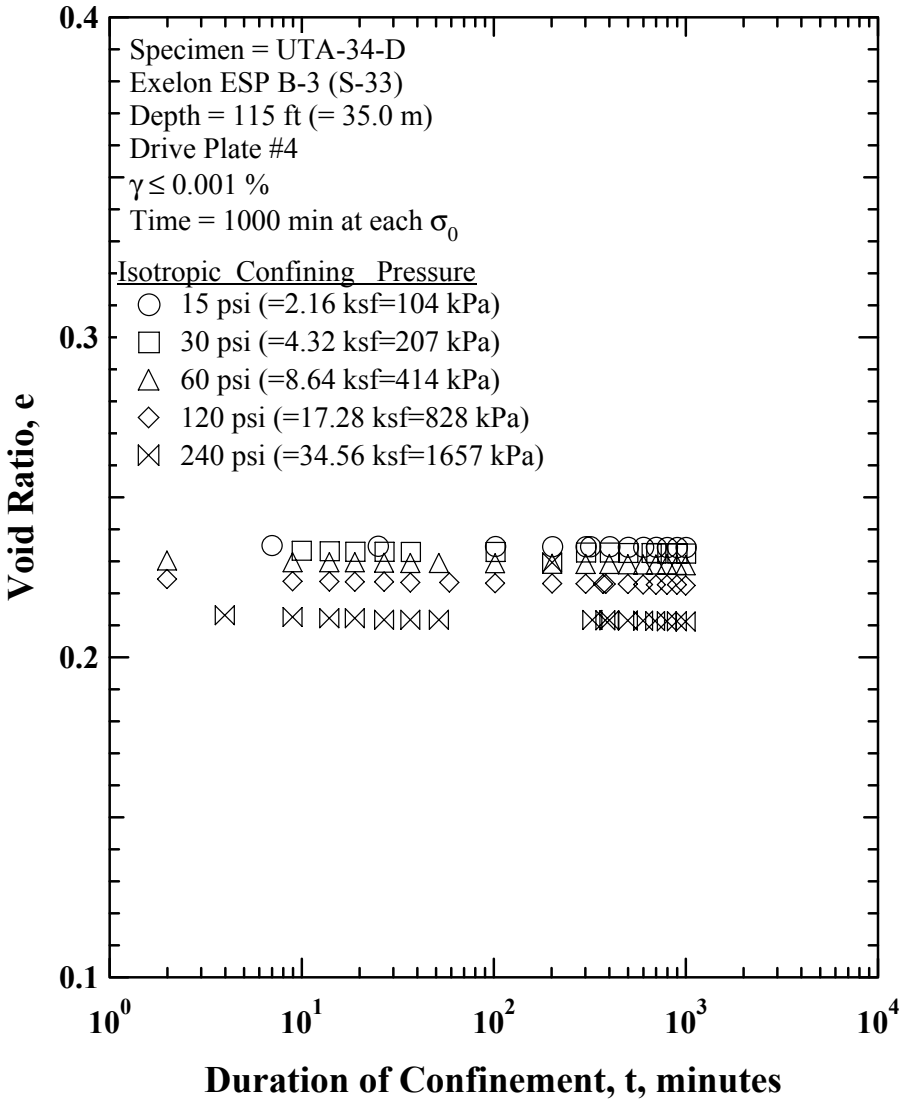

Figure D.3 Variation in Estimated Void Ratio with Magnitude and Duration of Isotropic Confining Pressure from Resonant Column Tests of Specimen UTA-34-D (Specimen No. 3)

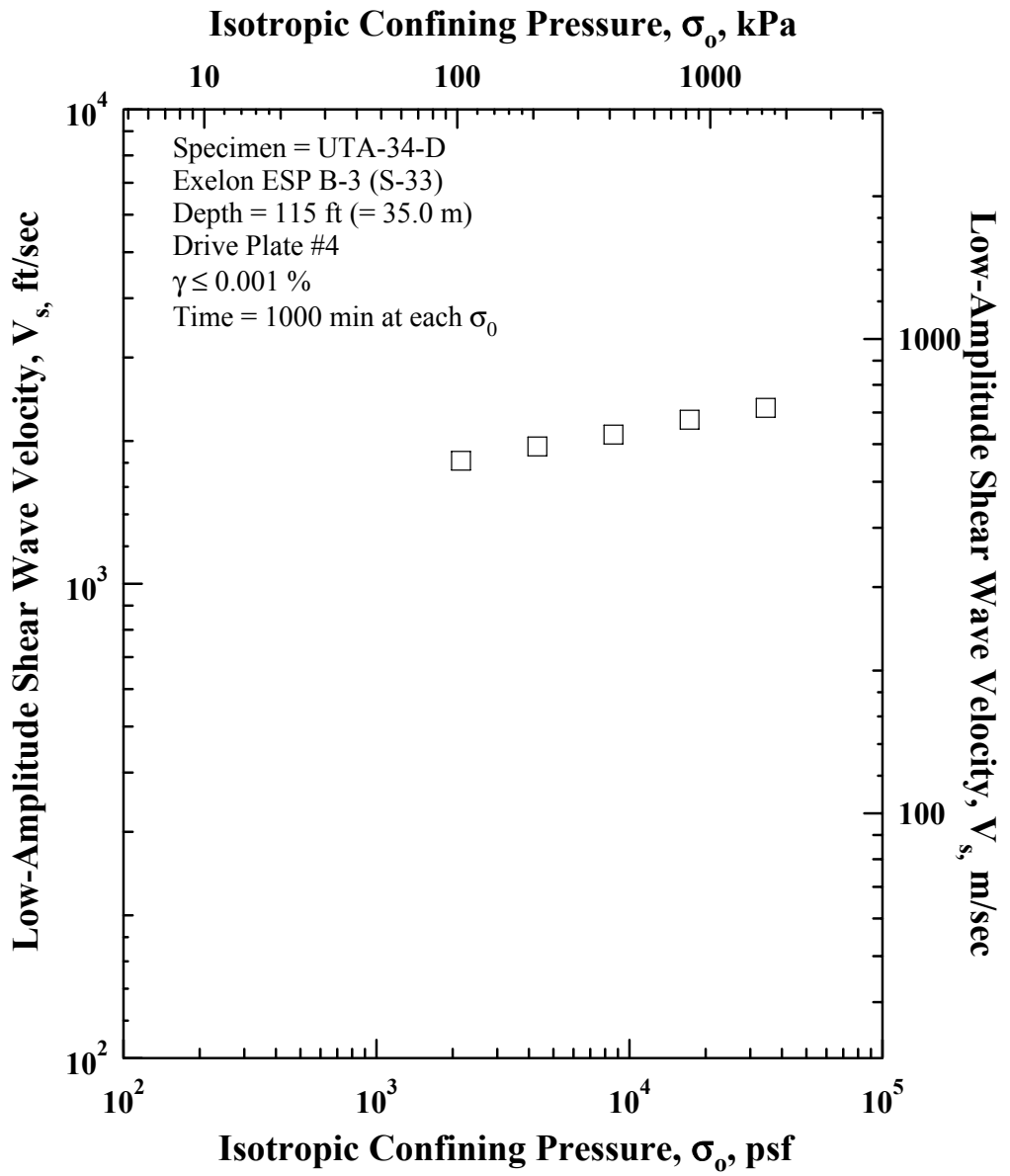

Figure D.4 Variation in Low-Amplitude Shear Wave Velocity with Isotropic Confining Pressure from Resonant Column Tests of Specimen UTA-34-D (Specimen No. 3)

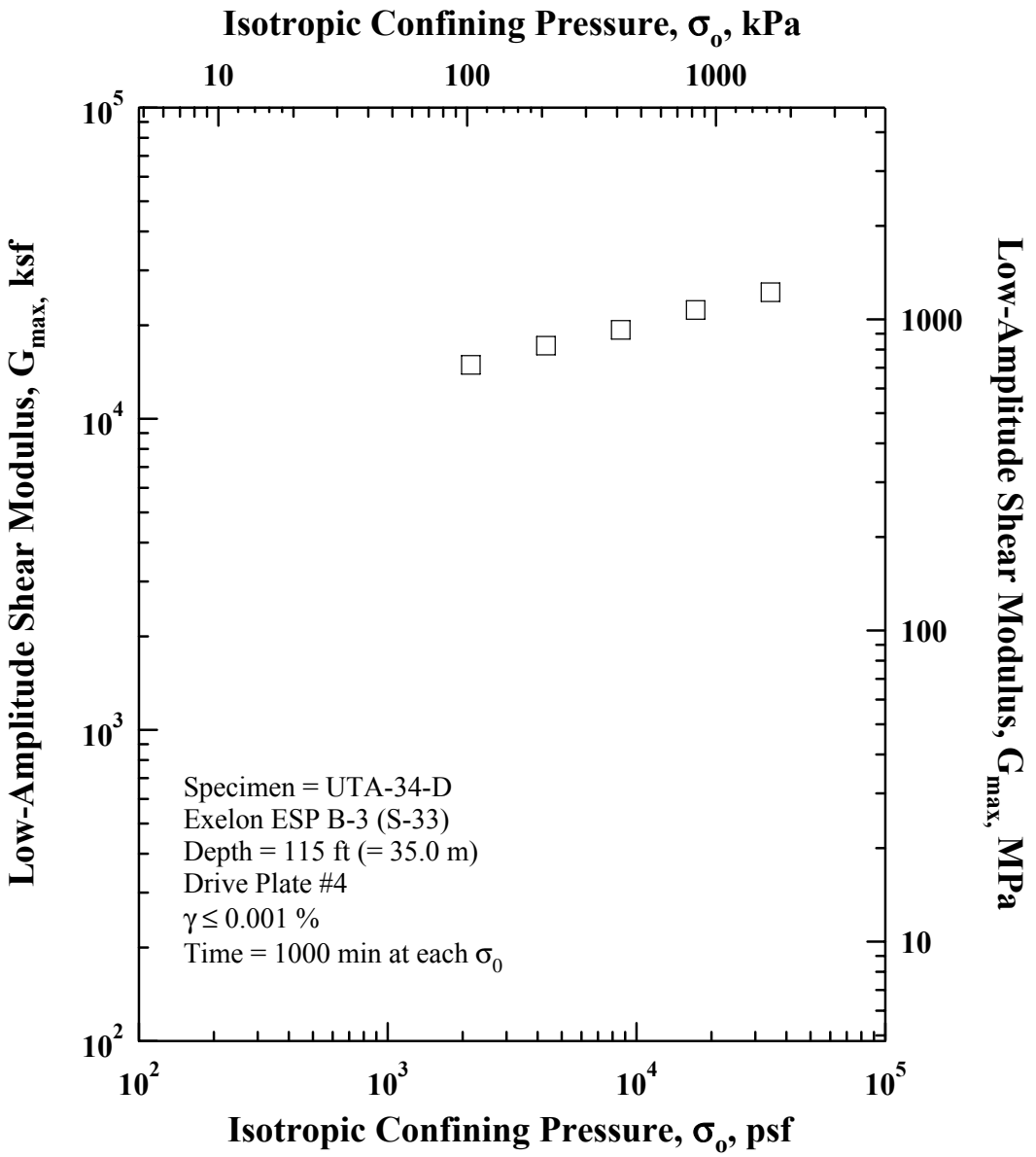

Figure D.5 Variation in Low-Amplitude Shear Modulus with Isotropic Confining Pressure from Resonant Column Tests of Specimen UTA-34-D (Specimen No. 3)

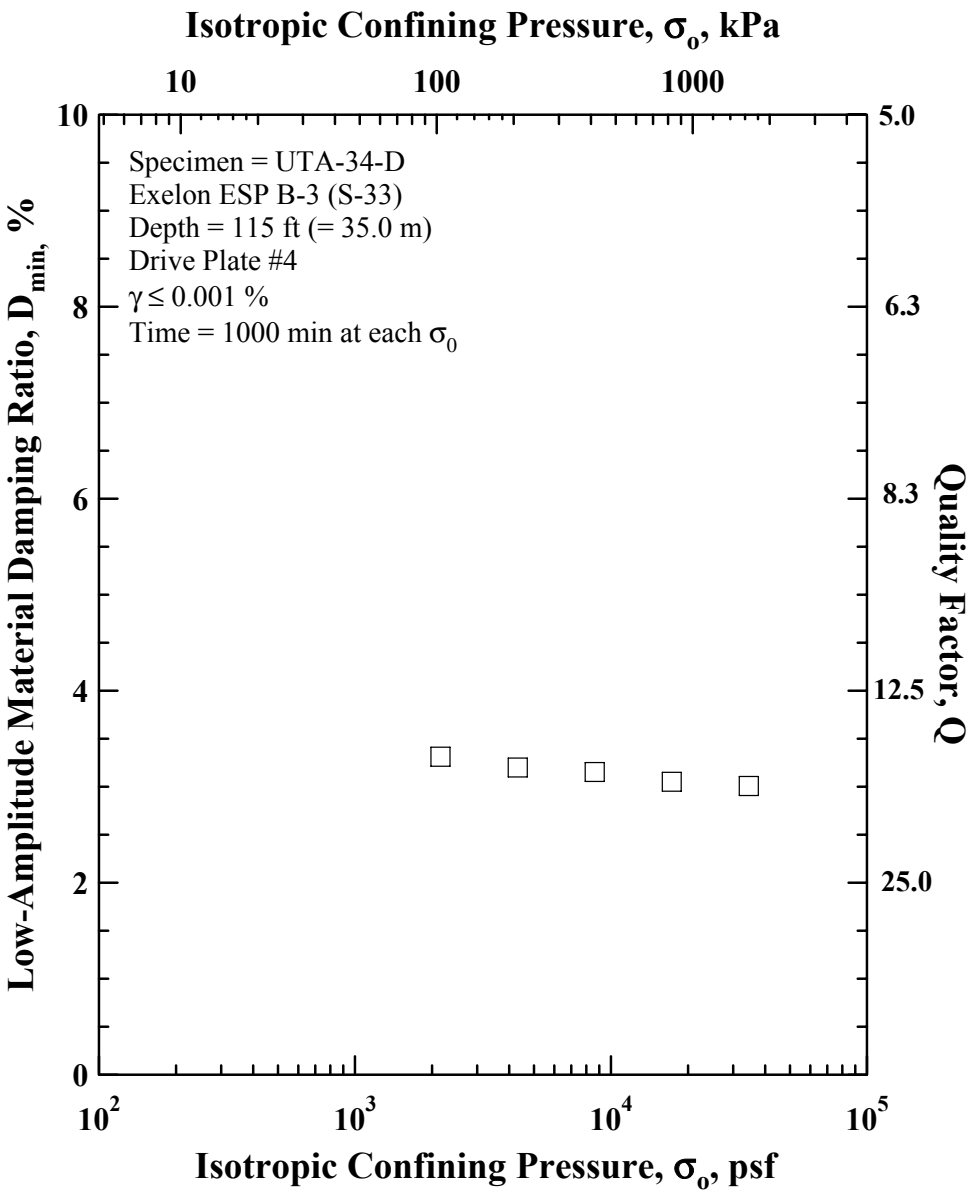

Figure D.6 Variation in Low-Amplitude Material Damping Ratio with Isotropic Confining Pressure from Resonant Column Tests of Specimen UTA-34-D (Specimen No. 3)

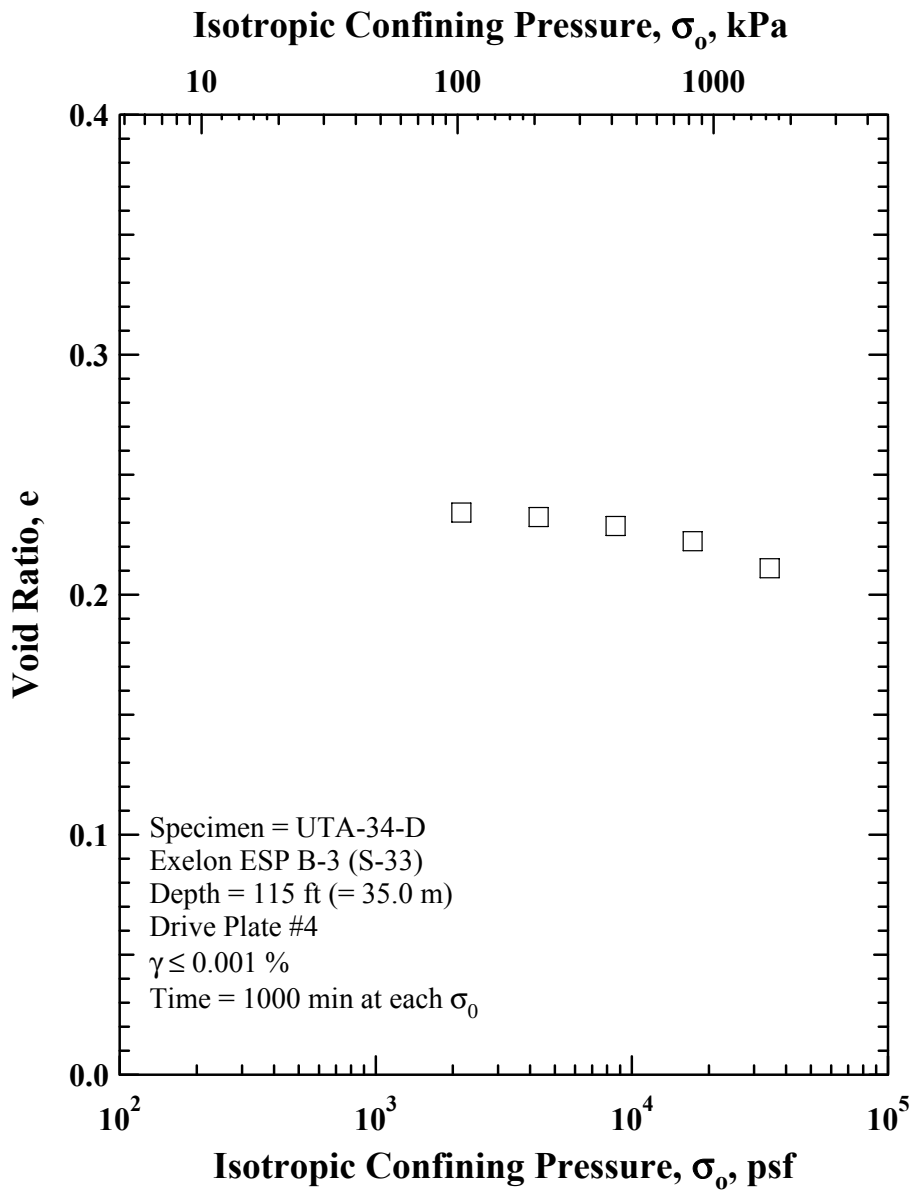

Figure D.7 Variation in Estimated Void Ratio with Isotropic Confining Pressure from Resonant Column Tests of Specimen UTA-34-D (Specimen No. 3)

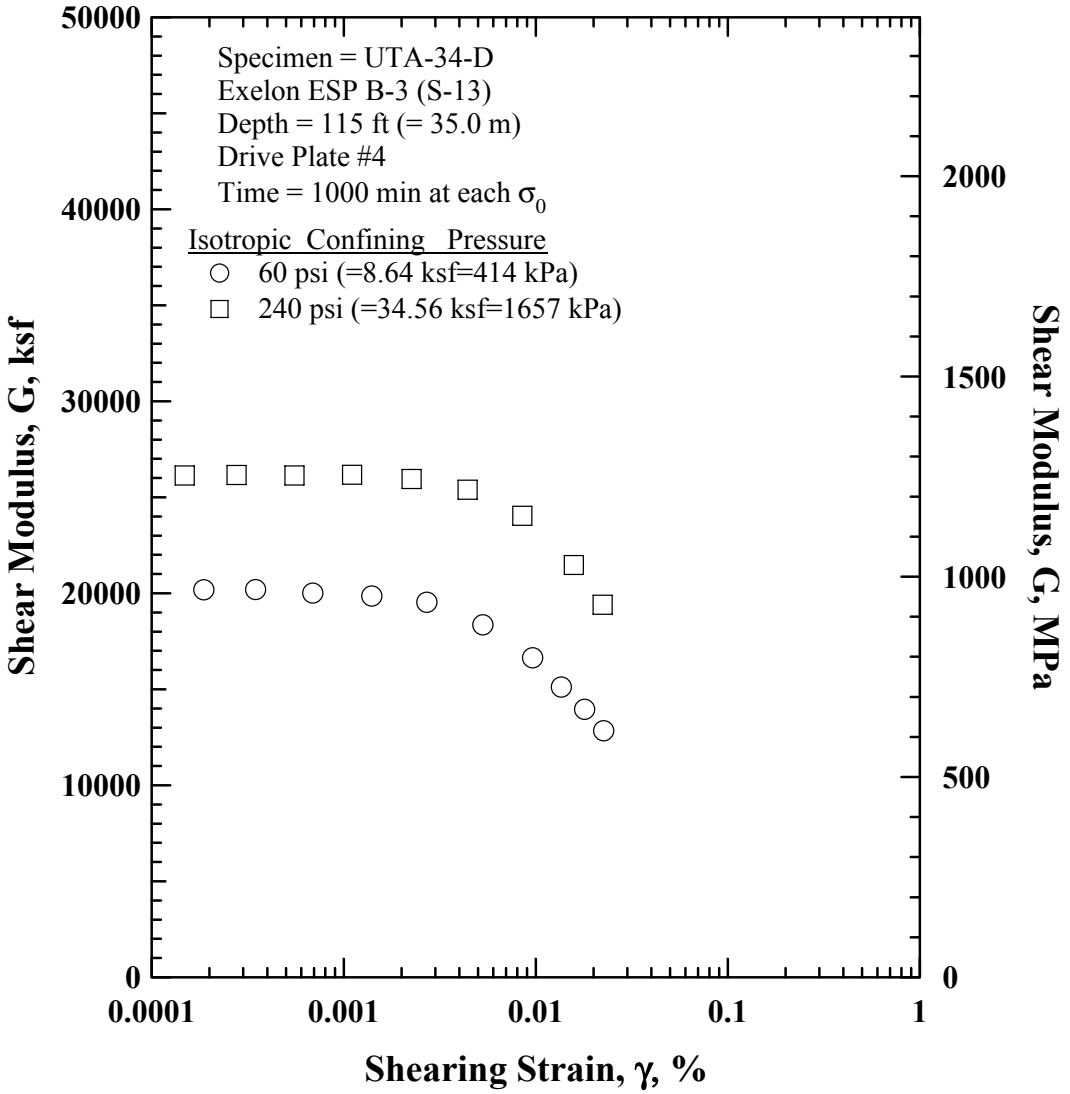

Figure D.8 Comparison of the Variation in Shear Modulus with Shearing Strain and Isotropic Confining Pressure from the Resonant Column Tests of Specimen UTA-34-D (Specimen No. 3)

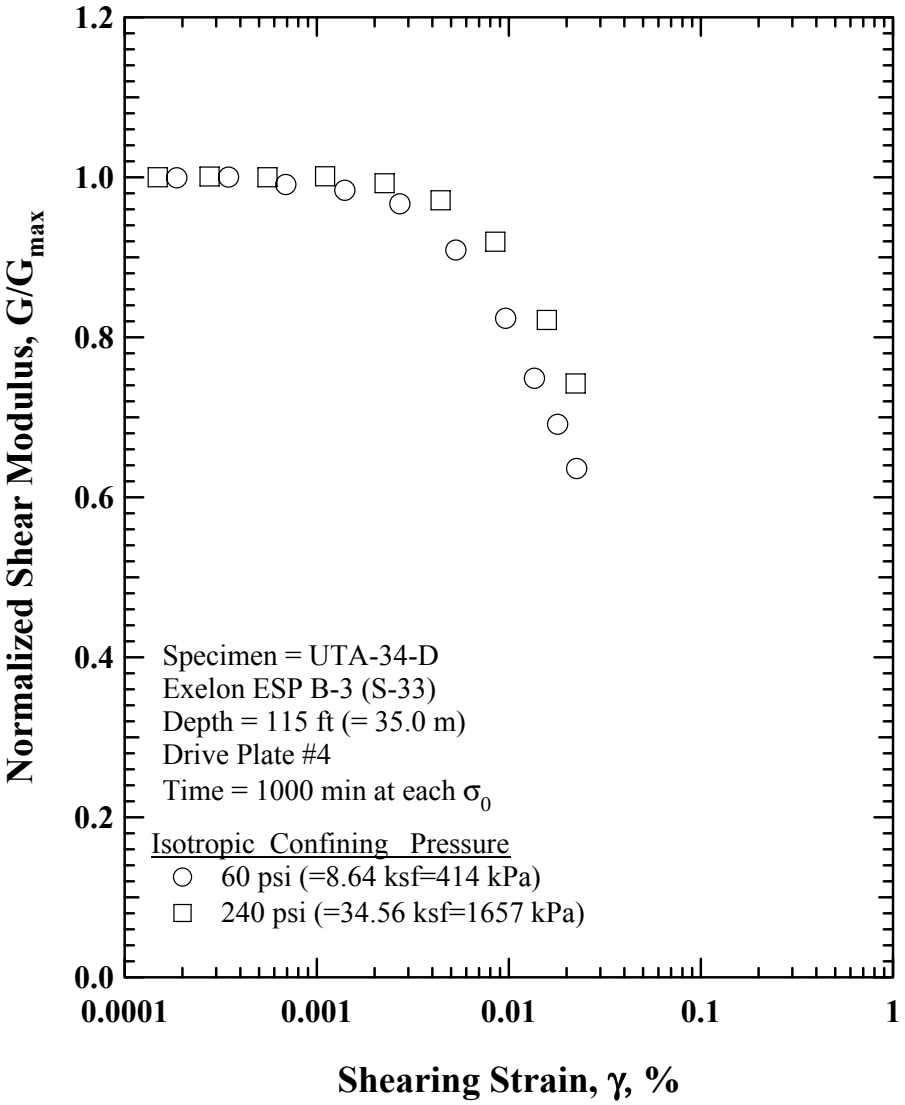

Figure D.9 Comparison of the Variation in Normalized Shear Modulus with Shearing Strain and Isotropic Confining Pressure from the Resonant Column Tests of Specimen UTA-34-D (Specimen No. 3)

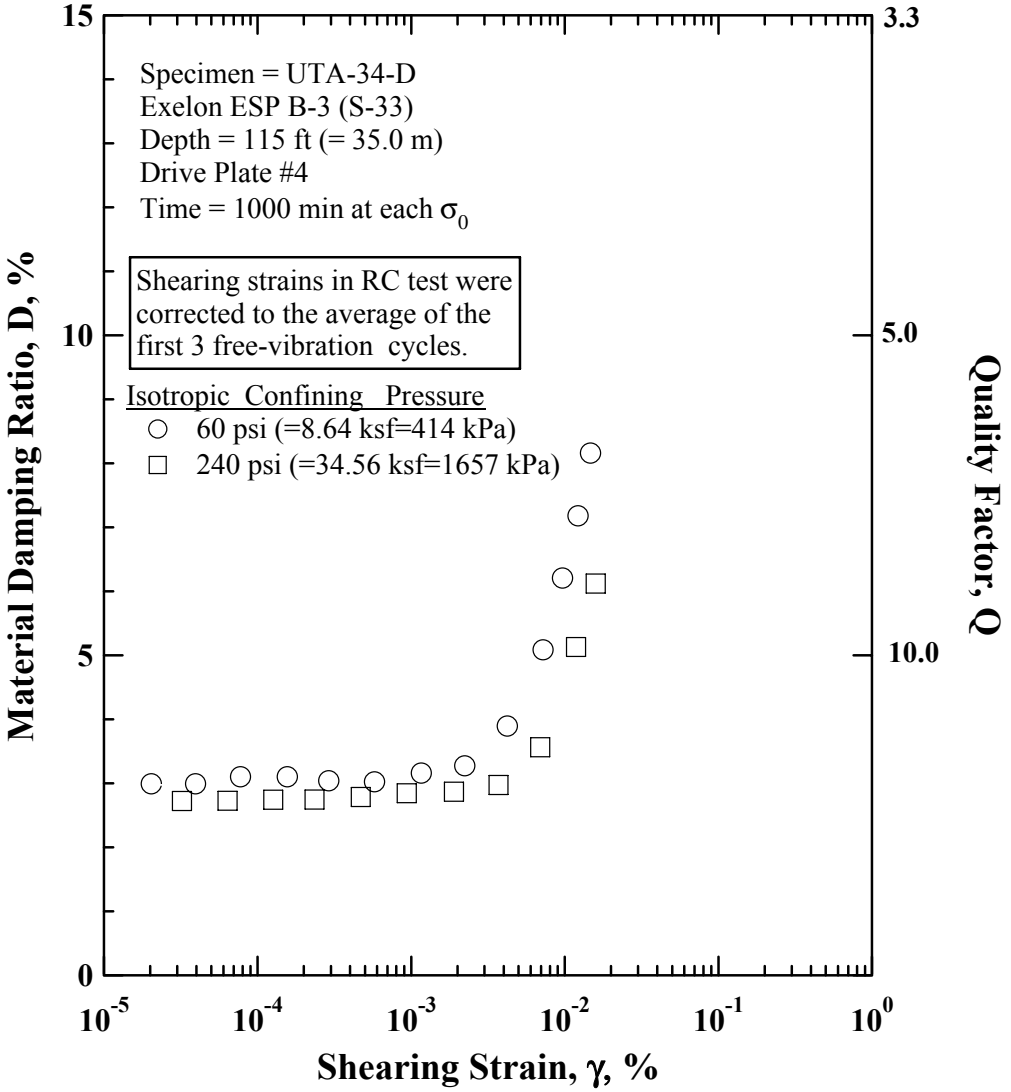

Figure D.10 Comparison of the Variation in Material Damping Ratio with Shearing Strain and Isotropic Confining Pressure from the Resonant Column Tests of Specimen UTA-34-D (Specimen No. 3)

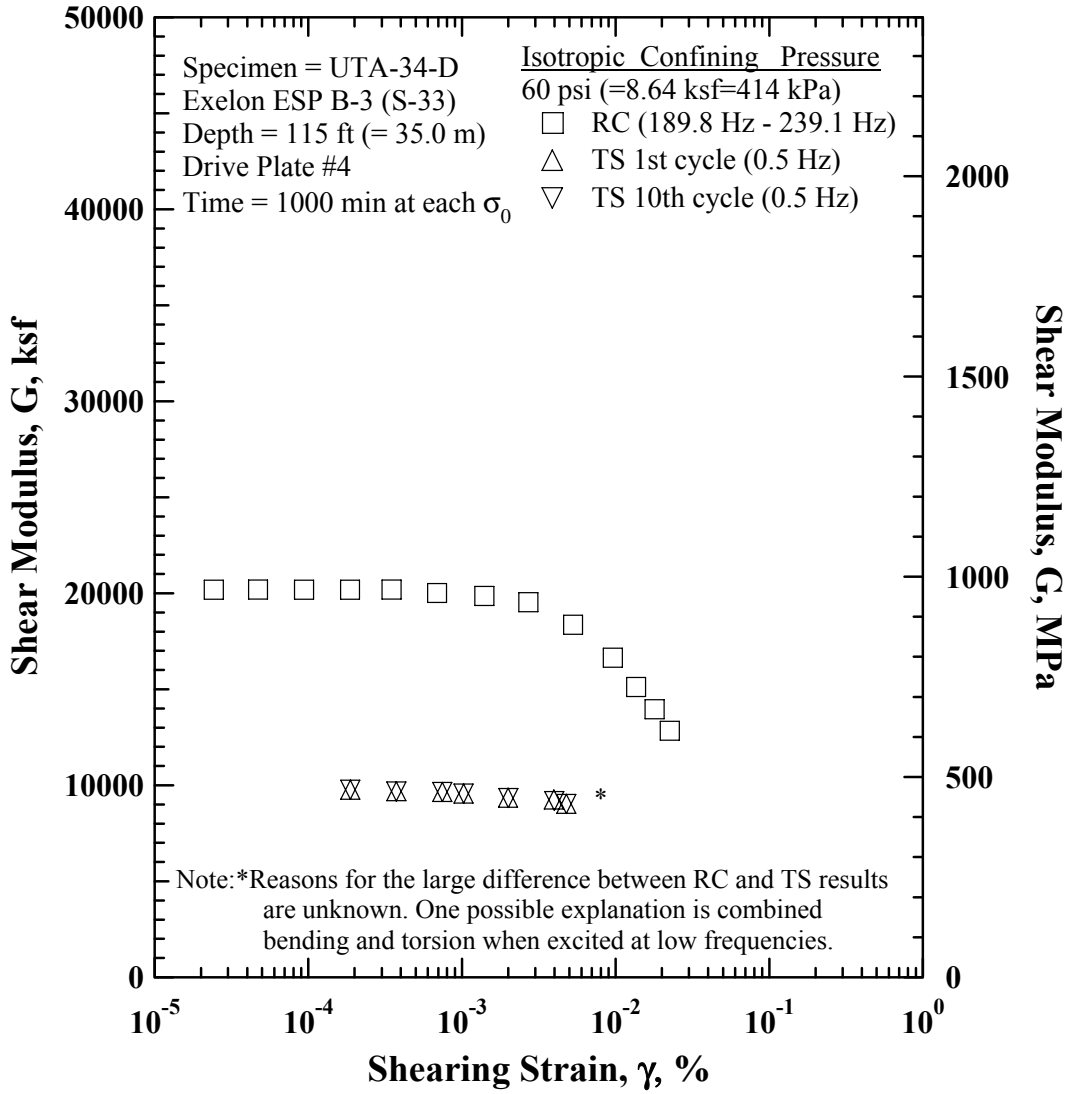

Figure D.11 Comparison of the Variation in Shear Modulus with Shearing Strain at an Isotropic Confining Pressure of 60 psi(=8.64 ksf=414 kPa)from the Combined RCTS Tests of Specimen UTA-34-D (Specimen No. 3)

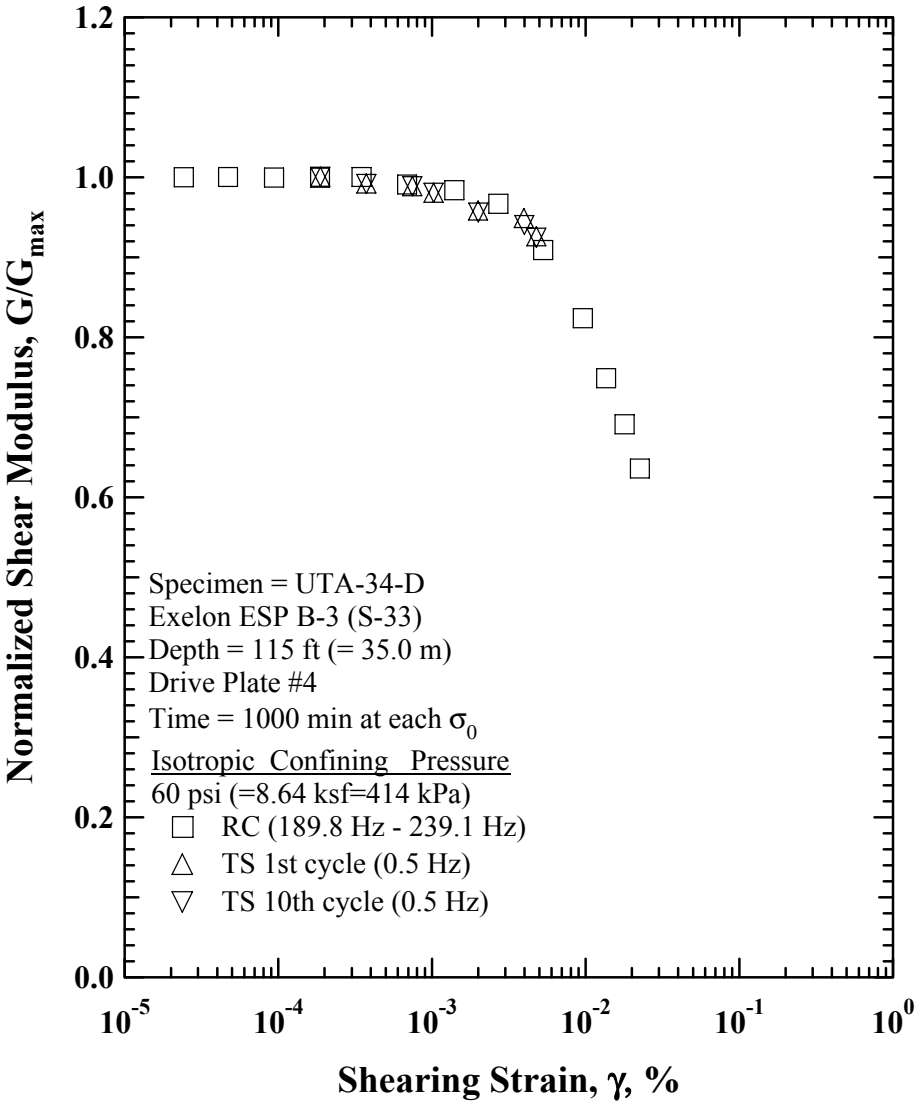

Figure D.12 Comparison of the Variation in Normalized Shear Modulus with Shearing Strain at an Isotropic Confining Pressure of 60 psi(=8.64 ksf=414 kPa)from the Combined RCTS Tests of Specimen UTA-34-D (Specimen No. 3)

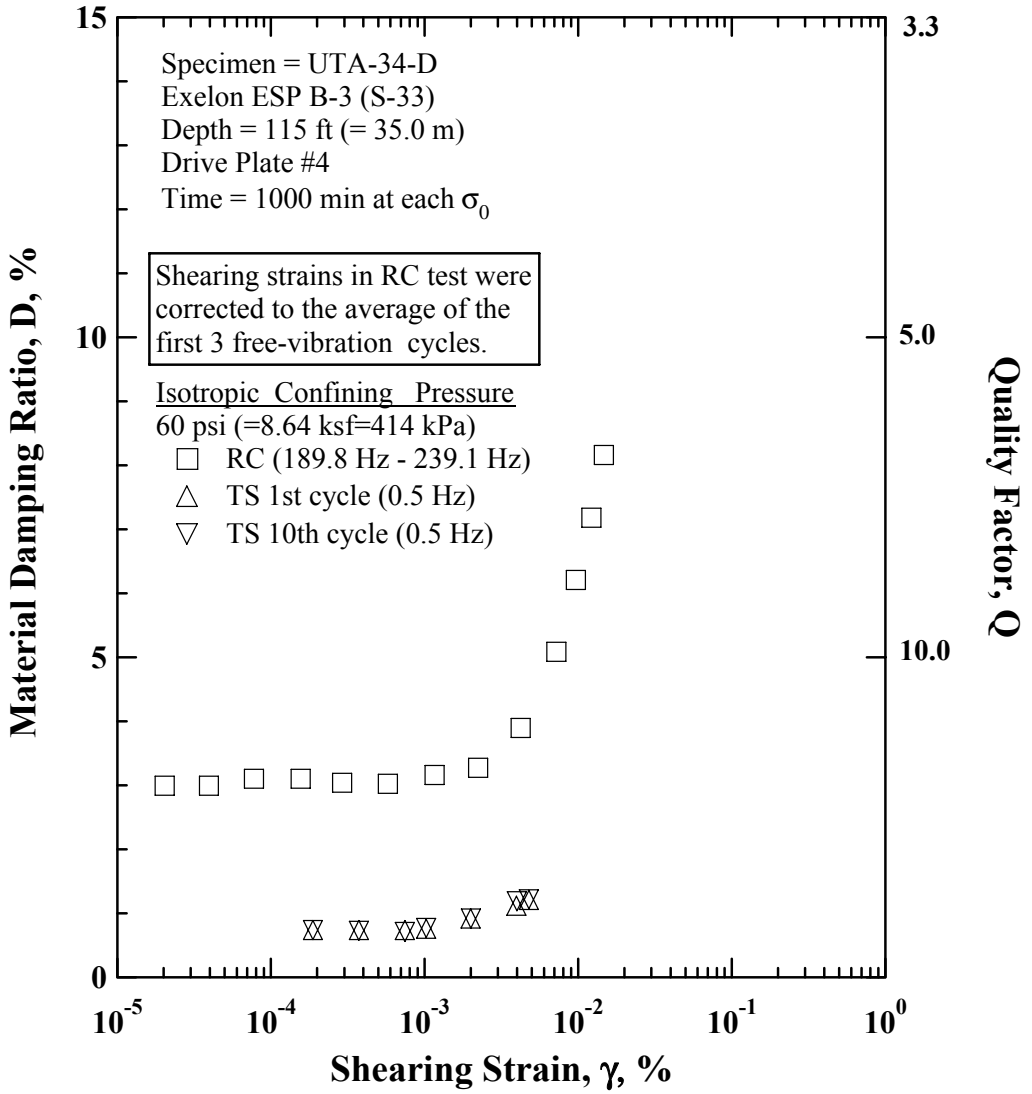

Figure D.13 Comparison of the Variation in Material Damping Ratio with Shearing Strain at an Isotropic Confining Pressure of 60 psi(=8.64 ksf=414 kPa)from the Combined RCTS Tests of Specimen UTA-34-D (Specimen No. 3)

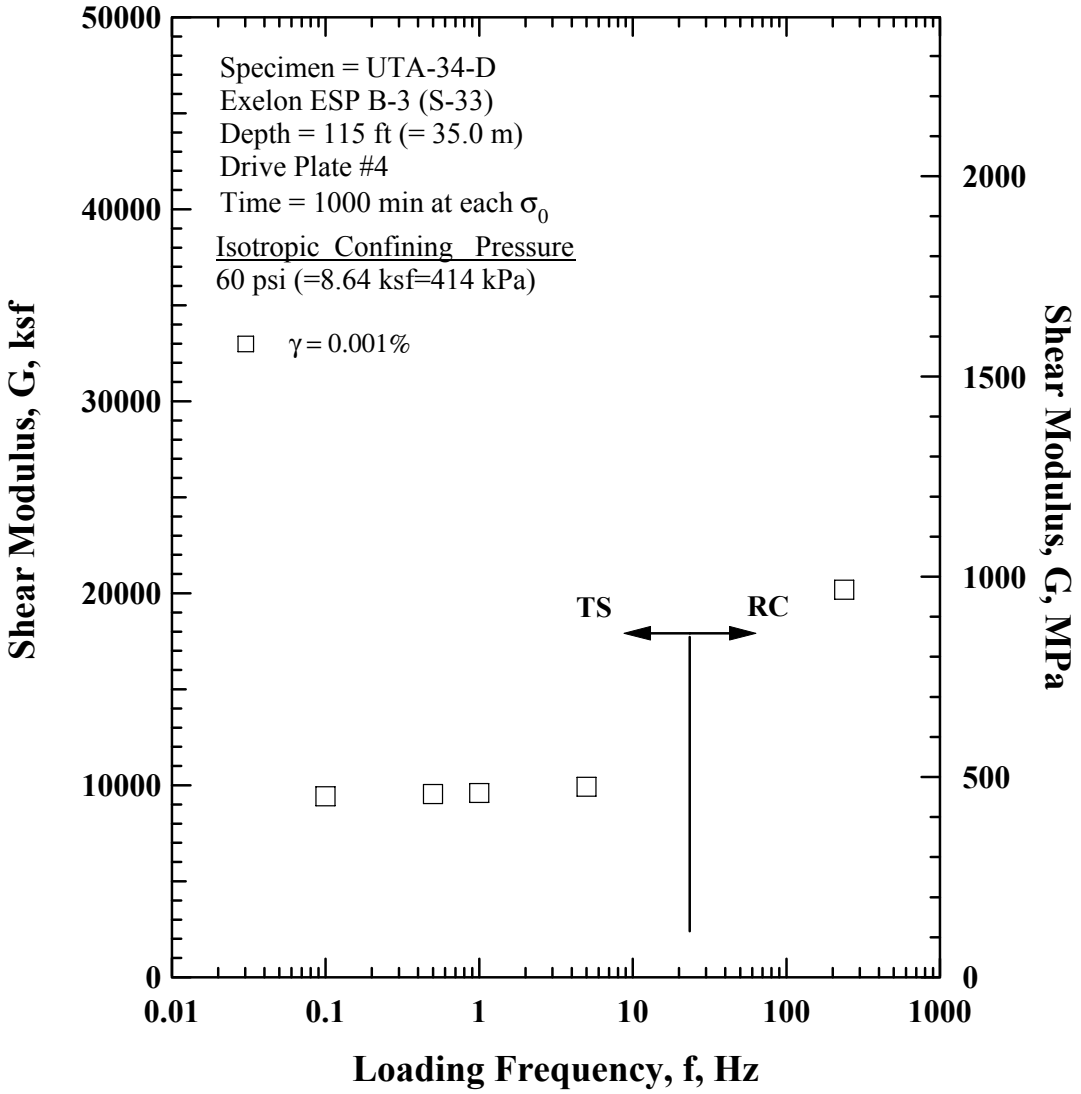

Figure D.14 Comparison of the Variation in Shear Modulus with Loading Frequency at an Isotropic Confining Pressure of 60 psi(=8.64 ksf=414 kPa)from the Combined RCTS Tests of Specimen UTA-34-D (Specimen No. 3)

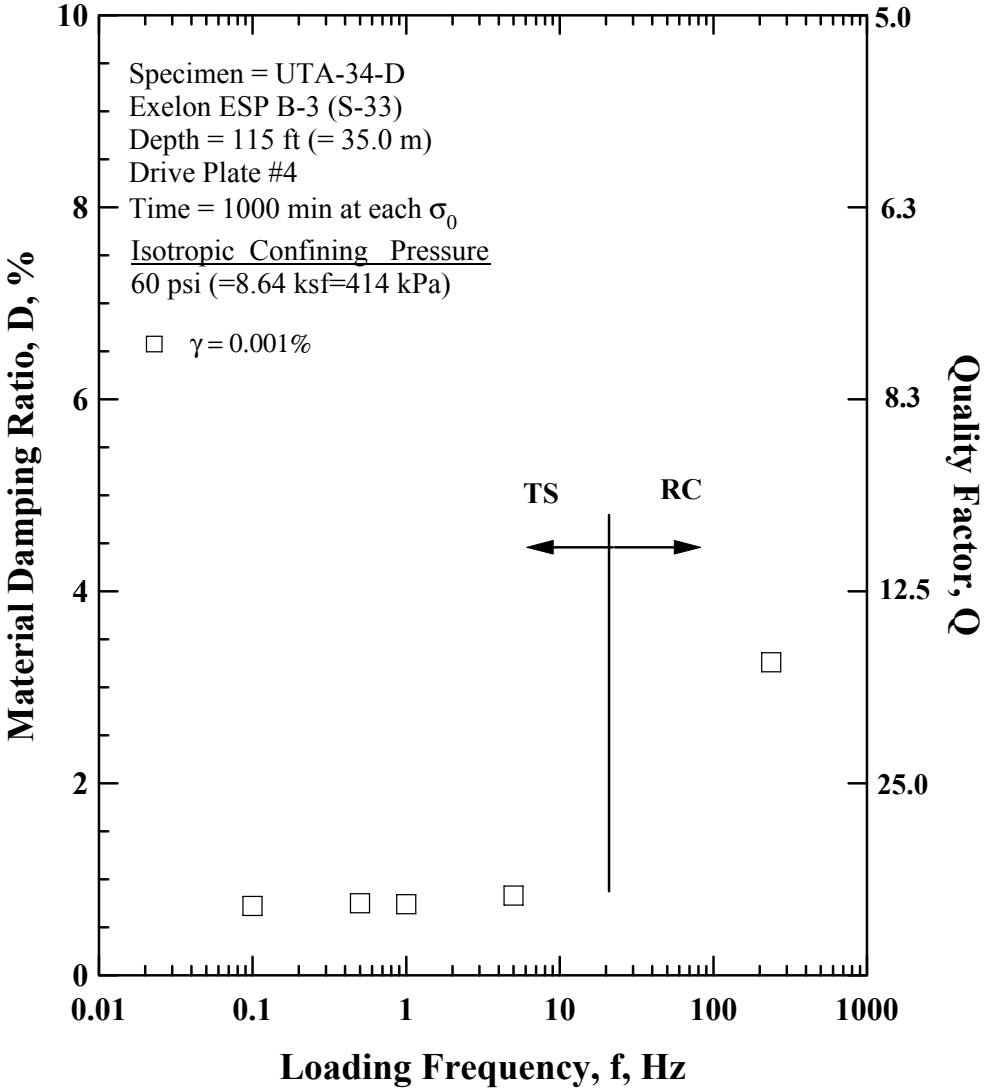

Figure D.15 Comparison of the Variation in Material Damping Ratio with Loading Frequency at an Isotropic Confining Pressure of 60 psi(=8.64 ksf=414 kPa)from the Combined RCTS Tests of Specimen UTA-34-D (Specimen No. 3)

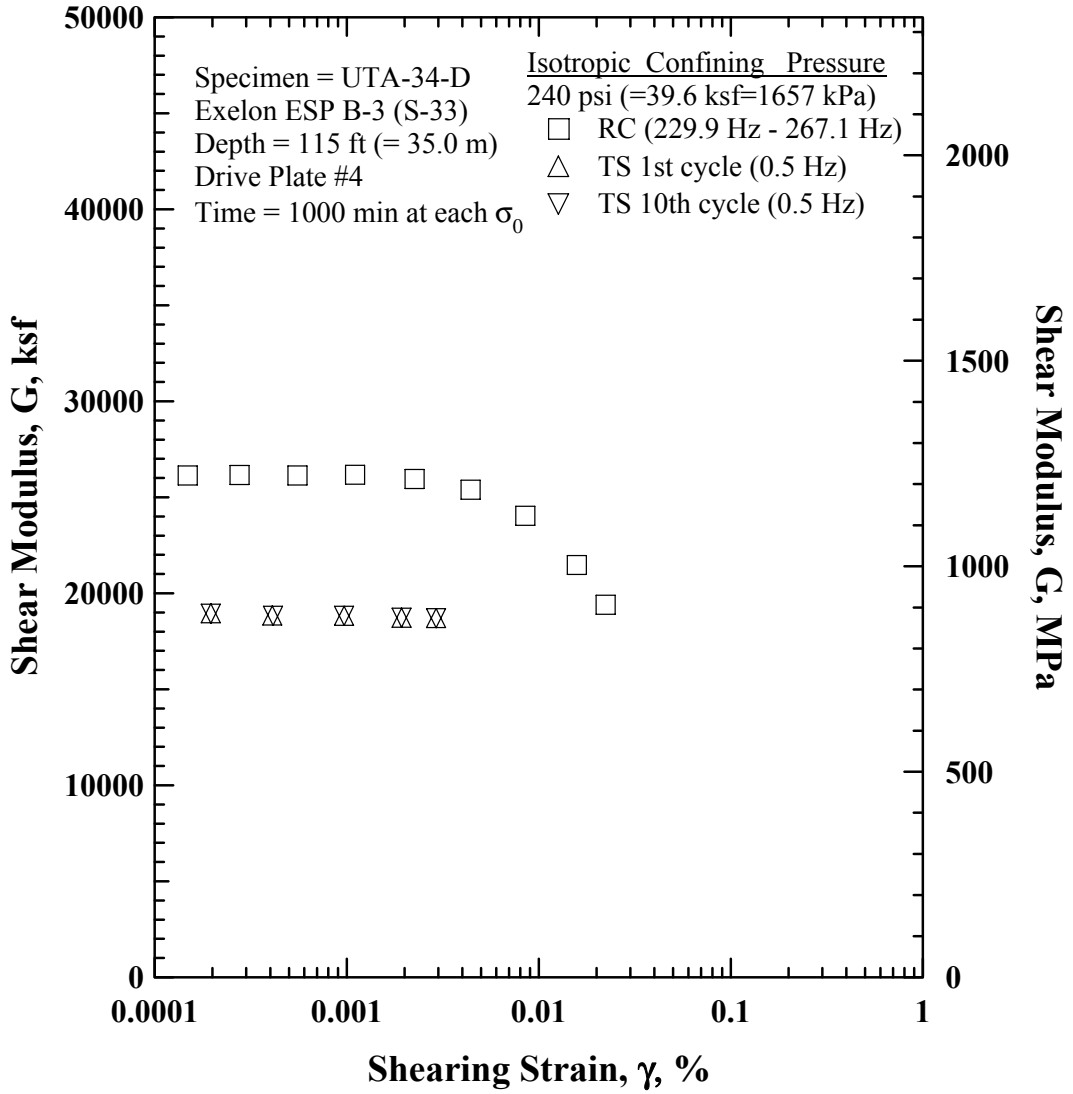

Figure D.16 Comparison of the Variation in Shear Modulus with Shearing Strain at an Isotropic Confining Pressure of 240 psi(=34.56 ksf=1657 kPa)from the Combined RCTS Tests of Specimen UTA-34-D (Specimen No. 3)

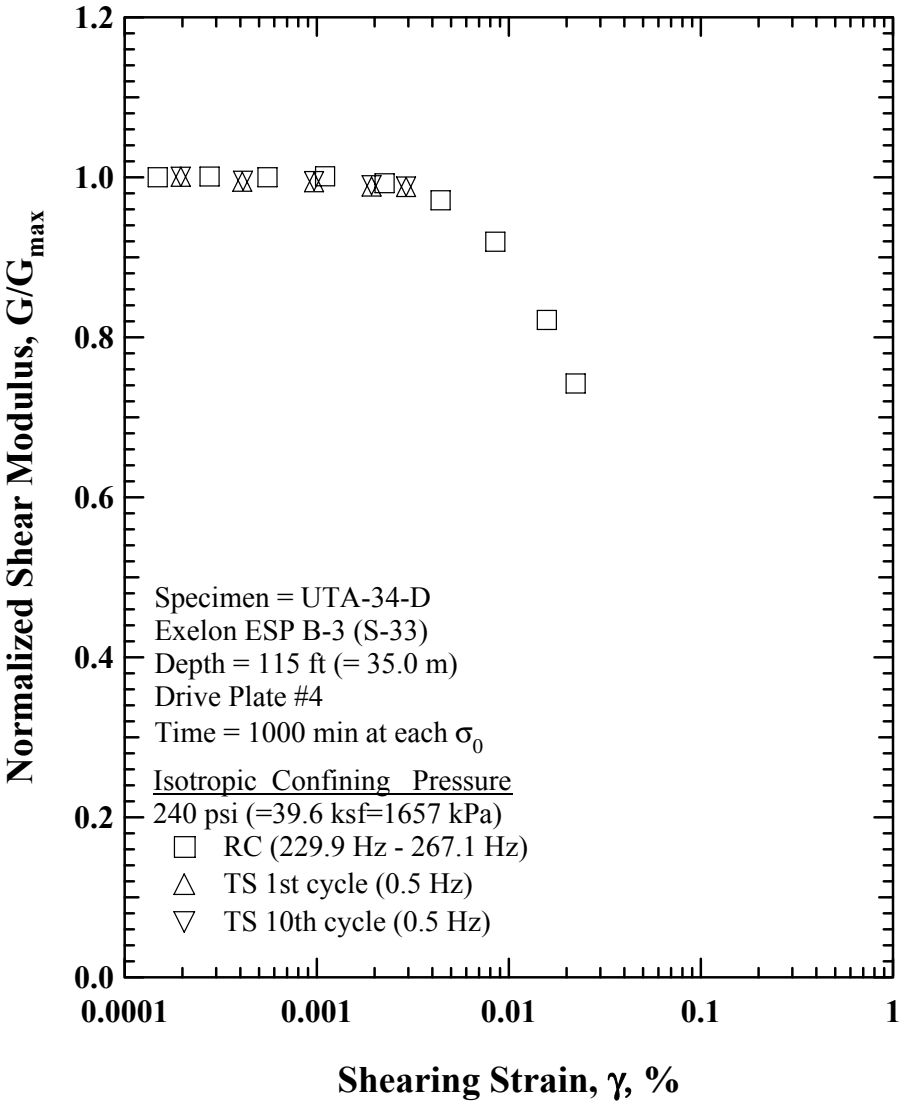

Figure D.17 Comparison of the Variation in Normalized Shear Modulus with Shearing Strain at an Isotropic Confining Pressure of 240 psi(=34.56 ksf=1657 kPa) from the Combined RCTS Tests of Specimen UTA-34-D (Specimen No. 3)

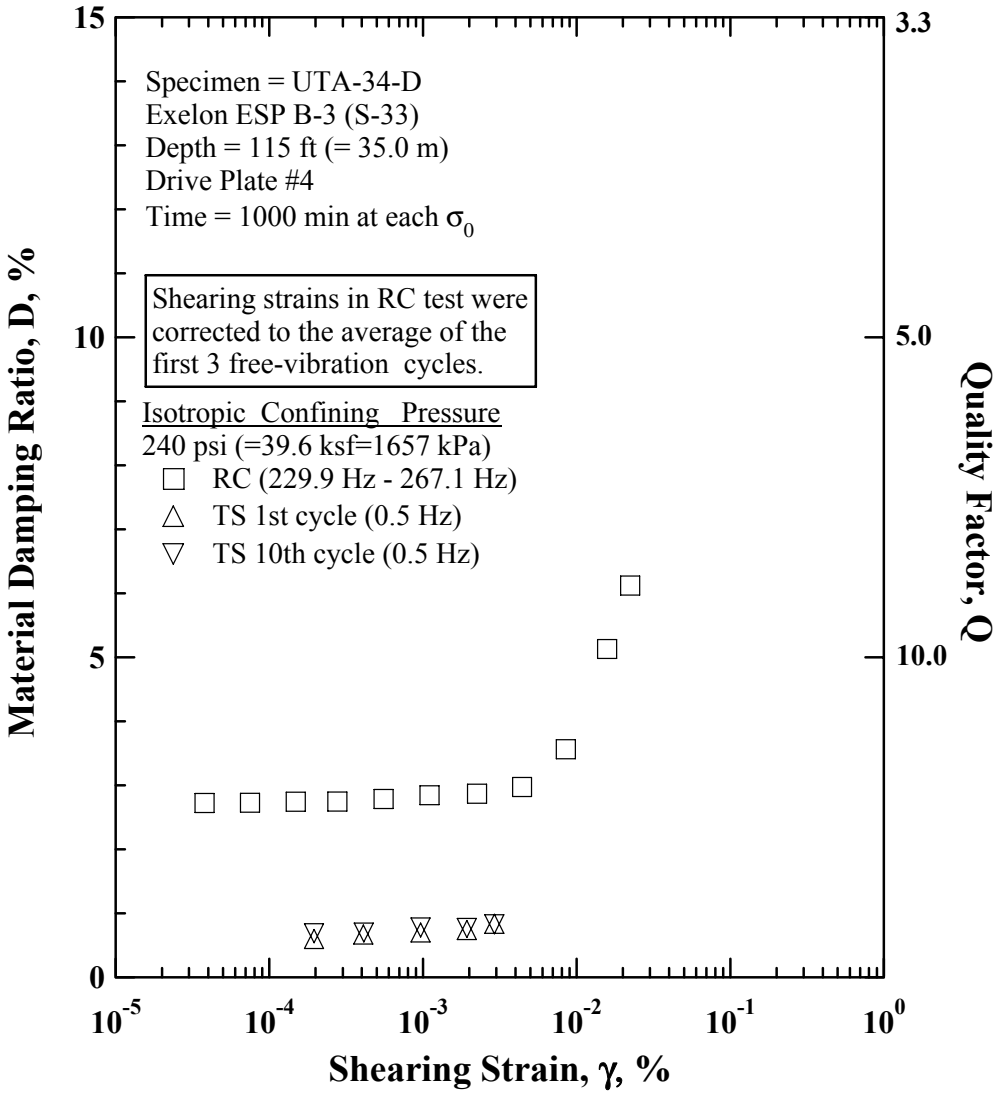

Figure D.18 Comparison of the Variation in Material Damping Ratio with Shearing Strain at an Isotropic Confining Pressure of 240 psi(=34.56 ksf=1657 kPa)from the Combined RCTS Tests of Specimen UTA-34-D (Specimen No. 3)

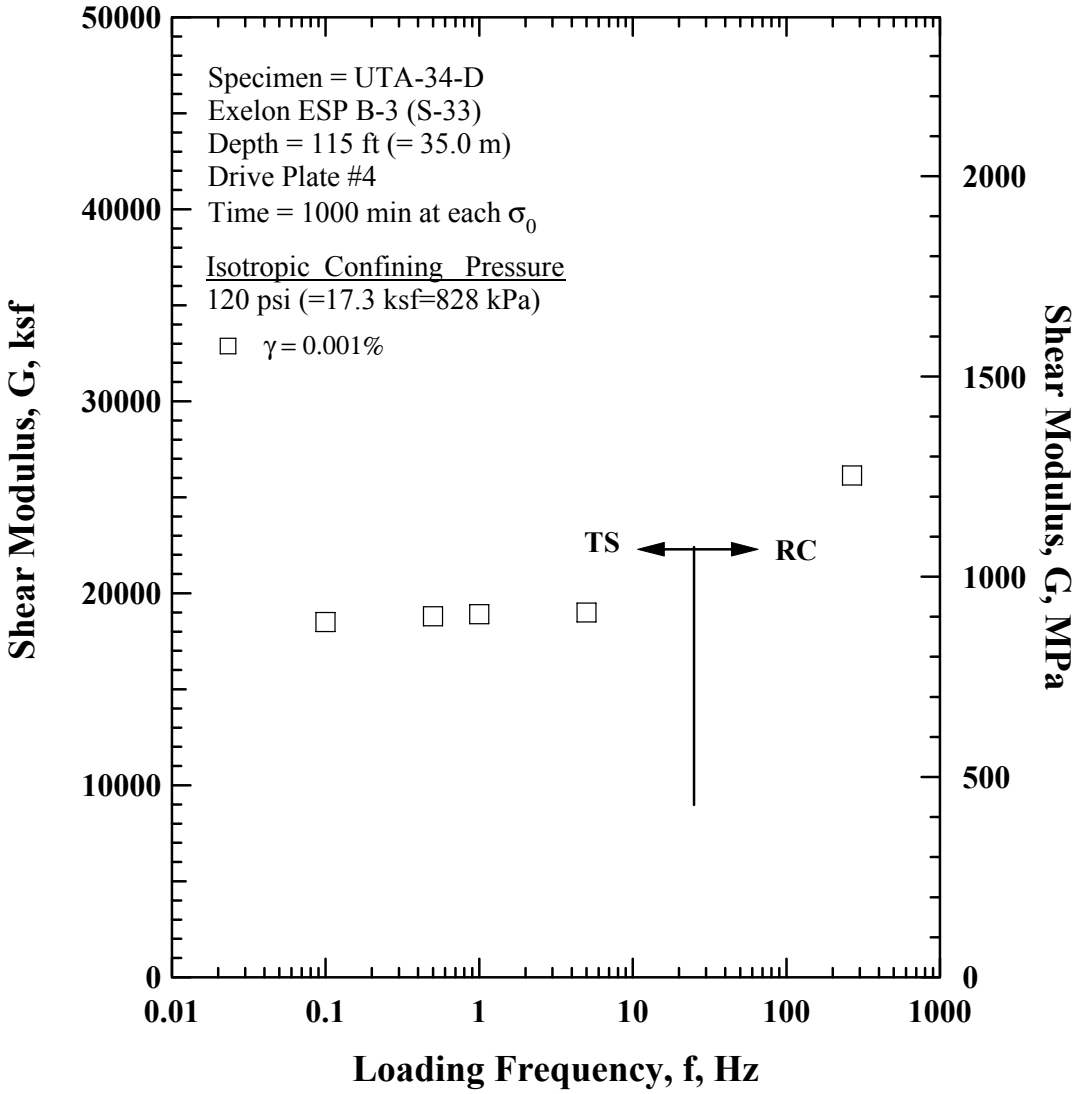

Figure D.19 Comparison of the Variation in Shear Modulus with Loading Frequency at an Isotropic Confining Pressure of 240 psi(=34.56 ksf=1657 kPa)from the Combined RCTS Tests of Specimen UTA-34-D (Specimen No. 3)

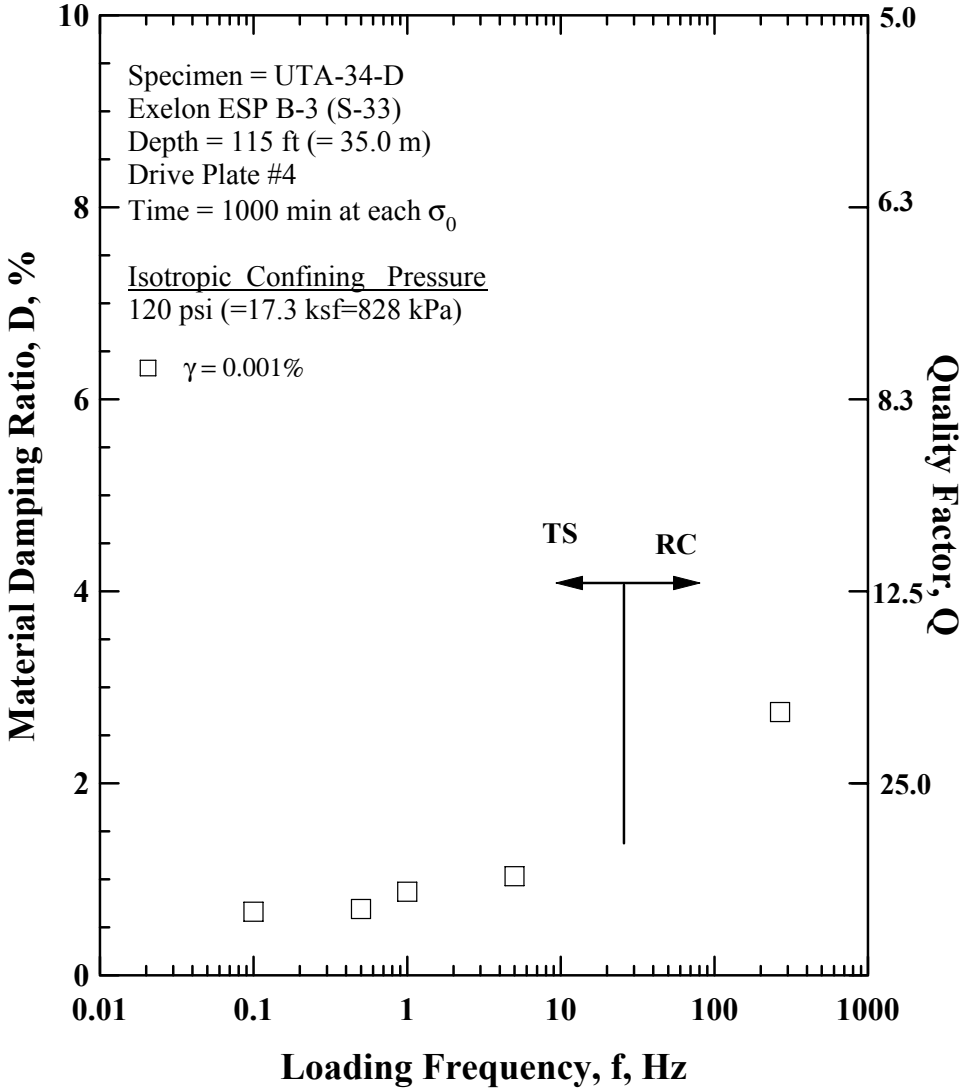

Figure D.20 Comparison of the Variation in Material Damping Ratio with Loading Frequency at an Isotropic Confining Pressure of 240 psi(=34.56 ksf=1657 kPa)from the Combined RCTS Tests of Specimen UTA-34-D (Specimen No. 3)

Table D.1 Variation in Low-Amplitude Shear Wave Velocity, Low-Amplitude Shear Modulus, Low-Amplitude Material Damping Ratio and Estimated Void Ratio with Isotropic Confining Pressure from RC Tests of Specimen UTA-34-D

Isotropic Isotropic Confining Pressure, so'			Low-Amplitude Shear Modulus, G_{max}		Low-Amplitude Shear Wave Velocity, Vs	Low-Amplitude Material Damping Ratio, D_{min}, %	Void Ratio, e
(psi)	(psf)	(kPa)	(ksf)	(MPa)	(fps)		
15	2160	103.5	14910	714.8	1816	3.31	0.234
30	4320	207.1	17186	823.9	1948	3.20	0.232
60	8640	414.2	19332	926.8	2064	3.15	0.229
120	17280	828.4	22382	1073.0	2217	3.05	0.222
240	34560	1656.8	25534	1224.1	2349	3.01	0.211

Table D.2 Variation in Shear Modulus, Normalized Shear Modulus and Material Damping Ratio with Shearing Strain from RC Tests of Specimen UTA-34-D; Isotropic Confining Pressure, σ_o = 60 psi(=8.64 ksf=414 kPa).

Peak Shearing Strain, %	Shear Modulus, G, ksf	Normalized Shear Modulus, G/G_{max}	Average[+] Shearing Strain, %	Material Damping Ratio[x], D, %
2.42E-05	20183	1.00	2.03E-05	2.99
4.71E-05	20201	1.00	3.95E-05	2.99
9.37E-05	20183	1.00	7.74E-05	3.10
1.87E-04	20180	1.00	1.56E-04	3.10
3.47E-04	20201	1.00	2.91E-04	3.04
6.89E-04	20012	0.99	5.76E-04	3.02
1.40E-03	19861	0.98	1.16E-03	3.16
2.70E-03	19525	0.97	2.23E-03	3.27
5.29E-03	18354	0.91	4.23E-03	3.89
9.60E-03	16636	0.82	7.22E-03	5.09
1.36E-02	15117	0.75	9.68E-03	6.21
1.79E-02	13955	0.69	1.22E-02	7.18
2.25E-02	12841	0.64	1.47E-02	8.16

[+] Average Shearing Strain from the First Three Cycles of the Free Vibration Decay Curve

[x] Average Damping Ratio from the First Three Cycles of the Free Vibration Decay Curve

Table D.3 Variation in Shear Modulus, Normalized Shear Modulus and Material Damping Ratio with Shearing Strain from TS Tests of Specimen UTA-34-D; Isotropic Confining Pressure, σ_o = 60 psi(=8.64 ksf=414 kPa).

First Cycle				Tenth Cycle			
Peak Shearing Strain, %	Shear Modulus, G, ksf	Normalized Shear Modulus, G/G_{max}	Material Damping Ratio, D, %	Peak Shearing Strain, %	Shear Modulus, G, ksf	Normalized Shear Modulus, G/G_{max}	Material Damping Ratio, D, %
1.89E-04	9738	1.00	0.73	1.89E-04	9738	1.00	0.73
3.76E-04	9657	0.99	0.73	3.76E-04	9649	0.99	0.72
7.51E-04	9621	0.99	0.73	7.51E-04	9621	0.99	0.70
1.03E-03	9543	0.98	0.75	1.03E-03	9543	0.98	0.76
2.01E-03	9326	0.96	0.91	2.02E-03	9304	0.96	0.91
3.99E-03	9235	0.95	1.11	4.02E-03	9150	0.94	1.18
4.81E-03	9014	0.93	1.20	4.82E-03	8996	0.92	1.21

Table D.4 Variation in Shear Modulus, Normalized Shear Modulus and Material Damping Ratio with Shearing Strain from RC Tests of Specimen UTA-34-D; Isotropic Confining Pressure, σ_o = 240 psi(=34.56 ksf=1657 kPa).

Peak Shearing Strain, %	Shear Modulus, G, ksf	Normalized Shear Modulus, G/G_{max}	Average[+] Shearing Strain, %	Material Damping Ratio[x], D, %
3.78E-05	26164	1.00	3.22E-05	2.72
7.48E-05	26141	1.00	6.36E-05	2.73
1.49E-04	26135	1.00	1.26E-04	2.74
2.76E-04	26164	1.00	2.35E-04	2.75
5.54E-04	26135	1.00	4.69E-04	2.79
1.10E-03	26167	1.00	9.34E-04	2.84
2.25E-03	25945	0.99	1.90E-03	2.87
4.41E-03	25389	0.97	3.70E-03	2.97
8.51E-03	24030	0.92	6.92E-03	3.56
1.58E-02	21476	0.82	1.18E-02	5.13
2.23E-02	19398	0.74	1.59E-02	6.12

[+] Average Shearing Strain from the First Three Cycles of the Free Vibration Decay Curve

[x] Average Damping Ratio from the First Three Cycles of the Free Vibration Decay Curve

Table D.5 Variation in Shear Modulus, Normalized Shear Modulus and Material Damping Ratio with Shearing Strain from TS Tests of Specimen UTA-34-D; Isotropic Confining Pressure, σ_o = 240 psi(=34.56 ksf=1657 kPa).

First Cycle				Tenth Cycle			
Peak Shearing Strain, %	Shear Modulus, G, ksf	Normalized Shear Modulus, G/G_{max}	Material Damping Ratio, D, %	Peak Shearing Strain, %	Shear Modulus, G, ksf	Normalized Shear Modulus, G/G_{max}	Material Damping Ratio, D, %
1.97E-04	18930	1.00	0.59	1.97E-04	18900	1.00	0.68
4.12E-04	18810	0.99	0.66	4.15E-04	18805	0.99	0.69
9.72E-04	18800	0.99	0.69	9.72E-04	18800	0.99	0.77
1.94E-03	18701	0.99	0.73	1.94E-03	18701	0.99	0.76
2.93E-03	18690	0.99	0.83	2.93E-03	18670	0.99	0.82

Exhibit E
to Attachment A-7

Specimen No.4
UT Specimen:UTA-34-C

Exelon ESP B-3
Depth = 171ft (=52.1m)
Soil Type:Sandy Lean Clay (CL)

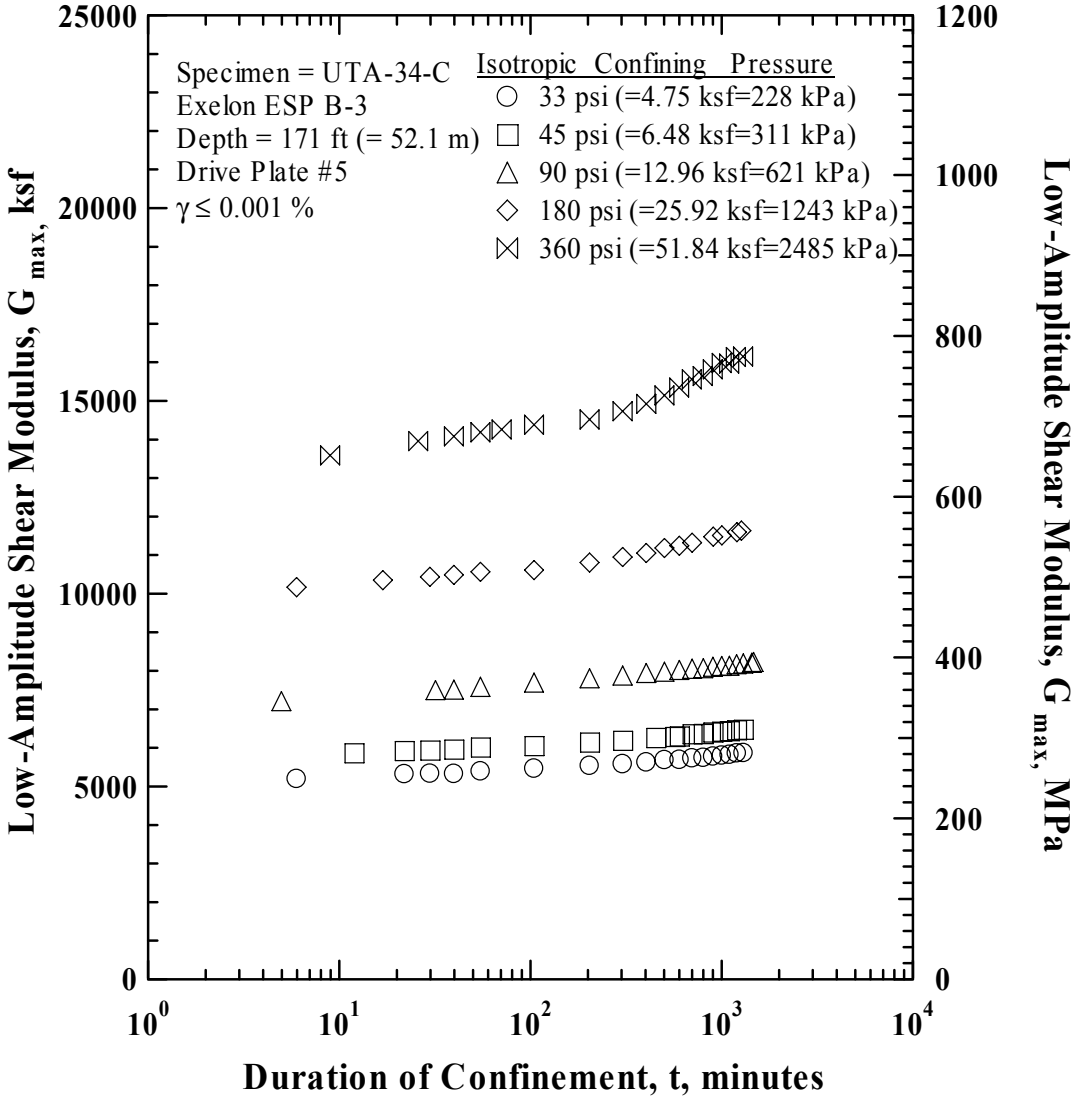

Figure E.1 Variation in Low-Amplitude Shear Modulus with Magnitude and Duration of Isotropic Confining Pressure from Resonant Column Tests of Specimen UTA-34-C (Specimen No. 4).

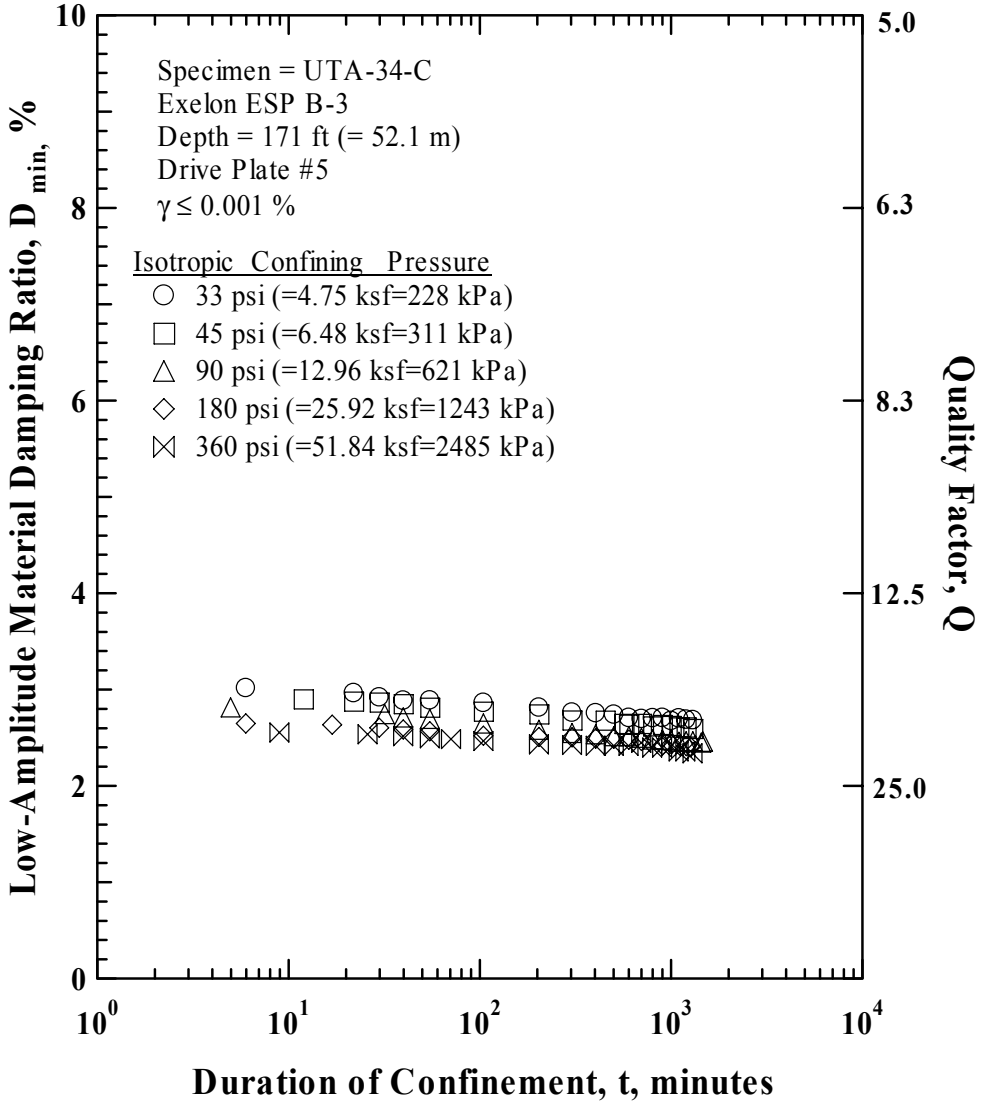

Figure E.2 Variation in Low-Amplitude Material Damping Ratio with Magnitude and Duration of Isotropic Confining Pressure from Resonant Column Tests of Specimen UTA-34-C (Specimen No. 4).

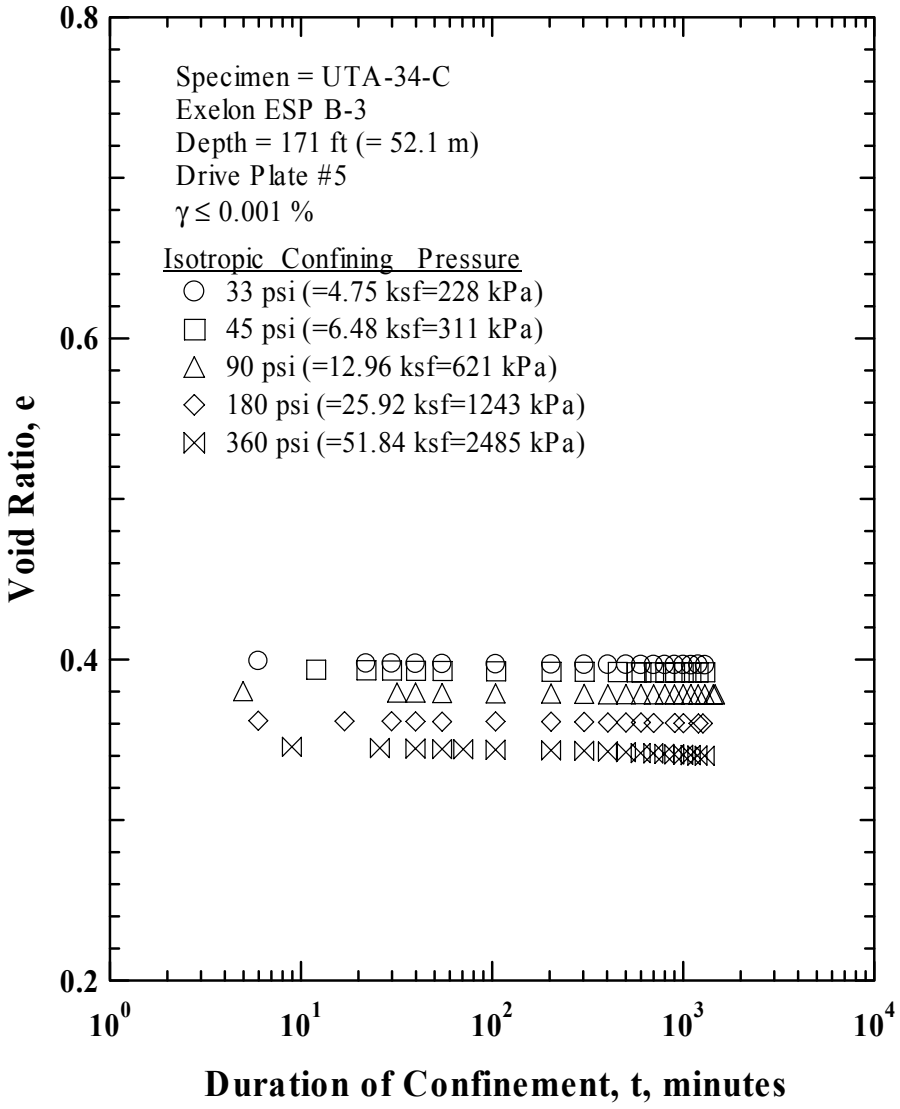

Figure E.3 Variation in Estimated Void Ratio with Magnitude and Duration of Isotropic Confining Pressure from Resonant Column Tests of Specimen UTA-34-C (Specimen No. 4).

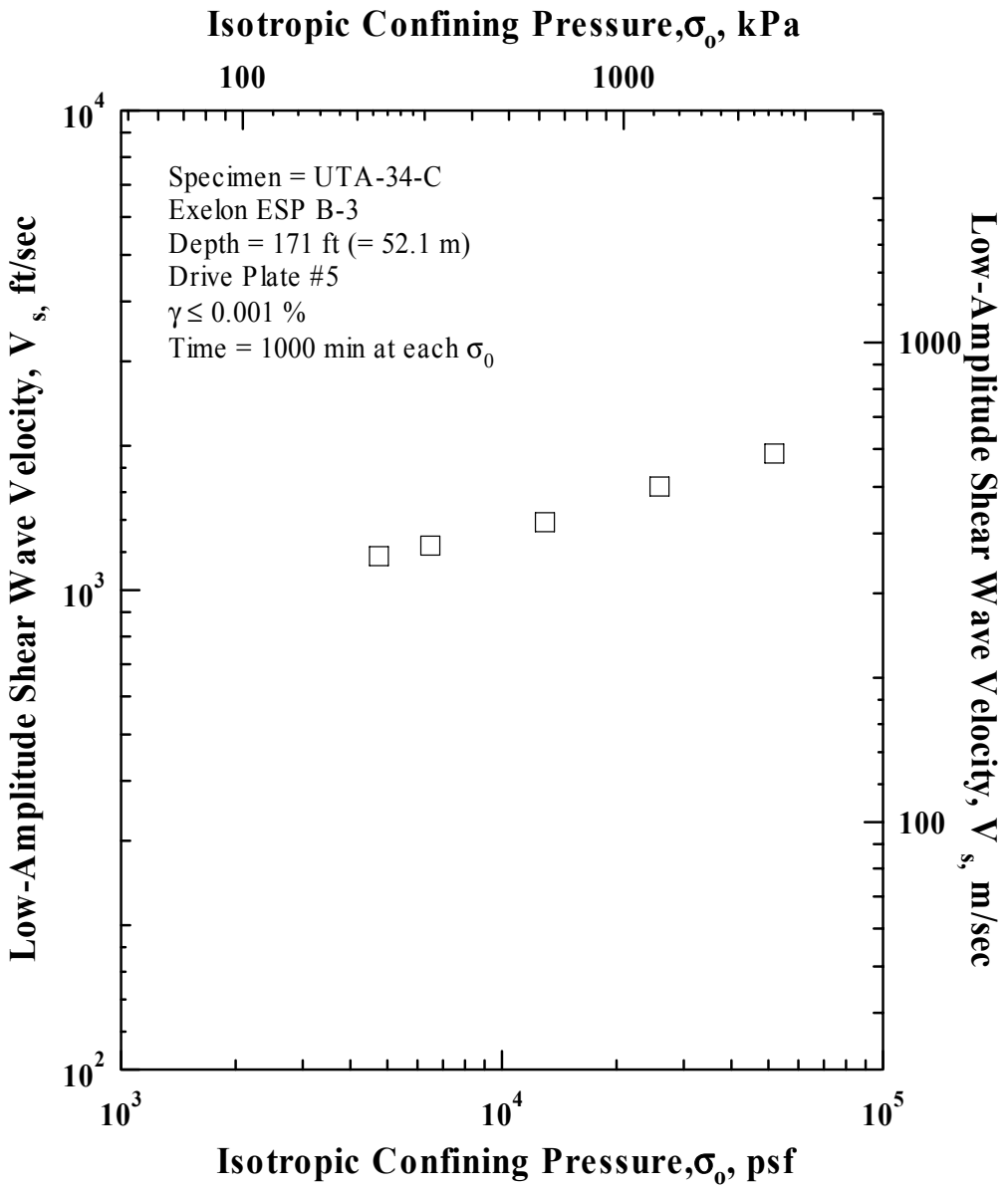

Figure E.4 Variation in Shear Wave Velocity with Isotropic Confining Pressure from Resonant Column Tests of Specimen UTA-34-C (Specimen No. 4).

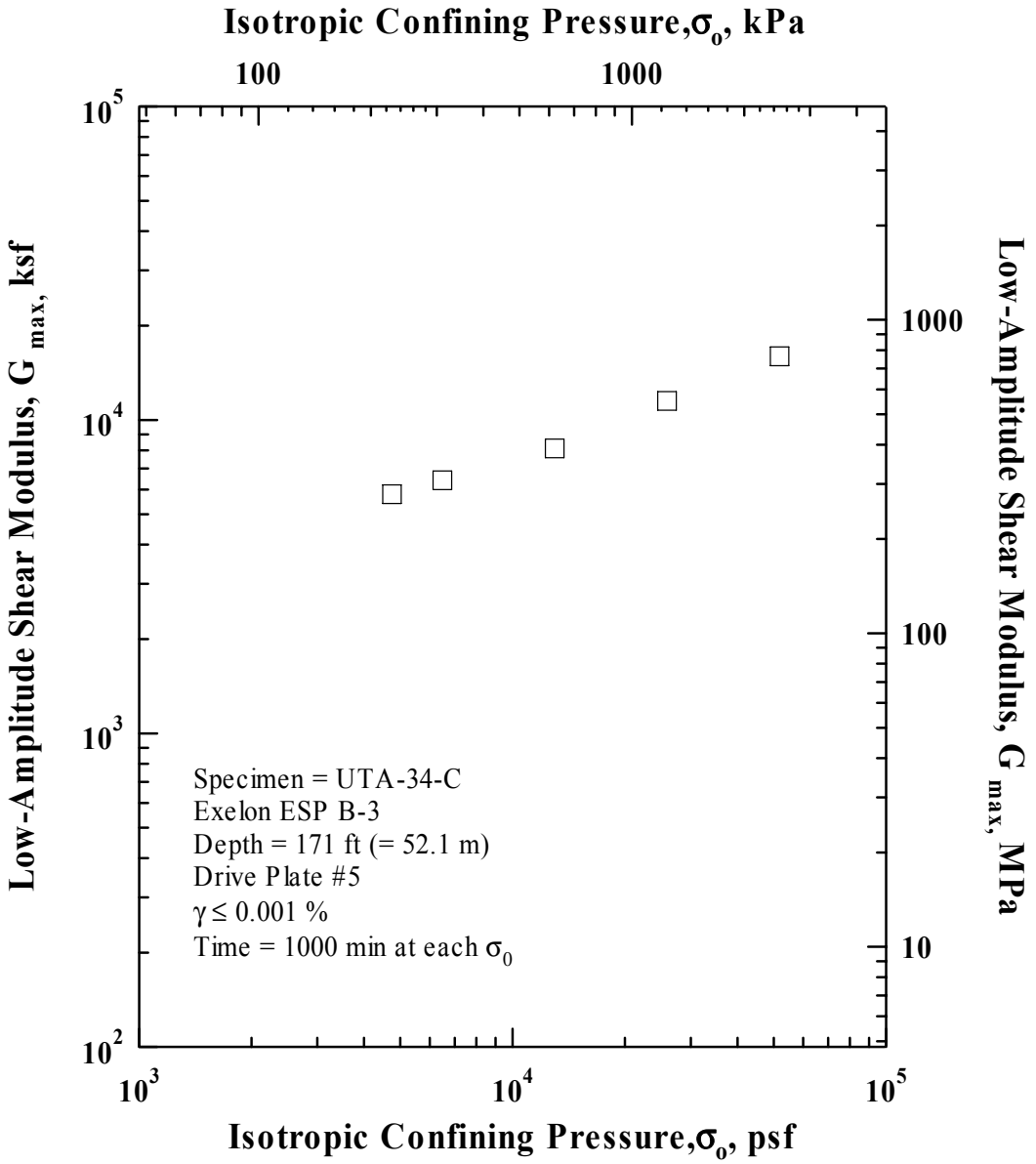

Figure E.5 Variation in Low-Amplitude Shear Modulus with Isotropic Confining Pressure from Resonant Column Tests of Specimen UTA-34-C (Specimen No. 4).

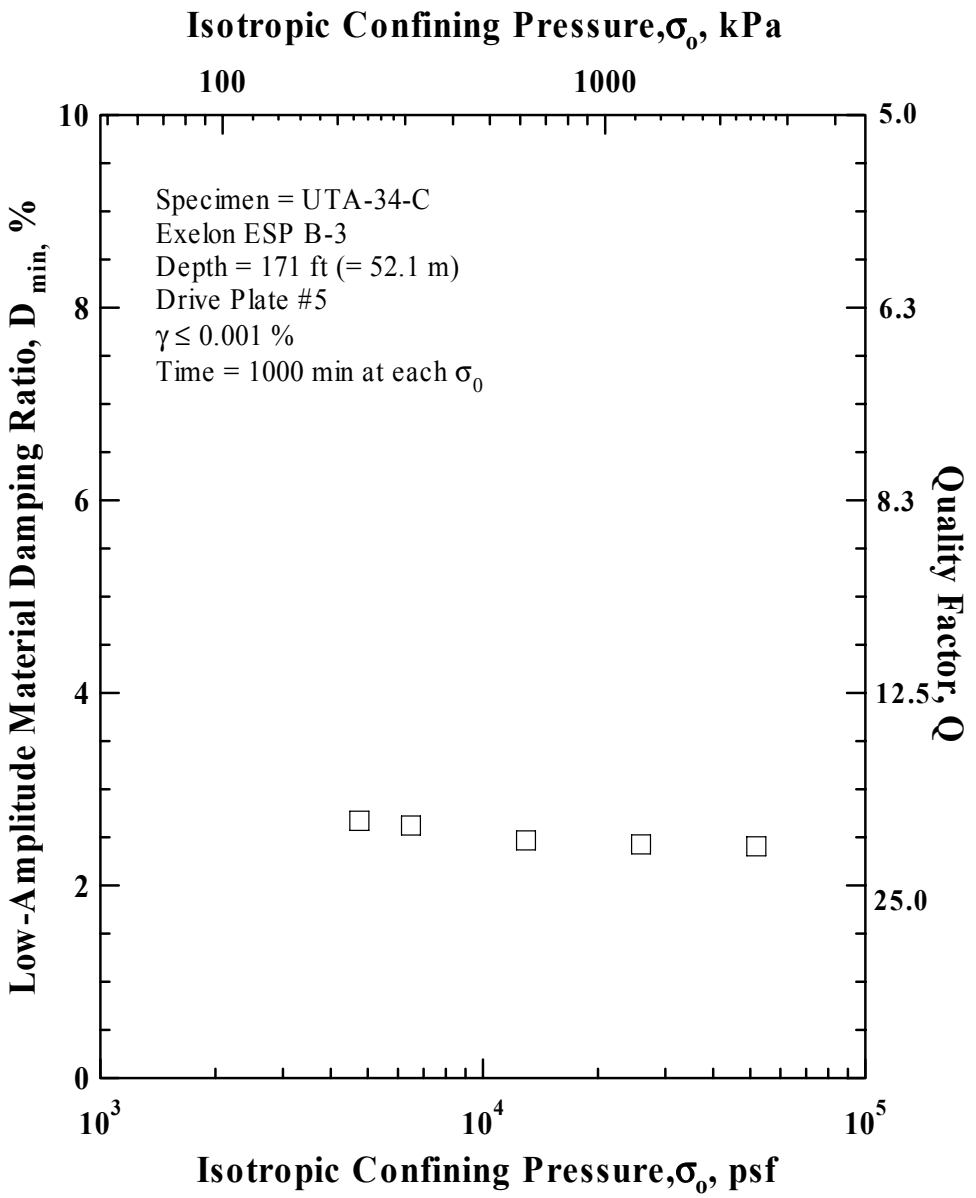

Figure E.6 Variation in Material Damping Ratio with Isotropic Confining Pressure from Resonant Column Tests of Specimen UTA-34-C (Specimen No. 4).

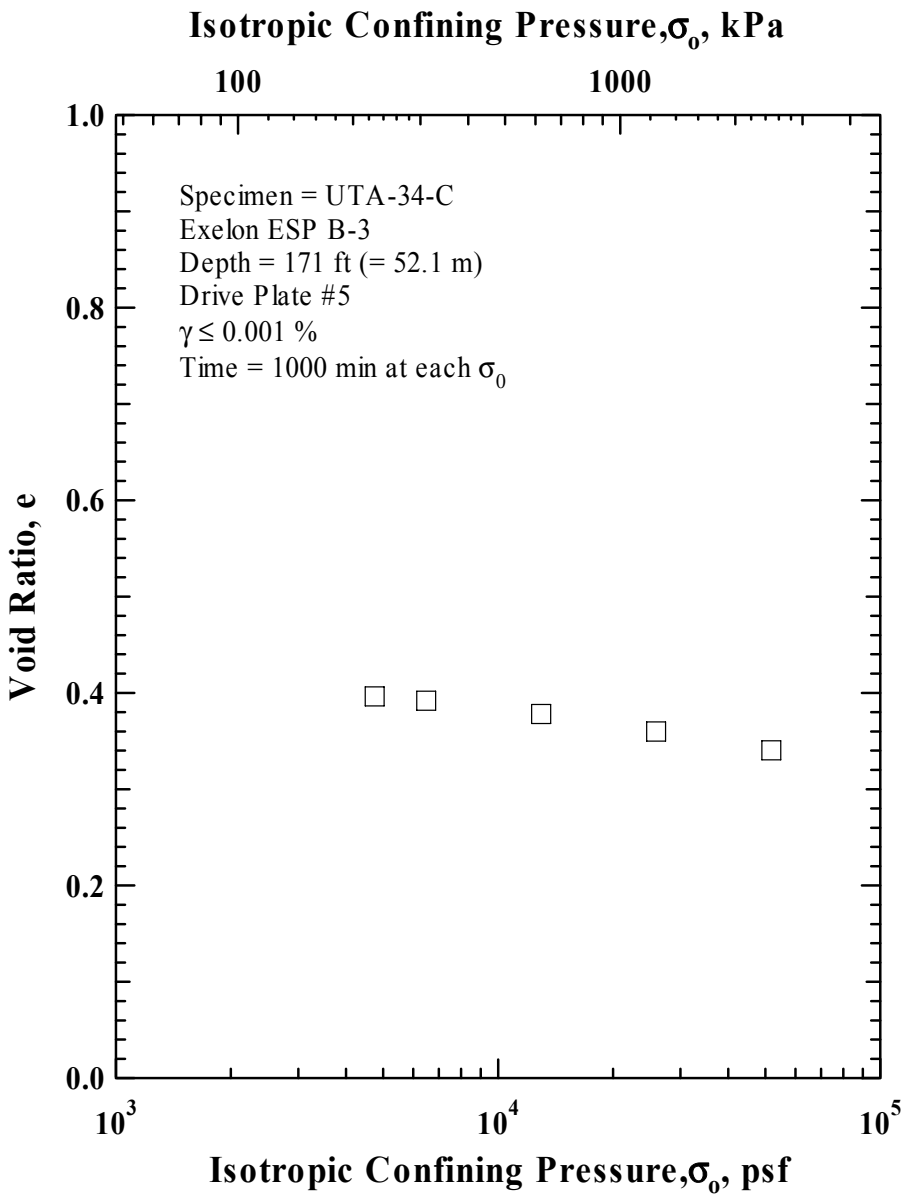

Figure E.7 Variation in Estimated Void Ratio with Isotropic Confining Pressure from Resonant Column Tests of Specimen UTA-34-C (Specimen No. 4).

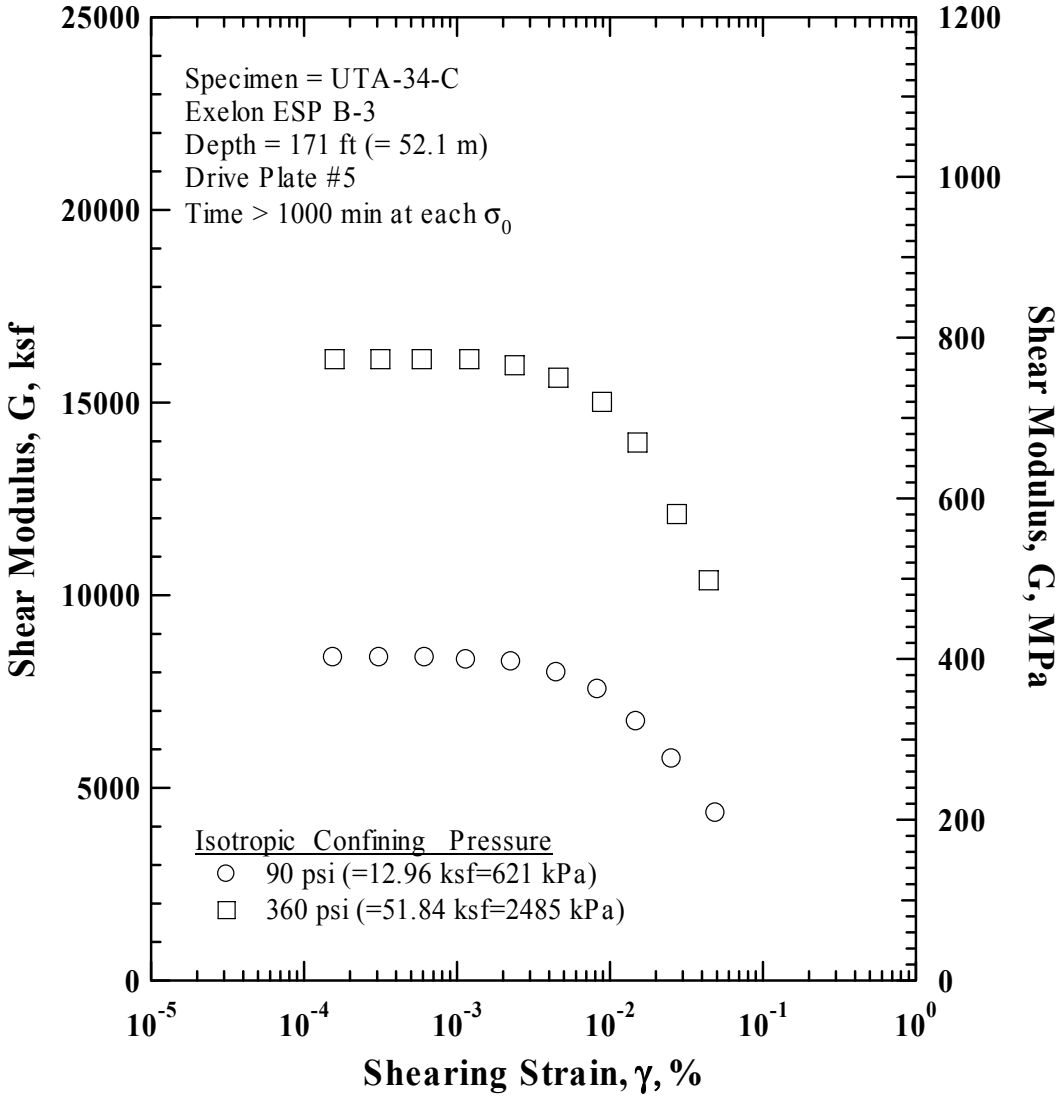

Figure E.8 Comparison of the Variation in Shear Modulus with Shearing Strain and Isotropic Confining Pressure from the Resonant Column Tests of Specimen UTA-34-C (Specimen No. 4).

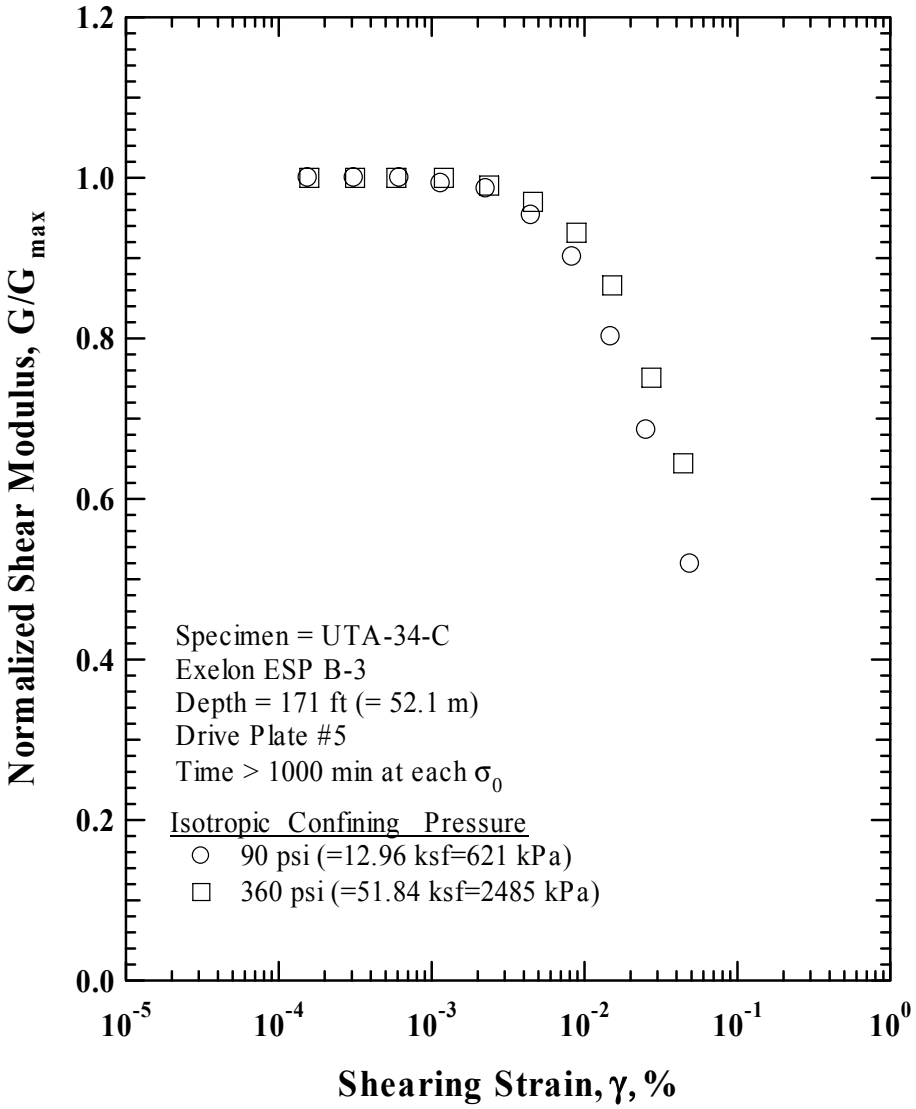

Figure E.9 Comparison of the Variation in Normalized Shear Modulus with Shearing Strain and Isotropic Confining Pressure from the Resonant Column Tests of Specimen UTA-34-C (Specimen No. 4).

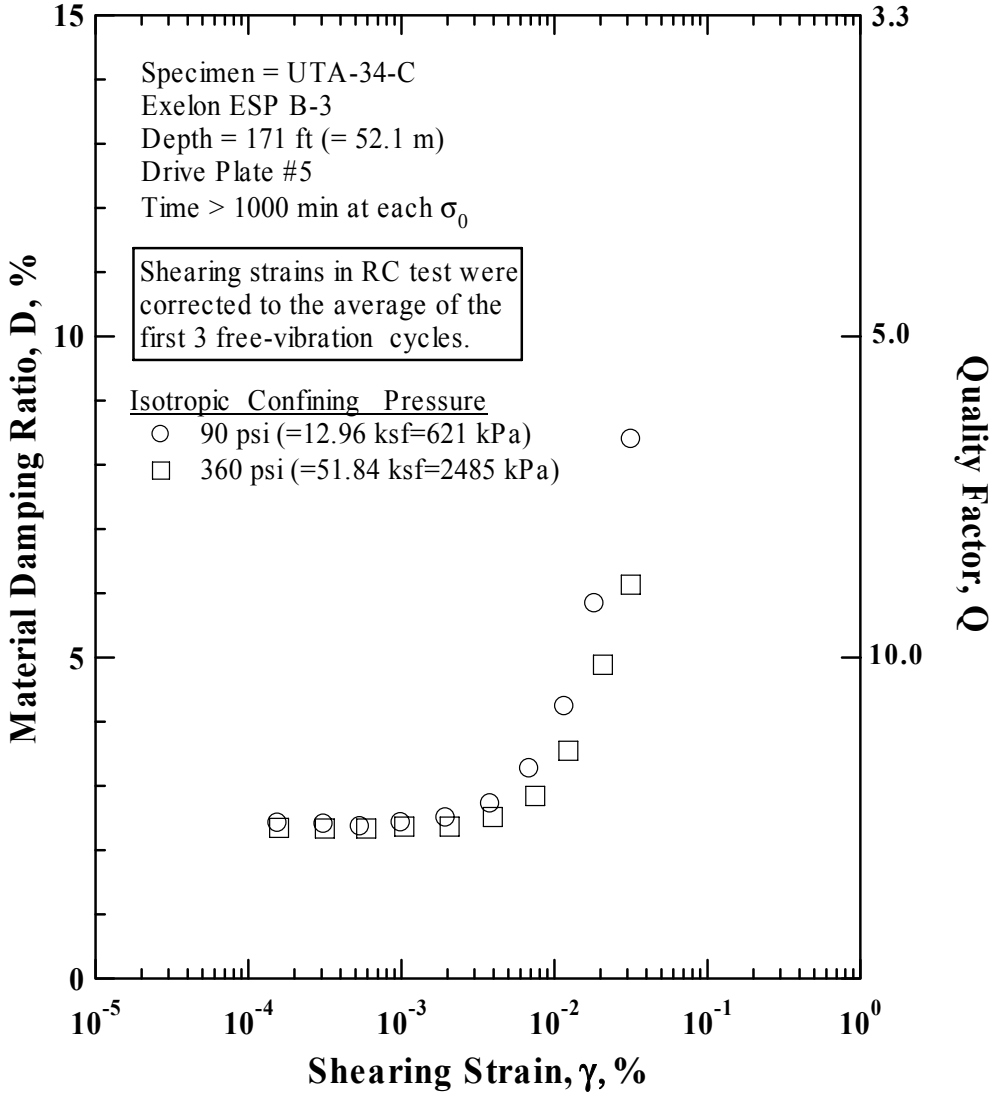

Figure E.10 Comparison of the Variation in Material Damping Ratio with Shearing Strain and Isotropic Confining Pressure from the Resonant Column Tests of Specimen UTA-34-C (Specimen No. 4).

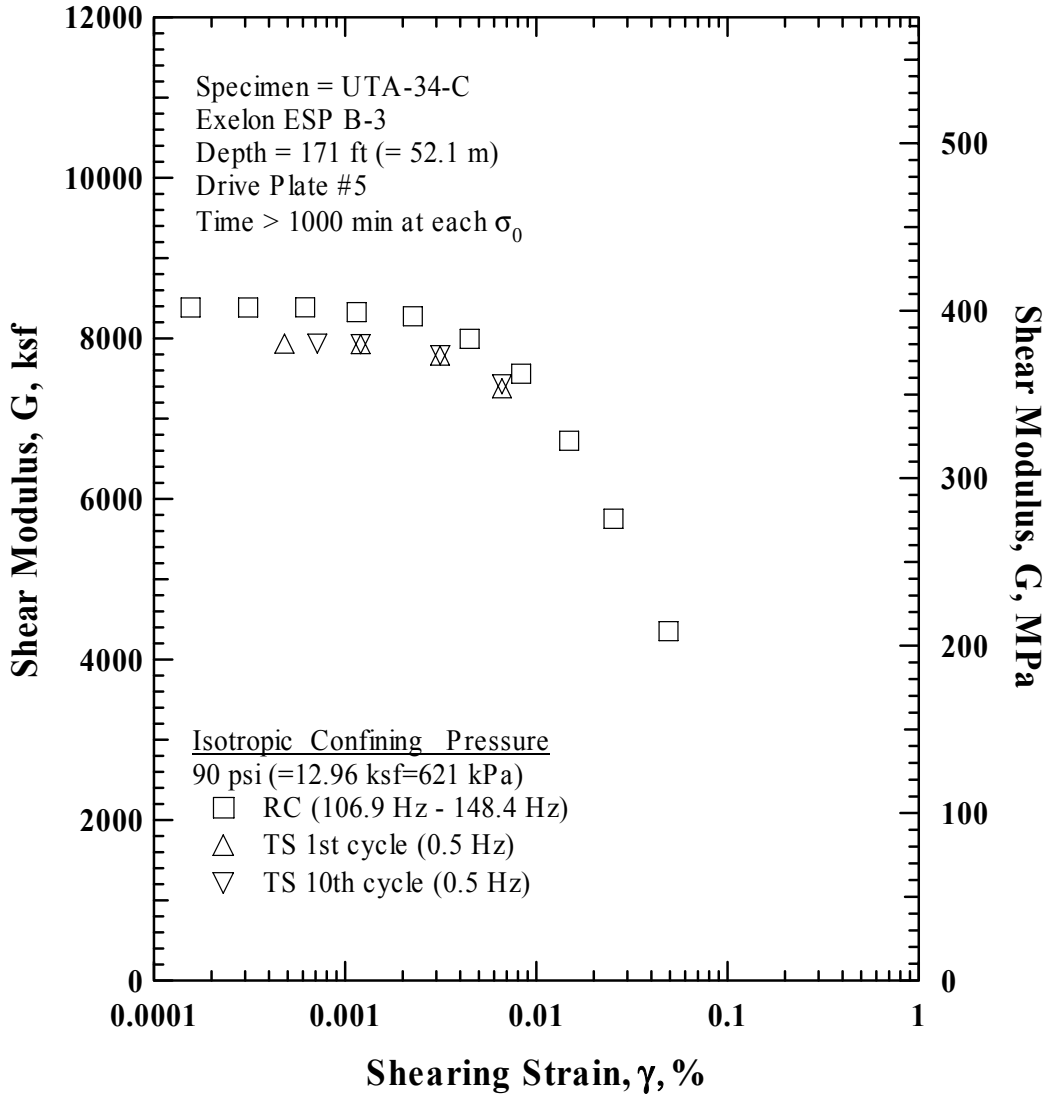

Figure E.11 Comparison of the Variation in Shear Modulus with Shearing Strain at an Isotropic Confining Pressure of 90 psi (=12.96 ksf=621 kPa) from the Combined RCTS Tests of Specimen UTA-34-C (Specimen No. 4).

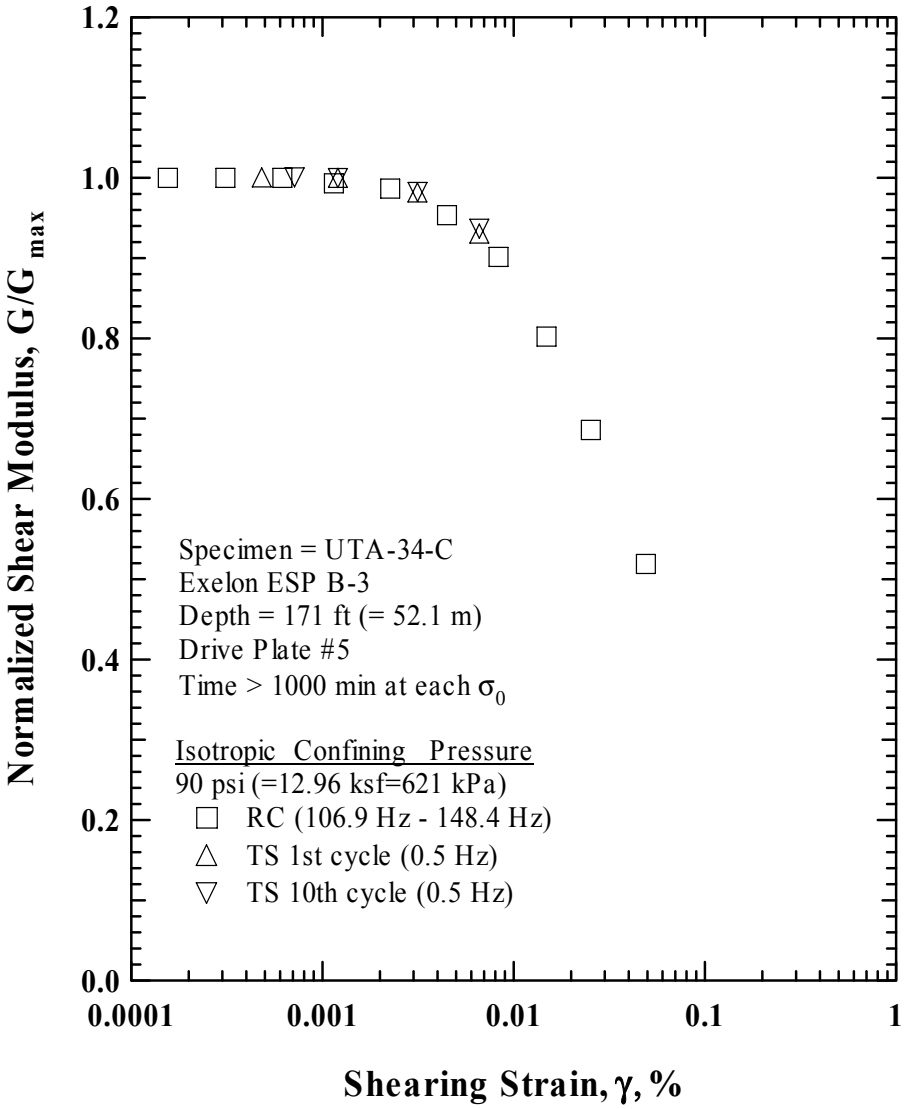

Figure E.12 Comparison of the Variation in Normalized Shear Modulus with Shearing Strain at an Isotropic Confining Pressure of 90 psi (=12.96 ksf=621 kPa) from the Combined RCTS Tests of Specimen UTA-34-C (Specimen No. 4).

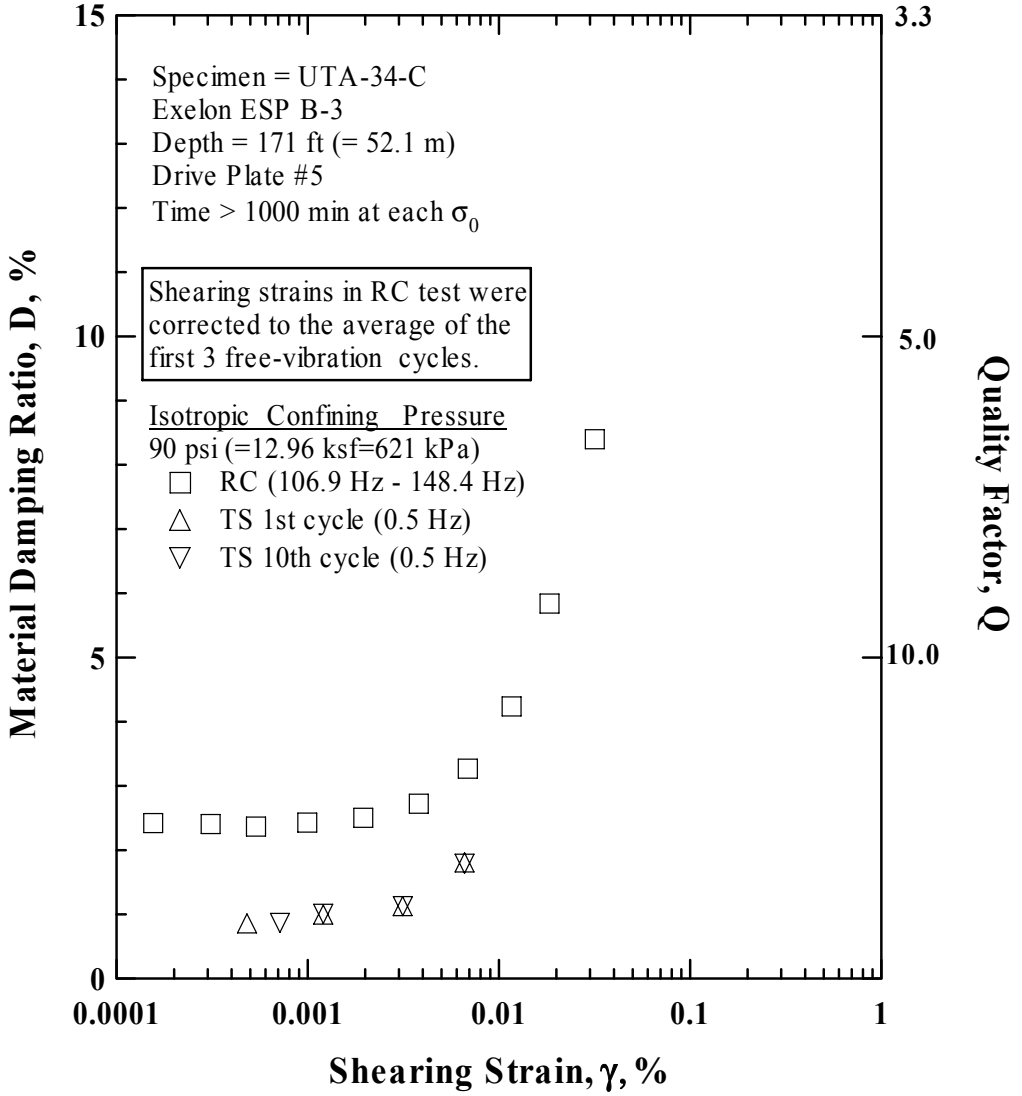

Figure E.13 Comparison of the Variation in Material Damping Ratio with Shearing Strain at an Isotropic Confining Pressure of 90 psi (=12.96 ksf=621 kPa) from the Combined RCTS Tests of Specimen UTA-34-C (Specimen No. 4).

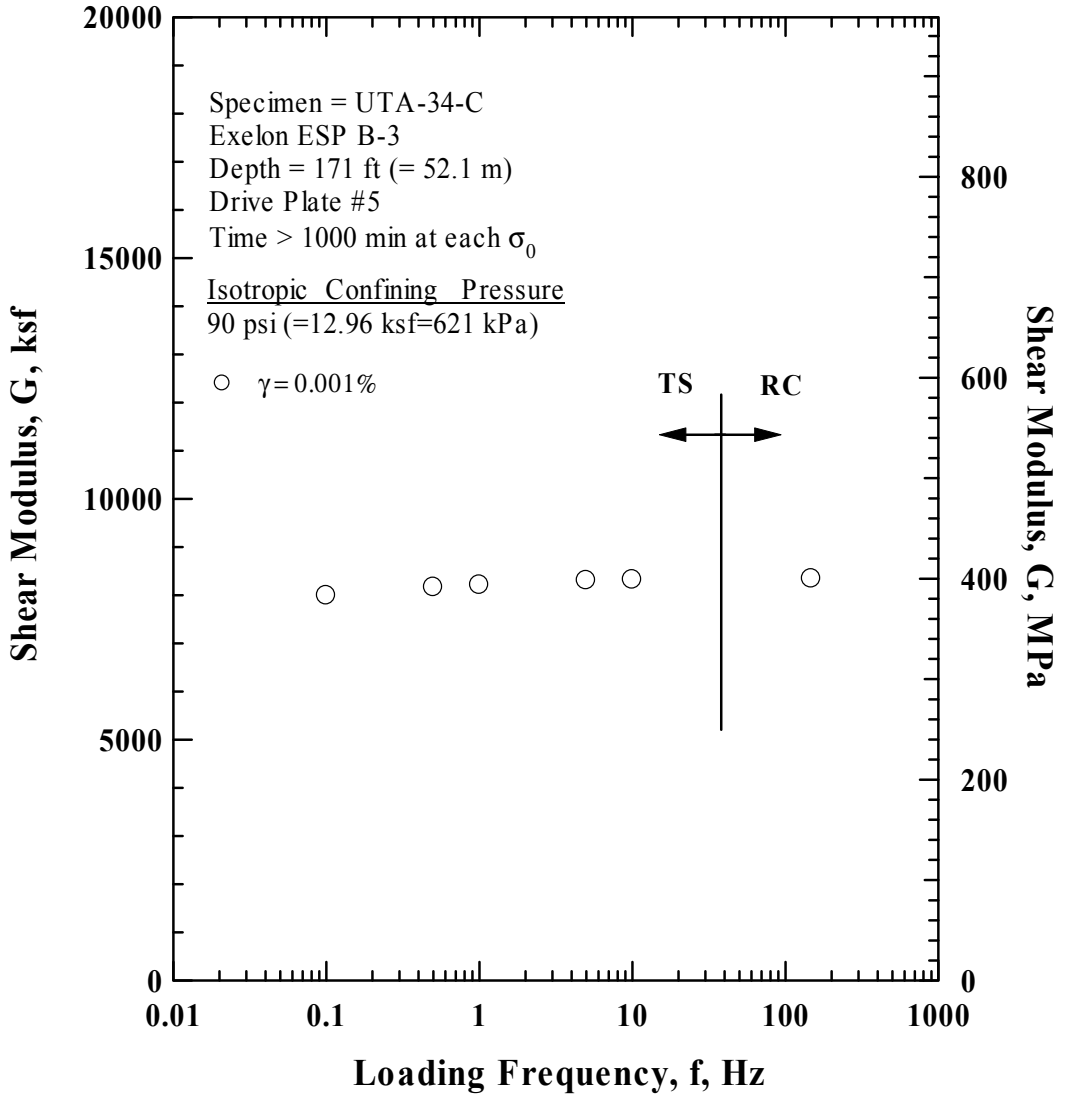

Figure E.14 Comparison of the Variation in Shear Modulus with Loading Frequency at an Isotropic Confining Pressure of 90 psi (=12.96 ksf=621 kPa) from the Combined RCTS Tests of Specimen UTA-34-C (Specimen No. 4).

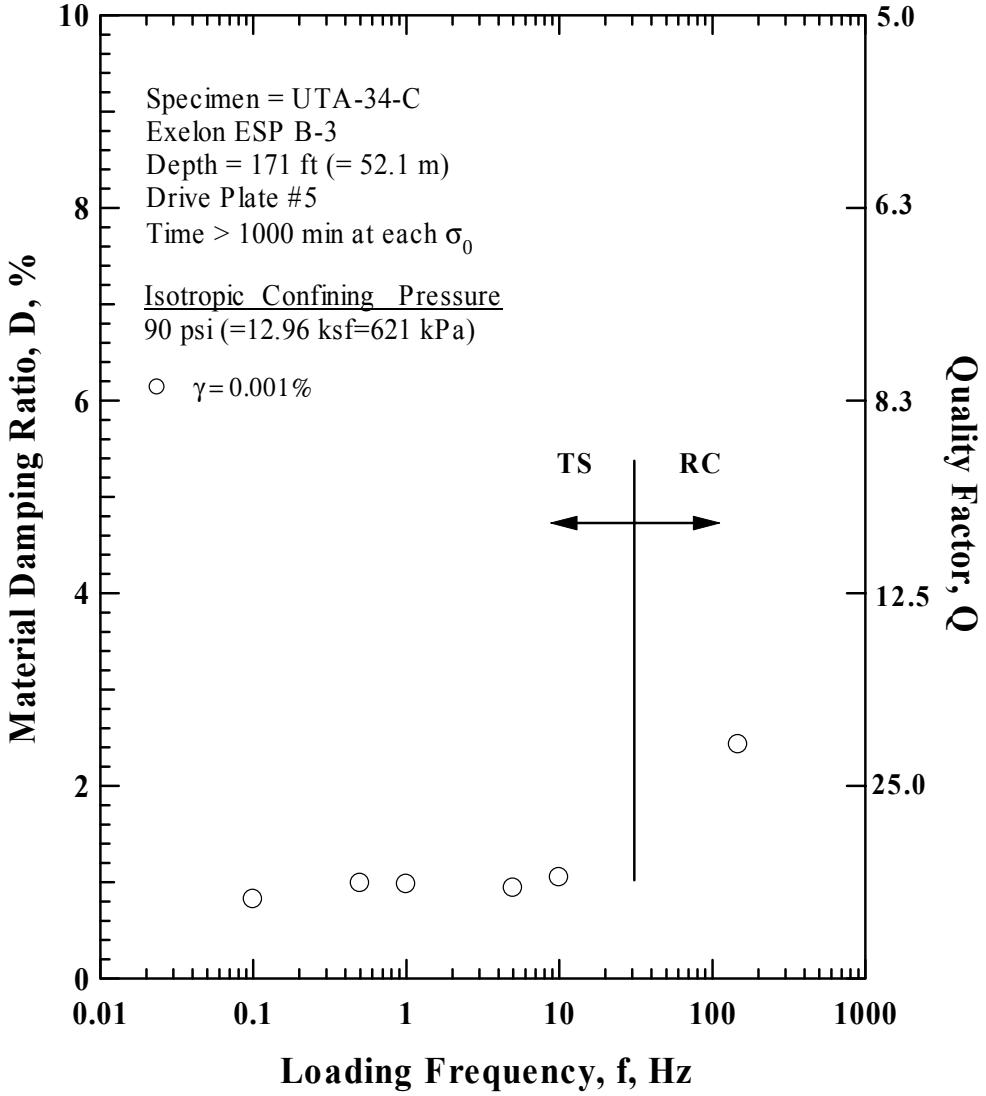

Figure E.15 Comparison of the Variation in Material Damping Ratio with Loading Frequency at an Isotropic Confining Pressure 90 psi (=12.96 ksf=621 kPa) from the Combined RCTS Tests of Specimen UTA-34-C (Specimen No. 4).

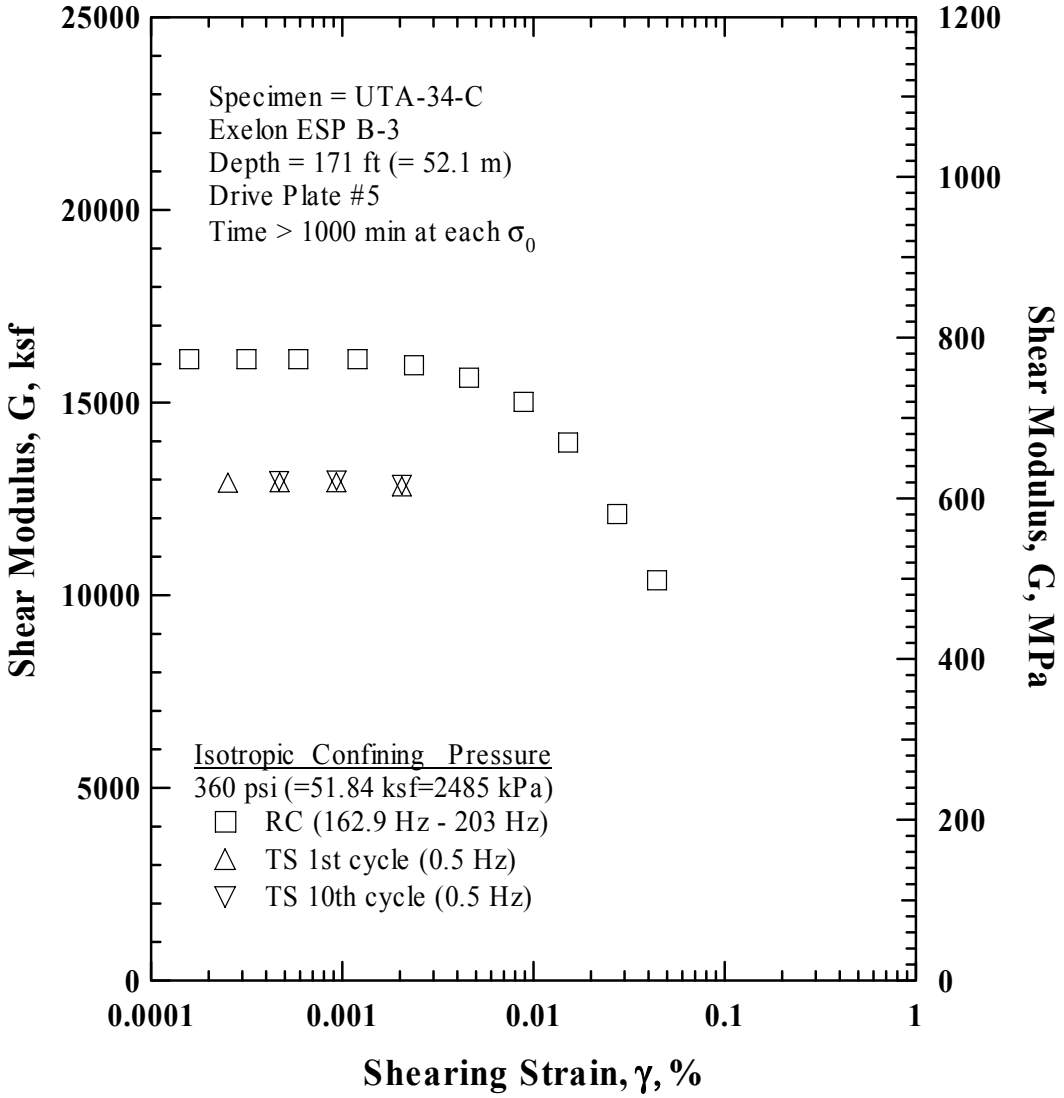

Figure E.16 Comparison of the Variation in Shear Modulus with Shearing Strain at an Isotropic Confining Pressure of 360 psi (=51.84 ksf=2485 kPa) from the Combined RCTS Tests of Specimen UTA-34-C (Specimen No. 4).

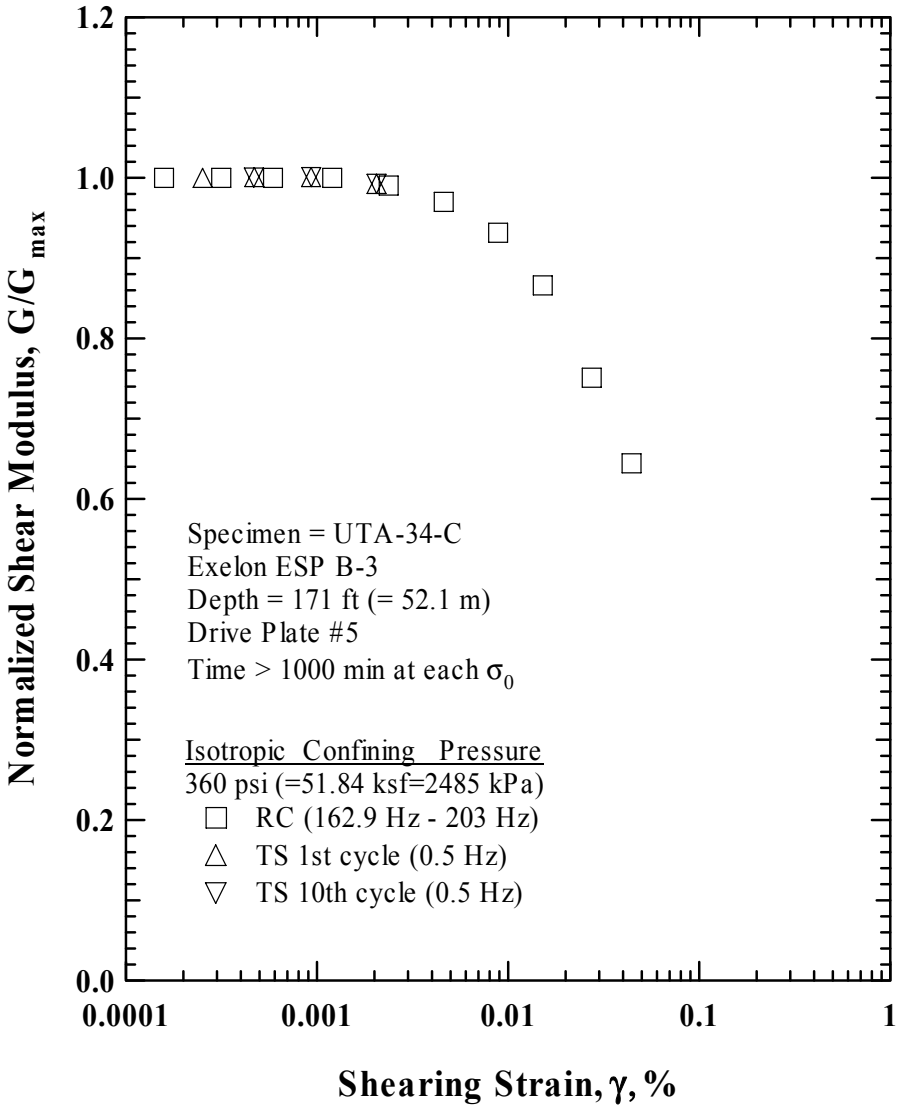

Figure E.17 Comparison of the Variation in Normalized Shear Modulus with Shearing Strain at an Isotropic Confining Pressure of 360 psi (=51.84 ksf=2485 kPa) from the Combined RCTS Tests of Specimen UTA-34-C (Specimen No. 4).

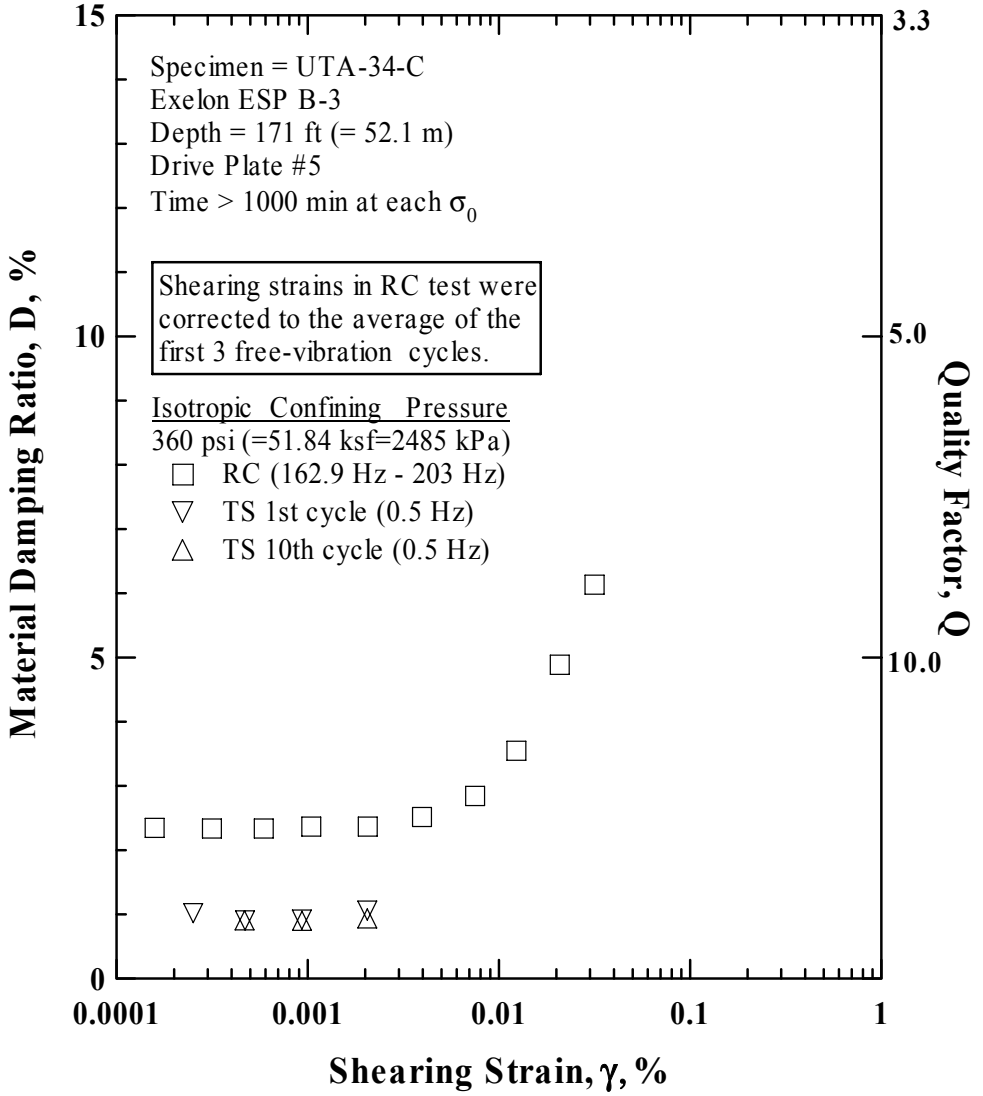

Figure E.18 Comparison of the Variation in Material Damping Ratio with Shearing Strain at an Isotropic Confining Pressure of 360 psi (=51.84 ksf=2485 kPa) from the Combined RCTS Tests of Specimen UTA-34-C (Specimen No. 4).

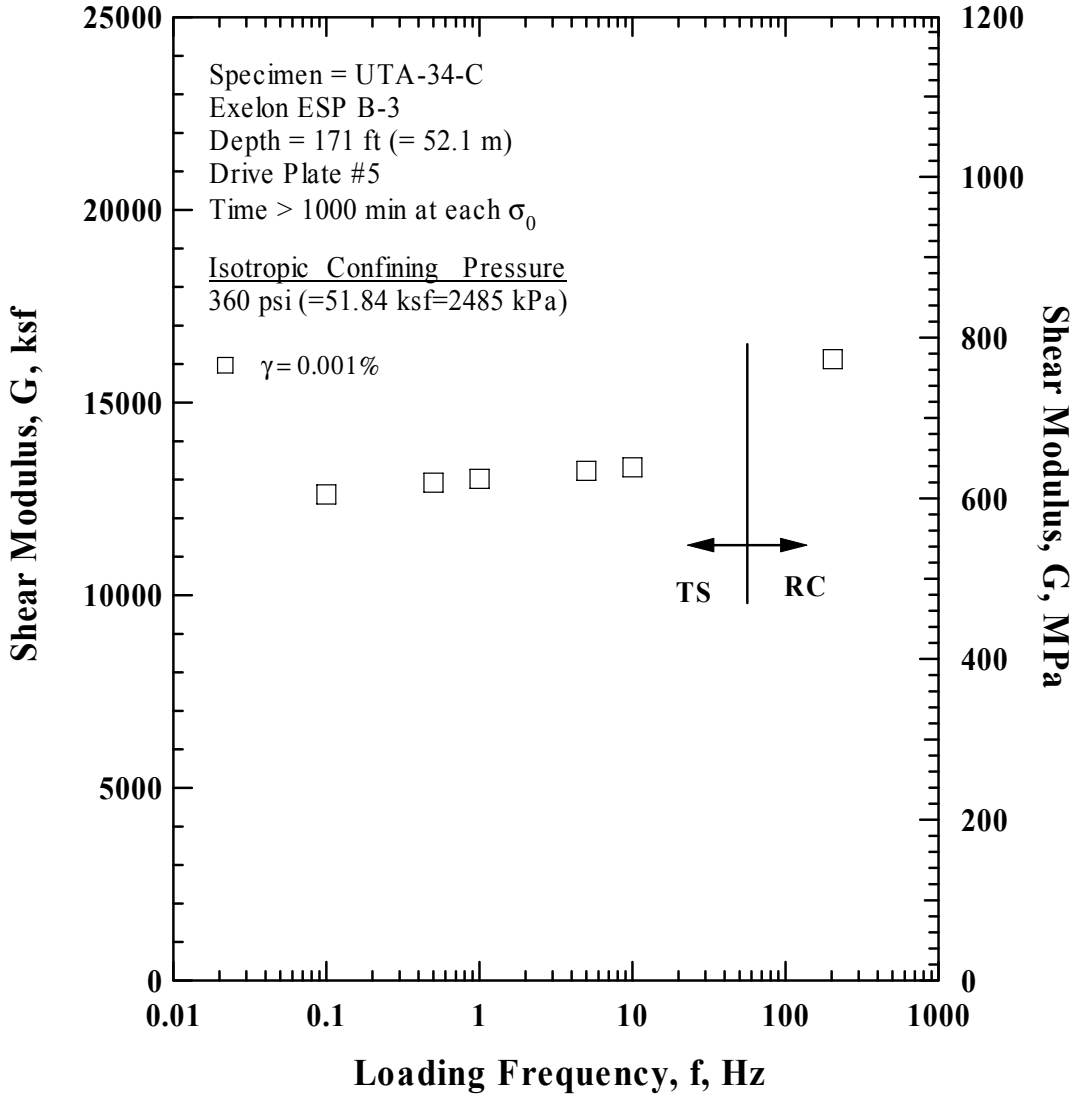

Figure E.19 Comparison of the Variation in Shear Modulus with Loading Frequency at an Isotropic Confining Pressure of 360 psi (=51.84 ksf=2485 kPa) from the Combined RCTS Tests of Specimen UTA-34-C (Specimen No. 4).

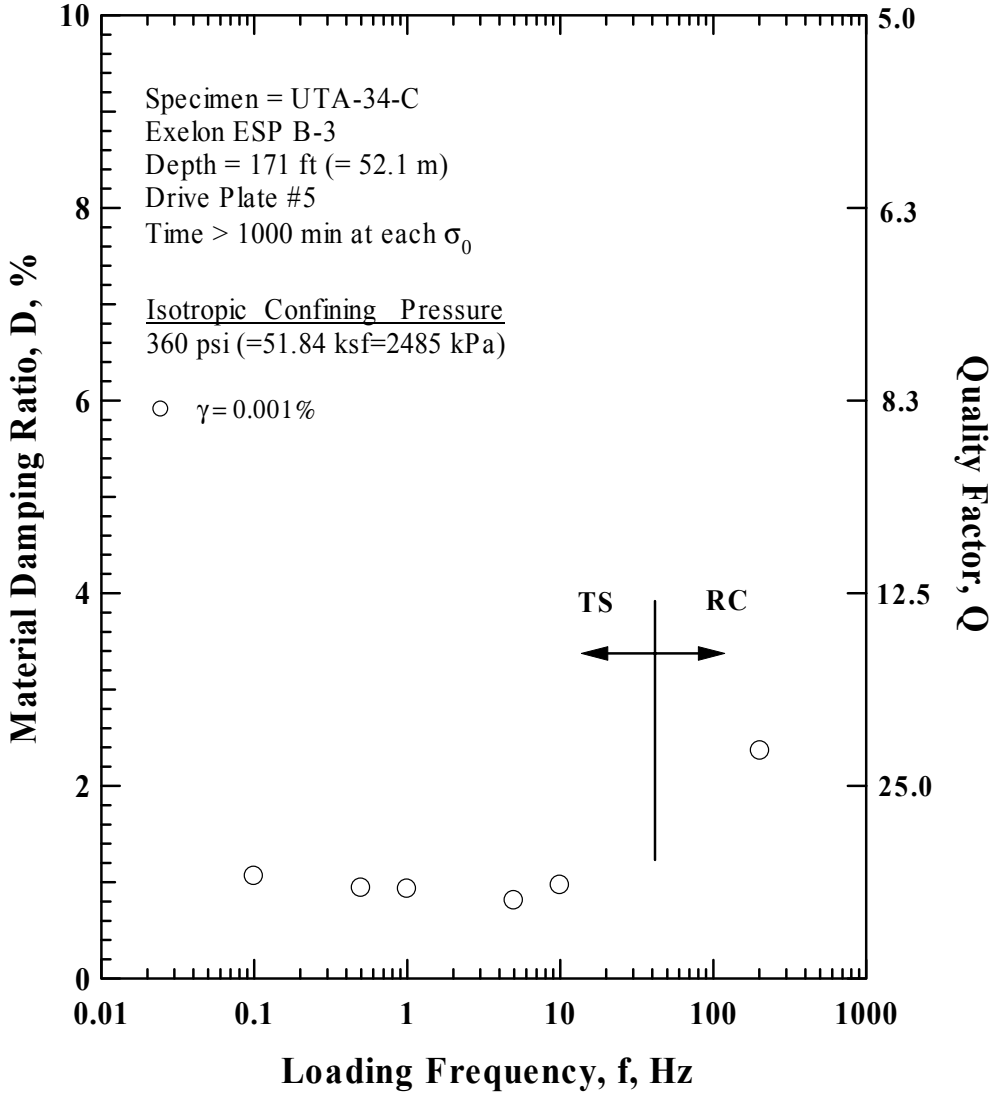

Figure E.20 Comparison of the Variation in Material Damping Ratio with Loading Frequency at an Isotropic Confining Pressure 360 psi (=51.84 ksf=2485 kPa) from the Combined RCTS Tests of Specimen UTA-34-C (Specimen No. 4).

Table E.1 Variation in Low-Amplitude Shear Wave Velocity, Low-Amplitude Shear Modulus, Low-Amplitude Material Damping Ratio and Void Ratio with Isotropic Confining Pressure from RC Tests of Specimen UTA-34-C.

Effective Isotropic Confining Pressure, σ_o'			Low-Amplitude Shear Modulus, G_{max}		Low-Amplitude Shear Wave Velocity, Vs	Low-Amplitude Material Damping Ratio, Dmin	Void Ratio, e
(psi)	(psf)	(kPa)	(ksf)	(MPa)	(fps)	(%)	
33	4752	228	5797	277.9	1177	2.67	0.40
45	6480	311	6420	307.8	1238	2.62	0.39
90	12960	621	8110	388.8	1386	2.47	0.38
180	25920	1243	11497	551.2	1644	2.43	0.36
360	51840	2485.2	15967	765.5	1928	2.41	0.34

Table E.2 Variation in Shear Modulus, Normalized Shear Modulus and Material Damping Ratio with Shearing Strain from RC Tests of Specimen UTA-34-C; Isotropic Confining Pressure, σ_o =90 psi (=12.96 ksf=621 kPa).

Peak Shearing Strain, %	Shear Modulus, G, ksf	Normalized Shear Modulus, G/G_{max}	Average[+] Shearing Strain, %	Material Damping Ratio[x], D, %
1.55E-04	8385	1.00	1.55E-04	2.42
3.10E-04	8385	1.00	3.10E-04	2.41
6.18E-04	8386	1.00	5.36E-04	2.37
1.15E-03	8329	0.99	9.94E-04	2.43
2.26E-03	8274	0.99	1.95E-03	2.50
4.48E-03	7994	0.95	3.81E-03	2.72
8.33E-03	7559	0.90	6.88E-03	3.27
1.48E-02	6726	0.80	1.16E-02	4.24
2.54E-02	5752	0.69	1.84E-02	5.84
4.92E-02	4352	0.52	3.18E-02	8.40

[+] Average Shearing Strain from the First Three Cycles of the Free Vibration Decay Curve

[x] Average Damping Ratio from the First Three Cycles of the Free Vibration Decay Curve

Table E.3 Variation in Shear Modulus, Normalized Shear Modulus and Material Damping Ratio with Shearing Strain from TS Tests of Specimen UTA-34-C; Isotropic Confining Pressure, σ_o =90 psi (=12.96 ksf=621 kPa).

First Cycle				Tenth Cycle			
Peak Shearing Strain, %	Shear Modulus, G, ksf	Normalized Shear Modulus, G/G_{max}	Material Damping Ratio, D, %	Peak Shearing Strain, %	Shear Modulus, G, ksf	Normalized Shear Modulus, G/G_{max}	Material Damping Ratio, D, %
4.84E-04	7927	1.00	0.85				
				7.20E-04	7929	1.00	0.86
1.21E-03	7922	1.00	0.99	1.21E-03	7922	1.00	1.00
3.15E-03	7779	0.98	1.12	3.16E-03	7785	0.98	1.12
6.65E-03	7372	0.93	1.80	6.66E-03	7421	0.94	1.78

Table E.4 Variation in Shear Modulus, Normalized Shear Modulus and Material Damping Ratio with Shearing Strain from RC Tests of Specimen UTA-34-C; Isotropic Confining Pressure, σ_o =360 psi (=51.84 ksf=2485 kPa).

Peak Shearing Strain, %	Shear Modulus, G, ksf	Normalized Shear Modulus, G/G_{max}	Average[+] Shearing Strain, %	Material Damping Ratio[x], D, %
1.58E-04	16127	1.00	1.58E-04	2.35
3.15E-04	16126	1.00	3.15E-04	2.34
5.88E-04	16126	1.00	5.88E-04	2.34
1.20E-03	16128	1.00	1.04E-03	2.37
2.37E-03	15969	0.99	2.06E-03	2.37
4.61E-03	15643	0.97	3.97E-03	2.52
8.87E-03	15021	0.93	7.50E-03	2.84
1.52E-02	13965	0.87	1.23E-02	3.55
2.74E-02	12111	0.75	2.08E-02	4.89
4.42E-02	10389	0.64	3.16E-02	6.13

[+] Average Shearing Strain from the First Three Cycles of the Free Vibration Decay Curve

[x] Average Damping Ratio from the First Three Cycles of the Free Vibration Decay Curve

Table E.5 Variation in Shear Modulus, Normalized Shear Modulus and Material Damping Ratio with Shearing Strain from TS Tests of Specimen UTA-34-C; Isotropic Confining Pressure, σ_o =360 psi (=51.84 ksf=2485 kPa).

First Cycle				Tenth Cycle			
Peak Shearing Strain, %	Shear Modulus, G, ksf	Normalized Shear Modulus, G/G_{max}	Material Damping Ratio, D, %	Peak Shearing Strain, %	Shear Modulus, G, ksf	Normalized Shear Modulus, G/G_{max}	Material Damping Ratio, D, %
2.53E-04	12910	1.00	1.01				
4.72E-04	12920	1.00	0.90	4.70E-04	12950	1.00	0.90
9.36E-04	12920	1.00	0.91	9.38E-04	12960	1.00	0.89
2.06E-03	12810	0.99	1.05	2.06E-03	12850	0.99	0.93

Exhibit F

to Attachment A-7

Specimen No. 5
UT Specimen: UTA-34-E

Exelon ESP B-3 (S-37)
Depth = 208ft (=63.4m)
Soil Type: Silty Clay (CL-ML)

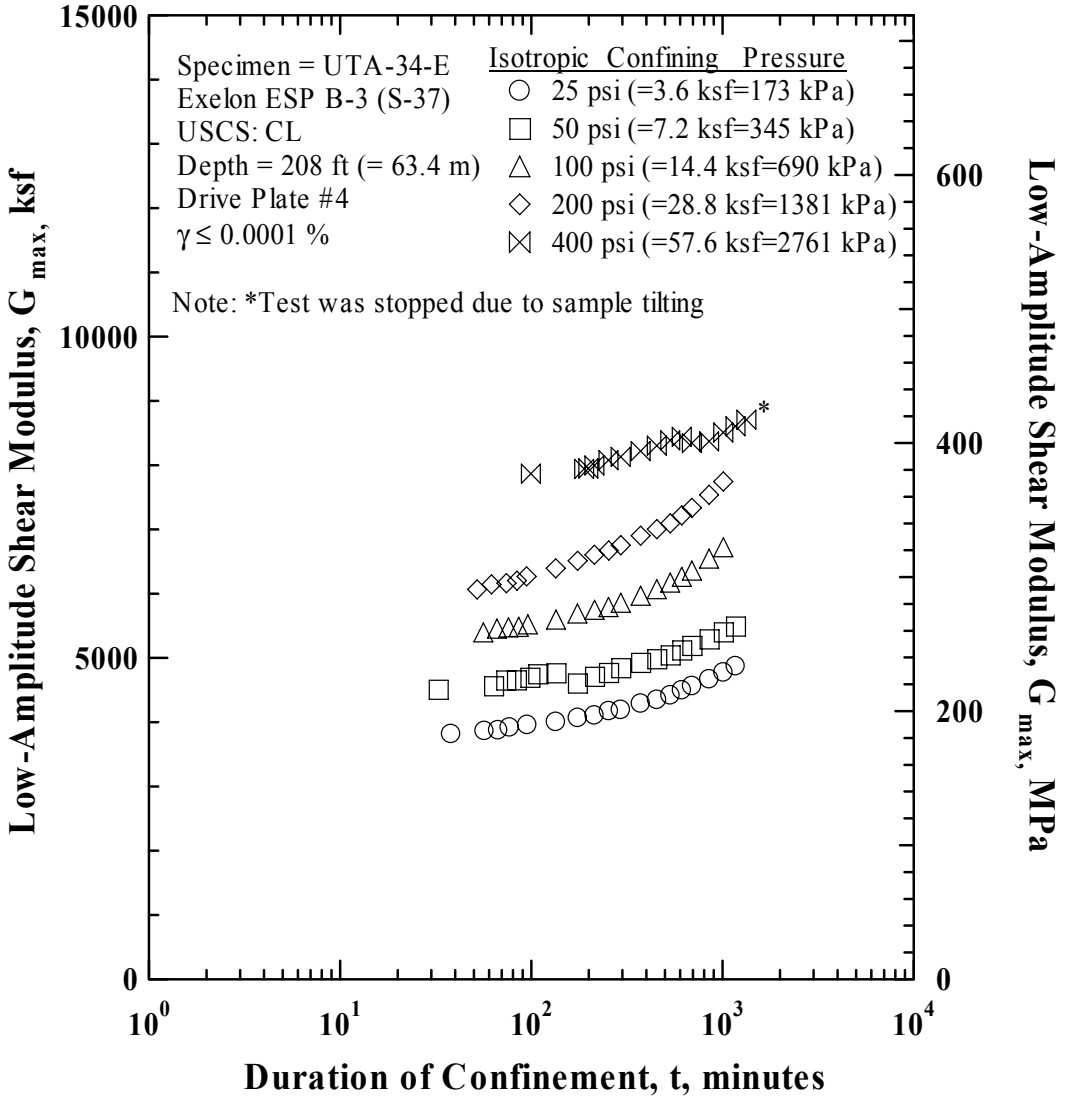

Figure F.1 Variation in Low-Amplitude Shear Modulus with Magnitude and Duration of Isotropic Confining Pressure from Resonant Column Tests of Specimen UTA-34-E (Specimen No. 5)

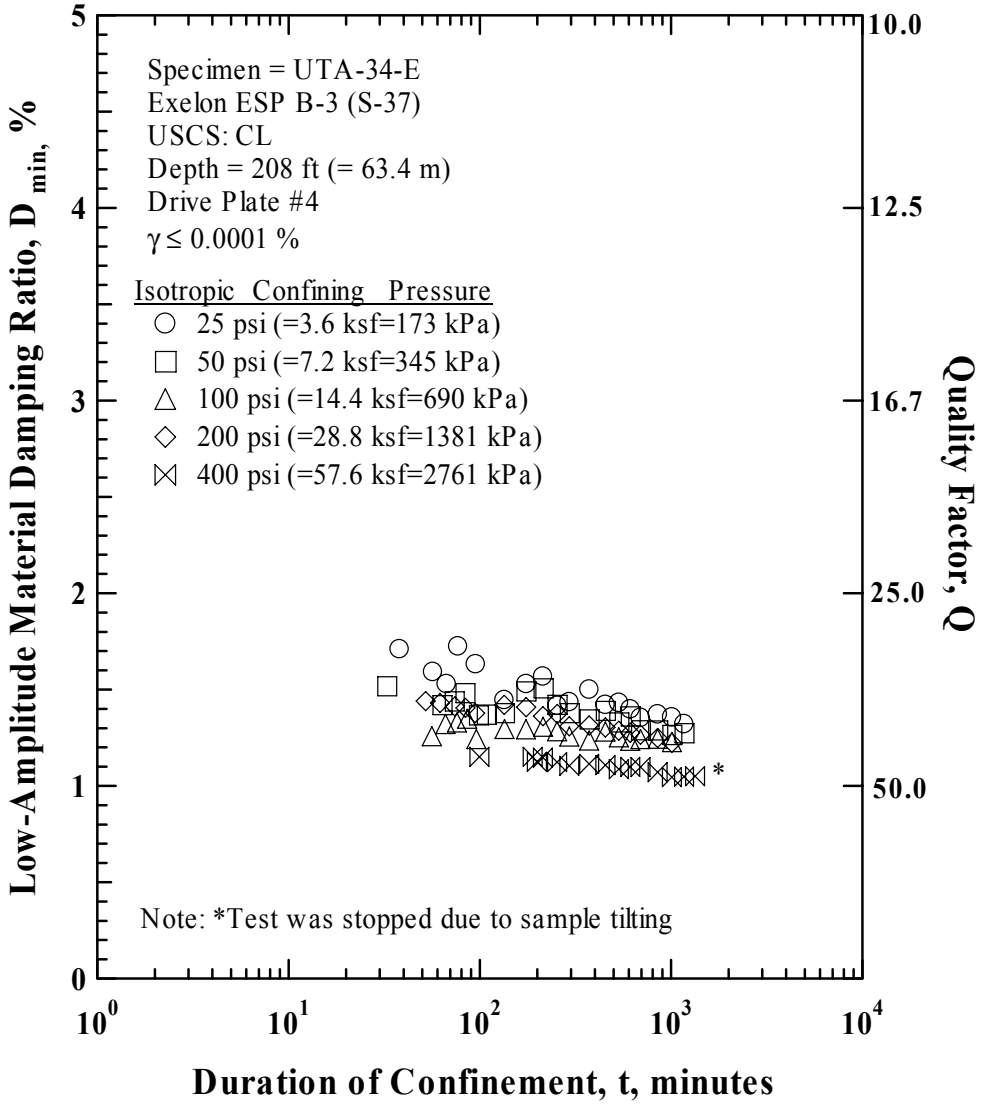

Figure F.2 Variation in Low-Amplitude Material Damping Ratio with Magnitude and Duration of Isotropic Confining Pressure from Resonant Column Tests of Specimen UTA-34-E (Specimen No. 5)

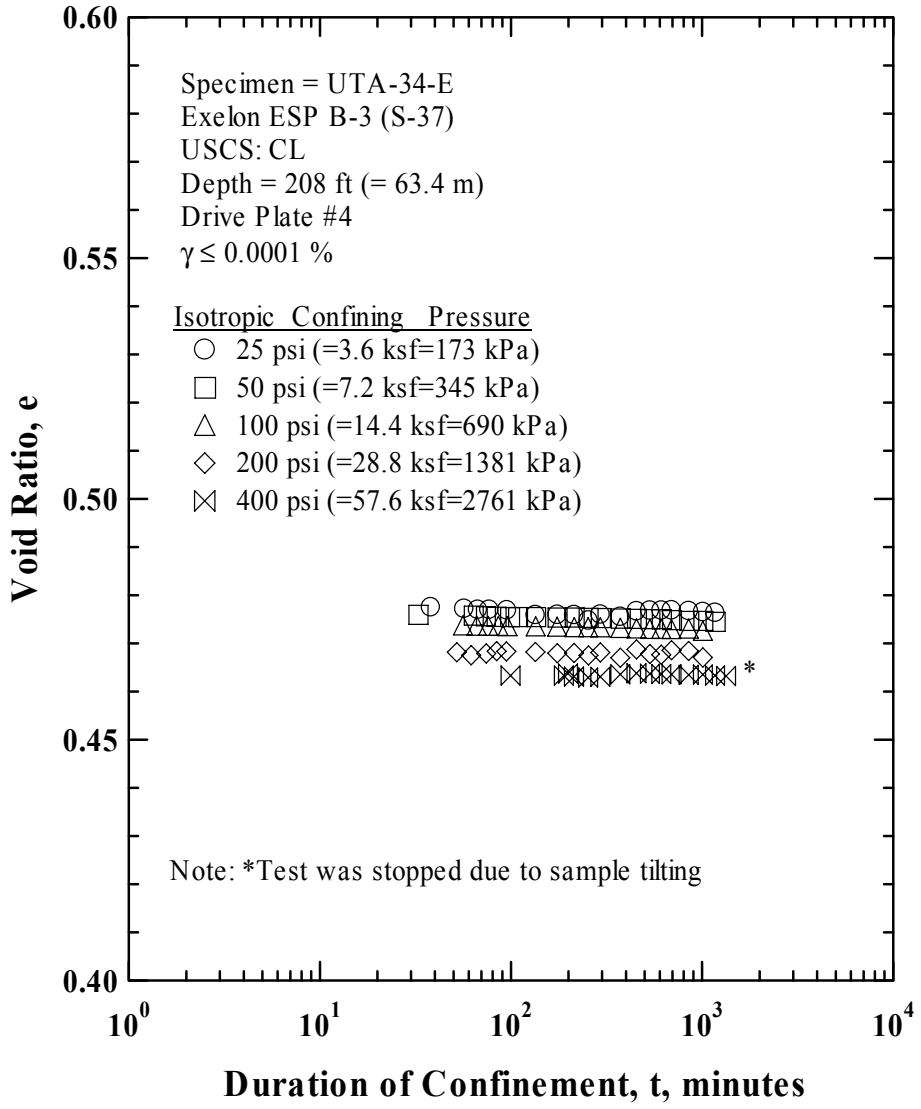

Figure F.3 Variation in Estimated Void Ratio with Magnitude and Duration of Isotropic Confining Pressure from Resonant Column Tests of Specimen UTA-34-E (Specimen No. 5)

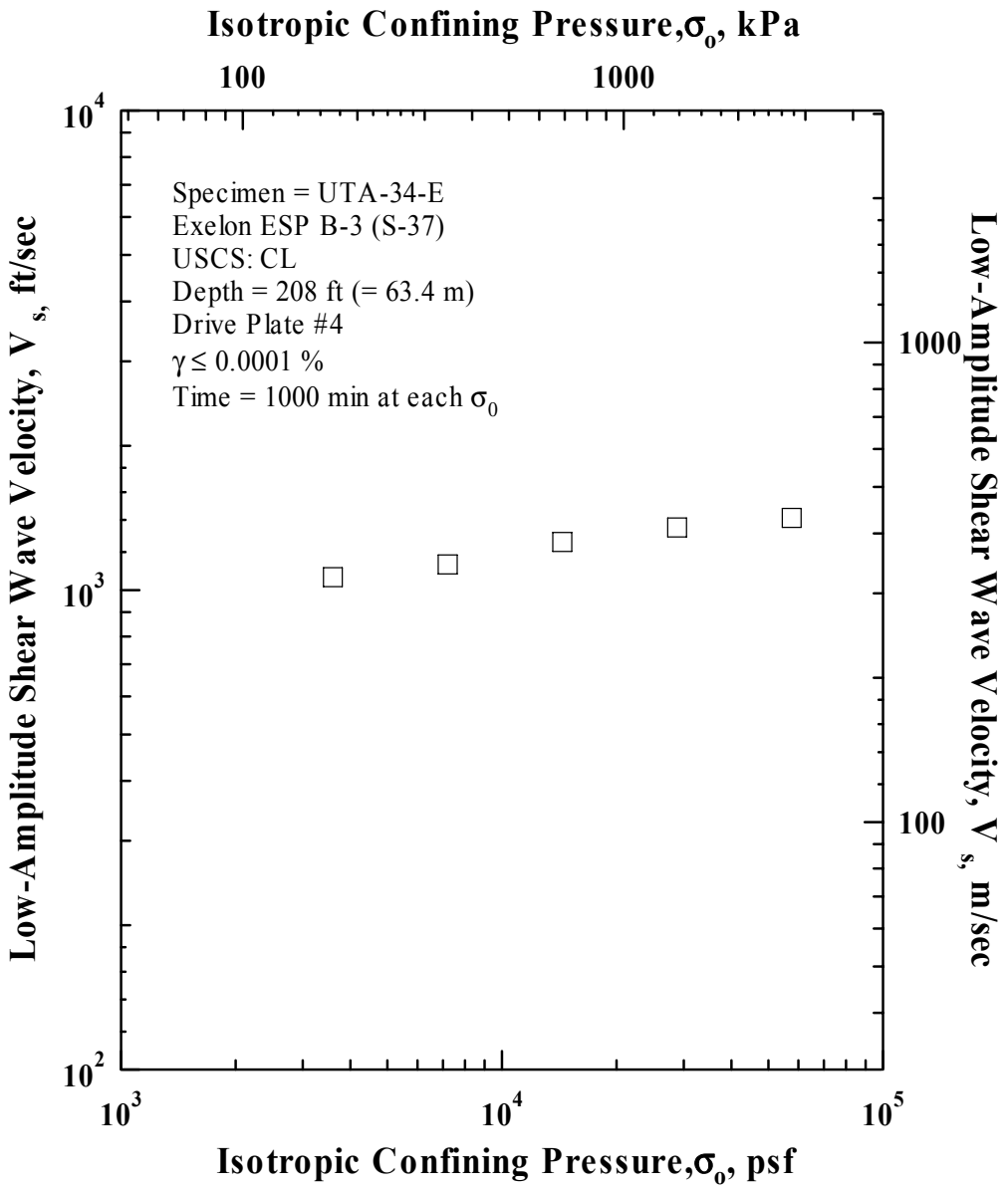

Figure F.4 Variation in Low-Amplitude Shear Wave Velocity with Isotropic Confining Pressure from Resonant Column Tests of Specimen UTA-34-E (Specimen No. 5)

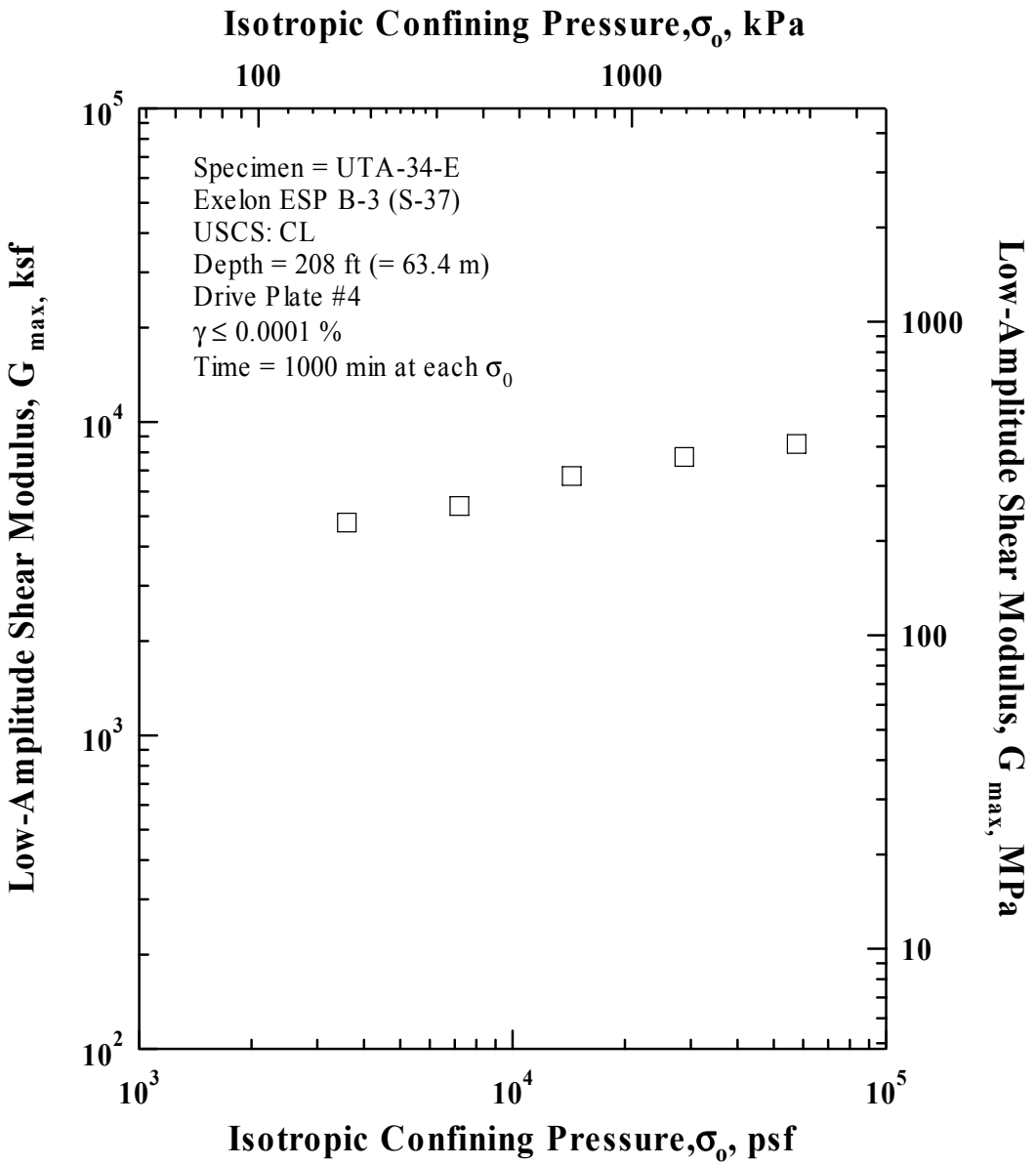

Figure F.5 Variation in Low-Amplitude Shear Modulus with Isotropic Confining Pressure from Resonant Column Tests of Specimen UTA-34-E (Specimen No. 5)

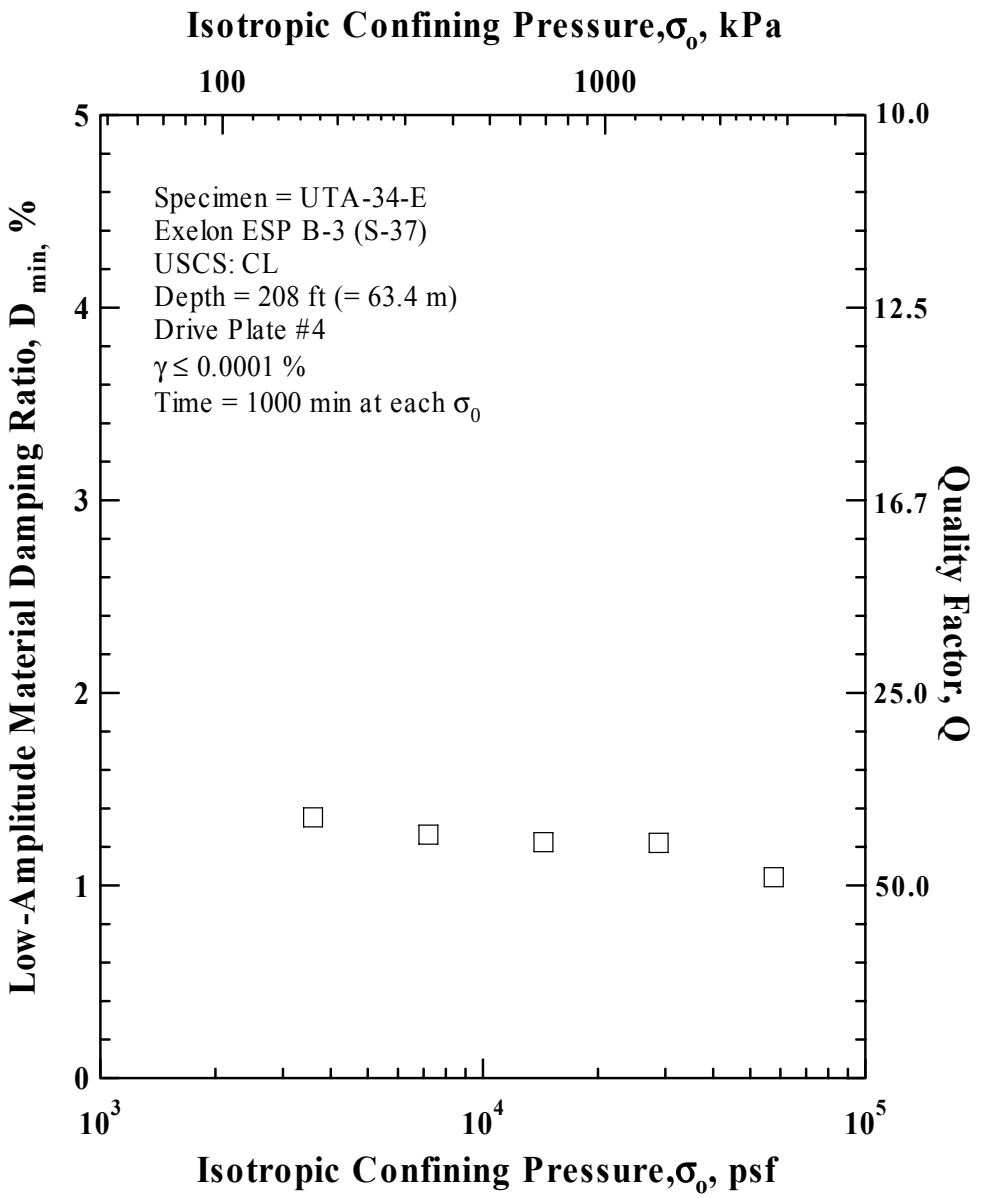

Figure F.6 Variation in Low-Amplitude Material Damping Ratio with Isotropic Confining Pressure from Resonant Column Tests of Specimen UTA-34-E (Specimen No. 5)

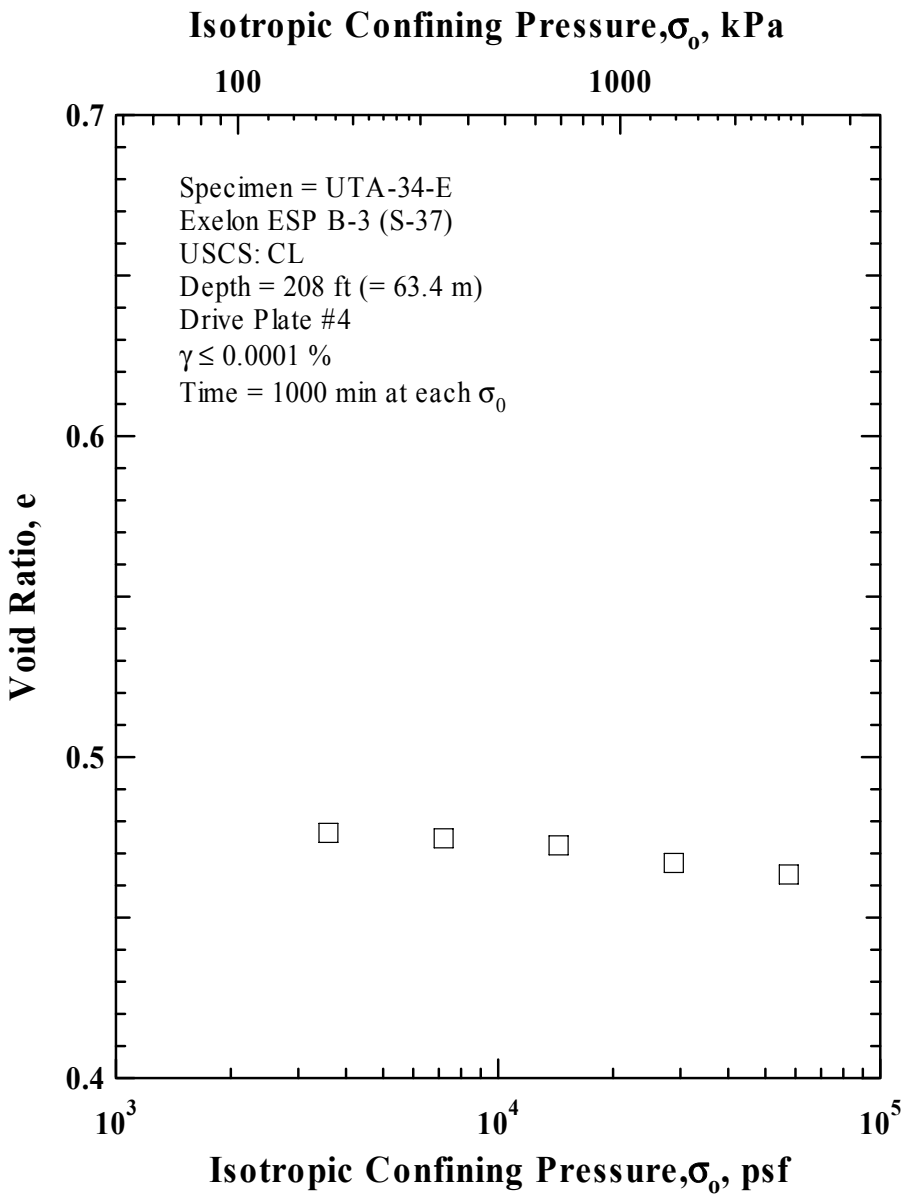

Figure F.7 Variation in Estimated Void Ratio with Isotropic Confining Pressure from Resonant Column Tests of Specimen UTA-34-E (Specimen No. 5)

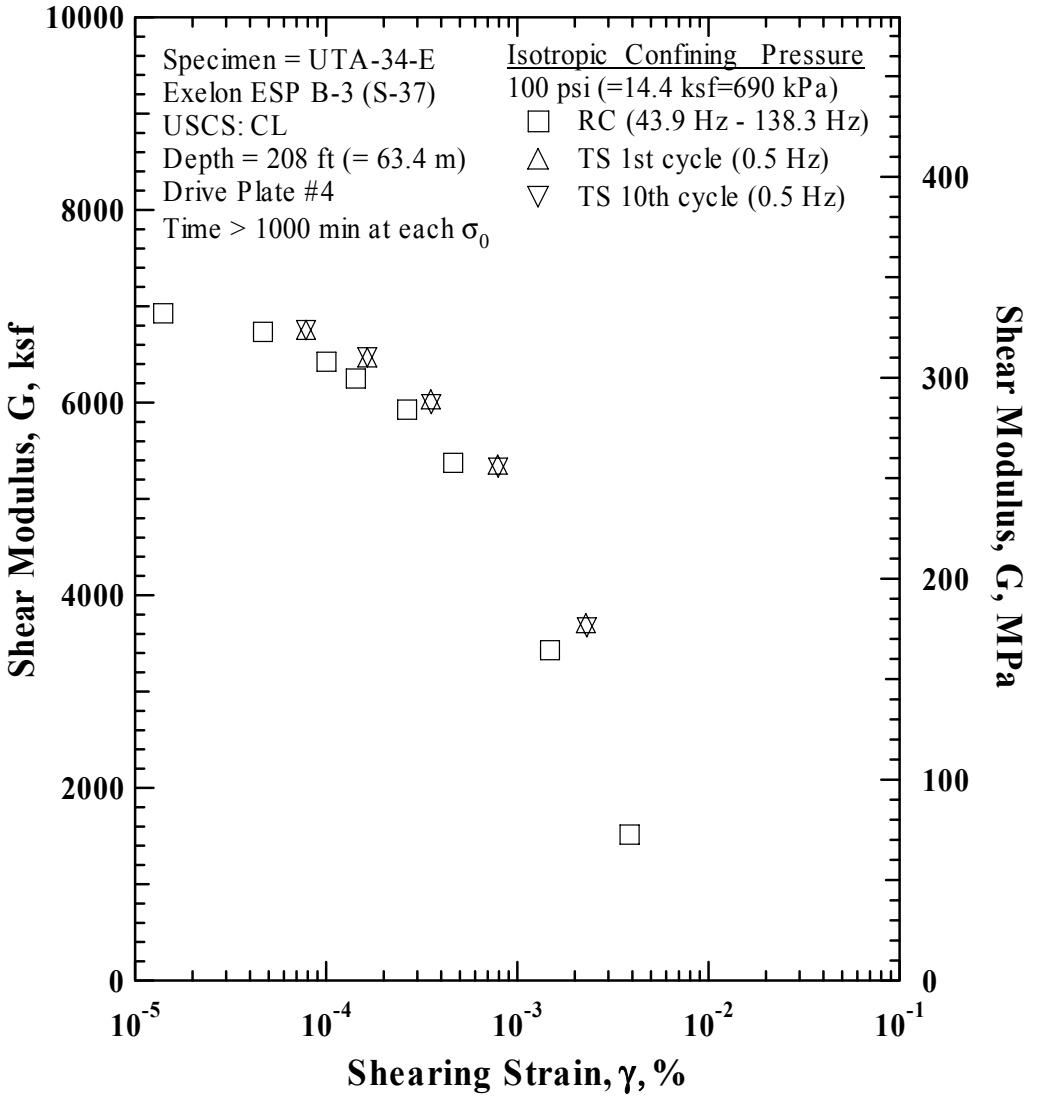

Figure F.8 Comparison of the Variation in Shear Modulus with Shearing Strain at an Isotropic Confining Pressure of 100 psi (=14.4 ksf=690 kPa) from the Combined RCTS Tests of Specimen UTA-34-E (Specimen No. 5)

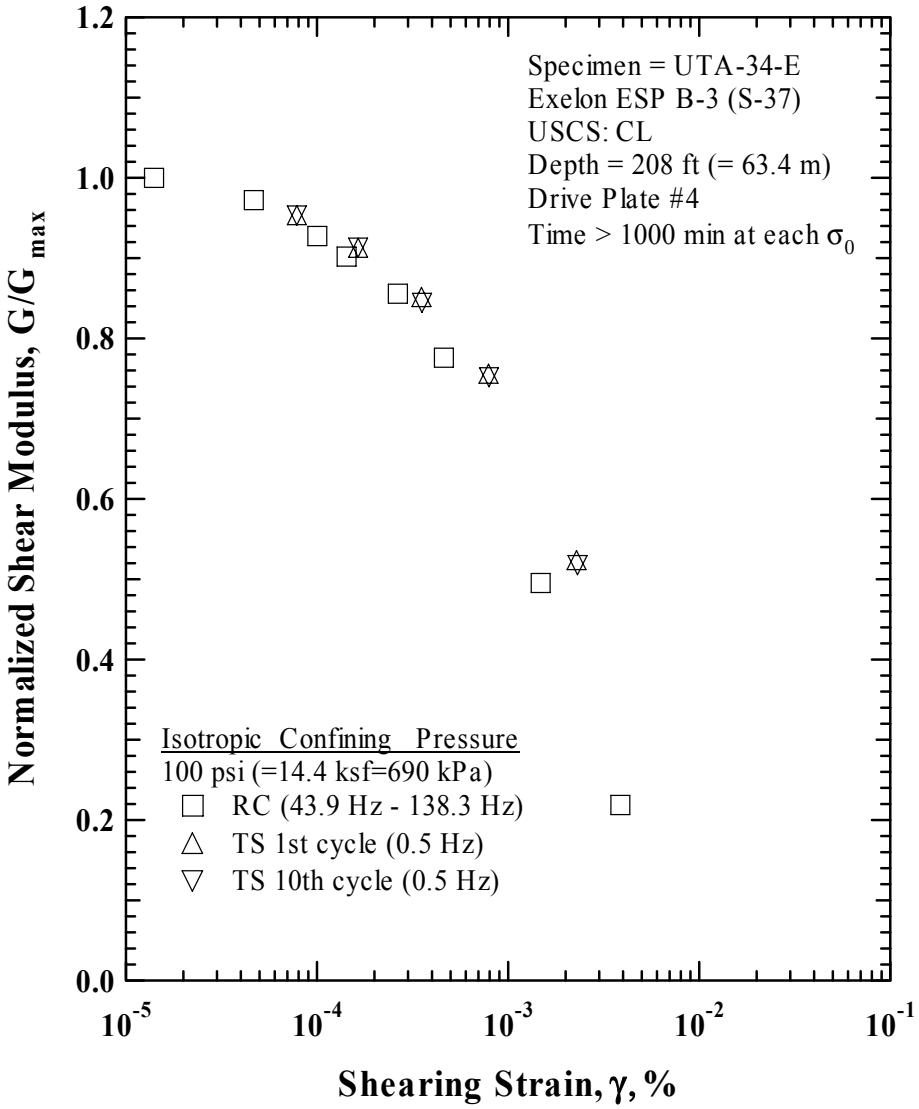

Figure F.9 Comparison of the Variation in Normalized Shear Modulus with Shearing Strain at an Isotropic Confining Pressure of 100 psi (=14.4 ksf=690 kPa) from the Combined RCTS Tests of Specimen UTA-34-E (Specimen No. 5)

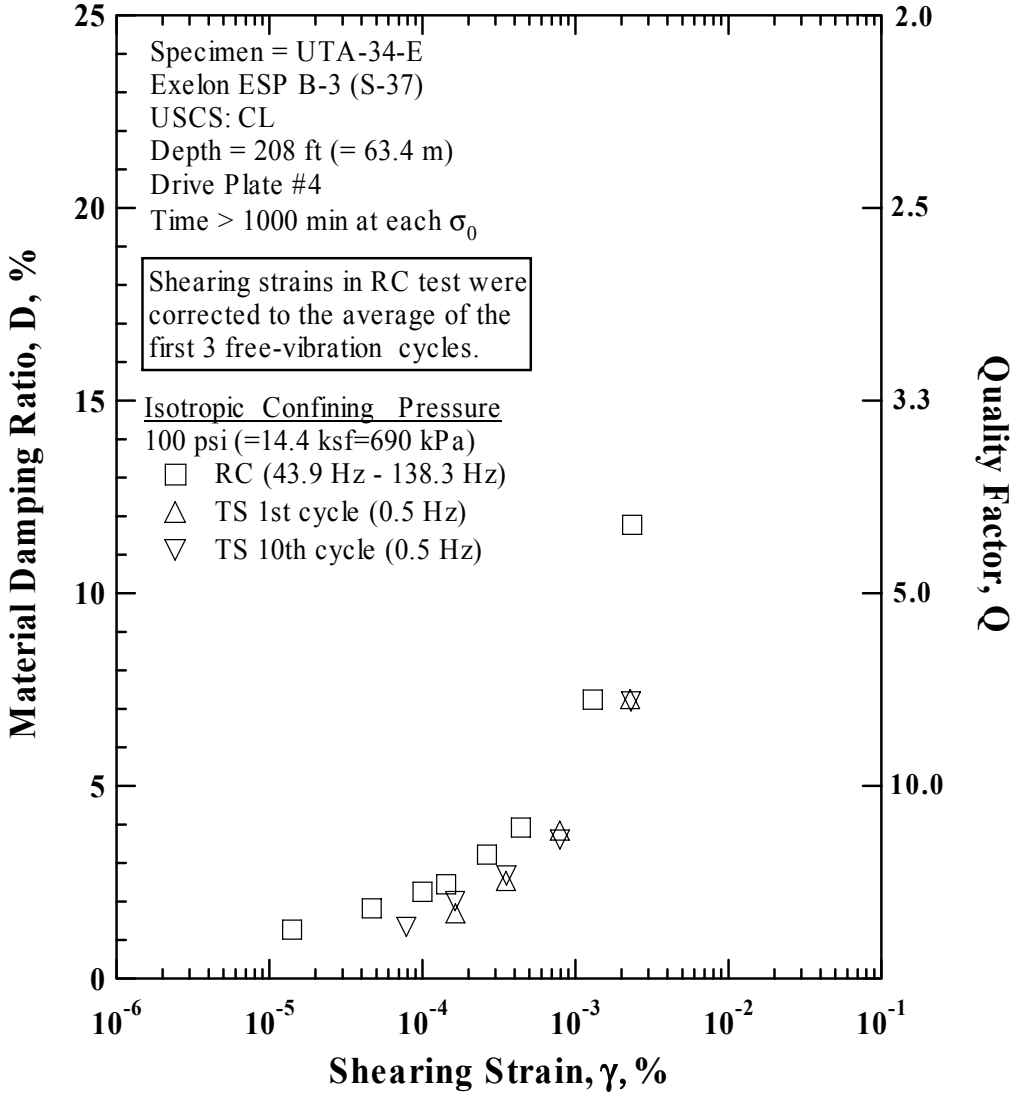

Figure F.10 Comparison of the Variation in Material Damping Ratio with Shearing Strain at an Isotropic Confining Pressure of 100 psi (=14.4 ksf=690 kPa) from the Combined RCTS Tests of Specimen UTA-34-E (Specimen No. 5)

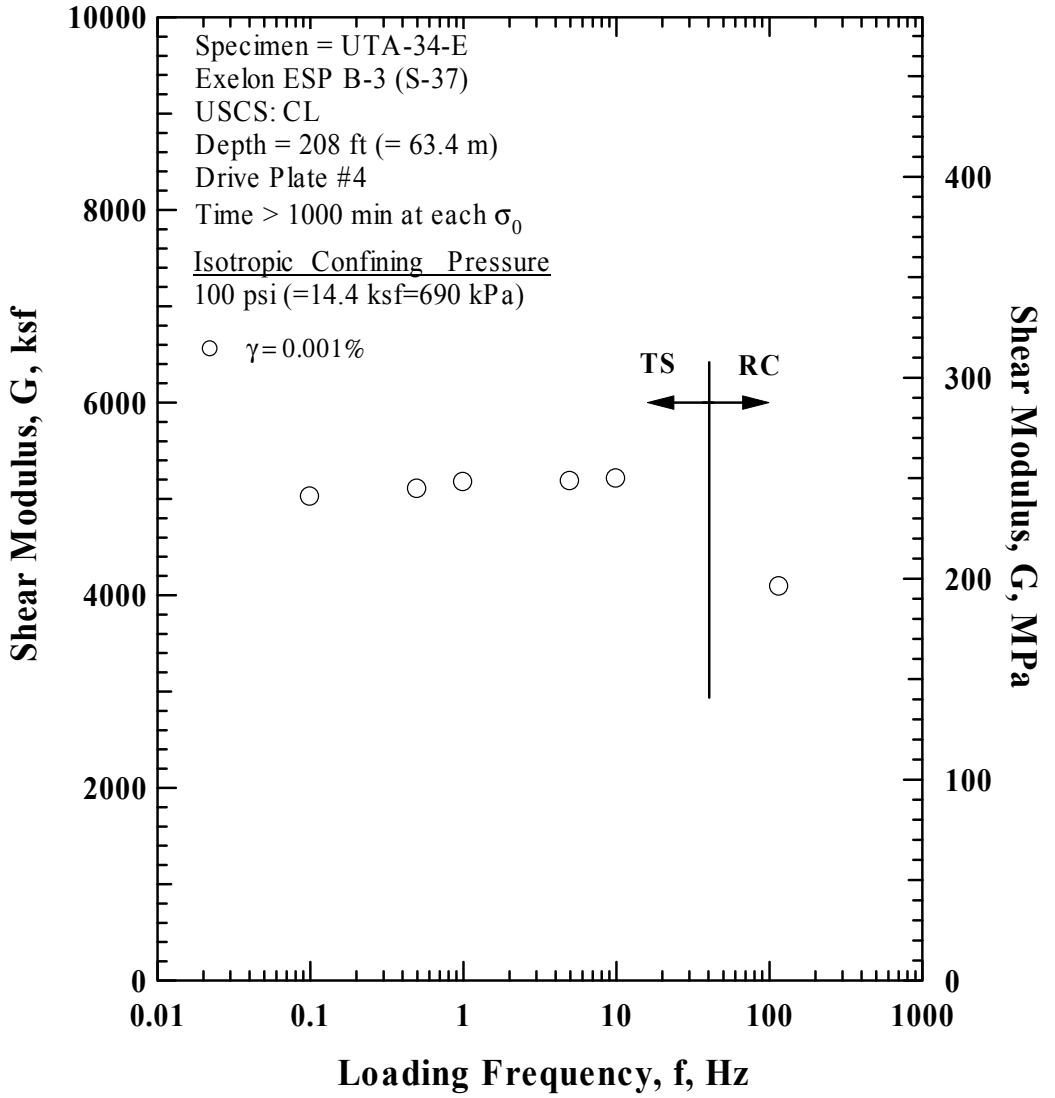

Figure F.11 Comparison of the Variation in Shear Modulus with Loading Frequency at an Isotropic Confining Pressure of 100 psi (=14.4 ksf=690 kPa) from the Combined RCTS Tests of Specimen UTA-34-E (Specimen No. 5)

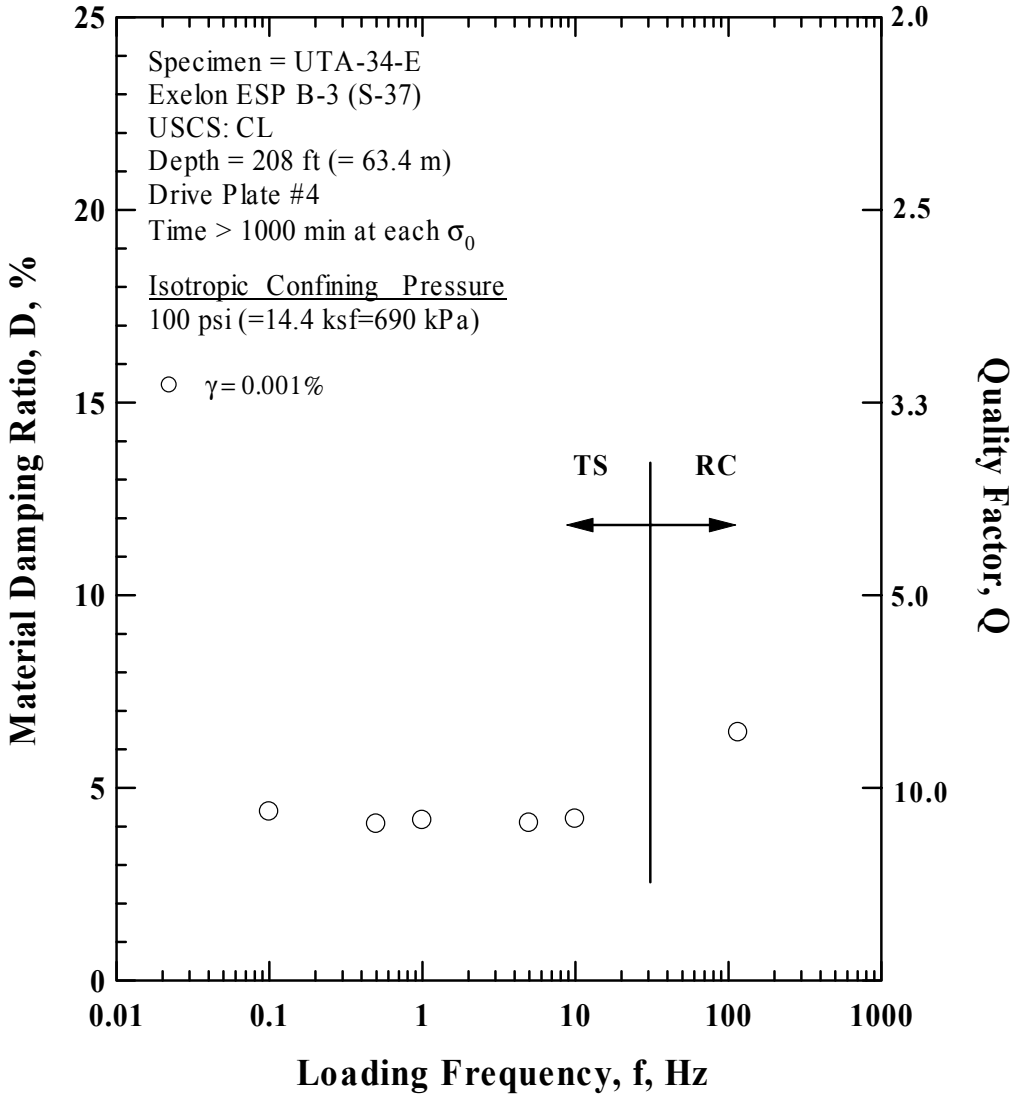

Figure F.12 Comparison of the Variation in Material Damping Ratio with Loading Frequency at an Isotropic Confining Pressure 100 psi (=14.4 ksf=690 kPa) from the Combined RCTS Tests of Specimen UTA-34-E (Specimen No. 5)

Table F.1 Variation in Low-Amplitude Shear Wave Velocity, Low-Amplitude Shear Modulus, Low-Amplitude Material Damping Ratio and Estimated Void Ratio with Isotropic Confining Pressure from RC Tests of Specimen UTA-34-E

Effective Isotropic Confining Pressure, σ_o'			Low-Amplitude Shear Modulus, G_{max}		Low-Amplitude Shear Wave Velocity, Vs	Low-Amplitude Material Damping Ratio, Dmin	Void Ratio, e
(psi)	(psf)	(kPa)	(ksf)	(MPa)	(fps)	(%)	
25	3600	173	4770	228.7	1064	1.35	0.48
50	7200	345	5397	258.7	1131	1.26	0.47
100	14400	690	6714	321.9	1261	1.23	0.47
200	28800	1381	7738	371.0	1351	1.22	0.47
400	57600	2761.3	8502	407.6	1414	1.04	0.46

Table F.2 Variation in Shear Modulus, Normalized Shear Modulus and Material Damping Ratio with Shearing Strain from RC Tests of Specimen UTA-34-E; Isotropic Confining Pressure, σ_o =100 psi (=14.4 ksf=690 kPa)

Peak Shearing Strain, %	Shear Modulus, G, ksf	Normalized Shear Modulus, G/G_{max}	Average[+] Shearing Strain, %	Material Damping Ratio[x], D, %
1.40E-05	6928	1.00	1.40E-05	1.27
4.67E-05	6735	0.97	4.67E-05	1.82
1.00E-04	6425	0.93	1.00E-04	2.25
1.43E-04	6249	0.90	1.43E-04	2.45
2.65E-04	5928	0.86	2.65E-04	3.22
4.61E-04	5376	0.78	4.40E-04	3.92
1.48E-03	3431	0.50	1.30E-03	7.24
3.86E-03	1515	0.22	2.35E-03	11.78

[+] Average Shearing Strain from the First Three Cycles of the Free Vibration Decay Curve

[x] Average Damping Ratio from the First Three Cycles of the Free Vibration Decay Curve

Table F.3 Variation in Shear Modulus, Normalized Shear Modulus and Material Damping Ratio with Shearing Strain from TS Tests of Specimen UTA-34-E; Isotropic Confining Pressure, σ_o =100 psi (=14.4 ksf=690 kPa)

First Cycle				Tenth Cycle			
Peak Shearing Strain, %	Shear Modulus, G, ksf	Normalized Shear Modulus, G/G_{max}	Material Damping Ratio, D, %	Peak Shearing Strain, %	Shear Modulus, G, ksf	Normalized Shear Modulus, G/G_{max}	Material Damping Ratio, D, %
7.90E-05	6751	0.95		7.90E-05	6749	0.95	1.33
1.65E-04	6462	0.91	1.68	1.65E-04	6465	0.91	2.00
3.54E-04	6029	0.85	2.52	3.57E-04	5979	0.84	2.66
7.94E-04	5351	0.76	3.83	7.99E-04	5321	0.75	3.59
2.30E-03	3707	0.52	7.24	2.32E-03	3662	0.52	7.18

Exhibit G
to Attachment A-7

Specimen No. 6
UT Specimen: UTA-34-F

Exelon ESP B-2 (S-38)
Depth = 242ft (=73.8m)
Soil Type: Silt (ML)

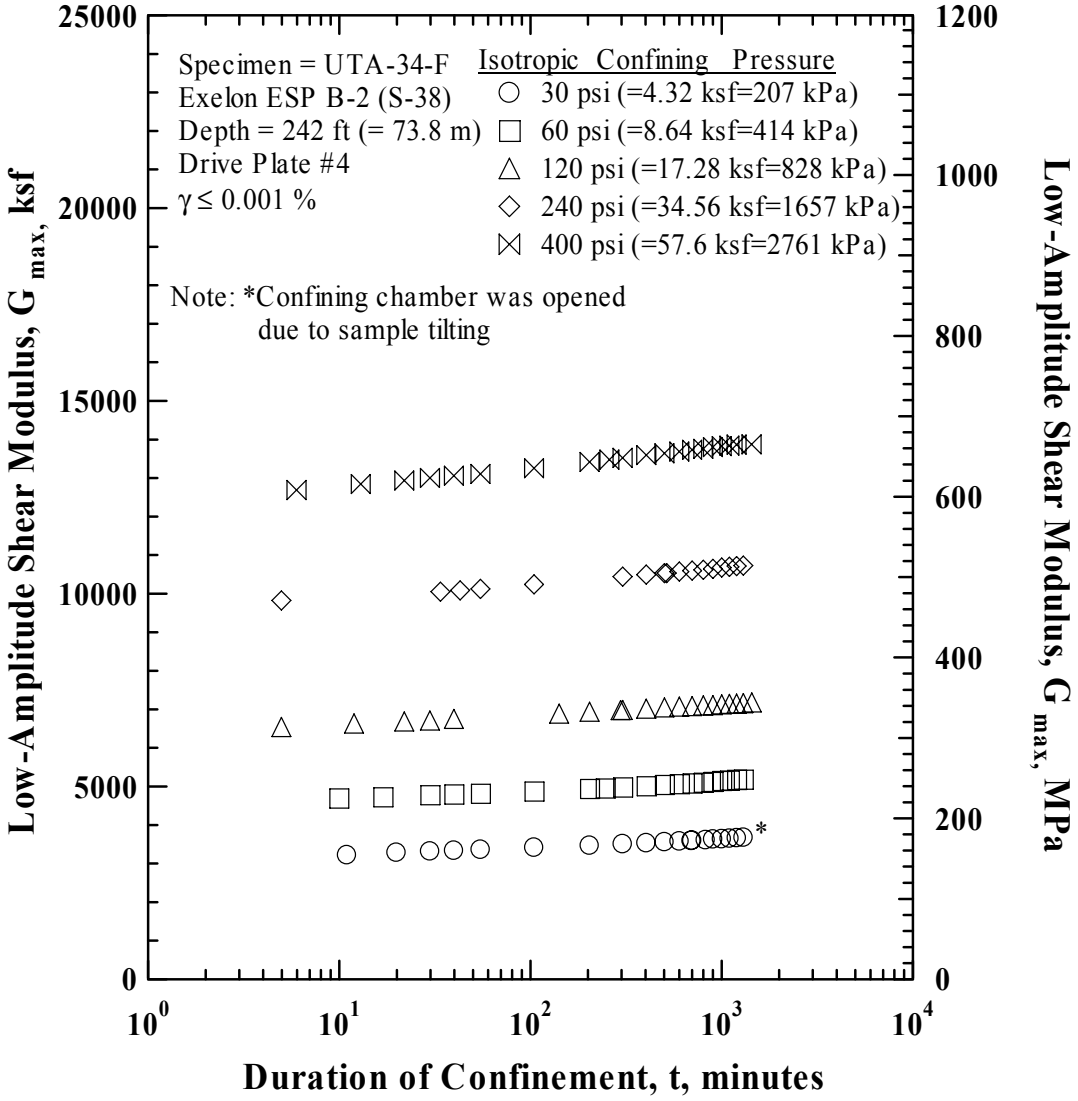

Figure G.1 Variation in Low-Amplitude Shear Modulus with Magnitude and Duration of Isotropic Confining Pressure from Resonant Column Tests of Specimen UTA-34-F (Specimen No. 6)

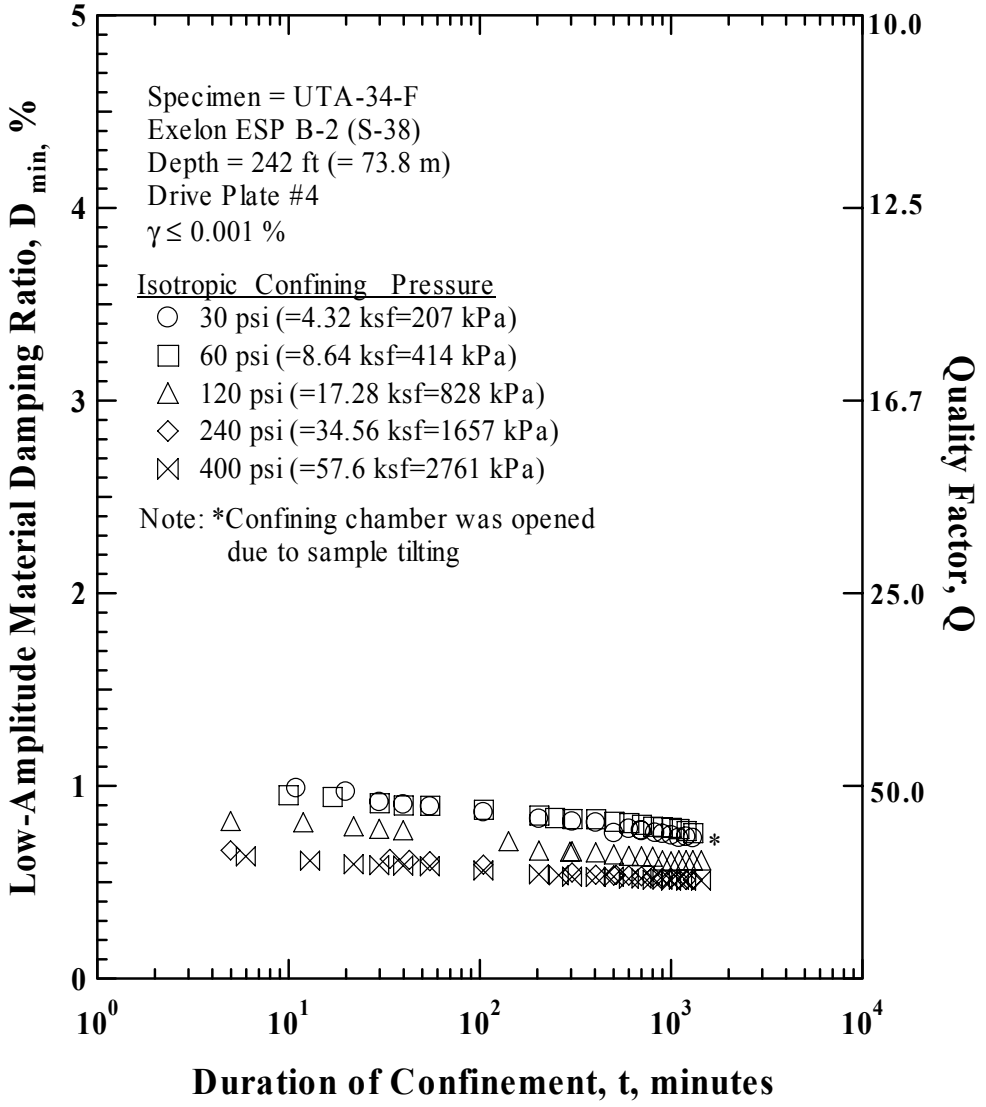

Figure G.2 Variation in Low-Amplitude Material Damping Ratio with Magnitude and Duration of Isotropic Confining Pressure from Resonant Column Tests of Specimen UTA-34-F (Specimen No. 6)

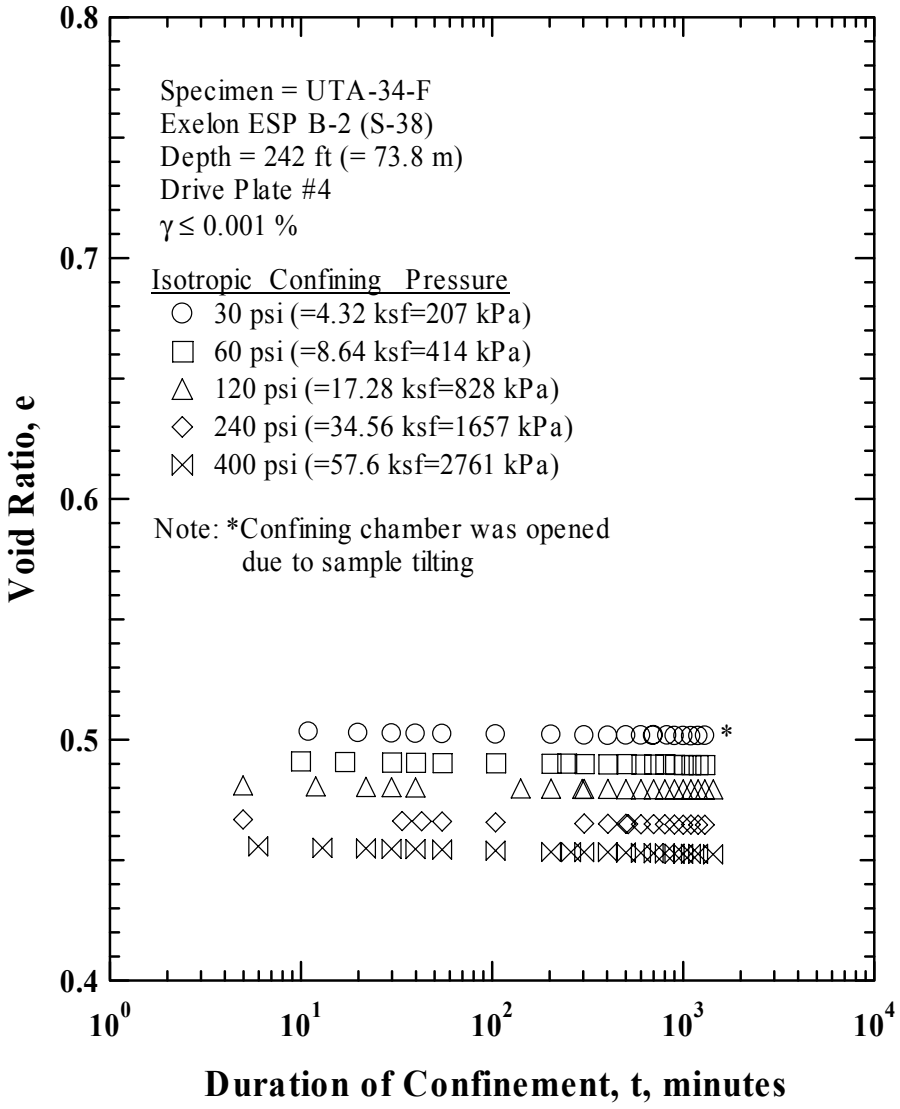

Figure G.3 Variation in Estimated Void Ratio with Magnitude and Duration of Isotropic Confining Pressure from Resonant Column Tests of Specimen UTA-34-F (Specimen No. 6)

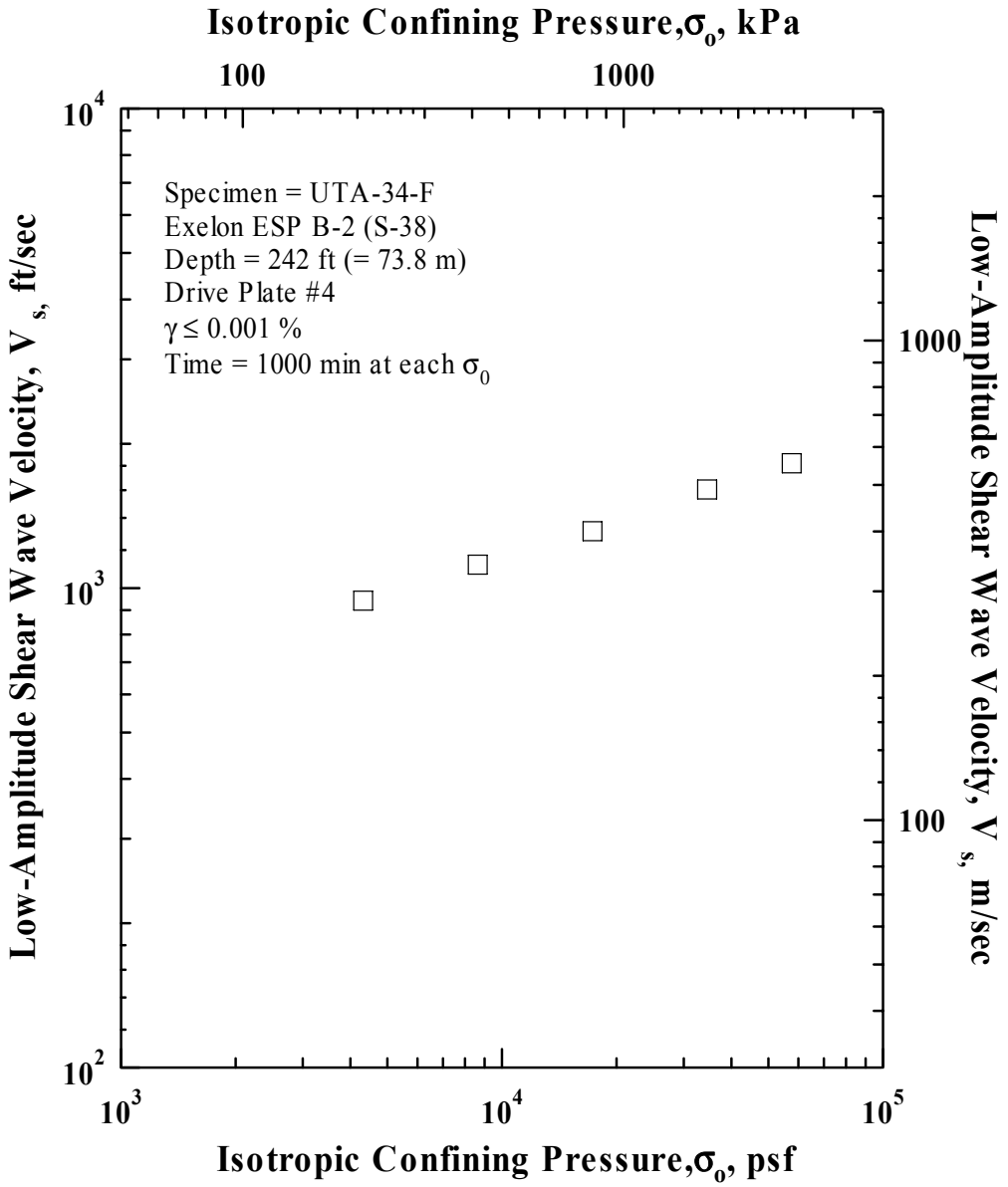

Figure G.4 Variation in Low-Amplitude Shear Wave Velocity with Isotropic Confining Pressure from Resonant Column Tests of Specimen UTA-34-F (Specimen No. 6)

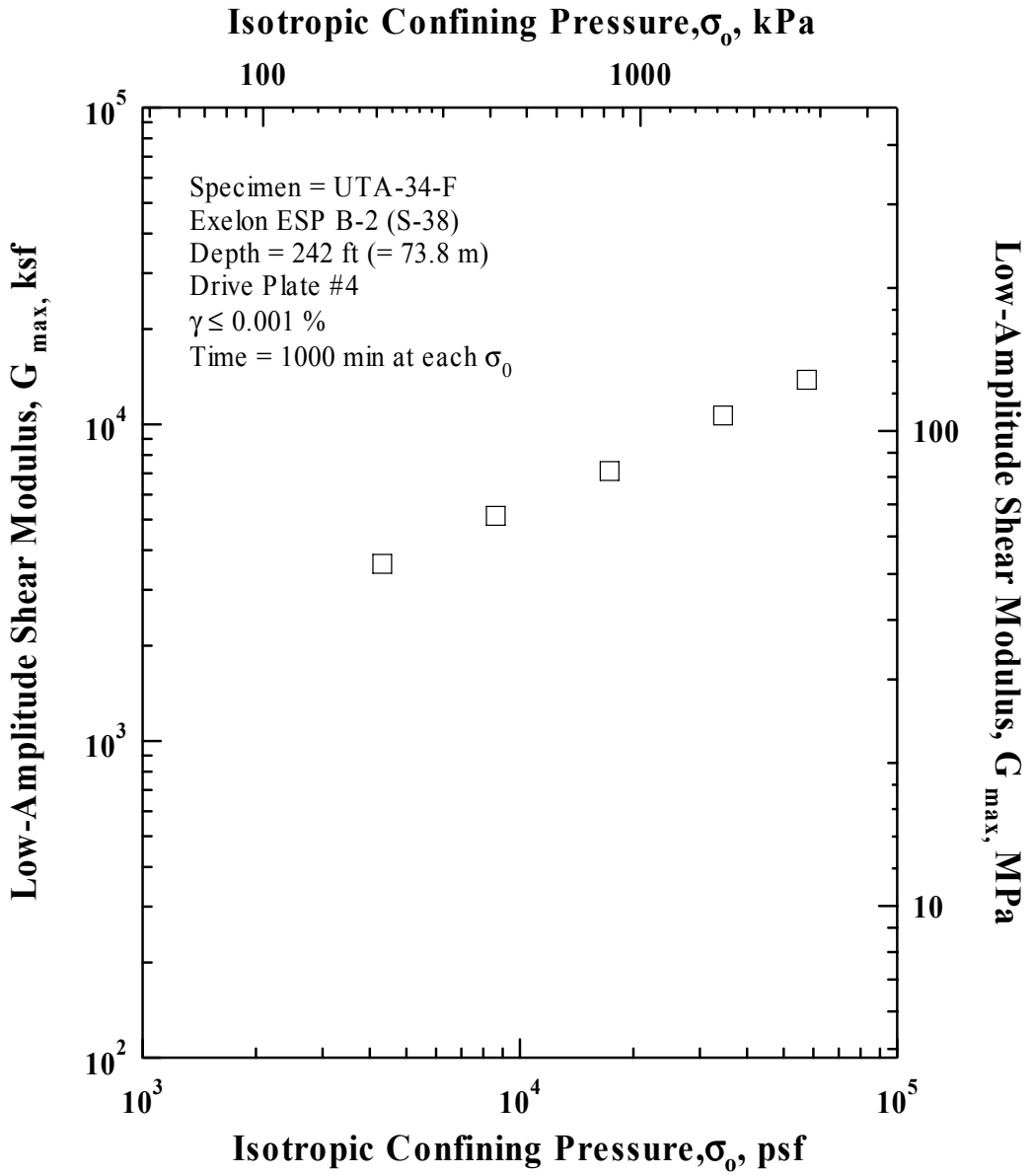

Figure G.5 Variation in Low-Amplitude Shear Modulus with Isotropic Confining Pressure from Resonant Column Tests of Specimen UTA-34-F (Specimen No. 6)

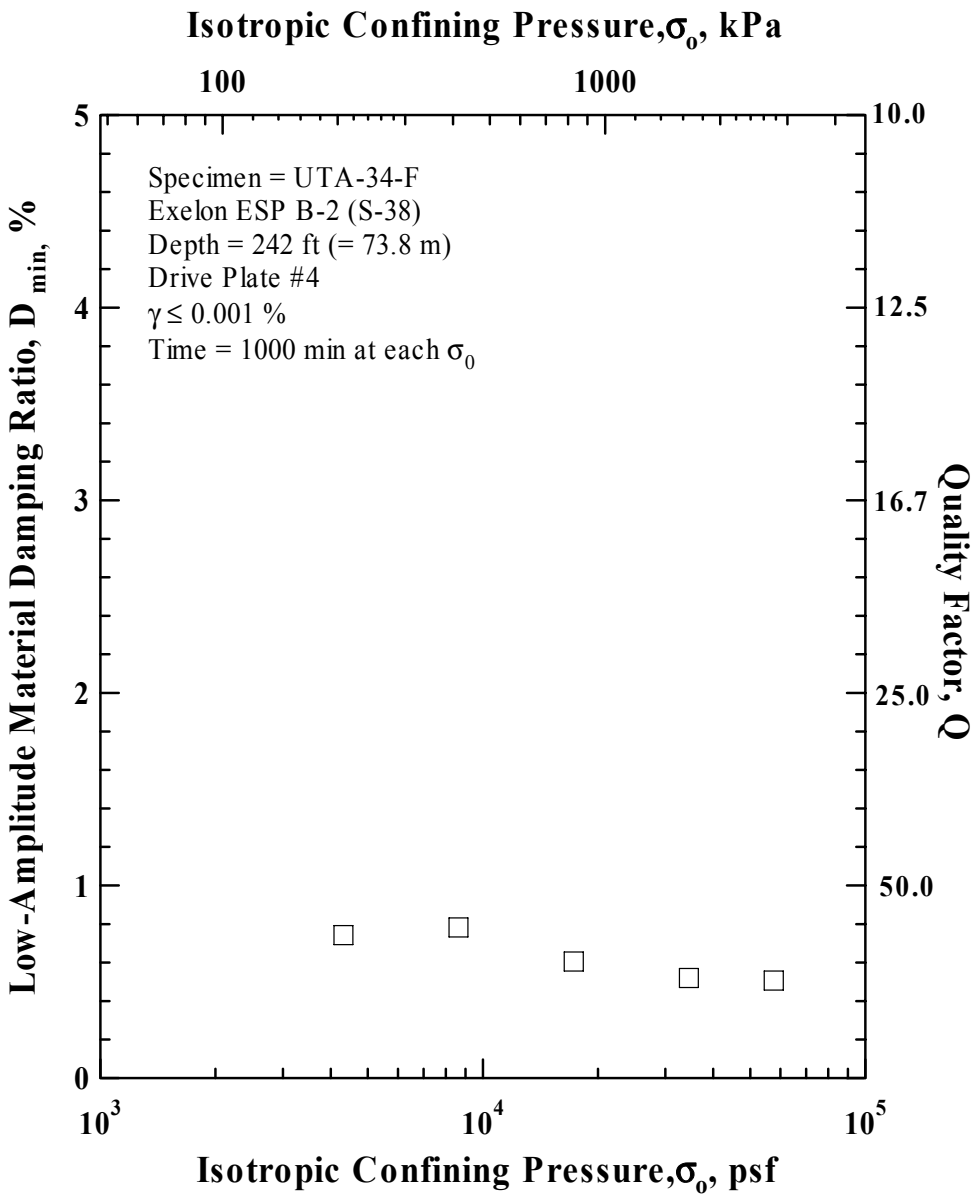

Figure G.6 Variation in Low-Amplitude Material Damping Ratio with Isotropic Confining Pressure from Resonant Column Tests of Specimen UTA-34-F (Specimen No. 6)

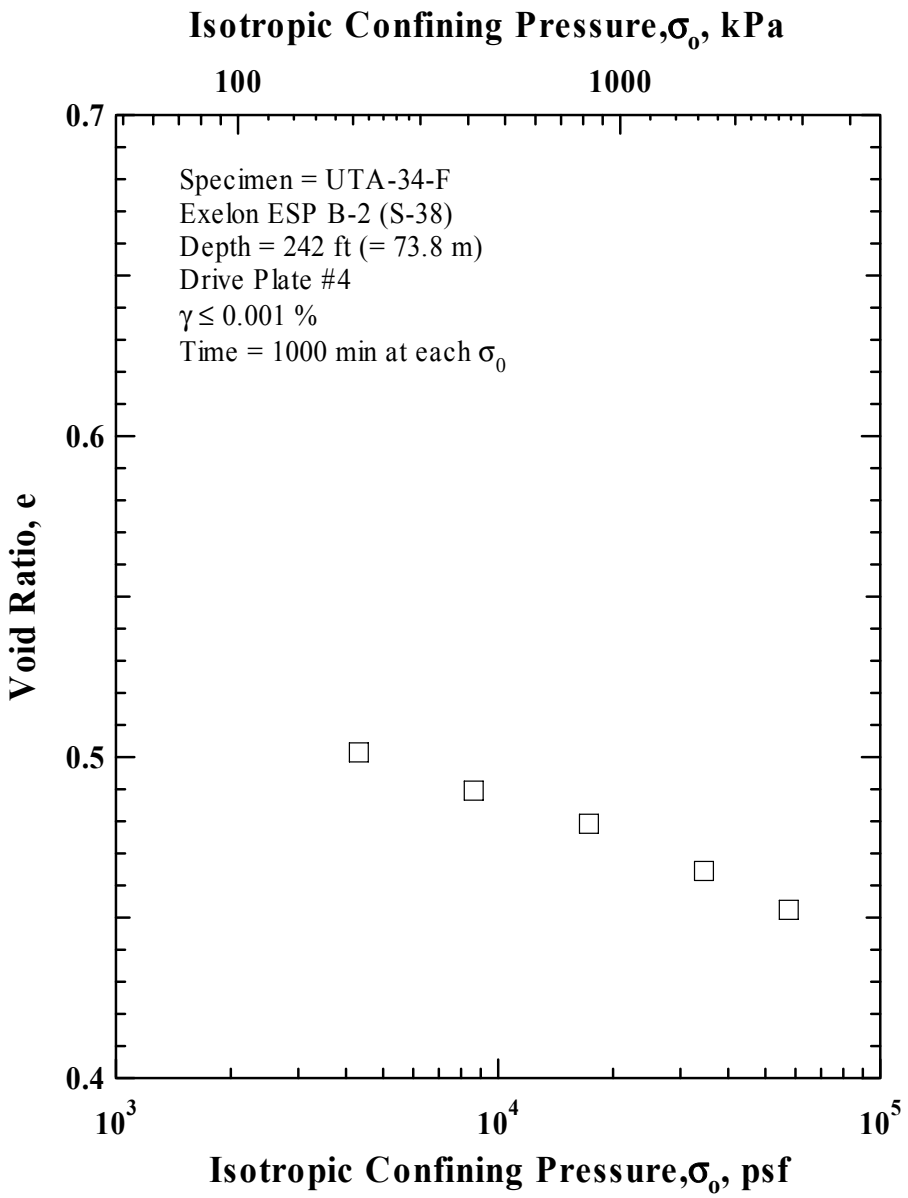

Figure G.7 Variation in Estimated Void Ratio with Isotropic Confining Pressure from Resonant Column Tests of Specimen UTA-34-F (Specimen No. 6)

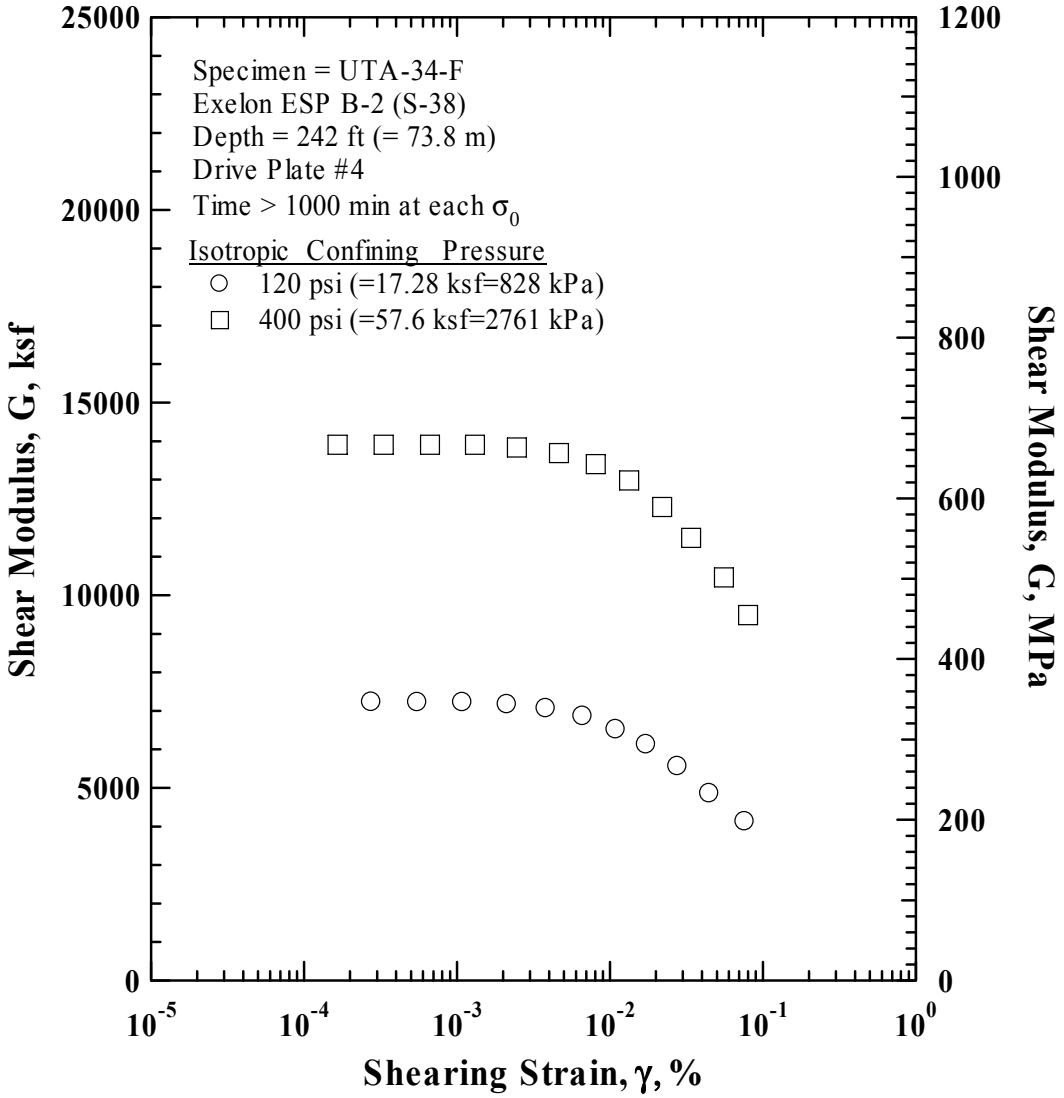

Figure G.8 Comparison of the Variation in Shear Modulus with Shearing Strain and Isotropic Confining Pressure from the Resonant Column Tests of Specimen UTA-34-F (Specimen No. 6)

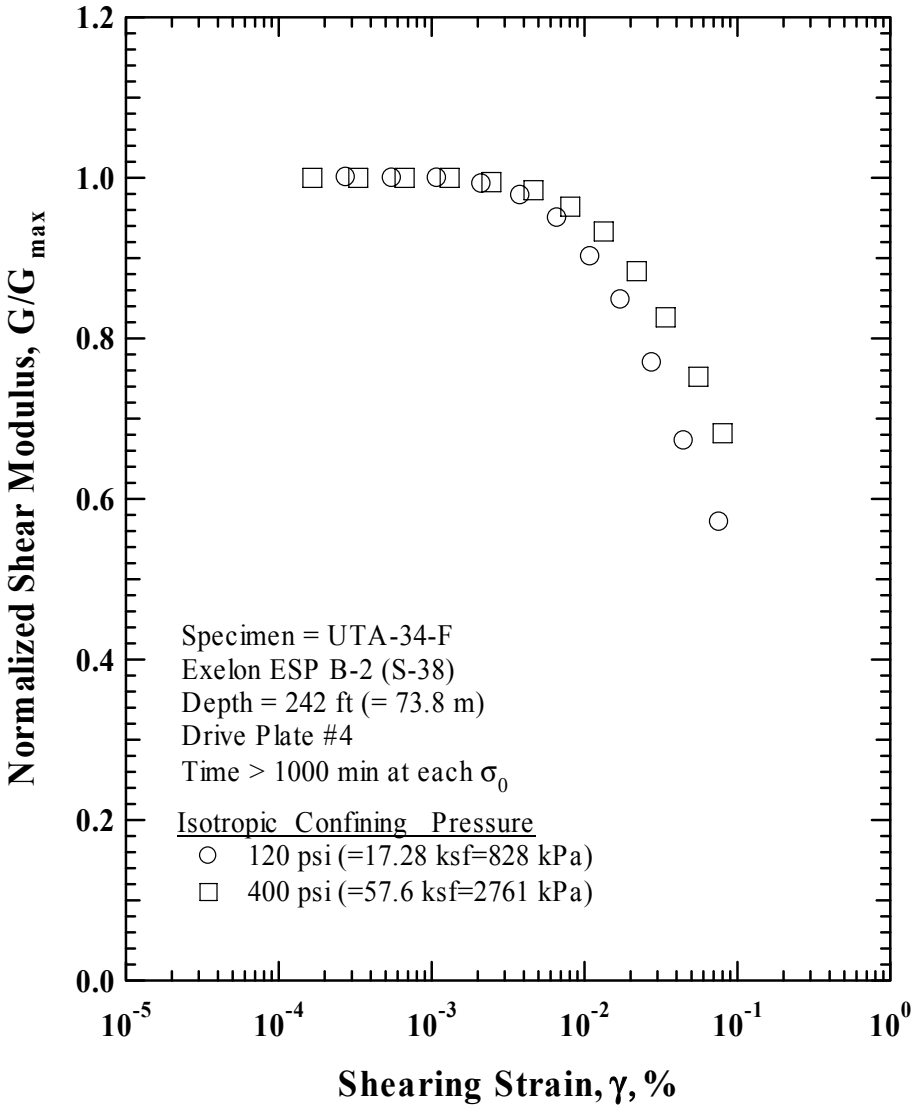

Figure G.9 Comparison of the Variation in Normalized Shear Modulus with Shearing Strain and Isotropic Confining Pressure from the Resonant Column Tests of Specimen UTA-34-F (Specimen No. 6)

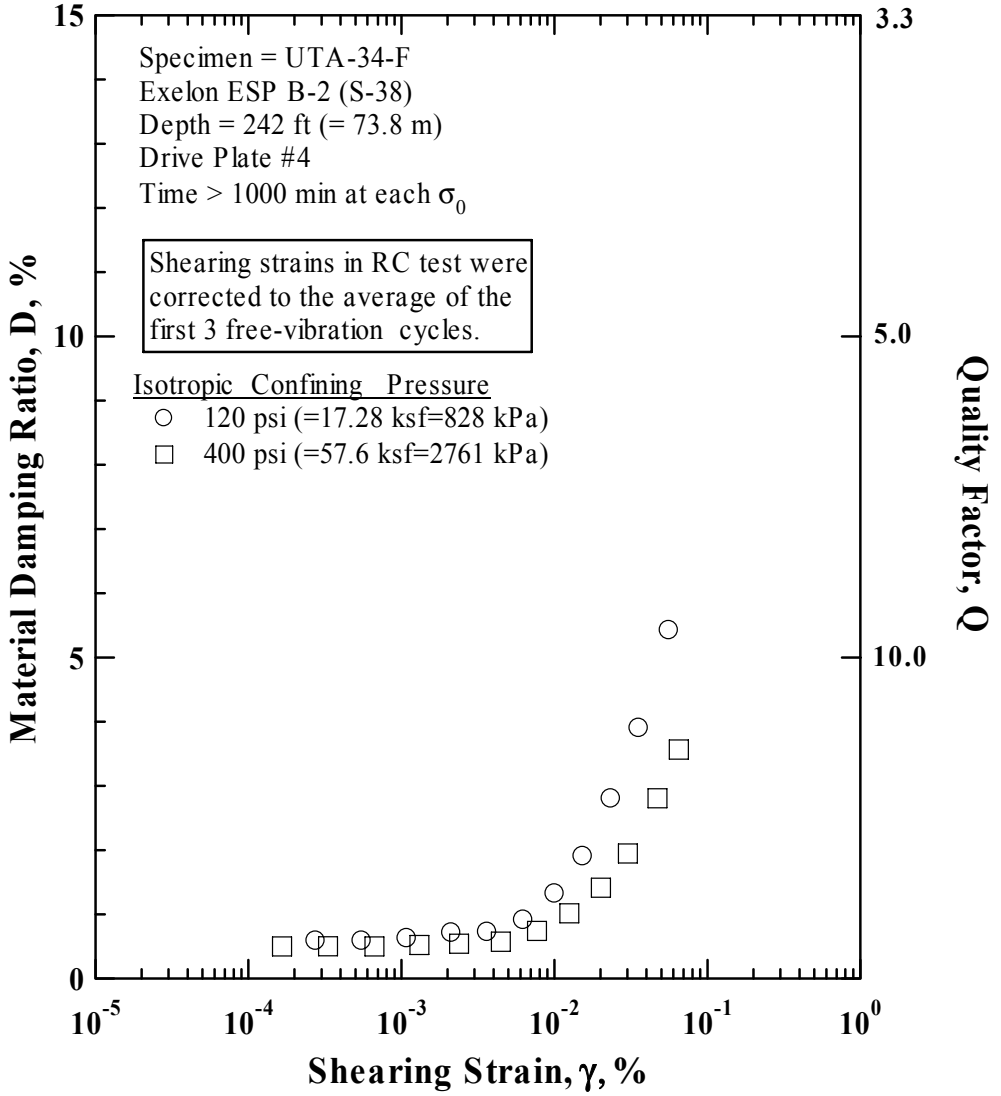

Figure G.10 Comparison of the Variation in Material Damping Ratio with Shearing Strain and Isotropic Confining Pressure from the Resonant Column Tests of Specimen UTA-34-F (Specimen No. 6)

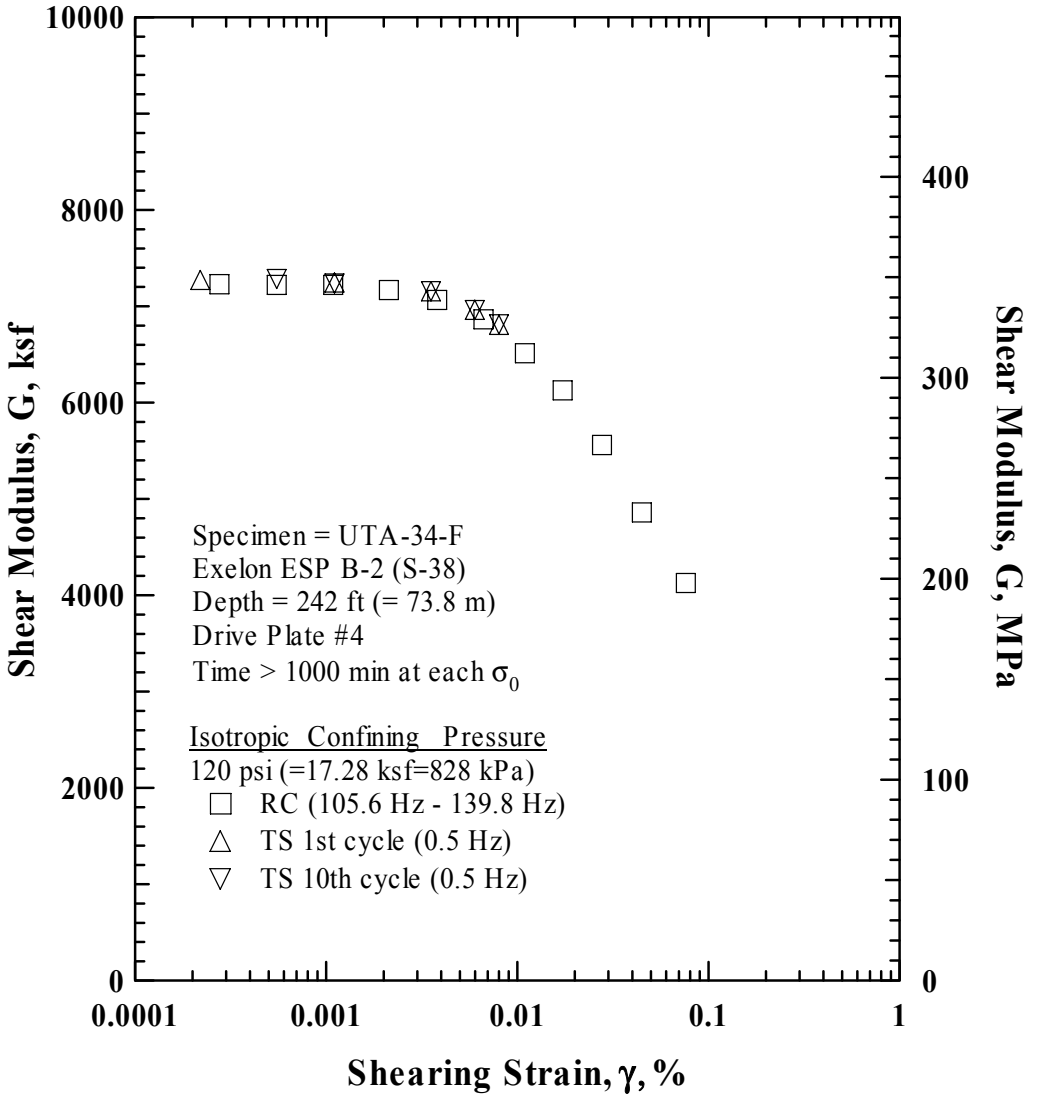

Figure G.11 Comparison of the Variation in Shear Modulus with Shearing Strain at an Isotropic Confining Pressure of 120 psi (=17.28 ksf=828 kPa) from the Combined RCTS Tests of Specimen UTA-34-F (Specimen No. 6)

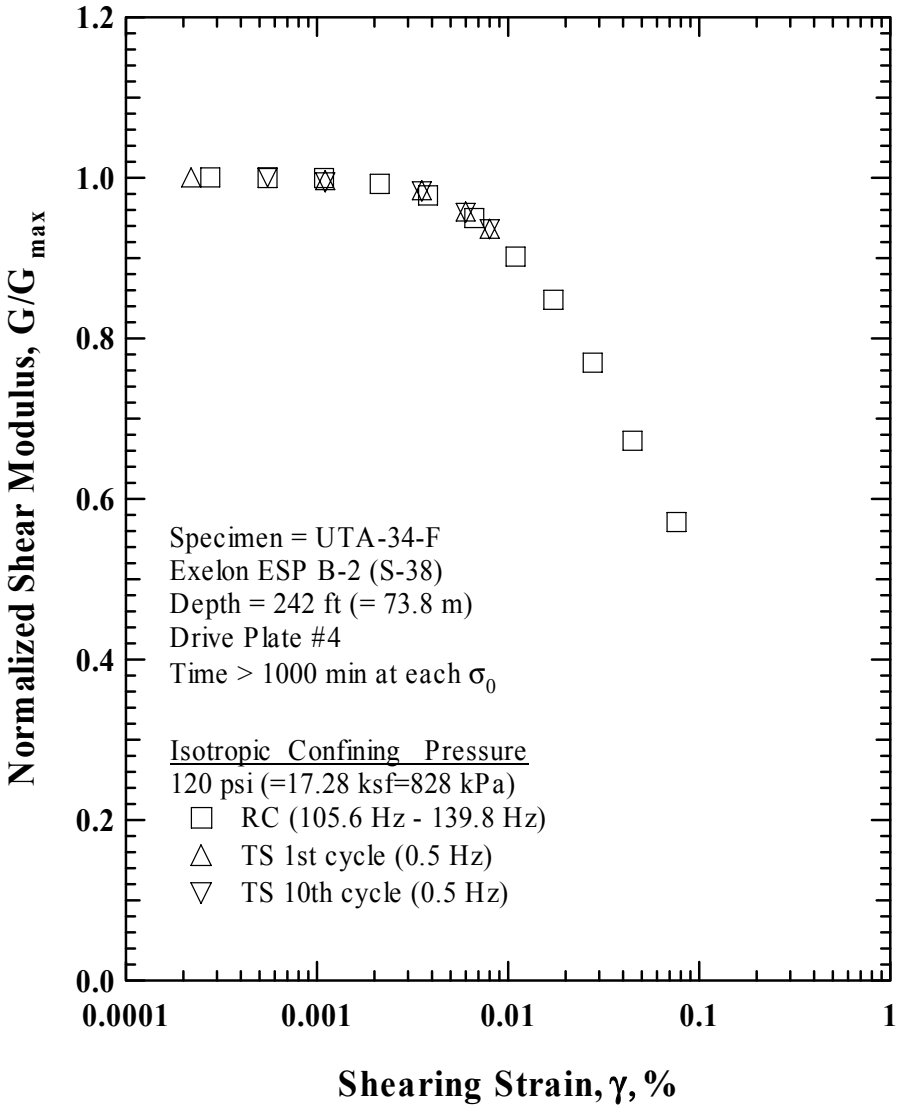

Figure G.12 Comparison of the Variation in Normalized Shear Modulus with Shearing Strain at an Isotropic Confining Pressure of 120 psi (=17.28 ksf=828 kPa) from the Combined RCTS Tests of Specimen UTA-34-F (Specimen No. 6)

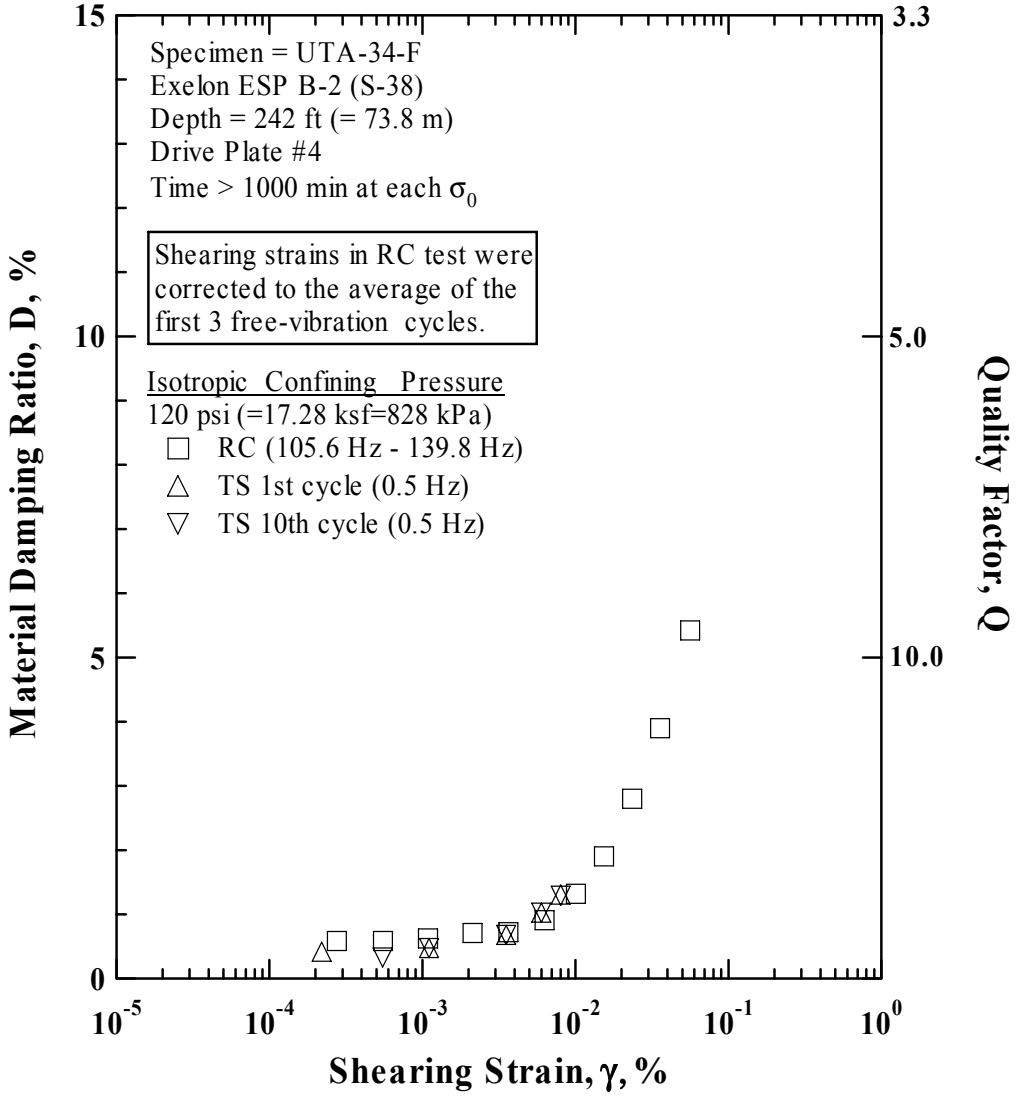

Figure G.13 Comparison of the Variation in Material Damping Ratio with Shearing Strain at an Isotropic Confining Pressure of 120 psi (=17.28 ksf=828 kPa) from the Combined RCTS Tests of Specimen UTA-34-F (Specimen No. 6)

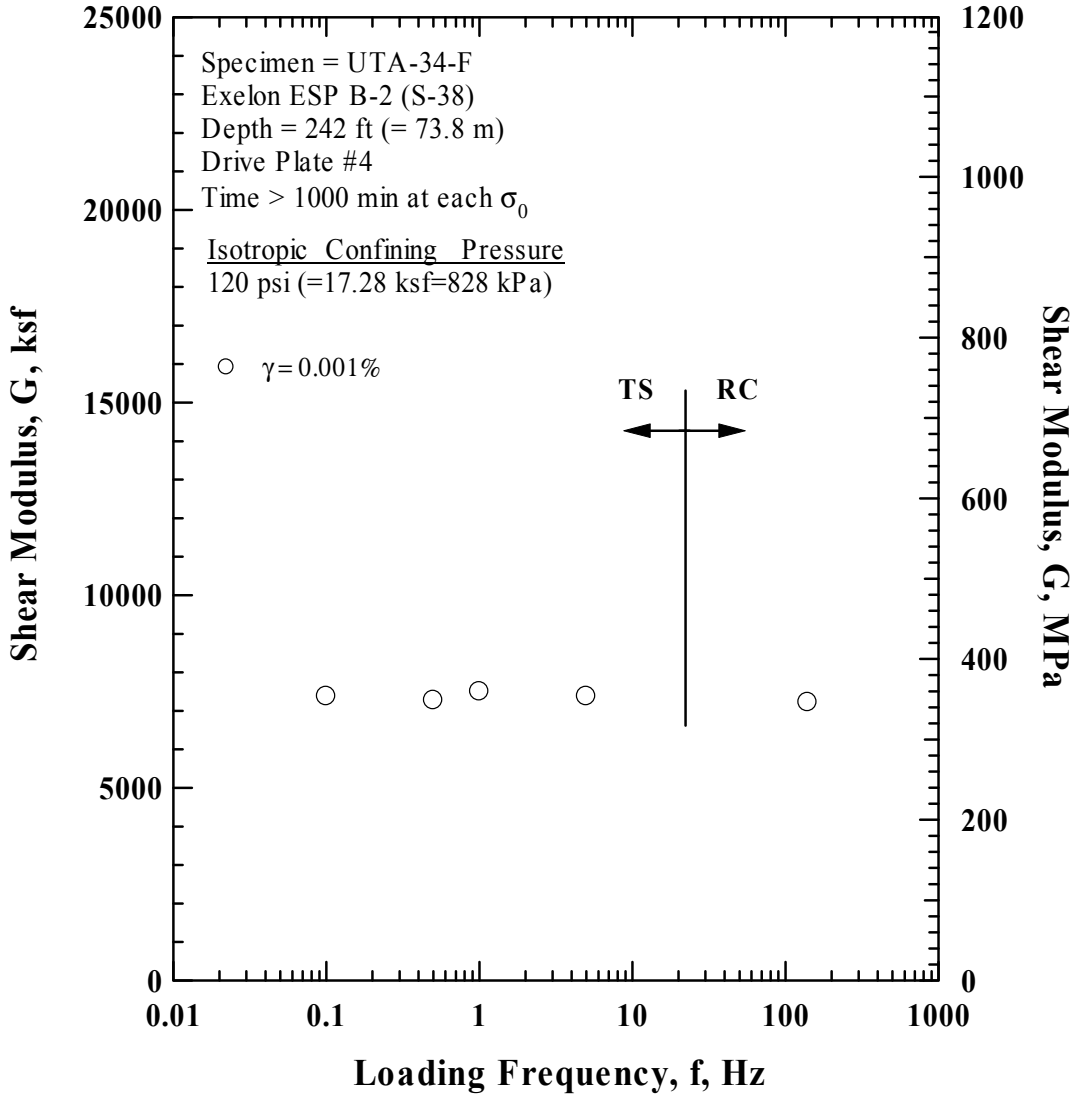

Figure G.14 Comparison of the Variation in Shear Modulus with Loading Frequency at an Isotropic Confining Pressure of 120 psi (=17.28 ksf=828 kPa) from the Combined RCTS Tests of Specimen UTA-34-F (Specimen No. 6)

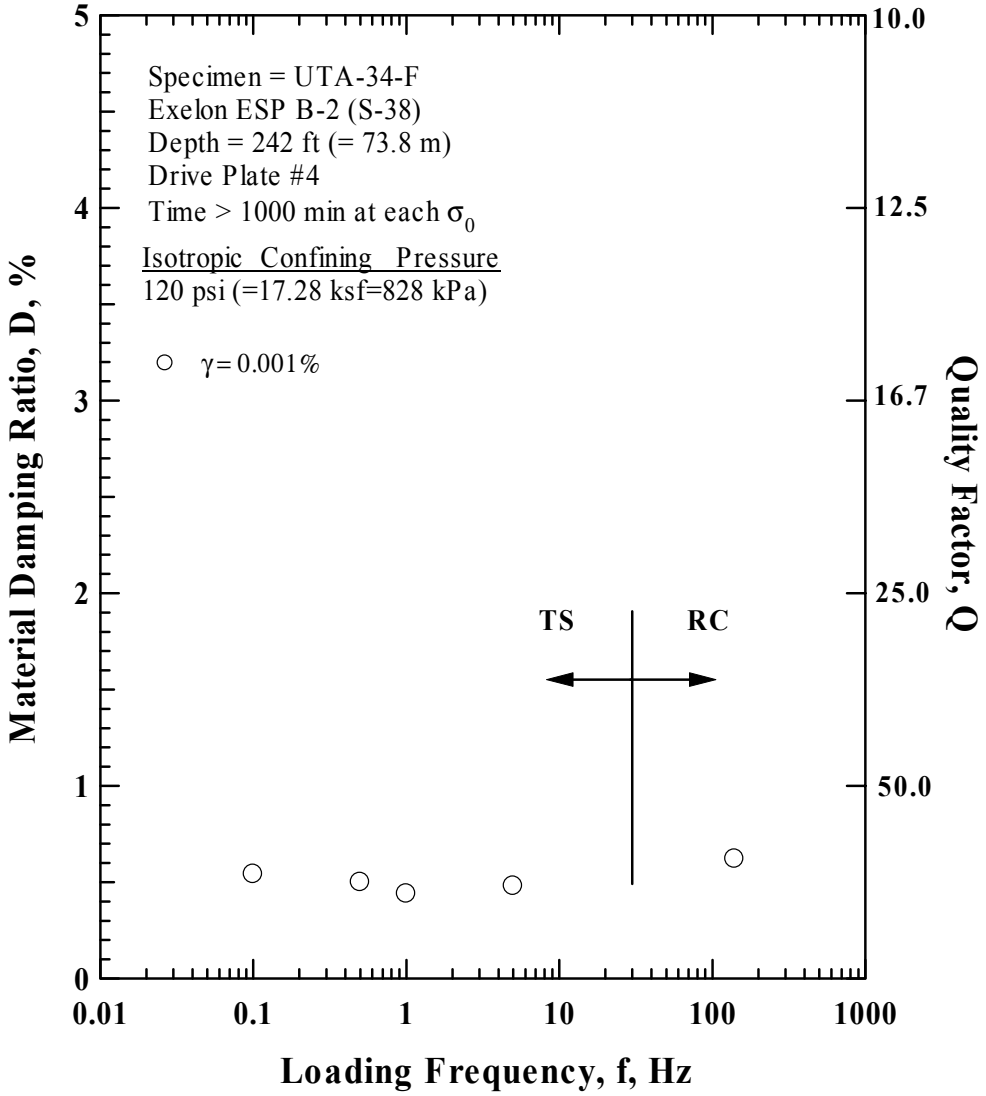

Figure G.15 Comparison of the Variation in Material Damping Ratio with Loading Frequency at an Isotropic Confining Pressure 120 psi (=17.28 ksf=828 kPa) from the Combined RCTS Tests of Specimen UTA-34-F (Specimen No. 6)

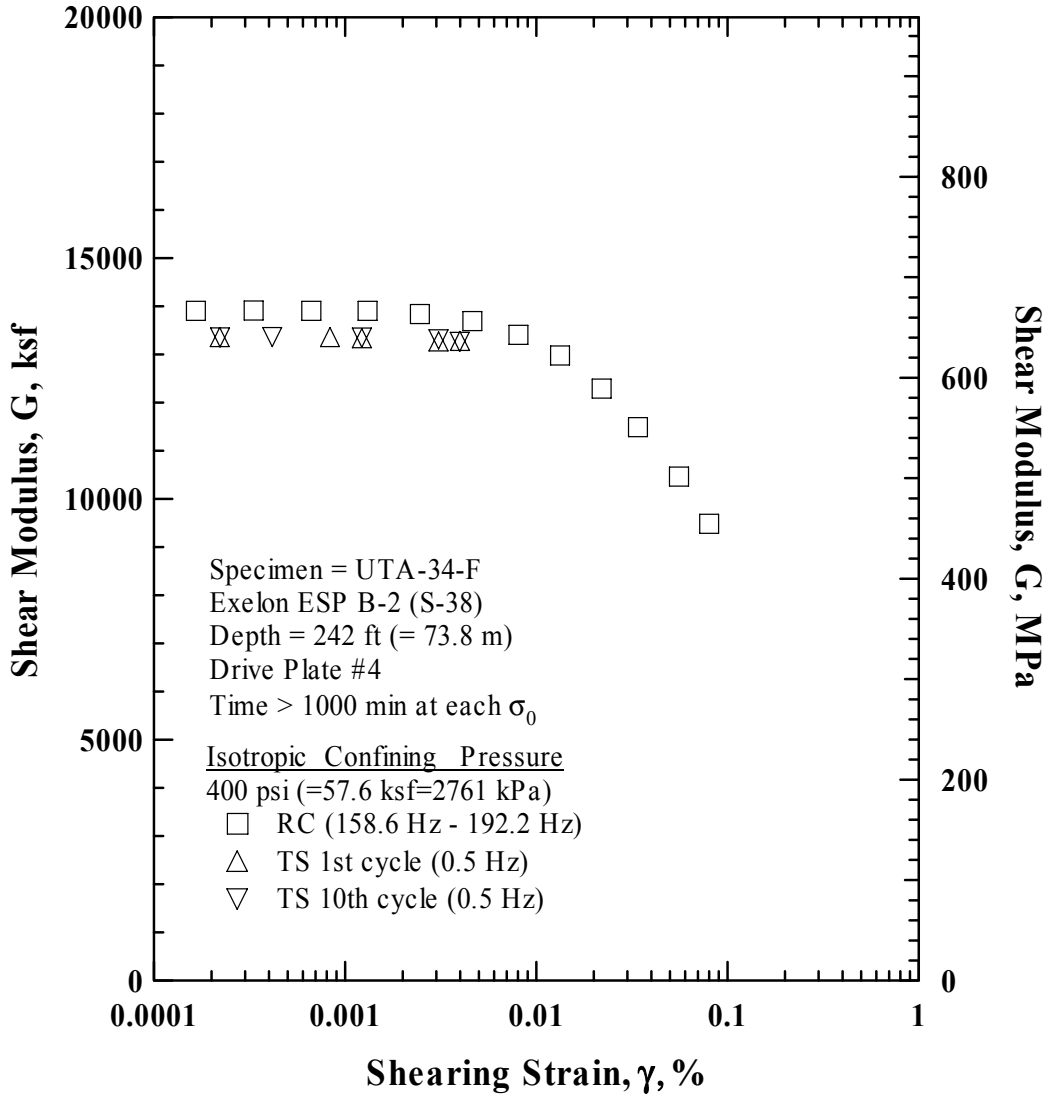

Figure G.16 Comparison of the Variation in Shear Modulus with Shearing Strain at an Isotropic Confining Pressure of 400 psi (=57.6 ksf=2761 kPa) from the Combined RCTS Tests of Specimen UTA-34-F (Specimen No. 6)

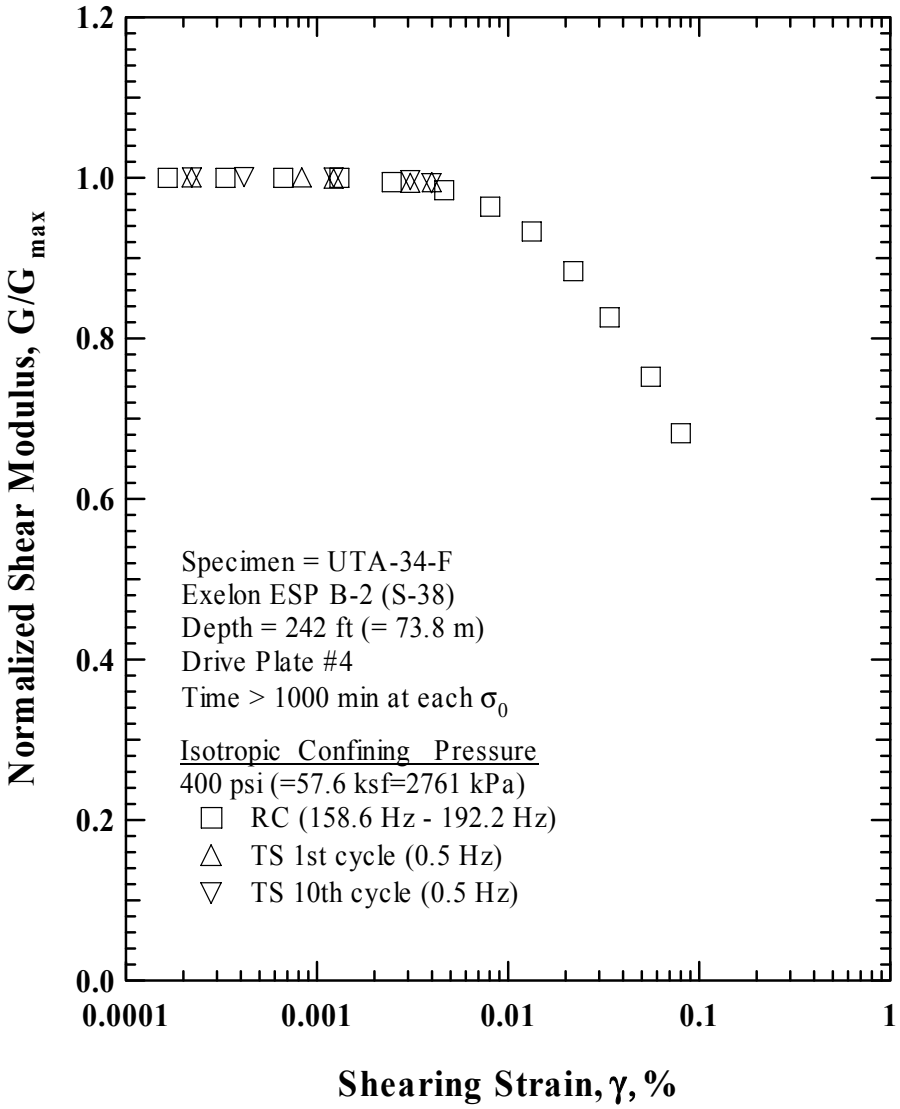

Figure G.17 Comparison of the Variation in Normalized Shear Modulus with Shearing Strain at an Isotropic Confining Pressure of 400 psi (=57.6 ksf=2761 kPa) from the Combined RCTS Tests of Specimen UTA-34-F (Specimen No. 6)

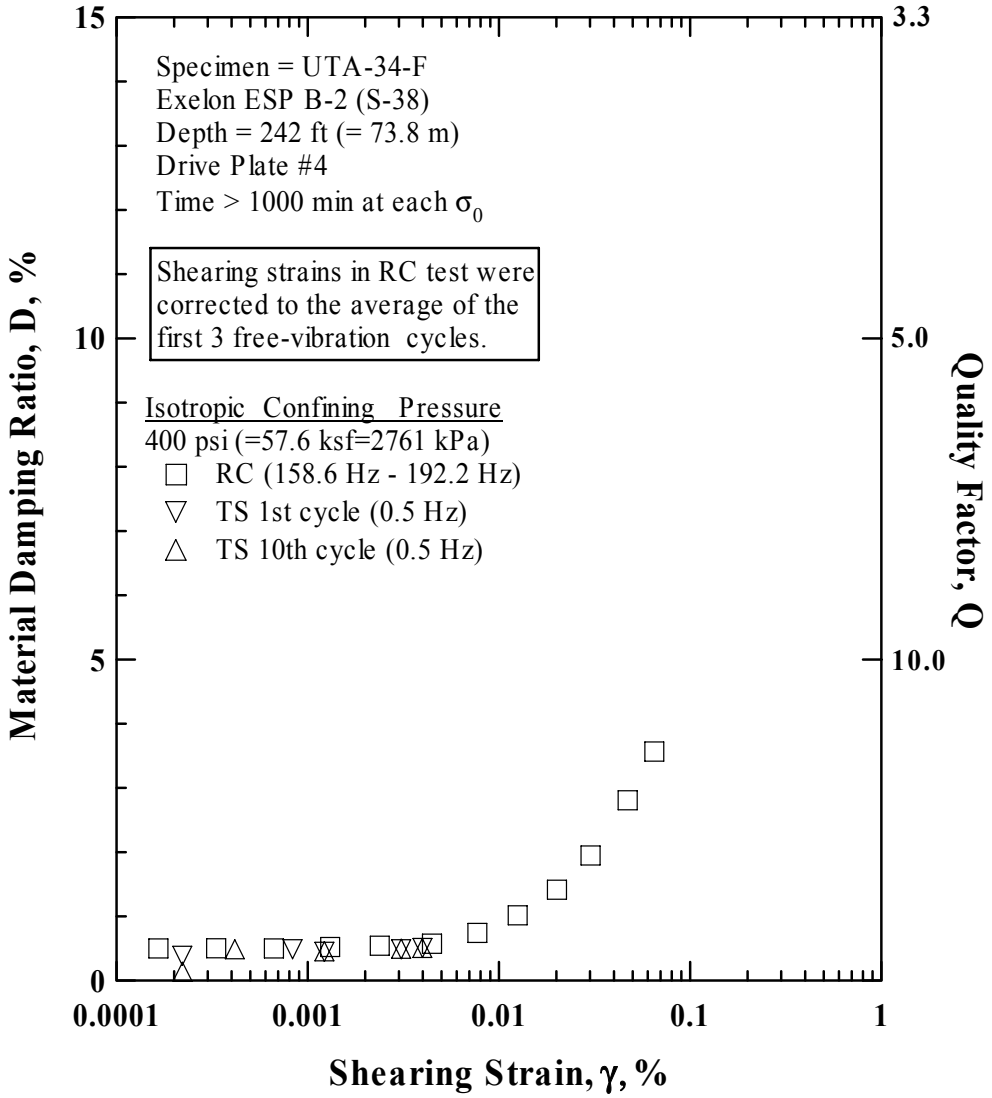

Figure G.18 Comparison of the Variation in Material Damping Ratio with Shearing Strain at an Isotropic Confining Pressure of 400 psi (=57.6 ksf=2761 kPa) from the Combined RCTS Tests of Specimen UTA-34-F (Specimen No. 6)

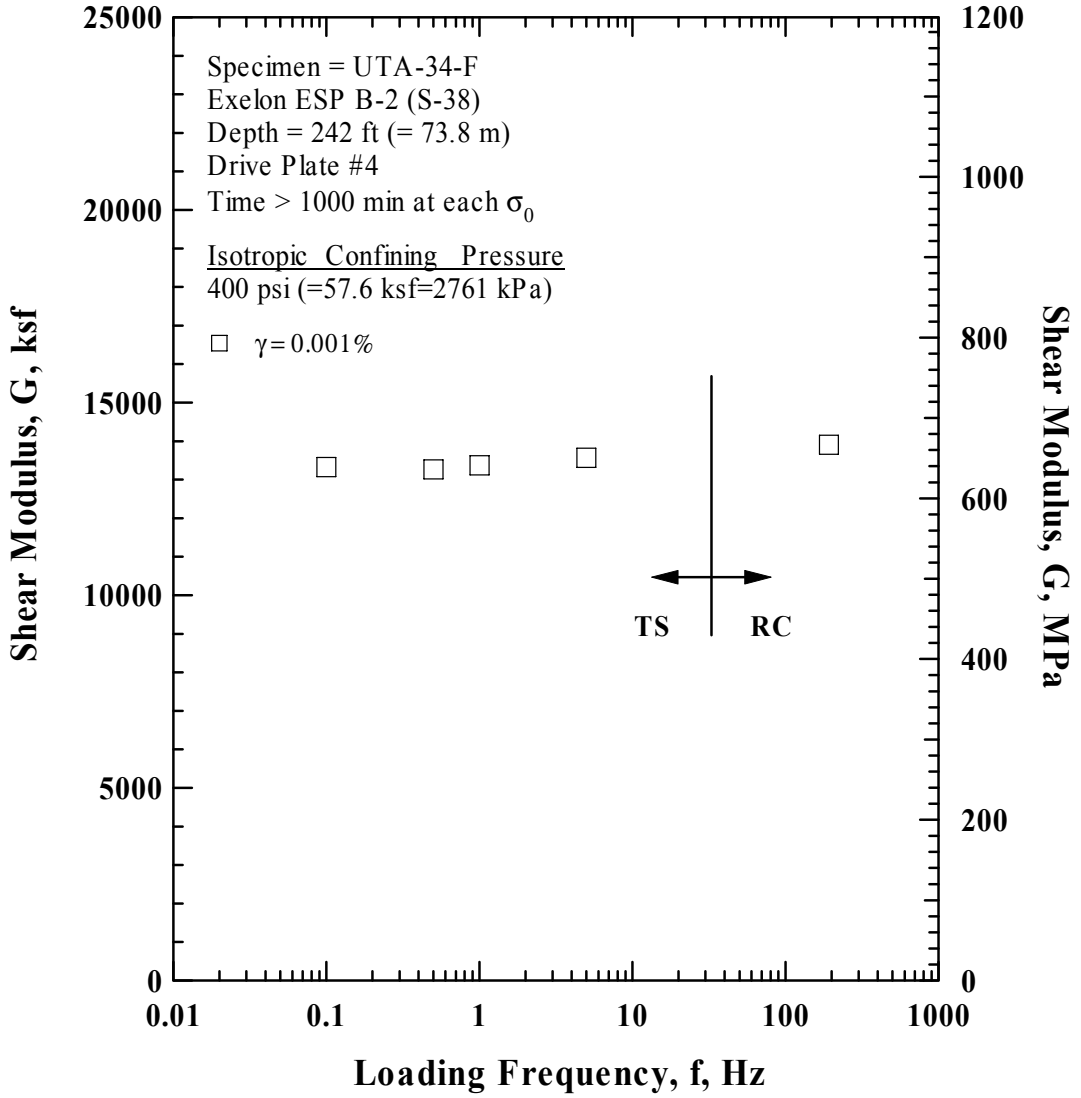

Figure G.19 Comparison of the Variation in Shear Modulus with Loading Frequency at an Isotropic Confining Pressure of 400 psi (=57.6 ksf=2761 kPa) from the Combined RCTS Tests of Specimen UTA-34-F (Specimen No. 6)

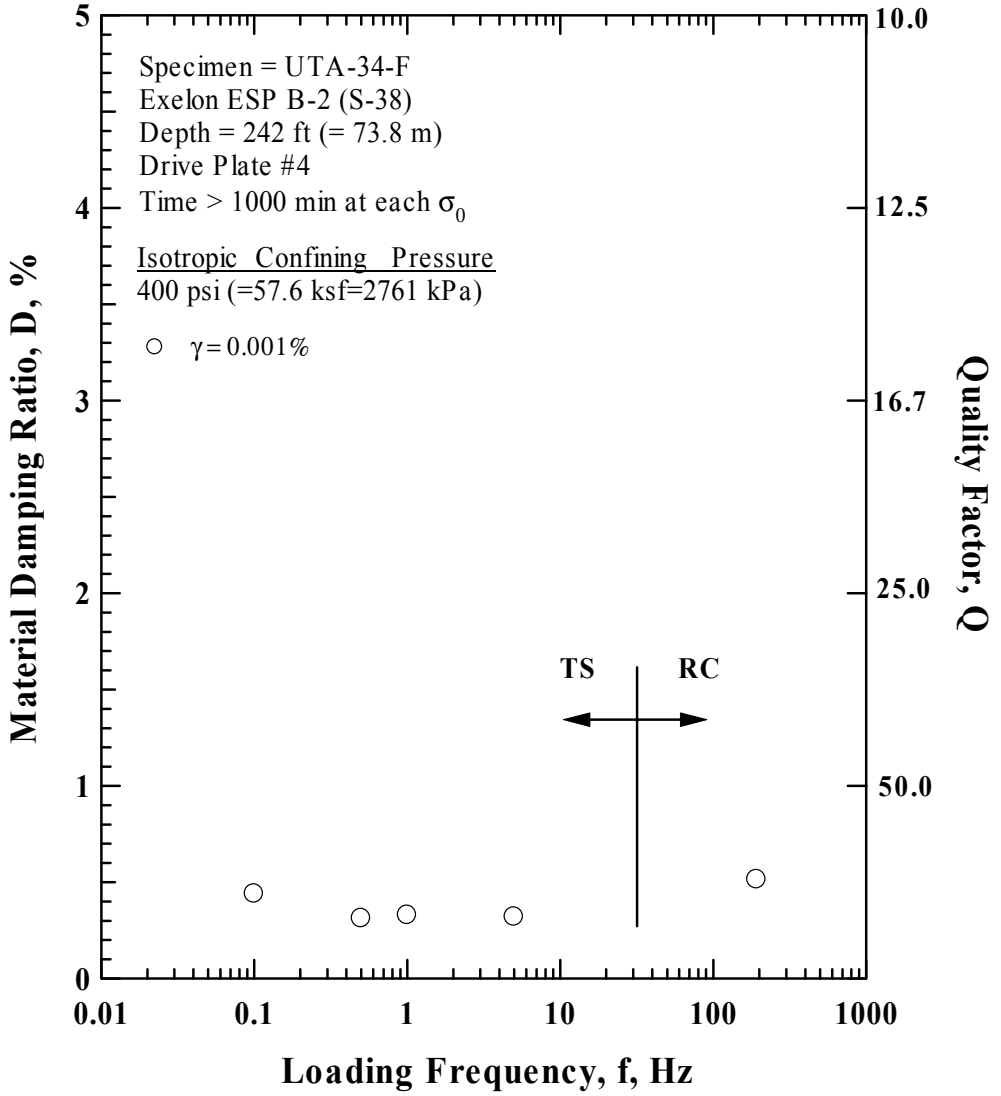

Figure G.20 Comparison of the Variation in Material Damping Ratio with Loading Frequency at an Isotropic Confining Pressure 400 psi (=57.6 ksf=2761 kPa) from the Combined RCTS Tests of Specimen UTA-34-F (Specimen No. 6)

Table G.1 Variation in Low-Amplitude Shear Wave Velocity, Low-Amplitude Shear Modulus, Low-Amplitude Material Damping Ratio and Estimated Void Ratio with Isotropic Confining Pressure from RC Tests of Specimen UTA-34-F

Isotropic Isotropic Confining Pressure, so'			Low-Amplitude Shear Modulus, G_{max}		Low-Amplitude Shear Wave Velocity, Vs	Low-Amplitude Material Damping Ratio, Dmin	Void Ratio, e
(psi)	(psf)	(kPa)	(ksf)	(MPa)	(fps)	(%)	
30	4320	207	3625	173.8	942	0.74	0.50
60	8640	414	5143	246.5	1120	0.78	0.49
120	17280	828	7119	341.3	1315	0.61	0.48
240	34560	1657	10662	511.1	1605	0.52	0.46
400	57600	2761.3	13814	662.2	1822	0.51	0.45

Table G.2 Variation in Shear Modulus, Normalized Shear Modulus and Material Damping Ratio with Shearing Strain from RC Tests of Specimen UTA-34-F; Isotropic Confining Pressure, σ_o =120 psi (=17.28 ksf=828 kPa)

Peak Shearing Strain, %	Shear Modulus, G, ksf	Normalized Shear Modulus, G/G_{max}	Average[+] Shearing Strain, %	Material Damping Ratio[x], D, %
2.76E-04	7230	1.00	2.76E-04	0.59
5.51E-04	7221	1.00	5.51E-04	0.59
1.09E-03	7221	1.00	1.09E-03	0.63
2.13E-03	7169	0.99	2.13E-03	0.71
3.81E-03	7066	0.98	3.64E-03	0.72
6.65E-03	6864	0.95	6.29E-03	0.91
1.09E-02	6514	0.90	1.01E-02	1.32
1.73E-02	6127	0.85	1.54E-02	1.90
2.77E-02	5561	0.77	2.35E-02	2.80
4.48E-02	4859	0.67	3.58E-02	3.90
7.62E-02	4127	0.57	5.63E-02	5.42

[+] Average Shearing Strain from the First Three Cycles of the Free Vibration Decay Curve

[x] Average Damping Ratio from the First Three Cycles of the Free Vibration Decay Curve

Table G.3 Variation in Shear Modulus, Normalized Shear Modulus and Material Damping Ratio with Shearing Strain from TS Tests of Specimen UTA-34-F; Isotropic Confining Pressure, σ_o =120 psi (=17.28 ksf=828 kPa)

First Cycle				Tenth Cycle			
Peak Shearing Strain, %	Shear Modulus, G, ksf	Normalized Shear Modulus, G/G_{max}	Material Damping Ratio, D, %	Peak Shearing Strain, %	Shear Modulus, G, ksf	Normalized Shear Modulus, G/G_{max}	Material Damping Ratio, D, %
2.21E-04	7268	1.00	0.41	2.21E-04			
				5.54E-04	7278	1.00	0.32
1.11E-03	7242	1.00	0.47	1.11E-03	7233	0.99	0.47
3.55E-03	7152	0.98	0.67	3.55E-03	7152	0.98	0.67
6.03E-03	6958	0.96	1.02	6.03E-03	6955	0.96	1.02
8.07E-03	6801.9	0.94	1.3	8.07E-03	6807.15	0.94	1.28

Table G.4 Variation in Shear Modulus, Normalized Shear Modulus and Material Damping Ratio with Shearing Strain from RC Tests of Specimen UTA-34-F; Isotropic Confining Pressure, σ_o =400 psi (=57.6 ksf=2761 kPa)

Peak Shearing Strain, %	Shear Modulus, G, ksf	Normalized Shear Modulus, G/G_{max}	Average[+] Shearing Strain, %	Material Damping Ratio[x], D, %
1.66E-04	13907	1.00	1.66E-04	0.50
3.32E-04	13909	1.00	3.32E-04	0.50
6.65E-04	13908	1.00	6.65E-04	0.50
1.31E-03	13908	1.00	1.31E-03	0.53
2.46E-03	13836	0.99	2.38E-03	0.54
4.63E-03	13693	0.98	4.47E-03	0.57
8.06E-03	13407	0.96	7.70E-03	0.74
1.33E-02	12980	0.93	1.25E-02	1.02
2.19E-02	12291	0.88	2.01E-02	1.41
3.39E-02	11490	0.83	3.02E-02	1.95
5.57E-02	10462	0.75	4.71E-02	2.81
8.01E-02	9484	0.68	6.50E-02	3.57

[+] Average Shearing Strain from the First Three Cycles of the Free Vibration Decay Curve

[x] Average Damping Ratio from the First Three Cycles of the Free Vibration Decay Curve

Table G.5 Variation in Shear Modulus, Normalized Shear Modulus and Material Damping Ratio with Shearing Strain from TS Tests of Specimen UTA-34-F; Isotropic Confining Pressure, σ_o =400 psi (=57.6 ksf=2761 kPa)

First Cycle				Tenth Cycle			
Peak Shearing Strain, %	Shear Modulus, G, ksf	Normalized Shear Modulus, G/G_{max}	Material Damping Ratio, D, %	Peak Shearing Strain, %	Shear Modulus, G, ksf	Normalized Shear Modulus, G/G_{max}	Material Damping Ratio, D, %
2.22E-04	13350	1.00	0.38	2.23E-04	13345	1.00	0.13
				4.18E-04	13350	1.00	0.48
8.37E-04	13350	1.00	0.48				
1.23E-03	13330	1.00	0.44	1.23E-03	13340	1.00	0.45
3.10E-03	13260	0.99	0.48	3.10E-03	13300	1.00	0.49
4.01E-03	13270	0.99	0.50	4.00E-03	13250	0.99	0.50